Institut für Erd- und Umweltwissenschaften
Mathematisch Naturwissenschaftliche Fakultät
Universität Potsdam

Biogeochemistry of ferruginous sediments of Lake Towuti, Sulawesi, Indonesia

Kumulative Dissertation
zur Erlangung des akademischen Grades
"doctor rerum naturalium"
(Dr. rer. nat.)
in der Wissenschaftsdisziplin "Geomikrobiologie"

eingereicht an der
Mathematisch-Naturwissenschaftlichen Fakultät
der Universität Potsdam

von

André Friese

Potsdam, den 24.10.2019

Published online on the
Publication Server of the University of Potsdam:
https://doi.org/10.25932/publishup-47535
https://nbn-resolving.org/urn:nbn:de:kobv:517-opus4-475355

Statement of original authorship

I, André Friese, hereby state that the work contained in this thesis has not previously been submitted for assessment, either in whole or in part, by either myself or any other person at either the Faculty of Mathematics and Natural Sciences at the University of Potsdam or at any other institution except where explicitly acknowledged.

To the best of my knowledge and belief, the thesis contains no material which has been previously published or written by any other person except where due reference is made.

Hiermit erkläre Ich, André Friese, dass diese Arbeit bisher weder von mir, noch von einer anderen Person, weder teilweise, noch in Gänze, weder an der Mathematisch-Naturwissenschaftlichen Fakultät der Universität Potsdam, noch einer anderen wissenschaftlichen Einrichtung, zum Zwecke der Promotion eingereicht wurde.

Zu meinem besten Wissen und Gewissen habe Ich diese Arbeit selbstständig verfasst und keine anderen als die darin angegebenen Quellen und Hilfsmittel benutzt.

Potsdam, den 24.10.2019 André Friese _____

Acknowledgements

I would like to express my sincerest thanks to Dr. Jens Kallmeyer for giving me the opportunity to conduct my PhD thesis under his direct supervision. Throughout my PhD he was there to give me advice, support and encouragement both scientifically and privately. I could not have wished for a better supervisor. Prof. Dr. Dirk Wagner is thanked for his support in scientific, bureaucratic and technical questions at all times.

I kindly thank the DFG, German Research Foundations for funding this project. The Ministry of Trade of the Republic of Indonesia (RISTEK) is thanked for permission to conduct research at Lake Towuti.

Many thanks are due to our technician Axel 'MacGyver' Kitte. His help and technical ideas in the field as well as in the laboratory were tremendous and his constant positive attitude was contagious.

My colleague Dr. Aurèle Vuillemin is thanked for countless scientific discussions and advices as well as for being a constant and competent partner in the field and in the lab.

I would also like to show my gratitude to Prof. Dr. Martin Trauth for a memorable visit to Kenya and Ethiopia during the Volkswagen Summer School in 2015 and 2016 in which I could get to know the fascinating geology of the East African Rift system and improve my skills in presenting scientific information.

Many thanks go out to the Crowe Lab in Vancouver, especially Dr. Sean Crowe, Kohen Bauer and Rachel Simister, for assistance in the field, numerous discussions and a productive and comfortable working environment in the field.

My colleagues from the Geomicrobiology group at GFZ are thanked for fruitful comments and critical questions during the numerous workgroup meetings. Verena Heuer and her colleagues at MARUM, Bremen are thanked for a very productive stay in which I could obtain critical data for my thesis.

Without support and encouragement from my parents and my sister I would not have been where I am today. Last but not least I would like to thank my girlfriend Anne for her love, patience and motivation at all times.

Abstract

Ferruginous conditions were a prominent feature of the oceans throughout the Precambrian Eons and thus throughout much of Earth's history. Organic matter mineralization and diagenesis within the ferruginous sediments that deposited from Earth's early oceans likely played a key role in global biogeochemical cycling. Knowledge of organic matter mineralization in ferruginous sediments, however, remains almost entirely conceptual, as modern analogue environments are extremely rare and largely unstudied, to date. Lake Towuti on the island of Sulawesi, Indonesia is such an analogue environment and the purpose of this PhD project was to investigate the rates and pathways of organic matter mineralization in its ferruginous sediments.

Lake Towuti is the largest tectonic lake in Southeast Asia and is hosted in the mafic and ultramafic rocks of the East Sulawesi Ophiolite. It has a maximum water depth of 203 m and is weakly thermally stratified. A well-oygenated surface layer extends to 70 m depth, while waters below 130 m are persistently anoxic. Intensive weathering of the ultramafic catchment feeds the lake with large amounts of iron(oxy)hydroxides while the runoff contains only little sulfate, leading to sulfate-poor (< 20 μM) lake water and anoxic ferruginous conditions below 130 m. Such conditions are analogous to the ferruginous water columns that persisted throughout much of the Archean and Proterozoic eons. Short (< 35 cm) sediment cores were collected from different water depths corresponding to different bottom water redox conditions. Also, a drilling campaign of the International Continental Scientific Drilling Program (ICDP) retrieved a 114 m long sediment core dedicated for geomicrobiological investigations from a water depth of 153 m, well below the depth of oxygen penetration at the time of sampling. Samples collected from these sediment cores form the fundament of this thesis and were used to perform a suite of biogeochemical and microbiological analyses.

Geomirobiological investigations depend on uncontaminated samples. However, exploration of subsurface environments relies on drilling, which requires the use of a drilling fluid. Drilling fluid infiltration during drilling can not be avoided. Thus, in order to trace contamination of the sediment core and to identify uncontaminated samples for further analyses a simple and inexpensive technique for assessing contamination during drilling operations was developed and applied during the ICDP drilling campaign. This approach uses an aqeous fluorescent pigment dispersion commonly used in the paint

industry as a particulate tracer. It has the same physical properties as conventionally used particulate tracers. However, the price is nearly four orders of magnitude lower solving the main problem of particulate tracer approaches. The approach requires only a minimum of equipment and allows for a rapid contamination assessment potentially even directly on site, while the senstitivity is in the range of already established approaches. Contaminated samples in the drill core were identified and not included for further geomicrobiological investigations.

Biogeochemical analyses of short sediment cores showed that Lake Towutis sediments are strongly depleted in electron acceptors commonly used in microbial organic matter mineralization (i.e. oxygen, nitrate, sulfate). Still, the sediments harbor high microbial cell densities, which are a function of redox conditions of Lake Towuti's bottom water. In shallow water depths bottom water oxygenation leads to a higher input of labile organic matter and electron acceptors like sulfate and iron, which promotes a higher microbial abundance. Microbial analyses showed that a versatile microbial community with a potential to perform metabolisms related to iron and sulfate reduction, fermentation as well as methanogenesis inhabits Lake Towuti's surface sediments.

Biogeochemical investigations of the upper 12 m of the 114 m sediment core showed that Lake Towuti's sediment is extremely rich in iron with total concentrations up to 2500 µmol cm^{-3} (20 wt. %), which makes it the natural sedimentary environment with the highest total iron concentrations studied to date. In the complete or near absence of oxygen, nitrate and sulfate, organic matter mineralization in ferruginous sediments would be expected to proceed anaerobically via the energetically most favorable terminal electron acceptors available - in this case ferric iron. Astonishingly, however, methanogenesis is the dominant (>85 %) organic matter mineralization process in Lake Towuti's sediment. Reactive ferric iron known to be available for microbial iron reduction is highly abundant throughout the upper 12 m and thus remained stable for at least 60.000 years. The produced methane is not oxidized anaerobically and diffuses out of the sediment into the water column. The proclivity towards methanogenesis, in these very iron-rich modern sediments, implies that methanogenesis may have played a more important role in organic matter mineralization thoughout the Precambrian than previously thought and thus could have been a key contributor to Earth's early climate dynamics.

Over the whole sequence of the 114 m long sediment core siderites were identified and characterized using high-resolution microscopic and spectroscopic imaging together with microchemical and geochemical analyses. The data show early diagenetic growth of siderite crystals as a response to sedimentary organic matter mineralization. Microchemical zoning was identified in all siderite crystals. Siderite thus likely forms during diagenesis through growth on primary existing phases and the mineralogical and chemical features of these siderites are a function of changes in redox conditions of the pore water and sediment over time. Identification of microchemical zoning in ancient siderites deposited in the Precambrian may thus also be used to infer siderite growth histories in ancient sedimentary rocks including sedimentary iron formations.

Zusammenfassung

Während des Präkambriums und damit während des Großteils der Erdgeschichte, zeichneten sich die Ozeane durch ihren hohen Eisengehalt aus. Sowohl die Remineralisierung von organischem Material, als auch die Diagenese in den Sedimenten, die in den frühen Ozeanen der Erde abgelagert wurden, hatte höchstwahrscheinlich bedeutende Auswirkungen auf die globalen biogeochemischen Stoffkreisläufe. Unser Verständnis des Abbaus von organischem Material in eisenhaltigen Sedimenten ist jedoch sehr begrenzt, da moderne Analogsysteme extrem selten sind und bis heute nicht erforscht wurden. Der Towutisee auf der Insel Sulawesi in Indonesien ist ein solches modernes Analogsystem und Ziel dieser Doktorarbeit war es, die Raten und Pfade des Abbaus von organischem Material in den modernen eisenhaltigen Sedimenten des Towutisees zu erforschen.

Der Towutisee ist der größte tektonische See in Südostasien und ist von mafischen und ultramafischen Gesteinen des Ost-Sulawesi-Ophioliten umgeben. Er hat eine maximale Wassertiefe von 203 m und ist schwach thermisch stratifiziert. Bis zu einer Tiefe von 70 m herrschen oxische Bedingungen, während die Wassersäule unterhalb von 130 m permanent anoxisch ist. Intensive Verwitterungsprozesse des ultramafischen Einzugsgebietes führen zu einem hohen Eintrag von Eisen(oxy)hydroxiden, während der Oberflächenabfluss nur wenig Sulfat enthält. Die Konzentrationen von Sulfat in der Wassersäule sind daher außergewöhnlich gering (< 20µM). Diese physikochemischen Verhältnisse sind analog zu denen der Ozeane des Archaikums und des Proterozoikums. Kurze (< 35 cm) Sedimentkerne wurden von verschiedenen Wassertiefen und unterschiedlichen Redox-Bedingungen des Bodenwassers entnommen. Darüber hinaus, wurde, im Zuge einer Bohrkampagne des International Continental Scientific Drilling Programs (ICDP) am Towutisee, ein 114 m langer Sedimentkern aus einer Wassertiefe von 153m, also deutlich unterhalb des Sauerstoffgradienten, erbohrt. Dieser war ausschließlich für geomikrobiologische Probenahmen und Untersuchungen vorgesehen. Die Proben, die aus diesen Sedimentkernen entnommen wurden, bilden das Fundament dieser Doktorarbeit und wurden für biogeochemische und mikrobiologische Untersuchungen verwendet.

Unkontaminierte Proben sind für geomikrobiologische Untersuchungen unabdingbar. Das Erforschen von Gebieten unterhalb der Oberfläche ist jedoch auf Bohrungen angewiesen, welche wiederum den Einsatz einer Bohrspülung erfordern. Leider ist es unvermeidlich, dass diese im Zuge des Bohrprozesses in den erbohrten Sedimentkern eindringen. Die einzige Möglichkeit unkontaminierte Proben zu gewinnen ist es daher, den Grad der Kontamination des Bohrkerns nachzuverfolgen und unkontaminierte Proben für weitere Analysen zu identifizieren. Dazu wurde im Zuge dieser Doktorarbeit eine einfache und kostengünstige Methode zur Kontaminationskontrolle während Bohroperationen entwickelt und während der ICDP Bohrkampagne auf dem Towutisee angewandt. Als Tracer kam eine Farbe zum Einsatz, deren physikalische Eigenschaften denen von partikulären Tracern ähnelt. Der Preis dieser Farbe ist im Vergleich zu bisher verwendeten partikulären Tracern, jedoch vier Größenordnungen geringer und löst damit das Hauptproblem dieser Tracer. Die Methode benötigt nur ein Mindestmaß an Equipment und ermöglicht eine schnelle Identifizierung von Kontaminationen, möglicherweise sogar vor Ort. Die Sensitivität der Methode ist im Bereich von etablierten Kontaminationskontrollen. Kontaminierte Proben des erbohrten Sedimentkerns wurden mit dieser Methode identifiziert und nicht für weitere geomikrobiologische Untersuchungen verwendet.

Biogeochemische Analysen der Kurzkerne zeigen, dass die Sedimente des Towutisees sehr arm an Elektronenakzeptoren sind, die für den mikrobiellen Abbau von organischem Material verwendet werden (d.h. Sauerstoff, Nitrat und Sulfat). Nichtsdestotrotz zeichnen sich die Sedimente des Towutisees durch hohe Zellzahlen aus, die von den Redox-Bedingungen des Bodenwassers abhängig sind. In niedrigen Wassertiefen führt oxygeniertes Bodenwasser zu einem erhöhten Eintrag von labilem organischen Material sowie Elektronenakzeptoren wie Eisen und Sulfat, wodurch hohe Zellzahlen resultieren. Mikrobiologische Analysen zeigen, dass die Sedimente des Towutisees durch eine vielseitige, mikrobielle Gemeinschaft bevölkert werden, die in der Lage ist, Stoffwechsel, wie Eisenreduktion, Sulfatreduktion, Fermentation sowie Methanogenese auszuführen.

Biogeochemische Untersuchungen der oberen 12 m des 114 m langen Sedimentkerns zeigen, dass die Sedimente des Towutisees mit 2500 $\mu M\ cm^{-3}$ extrem hohe Eisengehalte (20 Gew. %) aufweisen und damit das eisenreichste natürliche sedimentäre System sind, welches bisher erforscht wurde. Nach unserem bisherigen Verständnis über

biogeochemische Stoffkreisläufe sollte, in Abwesenheit von Sauerstoff, Nitrat oder Sulfat, organisches Material über den energetisch günstigsten verfügbaren Elektronenakzeptoren abgebaut werden – in dem Fall Eisen (III). Erstaunlicherweise jedoch, ist Methanogenese der dominante (> 85 %) Remineralisierungsprozess in den Sedimenten des Towutisees. Mikrobiell theoretisch verfügbares reaktives Eisen (III) hingegen bleibt stabil über die oberen 12 m des Sedimentkerns und damit über mehr als 60.000 Jahre. Produziertes Methan wird nicht anaerob oxidiert und diffundiert aus dem Sediment in die Wassersäule. Die Dominanz von Methanogenese in diesen eisenreichen Sedimenten impliziert, dass dieser Prozess im Präkambrium vermutlich eine viel bedeutendere Rolle in der Remineralisierung von organischem Material eingenommen hat, als bisher angenommen. Methan, als bedeutendes Treibhausgas, war demnach möglicherweise ein wichtiger Regulator des Klimas in der frühen Erdgeschichte.

Im gesamten 114 m Sedimentkern wurden Siderite identifiziert und mittels hochauflösender bildgebender Mikroskopie und Spektroskopie sowie mikrochemischer und geochemischer Analysen charakterisiert. Die Daten zeigen frühes diagenetisches Wachstum der Siderite als Folge des Abbaus von organischem Material im Sediment sowie mikrochemische Zonierung der Sideritkristalle. Siderit bildet sich während der Diagenese durch Wachstum auf bereits existierende Mineralphasen und die Chemie sowie Mineralogie der Sideritkristalle sind eine Funktion von Änderungen der Redox-Bedingungen im Porenwasser sowie im Sediment. Die Identifizierung von mikrochemischer Zonierung in Sideriten, die im Präkambrium gebildet wurden, kann daher womöglich genutzt werden, um Aussagen über die Bildungsgeschichte der Siderite in den sedimentären Eisenablagerungen der frühen Erdgeschichte zu treffen.

List of Figures

List of Tables

Abbreviations

AOM	Anaerobic oxidation of methane
aprAB	adenylysulfate reductase subunit alpha and beta
AVS	Acid volatile sulfur
ANME	Anaerobic methanotrophs
BIF	Banded iron formations
CCA	Canonical correspondence analysis
cmblf	Centimeters below lake floor
CRS	Chromium reducible sulfur
CTD	Conductivity-temperature-depth
DGGE	Denaturing gradient gel electrophoresis
DIC	Dissolved inorganic carbon
DM	Detergent Mix
DNA	deoxyribonucleic acid
dsrAB	dissimilatory sulfite reductase subunit alpha and beta
EDX	Energy-dispersive X-ray spectrometry
ENSO	El Nino Southern Oscillation
eDNA	extracellular deoxyribonucleic acid
ES	Elemental sulfur
FeRB	Iron-reducing bacteria
GC	Gas chromatography
GC-FID	Gas chromatography with flame ionization detector
GC-IRMS	Gas chromatography with isotope ratio mass spectrometry
GR	carbonate green rust
HPC	Hydraulic piston coring
IC	Ion chromatography
ICDP	International continental drilling program
IC-MS	Ion chromatography – mass spectrometry
iDNA	intracellular deoxyribonucleic acid
IF	Iron formations
IMM	interpolated Markov model
IPWP	Indo Pacific Warm pool

ITCZ	Intertropical convergence zone
LOD	Limit of detection
LOQ	Limit of quantification
mcrA	Methyl coenzyme M reductase
NSA	Naphthalene sulfonic acid
OM	Organic matter
ORF	Open reading frames
OTU	Operational taxonomic unit
PFT	Perfluorocarbon tracer
pSRR	potential sulfate reduction rate
PVPP	polyvinylpolypyrrolidone
RNA	Ribonucleic acid
SAED	Selected area electron microscopy
SEM	Scanning electron microscopy
SRB	Sulfate reducing bacteria
SRR	Sulfate reduction rate
SWI	Sediment water interface
S/N	Signal to noise ratio
TC	Total carbon
TDP	Towuti drilling project
TEM	Transmission electron microscopy
TN	Total nitrogen
TOC	Total organic carbon
TRIS	Total reduced inorganic sulfur
qPCR	quantitative polymerase chain reaction
VFA	volatile fatty acid
VSMOW	Vienna Standard Mean Ocean water
VPDB	Vienna Pee Dee Belemnite
WRC	Whole round cores

Contents

1 Introduction

1.1 Scope of the thesis

Although studies of subsurface life have expanded the range of habitats in recent years (Lever et al., 2013; Roussel et al., 2008), metal-rich environments other than hydrothermal systems (Nunoura et al., 2010) have not been studied so far. Ferruginous (Iron-rich, sulfate-poor) conditions prevailed throughout the Precambrian Eons and thus through much of Earth's history. Our knowledge of the biogeochemical processes that occurred under these conditions, however, remains largely conceptual, as modern analogue environments are extremely rare. The sediments of Lake Towuti represent such a modern analogue environment. Lake Towuti was chosen as a target for a drilling campaign conducted by the International Continental Drilling Program (ICDP), which included a dedicated core for geomicrobiological investigations. Further, several short (< 35 cm) cores were retrieved in two international pilot studies in preparation for the drilling campaign. The samples that were retrieved during the pilot study and the drilling campaign are the fundament of this thesis and were used to contribute to a better understanding of the biogeochemistry of anoxic, metal-rich environments similar to those that deposited from the stratified ferruginous oceans of the Precambrian Eons.

Geomicrobiological investigations rely on uncontaminated samples. However, drilling requires the use of a drilling fluid. As drilling fluid infiltration into the sediment core cannot be avoided it is of utmost importance to trace contamination of the sediment core in order to identify uncontaminated samples for further analyses. Several contamination control approaches were used in past drilling operations; each with their specific strengths and weaknesses. Given the special geochemical conditions of Lake Towuti and its remote location the second motivation of this thesis was to design a new contamination control approach. This approach should not only be applied during the Towuti drilling campaign but should also provide an alternative contamination control approach for future drilling operations.

The following introduction will give a general overview of microbial life in the subsurface as well as the geological and geochemical setting of Lake Towuti making it

a prime analogue environment for the ferruginous systems of Earth's early oceans. Further on it will introduce the Towuti Drilling Project (TDP) and will provide an overview of assessing contamination during drilling operations. Finally, the objectives of this thesis will be introduced.

1.2 General Background

1.2.1 Microbial Life in the Subsurface

The pore space of subsurface sediments provides a habitat for microbial life and it has been shown that the subsurface biosphere plays a significant role in global biogeochemical cycles (Jørgensen, 2012). Since their origin, microorganisms have shaped our planet by transforming inorganic and organic compounds for their nutritional and energetic needs, whereby they have significantly influenced biogeochemical and mineralogical processes through time (Konhauser, 2009). Numerous biogeochemical studies have been carried out so far in the marine realm (e.g. D'Hondt et al., 2004; Kallmeyer et al., 2012; Parkes et al., 2000; Parkes et al., 2005; Schippers et al., 2005; Webster et al., 2009) to get a broad understanding about population size and metabolic processes of deep biosphere microorganisms. Fewer studies exist on continental archives but in recent years progress has been made in the field of microbiology of terrestrial and lacustrine sediments (Deutzmann and Schink, 2011; Glombitza et al., 2013; Nelson et al., 2007; Sivan et al., 2011; Vuillemin et al., 2014). Still, our knowledge of the complex biogeochemical processes in the subsurface biosphere is intermittent.

The driving force of biogeochemical processes in sediments is the microbial degradation of organic matter (OM). The organic material is either incorporated into the system by allochthonous processes or autochthonously produced by primary production in the euphotic zone, which is controlled by insolation, water temperature and nutrient availability (Alin and Johnson, 2007). Most of the produced OM is remineralized in the water column by heterotrophic respiration so the amount of OM that finally reaches the sediment surface is a function of primary production and of water depth through which the detritus sinks while being gradually decomposed. Sedimentary OM consists of macromolecular complexes (structural carbohydrates, proteins, nucleic acids and lipids), which are too large to be taken up directly by prokaryotic organisms (Weiss et al.,

1991). Thus, the first step of the degradation of OM is the extracellular hydrolysis of macromolecular compounds via exoenzymes (Smith et al., 1992, Fig. 1.1), which are either excreted by the bacteria or tied in the outer cell wall. Microorganisms can use the produced depolymerized molecules for energy generation.

In the sediment carbon becomes oxidized by a gradual succession of redox reactions with different inorganic electron acceptors (Froelich et al., 1979). This sequence is related to a decrease in free energy G, which is the energy released per mole of reactant during a reaction. The change in free energy is expressed as ΔG [kJ mol^{-1}] and can be either positive (endergonic, energy is needed to drive the reaction) or negative (exergonic, reaction proceeds spontaneously or biologically catalyzed and yields energy). Electron acceptors that yield the highest energy output during respiration are favored. Based on this fact, Froelich et al. (1979) created a depth zonation model of oxidants used in the mineralization of OM, which corresponds to a gradual decrease in redox potential of the oxidant (Fig. 1.1). While a depth zonation of respiration processes is indeed commonly observed in marine and lacustrine sedimentary environments it has also been shown that several respiration processes can co-exist in the same depth interval (Wang et al., 2008).

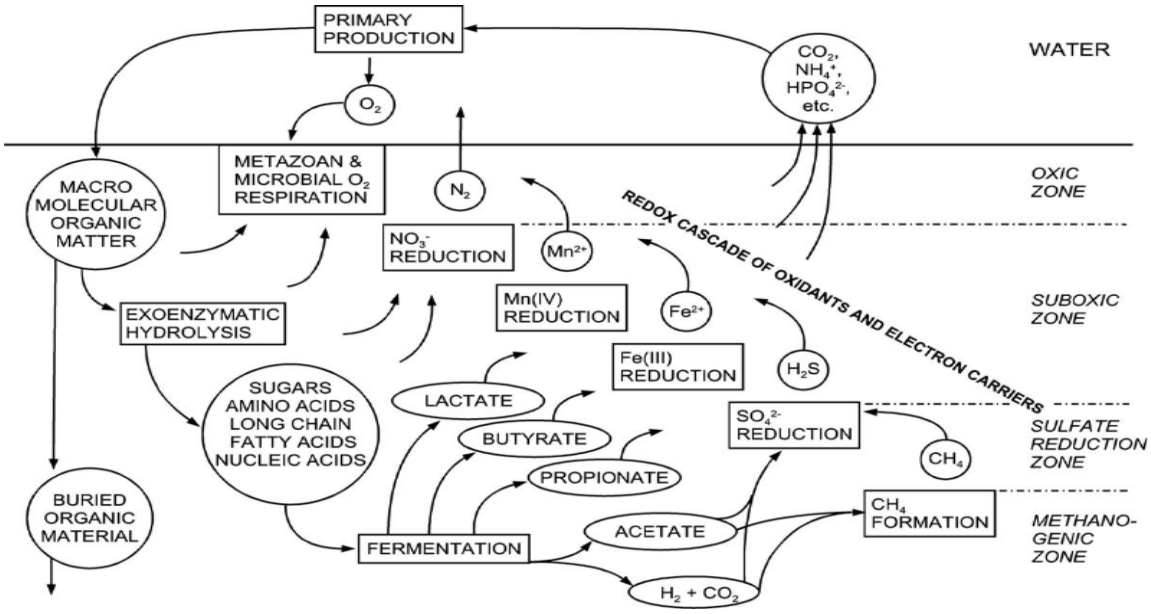

Figure 1.1: *Pathways of microbial organic matter degradation in the sediment and the resulting geochemical zonation of oxidants driven by the thermodynamic energy yield of oxidants (Jørgensen, 2006).*

Thermodynamically, oxygen yields the most energy and thus, aerobic respiration takes place in the uppermost sediment. Here, the freshly deposited OM at the sediment-

water interface forms a layer of high microbial activity and rapid organic matter degradation until oxygen is completely consumed. Below this zone, anaerobic respiration takes place with nitrate being the first oxidant being used followed by Mn (IV) reduction and Fe(III) reduction. Fe(III) reduction can account for up to 17% of the total carbon degradation and even up to 70% in non-sulfidic sediments (Thamdrup et al., 2000) and is thus one of the most important processes that occur in aquatic sediments (Lovley, 1991). The next step in microbial OM degradation is sulfate reduction. In marine sediments it is the most important process due to the fact that sulfate is abundant in high concentrations (mM range). Finally, methanogenesis is the terminal process in organic matter degradation (Fig. 1.1). This process is catalyzed by methanogenic archaea that can use hydrogen and carbon dioxide, acetate, formate, methanol, methylamine and carbon monoxide (Daniels et al., 1984). The produced methane in the methanogenic zone can diffuse upwards. When it reaches the sulfate reduction zone, methane can be oxidized anaerobically by a syntrophic consortium of methanogenic archaea and sulfate reducing bacteria, a process, which is called the anaerobic oxidation of methane (AOM) (Boetius et al., 2000). In this process sulfate as well as methane is consumed almost completely so that AOM is the most important methane sink in the sediment (Knittel and Boetius, 2009). In lacustrine environments, where sulfate is usually scarce, AOM has also been shown to proceed via the reduction of nitrate (Deutzmann and Schink, 2011) and ferric iron (Sivan et al., 2011).

Microorganisms able to perform aerobic respiration or nitrate reduction can use depolymerized organic macromolecules like sugars and amino acids (Fig. 1.1) as substrates. However, as the energy yield for microorganisms gradually decreases with depth, metal and sulfate reducers as well as methanogens are not able to respire these molecules (Jørgensen, 2006). These organisms are dependent on the activity of fermenting organisms. Fermenting bacteria can take up monomeric compounds like sugars and amino acids and convert them into simpler compounds including primarily volatile fatty acids (VFAs) such as lactate, butyrate, propionate, acetate, and formate, as well as some alcohols, H_2 and CO_2 (Fig. 1.1) (Fenchel et al., 1998). A second fermentation step may further reduce this spectrum of compounds to acetate, H_2 and CO_2 (Fig. 1.1). These compounds are the main substrates for metal and sulfate reducers, while methanogens can only use a very narrow spectrum of substrates, primarily H_2 plus CO_2 and acetate.

Microbial OM mineralization thus produces and consumes compounds that are dissolved in the pore water but also dissolution and production of solid phases are intrinsically linked to microbial OM mineralization. Thus, in order to obtain a full picture of the ongoing biogeochemical processes in the sediment a broad spectrum of analytical approaches is needed, which includes chemical analyses of the sediment pore water, analysis of sedimentary solid phases, quantification and characterization of the microbial community as well as quantification of turnover processes by using stable isotopes, radiotracers or numerical modeling based on concentration profiles of compounds dissolved in the pore water.

1.2.2 Geological setting and site description

With a surface area of 560 km^2 (Vaillant et al., 2011) Lake Towuti (2.75°S, 121.5°E) is the largest lake of the Malili Lake system, a chain of five tectonic lakes (Towuti, Matano, Mahalona, Lontoa and Masapi) situated on the eastern part of Sulawesi Island in central Indonesia. Sulawesi Island was formed by the convergence of three major lithospheric plates: The northward moving Indian-Australian Plate in the South, the southward moving Eurasian Plate in the North and the Pacific and Philippine Sea Plate in the East which are moving westward (Tierney and Russell, 2009). Eastern Sulawesi, was once part of a single block that separated from Australia in the Jurassic and collided with the Eurasian margin to form the Sulawesi orogen in the Oligocene/Early Miocene (Milsom et al., 2000). This collision was followed by a number of regional tectonic events including the formation of the Central Sulawesi thrust belt, the development of the sinistral Palu-Koro strike slip fault and the obduction of the East Sulawesi Ophiolite (Fig. 1.2) (Katili, 1971). This geological setting led to

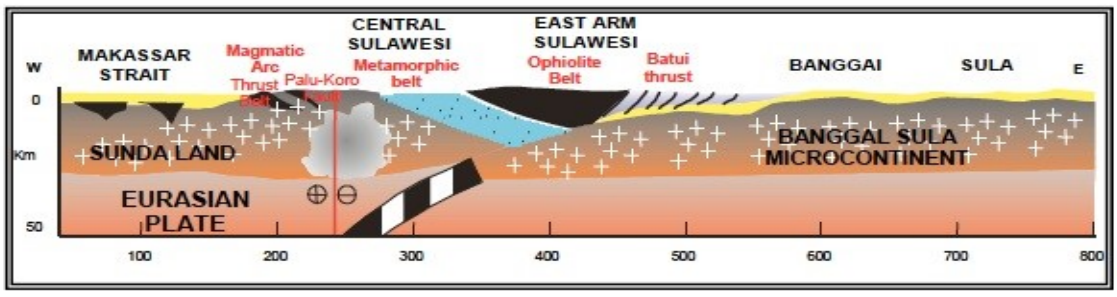

Figure 1.2: *Cross-section of the Neogene orogeny in Sulawesi after Simandjuntak and Barber (1996).*

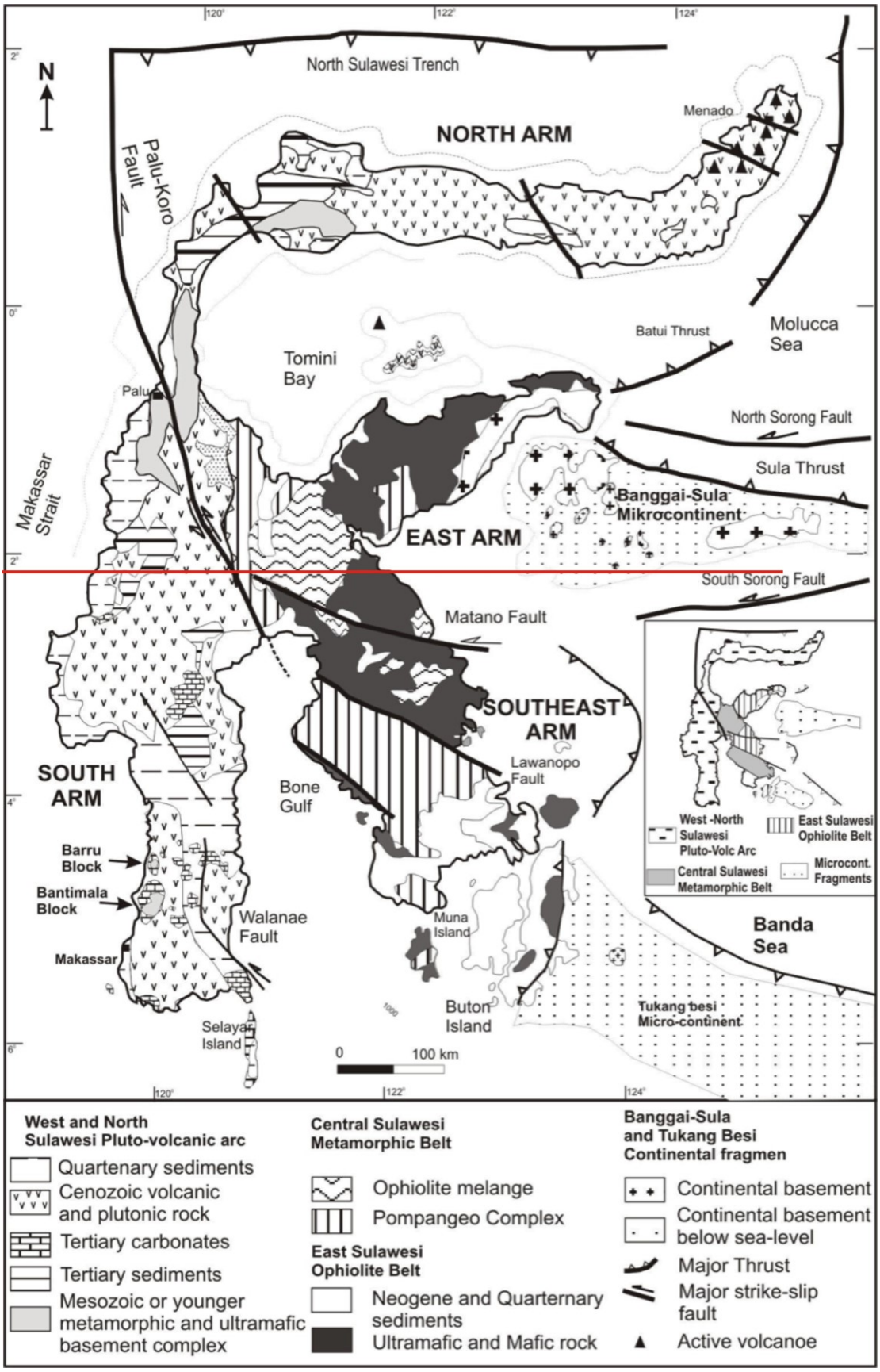

Figure 1.3: *Geological setting and lithotectonic division of Sulawesi Island (Katili, 1971). Red line indicates the location of the cross-section shown in Fig. 1.2.*

the formation of a complex zone of extensional faulting extending across central Sulawesi. Besides the Palu-Koro Fault in the West of Sulawesi this is represented by the Matano Fault and the Lawanopo Fault in Eastern Sulawesi narrowing the Malili Lake system in the North and South, respectively (Fig. 1.3). Within this tectonic regime the Malili Lakes were formed. The East Sulawesi Ophiolite forms the catchment of these lakes and consists of highly faulted mantle peridotites, cumulate gabbros, sheeted dolerites and Mid – Ocean Ridge Basalts (Kadarusman et al., 2004). While the Malili Lake system is thought to have been formed 1 - 2 million years ago, Lake Towuti's age is estimated to be approximately 600.000 years (Vaillant et al., 2011).

The region lies in the humid tropics and lacks marked seasonality or annual variability (Hope, 2001). Annual average air temperature is 25.7°C, with less than 1°C variation in monthly temperature (Costa et al., 2015). Lake Towuti has a maximum water depth of 203 m (Haffner et al., 2001) and with a surface water temperature of 29°C and a temperature gradient of less than 3.5°C Lake Towuti's water column is weakly thermally stratified (Costa et al., 2015). The rainy season lasts from November to May and is marked by a precipitation of more than 250 mm/month, while precipitation in the dry season from July to October drops below 200 mm per month. Annual precipitation is 2700 mm per year (Russell et al., 2014) and the combination of heavy rainfall and ultramafic bedrock results in intense weathering of the catchment that generates several meter thick lateritic soil horizons, which can contain more than 60% iron oxides (Hope, 2001).

1.2.3 Lake Towuti as a modern analogue for Earth's early oceans

The ultramafic catchment feeds the lake with large amounts of iron, nickel, manganese and many other metals, which is why Lake Towuti's sediments are very rich in iron with up to 20 wt% iron (hydr)oxides (Crowe et al., 2008b). In nearby Lake Matano the strong influx of iron(oxy)hydroxides to the lake and its sediments effectively scavenge most of the inorganic phosphorus from the oxic mixolimnion and thereby drive that lake, and by analogy likely Lake Towuti, towards phosphorus limited conditions (Crowe et al., 2008a). Sulfate concentrations are exceptionally low (< 20 µM) (Vuillemin et al., 2016). Due to the low seasonal variability, presently, an oxycline exists at a depth between 70 and 130 m with anoxic bottom water underneath and it has

been shown that modern climate does not fully mix the entire water column (Costa et al., 2015). Such physical and chemical characteristics of Lake Towuti lead to depositional conditions partly analogous to those of the stratified, ferruginous oceans that persisted throughout the Precambrian Eons (Bauer et al., 2017; Crowe et al., 2011; Crowe et al., 2008a). In sharp contrast to the modern, the Precambrian ocean-atmosphere system was weakly oxygenated, seawater was sulfate poor, and the oceans were characterized by ferruginous deep waters (Crowe et al., 2014; Poulton and Canfield, 2011). OM mineralization and diagenesis in the ferruginous sediments that deposited from these water bodies likely played a key role in global biogeochemical cycling throughout much of the Precambrian eons. Knowledge of OM mineralization in ferruginous sediments, however, remains almost entirely conceptual, as analogous modern sediments are extremely rare and remain largely unstudied, to date.

Also, sedimentary iron formations, composed of diverse iron oxides, silicates and carbonates, deposited under ferruginous conditions in the Precambrian and may provide an important record of environmental conditions at the time of deposition. For example, ancient iron carbonates, such as siderite, have been used to link their mineralogy to infer atmospheric and oceanic conditions on Early Earth (Holland, 2006). However, the interpretation of sedimentary iron formations and their depositional conditions depends on our knowledge of their mineral origins and formation pathways (Ohmoto et al., 2004), which is limited in part, again, due to the scarcity of ferruginous environments on Earth today (Konhauser et al., 2005; Posth et al., 2014). In nearby Lake Matano carbonate green rust forms below the chemocline via the reduction of ferrihydrite or via its reduction with dissolved ferrous iron and bicarbonate (Zegeye et al., 2012) but the fate of this green rust has not been investigated. Carbonate green rust has been shown to be a precursor to other mineral phases in banded iron formations (Halevy et al., 2017), the transformation of green rust to these phases, however, has not been observed in nature.

Thus, the ferruginous sediments of Lake Towuti offer the rare opportunity to study the microbial community and the related biogeochemical and diagenetic processes of a modern ferruginous sedimentary environment with possible implications for the sedimentary environments that deposited from Earth's early oceans. They may also hold promise to investigate mineral formation pathways that improve our understanding of the deposition of sedimentary iron formations in Precambrian times.

1.2.4 The Towuti Drilling Project

The following brief overview of the Towuti Drilling project has been published by Russell et al. (2016) in Scientific Drilling and can be found in the Appendix of this PhD thesis.

Lake Towuti is located within the center of the Indo-Pacific Warm Pool (IPWP), a vast pool of warm surface waters in the western tropical Pacific. By interacting with the El Niño-Southern Oscillation (ENSO), the Austral Asian monsoons, and the Intertropical Convergence Zone (ITCZ), the IPWP exerts a vast influence on global climate (Chiang, 2009; Pierrehumbert, 1999). In addition, Lake Towuti has high rates of floral and faunal endemism and is surrounded by one of the most diverse topical forests on Earth. Together with the already described unique biogeochemical setting of Lake Towuti and its sediments these features led to the proposal of different research questions from various research fields that motivated scientific drilling at Lake Towuti.

The Towuti Drilling Project (TDP) is an international research program that aims to understand long-term environmental and climatic changes in the tropical Western Pacific, the impact of geological and environmental changes on the biological evolution of aquatic taxa and finally the geomicrobiology and biogeochemistry of the ferruginous sediments of Lake Towuti. To address these questions an ICDP scientific drilling campaign was carried out on this lake in spring 2015. Here, a total of 1018 m of sediment core was retrieved from three primary drilling sites with water depths ranging from 156 to 200 m. The drilling sites were chosen based on three surveys between 2007 and 2013 that obtained a comprehensive seismic dataset that revealed two major sedimentary units in Lake Towuti (Russell and Bijaksana, 2012). Unit I covers the upper 100 m of sediment, is well stratified and consists of alternating red and green clays. It is underlain by Unit II that consists of a variety of lithologies including silts, massive sands, gravels and peat. This unit is thought to represent a diverse setting of lacustrine, fluvial and terrestrial sedimentation during the early stages of formation of Lake Towuti (Russell et al., 2016). Site 1 was the primary drilling target for the TDP, located in the central part of Towuti's northern basin in 153 m water depth. It consists of well-stratified sediments that are undisturbed by turbidites or other event deposits. Thus it is well suited to address most of TDP's key questions in paleoclimate, paleolimnology and paleoecology.

Towuti's pelagic microbial ecology, biogeochemistry and sediment mineralogy are tightly linked to climate variations through varying lake mixing regimes, soil erosion and weathering (Costa et al., 2015; Tamuntuan et al., 2015). These processes are directly or indirectly responsible for the production and deposition of many paleoclimate proxies and postdepositional alteration of those proxies is often linked to the activity of sedimentary microorganisms. Thus, Site 1 was chosen as the drilling target for geomicrobiological investigations. Scientific drilling retrieved a 114 m long sediment core dedicated for geomicrobiological investigations. However, there is a moratorium on publications about the whole sediment sequence as long as the complete age model is not established. As this is still the case, the detailed geochemical and microbiological studies made in this PhD thesis will mainly focus on the upper 12 m of the drill core that have already been subject of comprehensive paleoclimatic investigations (Costa et al., 2015; Konecky et al., 2016; Russell et al., 2014).

Environments such as Lake Towuti's sediment are rare and hence, are poorly understood. Thus, in order to get a first understanding of the biogeochemistry and microbiology of Lake Towuti's sediment two international pilot studies were carried out in autumn 2013 and 2014. Here, surficial sediments (< 35 cm) were retrieved from three different drilling sites corresponding to different bottom water redox conditions. The samples were used to investigate the relationship between the biogeochemistry and microbial processes in these iron rich, anoxic sediments as a function of varying bottom water redox conditions. The data provide a background for the geochemical and geomicrobiological analyses of the long drill core that was retrieved during the ICDP drilling campaign. Also, the pilot studies helped to improve sampling and analysis in order to identify and circumvent potential problems that might occur during the ICDP drilling campaign.

1.2.5 Assessing contamination during drilling

Exploration of subsurface environments relies on drilling. Based on the type of sediment or rock to be penetrated as well as the maximum depth that has to be reached, many different drilling techniques are being used. Irrespective of the drilling technique, almost always a drilling fluid is used for cooling the drill bit and transporting cuttings out of the borehole (Kallmeyer et al., 2006). This process inevitably causes infiltration of drilling fluid into the core. While drill fluid contamination is problematic for many analyses, it poses particular challenges for geomicrobiological studies. It is impossible to maintain sterile conditions during drilling operations as huge amounts of equipment (several tons) as well as massive amounts of drilling fluid (thousands of liters) come to use. Drilling fluid infiltration will thus introduce microorganisms from the surface and other contaminants into the sediment core. Using lake water or seawater as a drill fluid would translate into a microbial cell abundance of approximately 10^6 cells mL^{-1} drilling fluid. Thus, for deep subsurface environments with only a few hundred or thousand cells cm^{-3} even the slightest infiltration in the range of nanoliters of drilling fluid into one cm^{-3} sediment would render the sample unsuitable for geomicrobiological analyses (Yanagawa et al., 2013). Because contamination cannot be avoided completely, it is essential to trace contamination of the sediment core in order to identify uncontaminated samples for geomicrobiological investigations. To do this, a tracer is added to the drilling fluid prior to drilling. Detection of this tracer in a sediment sample identifies a contaminated sample that cannot be used for microbiological and/or chemical analyses. Several tracers have been used in past drilling operations to assess microbial contamination including microbiological (Pedersen et al., 1997; Yanagawa et al., 2013), chemical (Lever et al., 2006) and particulate tracers (Colwell et al., 1992; Kallmeyer et al., 2006). Before choosing a tracer for assessing contamination various questions have to be considered (Kallmeyer, 2017).

(1) Does a particular tracer work under the given circumstances?

Certain environmental conditions can render a tracer unsuitable for an accurate contamination assessment. Some tracers might be affected by the chemistry of the drilling fluid or the environment that has to be drilled. For example it has been shown that fluorescent dyes are sensitive to light, pH and high iron concentrations (Krause et al., 2005; Smart and Laidlaw, 1977). These parameters will thus decrease the fluorescence signal. Also, the thermal regime of a drilling site can be important.

Fluorescent dyes as well as particulate tracers will undergo complete thermal degradation at temperatures above 100 °C. These tracers are thus unsuitable for high temperature drilling operations. Here, other tracers like Perfluorocarbon tracers (PFTs) or naphtalene sulfonic acids would be the better option.

(2) Is it technically/logistically/legally possible to use a particular tracer?

The location of a drill site is an important factor that has to be considered when choosing the right tracer. Drilling in a remote location might render certain contamination control approaches logistically unsuitable. In this context it is also important to consider, if tracer detection has to be done on- or off-site. Some tracers like PFTs have to be detected immediately after core retrieval and thus require the corresponding equipment on-site. Drilling operations in remote locations and on small lake drilling platforms will thus become problematic for PFTs as tracer detection requires significant working space for a gas chromatograph. Also, the location of a drilling site might be problematic for drill mud disposal. Some tracers like naphtalene sulfonic acids have legal constraints in that they are toxic to aquatic life and can be harmful for humans. Thus, their use is problematic in many drilling locations. But even if the tracer is non-toxic and environmentally harmless it might be problematic to use and dispose brightly coloured drilling fluid when drilling in an urban and/or agricultural setting. In this setting the use of fluorescent dyes might be problematic.

(3) What is the required minimum detection limit?

Different contamination approaches have different sensitivities. If the sensitivity of a certain approach is not sufficient, contamination will pass unnoticed. To choose an adequate tracer one has to consider the cell concentration in the drill fluid as well as the minimum cell concentrations in the sediment samples. This will eventually determine the tracer concentration that is needed in the drill fluid in order to achieve a suitable detection limit.

In light of the high total iron content of Lake Towuti's sediments that may interfere with several tracers (Krause et al., 2005; Smart and Laidlaw, 1977) as well as the remote location of Lake Towuti, none of the established contamination control approaches could meet the requirements for a contamination assessment during the ICDP drilling campaign at Lake Towuti. These included:

(1) Long term tracer stability allowing for a contamination assessment of archived core material
(2) Cost-effectivity
(3) Minimum of equipment that is necessary for tracer detection on- and off-site
(4) High sensitivity despite high iron concentrations

Thus, a major motivation of this thesis was to develop a contamination control approach that meets all these criteria. This approach should be applied at the ICDP drilling in Lake Towuti.

1.3 Objectives

The main objectives of this PhD thesis are:

1. Development of a simple and inexpensive technique for assessing contamination not only for the ICDP drilling campaign at Lake Towuti, but also as an alternative approach for future drilling operations (Chapter 2).
2. Getting a first understanding of the biogeochemistry of surficial sediments of this modern ferruginous environment as well as the metabolic potential of the microbial community inhabiting this poorly understood environment (Chapter 3 and 4).
3. Investigation of microbial organic matter mineralization in modern ferruginous environments similar to those that deposited in Earth's early oceans (Chapter 5).
4. Identification of iron minerals in the sediments of Lake Towuti and investigation of their formation pathways (Chapter 6).

To achieve these aims, intense scientific collaboration was carried out with other institutions including the University of British Columbia, Vancouver, the University of Geneva, the MARUM Bremen, Brown University as well as the Research Center for Limnology Indonesia.

1.4 Outline of the thesis

This cumulative thesis consists of seven chapters. Out of these, five chapters (Chapters 2 – 6) are in the form of manuscripts for international peer-reviewed journals. Chapters 2, 3, 4 and 6 are already published, whereas Chapter 5 was submitted and accepted for review.

Chapter 1: Introduction

This chapter introduces the scope and the aims of the thesis. It further provides a general overview of microbial organic matter mineralization in subsurface sedimentary environments, the geologic setting of Lake Towuti, the Towuti Drilling Project as well as the necessity to assess contamination during drilling operations for microbiological and chemical analyses.

Chapter 2: A simple and inexpensive technique for assessing contamination during drilling operations

A. Friese, J. Kallmeyer, J.A. Kitte, I. M. Martinez, S. Bijaksana, D. Wagner, the ICDP Lake Chalco Drilling Science Team and the ICDP Lake Towuti Drilling Science Team

Limnology and Oceanography: Methods (2017), Vol. 15 (2): 200 – 211

In Chapter 2, a new method for assessing contamination during drilling operations was developed. Here, a particular tracer comes to use, whose price is nearly four orders of magnitude cheaper compared to conventionally used particulate tracers. The approach allows for a long-term contamination assessment even several months after core retrieval, requires only a minimum of equipment and allows for a contamination assessment directly on site, even in remote locations and on small drill platforms.

I developed the protocol, produced all data, designed the figures and wrote the manuscript. My PhD supervisor Jens Kallmeyer designed the study and supervised laboratory experiments as well as the writing of the manuscript. Jan Axel Kitte supervised flow cytometry analyses and helped to develop the protocol for tracer detection via flow cytometry. Ivan Montano Martinez sampled in the field of the Lake Chalco Drilling. Satria Bijaksana supervised the Lake Towuti Drilling and Dirk Wagner provided important financial and technical support and supervised the writing of the manuscript.

Chapter 3: Geomicrobiological features of ferruginous sediments from Lake Towuti, Indonesia

A. Vuillemin, A. Friese, M. Alawi, C. Henny, S. Nomosatryo, D. Wagner, S.A. Crowe and J. Kallmeyer

Frontiers in Microbiology (2016), Vol. 7, Article 1007

Chapter 3 characterizes the biogeochemistry of surficial (< 35 cm) ferruginous sediments with varying redox conditions at the sediment water interface. It shows that cell densities are controlled by redox changes in the lake and that Lake Towuti's sediments have a limited availability of electron acceptors like oxygen, nitrate and sulfate. Still, the sediments support microorganisms with a variety of metabolic capabilities related to sulfur, iron and methane cycling. Also, it is investigated if ferruginous sediments have the potential to adsorb extracellular DNA, which would lead to its preservation and persistence in the sedimentary record. The results show that extracellular DNA is substantially degraded by microorganisms within the sediment leading to the gradual loss of genetic information with depth. Thus, Lake Towuti's sediment is not a valuable archive of genetic information. The samples were obtained during the pilot study in autumn 2013 and the results provide a background for more detailed biogeochemical and geomicrobiological studies on the 114 m long drill core retrieved during the ICDP drilling campaign.

Aurèle Vuillemin and me contributed equally to this work and thus have a shared first-authorship. I sampled during the field campaign, performed all geochemical analyses, cell counts and contributed to writing the manuscript. Aurèle Vuillemin performed DNA extractions, DGGE procedure, genetic and image analyses, designed the figures and led the writing of the manuscript. Mashal Alawi designed and supervised DNA extractions and genetic analyses. Sean A. Crowe sampled during the field campaign and conducted the CTD cast measurements. Cynthia Henny and Sulung Nomosatryo fulfilled the research permit procedure and sampled during field campaign. Dirk Wagner provided important technical and financial support, supervised genetic analyses and writing of the manuscript. My PhD supervisor Jens Kallmeyer designed the study, sampled in the field, supervised all geochemical analyses and cell counts as well as writing of the manuscript.

Chapter 4: Metabolic potential of microbial communities from ferruginous sediments

A. Vuillemin, F. Horn, A. Friese, M. Winkel, M. Alawi, D. Wagner, C. Henny, W. D. Orsi, S. A. Crowe, and J. Kallmeyer

Environmental Microbiology (2018), Vol 20 (12): 4297-4313

In Chapter 4, biogeochemical studies of Chapter 3 were expanded with microbiological analyses. For this, surficial sediment cores were retrieved in a second pilot campaign in 2014 to perform metagenomic analyses in order to assess whether metabolic potential correlated with geochemical processes. The results show that microbial communities in the upper few cm show a metabolic versatility for iron and sulfur reduction as well as fermentation. Also, methanogenic and methanotrophic microorganisms could be detected throughout the core. The microbial communities in these ferruginous sediments exhibit a vertical succession of sulfate reducers, iron reducers, methanogens and methanotrophs that have the potential to markedly influence the iron and sulfur geochemistry in the sediment.

As a co-author I sampled in the field, performed pore water chemistry analyses, sulfate reduction rate experiments and extracted the different fractions of the total reduced inorganic sulfur pool. Aurèle Vuillemin performed laboratory analyses, including DNA extractions, qPCR, Illumina MiSeq sequencing, phylogenetic and statistical analyses, designed all figures and led the writing of the manuscript. Fabian Horn treated the raw sequencing data, supervised genetic and statistical analyses and contributed to writing the manuscript. Matthias Winkel assisted in metagenomic analyses and phylogenetic tree construction and contributed to writing the manuscript. Mashal Alawi designed and supervised DNA extractions and genetic analyses. Dirk Wagner provided important technical and financial support, supervised genetic analyses and writing of the manuscript. Cynthia Henny fulfilled the research permit procedure. William D. Orsi supervised genetic and statistical analyses and contributed to writing the manuscript. Sean A. Crowe assisted in the permit procedure, sampled during the field campaign and contributed to writing the manuscript. Jens Kallmeyer designed the study, sampled in the field, supervised all geochemical analyses and cell counts as well as writing of the manuscript.

Chapter 5: Iron oxide reactivity controls organic matter mineralization in ferruginous sediments

A. Friese, K. Bauer, J. Kallmeyer, S. A. Crowe, C. Glombitza, L. O. Rendon, V. B. Heuer, R. Simister, A. Vuillemin, S. Nomosatryo, C. Henny, D. Ariztegui, S. Bijaksana, H. Vogel, M. Melles, J. M. Russell, D. Wagner and the ' Drilling Project Science Team

under review in *Nature Communications (2020)*

In Chapter 5 a suite of biogeochemical analyses is used to assess the rates and pathways of microbial organic matter mineralization in the upper 12 meters of Lake Towuti's ferruginous sediments spanning the last 60.000 years. The results show that Lake Towuti's sediment has extremely high total iron concentrations, with more than 2.500 μmol cm^{-3} (20 % dry wt.). According to thermodynamic arguments, the high abundance of iron in the sediment should preclude methanogenesis. However, organic matter mineralization in Towuti's sediment is predominantly (> 85% of total organic carbon mineralization) channeled via methanogenesis, despite the abundance of ferric iron minerals known to support microbial respiration in laboratory experiments. The absence of oxygen and nitrate, the scarcity of sulfate and the poor reactivity of iron(oxy)hydroxides likely suppress anaerobic methane oxidation and leads to a methane efflux from the sediment into the water column. By analogy to Lake Towuti, sedimentary methanogenesis fueled by organic matter may have led to significant effluxes of methane to Precambrian oceans. In scarcity of oxygen and sulfate in Earth's early oceans much of this methane likely escaped to the atmosphere where it contributed to warming under a faint young sun.

I sampled in the field during the drilling campaign, analyzed the pore water chemistry as well as the isotopic composition of methane and carbon dioxide. Also, I performed geochemical modeling, incubation experiments and sulfate reduction rate experiments. Finally, I designed the figures and led the writing of the manuscript. Kohen Bauer and me contributed equally to this study and thus share the firs-authorship. Kohen Bauer sampled in the field, performed iron speciation experiments, calculated iron reduction rates and contributed to writing the manuscript. Jens Kallmeyer designed the study, sampled in the field and supervised geochemical experiments and manuscript writing. Sean A. Crowe sampled in the field, supervised iron speciation experiments and contributed to writing the manuscript. Clemens

Glombitza analyzed volatile fatty acids using 2D ion chromatography – mass pectrometry. Luis O. Rendon sampled in the field and analyzed total organic carbon. Verena B. Heuer provided important technical support and supervised methane analysis. Rachel Simister, Aurèle Vuillemin and Sulung Nomosatryo sampled in the field. Cynthia Henny fulfilled the research permit. As principal investigators of the Towuti Drilling Project, Daniel Ariztegui, James M. Russell, Satrija Bijaksana, Hendrik Vogel and Martin Melles sampled on the field, processed drill core splitting and imaging at LacCore, and supervised the writing of the present manuscript. Dirk Wagner provided important financial and technical support, supervised incubation experiments and the writing of the manuscript.

Chapter 6: Formation of diagenetic siderite in modern ferruginous sediments

A. Vuillemin, R. Wirth, H. Kemnitz, A. M. Schleicher, A. Friese, K. W. Bauer, R. Simister, S. Nomosatryo, L. Ordoñez, D. Ariztegui, C. Henny, S. A. Crowe, L. G. Benning, J. Kallmeyer, J. M. Russell, S. Bijaksana, H. Vogel and the Towuti Drilling Project Science Team

Geology (2019), Vol 47 (6): 540 – 544

In Chapter 6, detailed mineralogical studies were performed on the whole sequence of the 114 m drill core. Here, siderites were identified and characterized using high-resolution microscopic and spectroscopic imaging combined with microchemical and geochemical analyses. The data show early diagenetic growth of siderite crystals as a response to sedimentary organic matter mineralization. Microchemical zoning is identified in all siderite crystals. Siderite thus likely forms during diagenesis through growth on primary existing phases and the mineralogical and chemical features of these siderites, together with their irregular distribution down core, are a function of changes in redox conditions of the pore water and sediment over time. Identification of microchemical zoning in ancient siderites deposited in Archean and Proterozoic eons may thus also be used to infer siderite growth histories in ancient sedimentary rocks including sedimentary iron formations.

I sampled in the field and performed all pore water analyses. Aurèle Vuillemin designed the study, led the writing of the manuscript, designed the figures, sampled in the field and at LacCore and took part in TEM, SEM and XRD analyses. Richard Wirth,

Helga Kemnitz and Anja M. Schleicher performed TEM, SEM and XRD analyses, respectively. Kohen Bauer, Rachel Simister, Sulung Nomosatryo and Luis Ordoñez assisted during field sampling. Cynthia Henny fulfilled research permit procedure in Indonesia. Sean A. Crowe is principal investigator of the Towuti Drilling Project, sampled in the field and modeled pore water geochemistry. Jens Kallmeyer designed the study, sampled in the field and at LacCore and supervised geochemical analyses as well as manuscript writing. Daniel Ariztegui, James M. Russell, Satria Bijaksana and Hendrik Vogel are principal investigators of the Towuti Drilling Project, sampled in the field and supervised manuscript writing.

Chapter 7: Conclusions and outlook

This chapter summarizes all findings and conclusions and provides an outlook for future work.

Chapter 8: Appendix

Additional manuscript I

The Towuti Drilling Project: Paleoenvironments, Biological Evolution, and Geomicrobiology of a Tropical Pacific Lake

J. M. Russell, S. Bijaksana, H. Vogel, M. Melles, J. Kallmeyer, D. Ariztegui, S. A. Crowe, S. Fajar, A. Hafidz, D. Haffner, A. Hasberg, S. Ivory, C. Kelly, J. King, K. Kirana, M. Morlock, A. Noren, R. O'Grady, L. Ordonez, J. Stevenson, T. v. Rintelen, A. Vuillemin, I. Watkinson, N. Wattrus, S. Wicaksono, T. Wonik, K. Bauer, A. Deino, A. Friese, C. Henny, Imran, R. Marwoto, L. O. Ngkoimani, S. Nomosatryo, L. O. Safiuddin, R. Simister, G. Tamuntuan

Scientific Drilling (2016), Vol 21, 29-40

The first additional manuscript presents the purpose and the objectives of the Towuti Drilling Project as a whole. It also introduces the different research questions of the respective working groups involved and the geochronological, sedimentological,

geochemical, geophysical and biological methods that will be applied answering these. Finally, initial coring and core description results are presented.

All scientists involved in the Towuti Drilling Project were included in the author list. I did not contribute to writing the manuscript and also did not provide any data that are presented. As the manuscript presents the big picture of the Towuti Drilling Project and what makes Lake Towuti such an exciting research site, it is included in the Appendix of the PhD thesis.

Additional manuscript II

Empowering conventional Rock-Eval pyrolysis for organic matter characterization of the siderite-rich sediments of Lake Towuti (Indonesia) using End-Member Analysis

L. Ordoñez, H. Vogel, D. Sebag, D. Ariztegui, T. Adatte, J. M. Russell, J. Kallmeyer, A. Vuillemin, A. Friese, S. A. Crowe, K. W. Bauer, R. Simister, C. Henny, S. Nomosatryo, S. Bijaksana and the Towuti Drilling Project Scientific Team

Rock-Eval Analysis allows for assessment of proxies used to reconstruct past environments, paleoproductivity and sediment provenance, like total organic carbon, mineral carbon as well as hydrogen and oxygen indices of organic matter. So far a major limitation of this approach were carbonate minerals with low cracking temperatures that induce significant matrix effects, biasing the mentioned parameters. The second additional manuscript presents an approach that enables correction of Rock-Eval Analysis for these matrix effects using End-Member Analysis. This approach is then used to characterize the type and source of organic matter in the sediments of Lake Towuti.

I sampled in the field and contributed to writing the manuscript by discussing the dataset and providing comments to the different manuscript versions. As this manuscript does not fit into the scope of this thesis it is included in the Appendix of this thesis.

2 A simple and inexpensive technique for assessing contamination during drilling operations

Subsurface exploration relies on drilling. Normally drilling requires a drilling fluid that will infiltrate into the drill core. Drilling fluid contains non-indigenous materials and microbes from the surface, so its presence renders a sample unsuitable for microbiological and many other analyses. Because infiltration cannot be avoided, it is of paramount importance to assess the degree of contamination to identify uncontaminated samples for geomicrobiological investigations. To do this, usually a tracer is mixed into the drilling fluid. In past drilling operations a variety of tracers have been used; each has specific strengths and weaknesses. For microspheres the main problem was the high price, which limited their use to spot checks or drilling operations that require only small amounts of drilling fluid.

Here, we present a modified microsphere tracer approach that uses an aqueous fluorescent pigment dispersion with a similar concentration of fluorescent particles as previously used microsphere tracers. However, it costs four orders of magnitude less, allowing for a more liberal use even in large operations. Its applicability for deep drilling campaigns was successfully tested during two drilling campaigns of the International Continental Drilling Program (ICDP) at Lake Towuti, Sulawesi, Indonesia, and Lake Chalco, Mexico. Quantification of the tracer requires only a fluorescence microscope or a flow cytometer. The latter allowing for high-resolution data to be obtained directly on-site within minutes and with minimal effort, decreasing sample processing times substantially relative to traditional tracer methods. This approach offers an inexpensive, rapid, but powerful alternative technique for contamination assessment during drilling campaigns.

2.1 Introduction

Exploration of deep subsurface environments relies on drilling, which requires the use of drilling fluid for cooling the bit and transporting cuttings out of the borehole

(Kallmeyer, 2011; Kallmeyer et al., 2006). This process inevitably causes infiltration of drilling fluid into the core, either by advection through the pore space of coarser and looser sediments or by being pushed through small fissures that can be created by drilling more fine-grained and more cohesive or brittle sediments (Lever et al., 2006). While drill fluid contamination is problematic for many analyses, it poses particular challenges for geomicrobiological studies. Microbial cell abundances in the subsurface are several orders of magnitude lower than those of surface environments (e.g. D'Hondt et al., 2015; Kallmeyer et al., 2012). Thus, even the slightest infiltration of drilling fluid into the sediment (nanoliters per cm^3 sediment) renders the sample unsuitable for microbiological and also certain geochemical investigations (Yanagawa et al., 2013). Therefore, it is essential to trace contamination of the sediment core in order to identify uncontaminated samples for geomicrobiological investigations. In order to attribute the detected tracer to the infiltration of drilling fluid into the sample it is necessary that tracers (1) have no natural source, (2) are easy to detect even at extremely low concentrations, (3) are chemically inert.

Several techniques have been used in past drilling operations to assess microbial contamination, including fluorescent dyes (Pellizzari et al., 2013; Phelps et al., 1989; Russell et al., 1992), Perfluorocarbon tracers (PFT) (Colwell et al., 1992; House et al., 2003; Lever et al., 2006; Russell et al., 1992; Senum and Dietz, 1991; Smith et al., 2000b) and microsphere tracers (Colwell et al., 1992; Kallmeyer et al., 2006; Smith et al., 2000b; Yanagawa et al., 2013). Fluorescent dyes like fluorescein or Rhodamine are inexpensive, easy to handle on-site and allow sensitive detection of contamination (Russell et al., 1992). However, they are sensitive to light degradation (Diehl and Horchak-Morris, 1987), pH and water chemistry (Krause et al., 2005; Smart and Laidlaw, 1977). Furthermore, significant sorption onto clays, which are a common component of drilling fluids, and the presence of humic substances, can decrease the fluorescence signal (Hafuka et al., 2015; Magal et al., 2008). These features limit the applicability of fluorescent dyes in deep drilling campaigns. Moreover, fluorescent dyes will stain the entire drilling fluid in a bright color, which might cause problems for disposal of the mud after drilling.

Perfluorocarbon tracers (PFT) are chemically inert hydrophobic compounds that can be detected with high sensitivity (picogram per gram) via gas chromatography (Smith et al., 2000a). Detection of PFTs thus requires a gas chromatograph on-site in

order to identify uncontaminated samples for immediate biogeochemical and geomicrobiological analyses that have to be carried out on fresh sample material. While this is a minor issue on large oceanographic vessels (PFT is currently the standard contamination control method on board the IODP drill ship JOIDES Resolution), it poses challenges for operations at remote locations or on smaller drilling platforms. Also, samples have to be taken immediately after core retrieval as the volatile tracer diffuses rapidly out of the core. Diffusive loss after core retrieval can severely affect the ability to detect contamination even though substantial amounts of drilling fluid might have infiltrated into a sediment sample.

Microsphere tracers are small (0,2 – 0,5 µm diameter) fluorescent particles and have been used in both terrestrial and ocean drilling campaigns (Colwell et al., 1992; Kallmeyer et al., 2006; Smith et al., 2000b; Yanagawa et al., 2013). They are either mixed directly into the drilling fluid, or filled into a small plastic bag that is taped on the lower end of the core barrel. The bag bursts open when the core barrel hits the sediment and the released microspheres are supposed to mix locally with the drill mud and surround the drill core while entering the core barrel. It has been shown, however, that the distribution of tracer derived from these bags is rather uneven (Biddle et al., 2014) so the results have to be interpreted with caution. For analysis the microspheres are either extracted from the sediment by density centrifugation (Kallmeyer et al., 2006) or the sample slurry is counted directly, similar to Acridine Orange Direct Counting for microbial cells (Cragg et al., 1990; Fry, 1988). Irrespective of preparation, the sample is transferred onto a filter membrane and counted by fluorescence microscopy, with which a detection limit of 10^3 particles g^{-1} of sediment can be achieved (Colwell et al., 1992). However, microsphere tracers are exceptionally expensive, costing tens of dollars per milliliter, which renders them unsuitable for drilling campaigns that use large amounts of drilling fluid and therefore would require liters to tens of liters of microsphere solution. Also, microsphere quantification by fluorescence microscopy is rather time consuming.

Here, we present an inexpensive contamination control approach based upon fluorescent pigments that are normally used for paints or plastics. Their physical properties are similar to those of microsphere tracers but their price is nearly four orders of magnitude lower. Quantification of contamination can be achieved by fluorescence microscopy or by flow cytometry, the latter allowing for more rapid analysis. This study

thus presents an inexpensive and simple contamination control approach that only requires a minimum of equipment and that offers a powerful technique to assess microbial contamination during terrestrial and marine drilling campaigns.

2.2 Materials and Methods

Tracer properties – As a tracer we used SPL-N fine grind fluorescent pigment dispersion (DayGlo, Cleveland, OH, USA) with a pigment content of ca. 45%. The pigments are available in several colors and normally used for coatings, plastics and water-based inks. According to the data sheet provided by the supplier, the dispersion contains no organic solvents and is free from heavy metals, its specific gravity is 1 – 1.1 g/ml and viscosity ranges between 50 and 300 cP at 25°C. In contrast to normal microspheres, which have a very narrow size range and usually come in very precisely controlled concentrations, the size of fluorescent pigment particles ranges between 0.25 and 0.45 µm and the concentration may also vary by several percent. Given the normal size range of deep subsurface microbes (Kallmeyer et al., 2012), the pigments cover the natural range quite well. The few percent variability in tracer concentration is within the usual level of accuracy of our detection techniques. In Europe these pigment suspensions are supplied through Radiant Color NV, Houthalen, Belgium, and labeled RADGLO AFN. The pigment concentration is about 1 x 10^{15} particles per liter in undiluted form, which is in the same range as common microsphere tracers.

Drilling - The applicability of the pigment tracer for large drilling campaigns was tested during two ICDP Deep Drilling campaigns at Lake Towuti and Lake Chalco.

Lake Towuti: In June/July 2015, a 114m long sediment core was retrieved for geomicrobiological investigations from Lake Towuti, located in Sulawesi, Indonesia (Russell et al., 2016). DOSECC Exploration Services carried out drilling operations using the ICDP Deep Lakes Drilling System (DLDS, 2010). The borehole was drilled with specialized lake drilling tools. Cores were collected in standard IODP-style butyrate liners (66mm core diameter) in 3m intervals using P size drill rods (122,6 mm borehole diameter) (Russell et al., 2016). Hydraulic piston coring (HPC) was applied for soft unconsolidated sediment, and the rotating Alien corer (ALN) was used for more resistant layers such as lithified tephras. Surface Lake Towuti water was used as drilling fluid without any additives. We used a blue tracer with a green fluorescence under blue

excitation (DayGlo SPL-19N; RADGLO AFN-29), The drilling fluid was stored in a 4000 L holding tank in which the pigment tracer was diluted 1:1000 to a final concentration of approximately 1 x 10^9 particles per ml drilling fluid, which colored the drilling fluid bright blue. The flow rate of the drilling fluid was highly variable, ranging from tens to hundreds of liters per minute depending on the lithology. Drilling fluid was not recirculated and flowed out of the borehole on the lake floor into the lake.

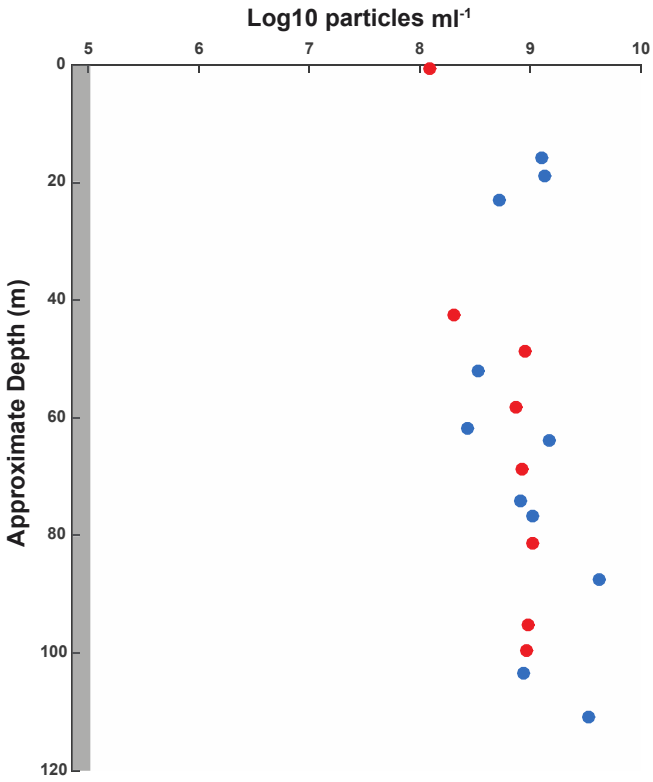

Figure 2.1: *Pigment particle concentrations per milliliter of liner fluid (blue circles) and drilling fluid samples (red circles) from the Lake Towuti drilling. Concentrations are within one order of magnitude. The limit of detection (LOD) is indicated in dark grey.*

Additionally, small plastic bags with undiluted tracer were attached to the bottom of the core to increase the tracer concentration right at the bottom of the drill hole. However, several of the bags did not burst and were pushed through the liner by the entering sediment. Only in two instances the fluid that was collected from the gap between the drill core and the liner, i.e. the so-called liner fluid showed significantly higher (>1 order of magnitude) particle concentrations than the drill mud (Fig. 2.1). We interpret this as a general failure of the tracer bags at the bottom of the core. Only in two instances did this technique lead to a significantly higher particle concentration around the core.

Lake Chalco: Drilling of the ICDP Mexidrill drilling project at Lake Chalco was carried out with a track mounted diamond wireline drill rig. The cores were collected in plastic liners in 1.5 m intervals using H size (~96.3 mm diameter hole, 61.1 mm diameter core) drilling tools. The core reached a maximum depth of 500 m but only the upper 100 m were investigated for geomicrobiological and biogeochemical purposes. In the upper 100 m the drillers were using minimal rotation in an effort to maximize recovery of the relatively soft sediments. Field observations indicated good recovery of undisturbed sediment. However, upon subsequent splitting and initial description of cores, significant disturbances – interpreted as drilling artifacts – were frequently observed in core sections from this upper sequence.

A whitish tracer with light blue fluorescence under UV excitation (DayGlo SPL-594N; RADGLO AFN-09) was mixed into the mud holding system. Due to the agricultural/urban setting of the drill site, this tracer was chosen because it did not add any coloration to the drilling fluid. It would not have been possible to use and later dispose brightly colored drilling fluid, despite being non-toxic and environmentally harmless. After the initial amendment of the drill mud with tracer (dilution ca. 1:1000, ca. 1 x 10^9 particles per ml drilling fluid), about half of the initial amount of fresh tracer was added daily to make up for the loss of particles due to continual separation and removal of cuttings from the drill mud or to loss of drilling fluid into permeable sedimentary layers. As no fluorescence microscope or flow cytometer was available on site, this addition was based on the experiences of Kallmeyer et al. (2006). Upon later analysis we found that the tracer addition was not completely sufficient as the tracer concentration dropped by over one order of magnitude over the course of the drilling (Fig. 2.2).

Sample collection and particle quantification – Immediately after core retrieval, liner fluid was collected either from a fresh cut between sections or from the bottom of the core. At Lake Towuti the sediment core was cut into two subsections of 1,5m length whereas at Lake Chalco the core was recovered in 1.5 m intervals. Unfortunately at Lake Towuti it was only possible to obtain 11 liner fluid samples from a total number of 61 core sections, due to gas expansion in the sediment caused by pressure loss during retrieval, which pushed out any remaining fluid and completely filled out the liner. Additionally, samples of the drilling fluid were collected in regular intervals from the holding tank. At Lake Chalco liner fluid could be collected from every core.

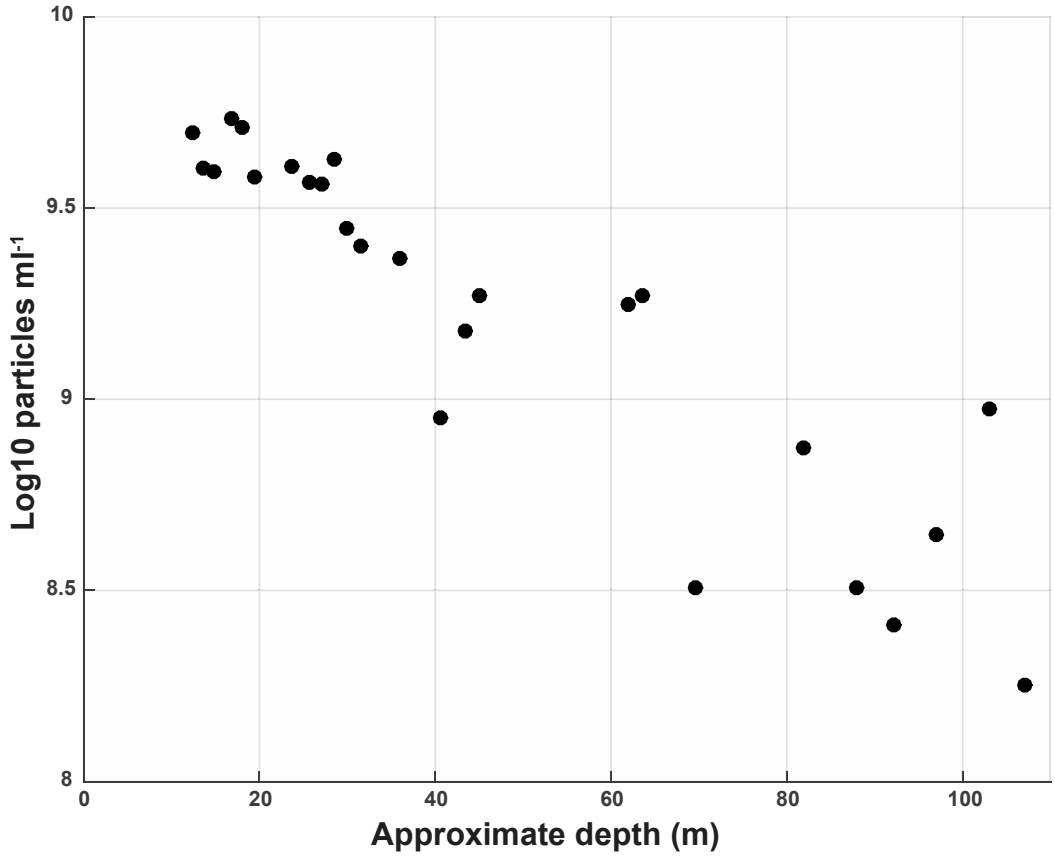

Figure 2.2: *Tracer concentration in the drilling fluid over the course of the ICDP Lake Chalco drilling. The samples were taken directly from the gap between core and liner, i.e. as so-called liner fluid. Despite daily addition of tracer the concentration decreased over the course of the drilling operations.*

Samples for contamination control were either taken from whole round cores (WRC, Lake Towuti) or from the lower ends of freshly cut core segments (Lake Chalco). In either case a few mm of the cut core surface was scraped off with a sterile scalpel and sediment samples of 1 cm^3 and 2 cm^3 for the Towuti and Chalco cores, respectively, were retrieved with a sterile cutoff syringe from the rim, the center and an intermediate position of the core. The syringes were inserted by hand into the sediment perpendicular to the cut surface and the subsamples were transferred into a 15 ml Falcon tube containing 9 ml and 8 ml of MilliQ water for Lake Towuti and Lake Chalco, respectively, followed by homogenization.

For initial analysis by fluorescence microscopy, 100 µl of the sediment slurry from the Towuti drilling were diluted 1:100 with MilliQ water and filtered through a white 0.2 µm polycarbonate track-etched membrane filter (Ø 25 mm, Cyclopore, Whatman International Ltd, Maidstone, England). For the Chalco samples it was necessary to disperse pigment-particle aggregates prior to analysis. Therefore, 30µl of

the sediment slurry were mixed with 2670 µl MilliQ water and 150 µl each of methanol and Detergent Mix (36.8 g L^{-1} $Na_2EDTA \times 2\ H_2O$, 22.3 g L^{-1} Na-pyrophosphate × 10 H_2O and 5 mL TWEEN 80). This suspension was sonicated 1x 10 sec and 1x 5 sec with a 30 sec cooling pause in between at 90% amplitude with a Bandelin MS73 ultrasonic probe (Bandelin electronic, Berlin, Germany). 500 µl of this mixture was filtered through a white 0.2 µm polycarbonate track-etched membrane filter. Filter towers were cleaned with MilliQ after each filtration in order to avoid cross contamination between samples. Filters were embedded in glycerol, diluted 1:2 with MilliQ water, with 10 µl of this solution on both the microscope slide and cover slip. On each filter a total of 200 fields of view were counted on a Leica DM2000 fluorescence microscope using non-fluorescent immersion oil (Leica type F oil, $n_e^{23} = 1.518$, $v_e = 46$) and 63x or 100 x objectives (Leica Plan Apo), depending on the amount of minerals on the filter. For enumeration of the tracer used at Lake Towuti, we employed a blue filter set (Leica Filter Cube F1/RH, excitation 490/15; 560/25 nm, dichromatic mirror 500; 580 nm, suppression 525/20; 605/30 nm). For the Lake Chalco tracer a UV filter set (Leica Filter Cube A, excitation BP340-380 nm, dichromatic mirror 400 nm, suppression LP425 nm) was used.

Quantification via flow cytometry – In order to expedite sample turnover, we combined the microscopy approach with flow cytometry. For Lake Towuti samples we used a portable cytometer (BD Accuri C6, BD Biosciences, San Jose, USA), which is small and rugged enough to be taken into the field, enabling automatic and rapid determination of contamination directly on-site. For each analysis 100 µl of sediment slurry or drilling fluid was diluted 1:100 in MilliQ water and the slurry fed into the cytometer by a peristaltic pump at a constant flow rate of 35 µl/min. MilliQ water was used as sheath fluid. A blue 488 nm laser and fluorescence detectors with optical filters at 533/30 nm and 585/40 nm were used. For the 533/30 nm filter a threshold was set to 900 to remove background noise events that are not associated with sediment or tracer particles.

For the Lake Chalco samples we used a FACS Aria III (BD Biosciences, San Jose, USA) instead of the Accuri C6 because the excitation wavelength of the tracer is in the UV range and therefore outside the range of the red and blue lasers of the Accuri. For analysis, 1 ml of the remaining slurries from the microscopy filter preparation was transferred into round bottom tubes through a 40 µm cell strainer cap to remove larger

particles, which may clog the flow cell. The sample was fed to the flow cell by air pressure at a flow rate of ca. 20 µl/min. The exact flow rates for each sample were determined from the mass difference of the sample tubes before and after each measurement. BD FACS flow (BD Biosciences, San Jose, USA) was used as sheath fluid. A UV 375 nm laser and fluorescence detectors with optical filters at 510/50 nm and 450/40 nm were used. For the 510/50 nm filter a threshold was set to 300. These parameters allowed the instrument to ignore background noise events.

2.3 Assessment

Before applying the approach in the field, several tests were conducted to assess fluorescence stability of the pigment tracer under a wide range of parameters. First, we tested, whether tracer particles (DayGlo SPL-19N) remain detectable when they are mixed into a sediment slurry. A 1:10 diluted sediment slurry containing 1 cm^3 sediment from Lake Towuti was spiked with a tracer particle concentration of ca. 1 x 10^8 particles per milliliter and 10 µl of this mixture was diluted in 1 ml MilliQ water and transferred onto a white 0.2 µm polycarbonate track-etched membrane filter.

Figure 2.3 shows a microscopic image of this filter and illustrates that the tracer particles do not attach to sediment particles and can easily be quantified. This is also important for analysis with flow cytometers, where aggregates of sediment and tracer particles might not be clearly identifiable. Particle quantification by fluorescence microscopy could reproduce the known particle concentration.

Occasionally, scientific drilling operations are carried out in acidic, alkaline or saline environments. In order to determine the applicability of the pigment tracer in these environments, we tested the tracer stability under extreme pH and salinity conditions. We prepared three solutions:

(1) A 0,1M HCl solution with a pH of 1
(2) A 0,1M NaOH solution with a pH of 13
(3) A saturated NaCl solution.

Each of the three solutions was spiked with a tracer particle concentration of 10^6 particles per milliliter. After two hours, the particle concentration was quantified. In all three experiments the fluorescence intensity of the tracer particles remained unchanged

and microscopic counts could reproduce the known particle concentration showing that the tracer is applicable over a wide range of pH or salinity conditions.

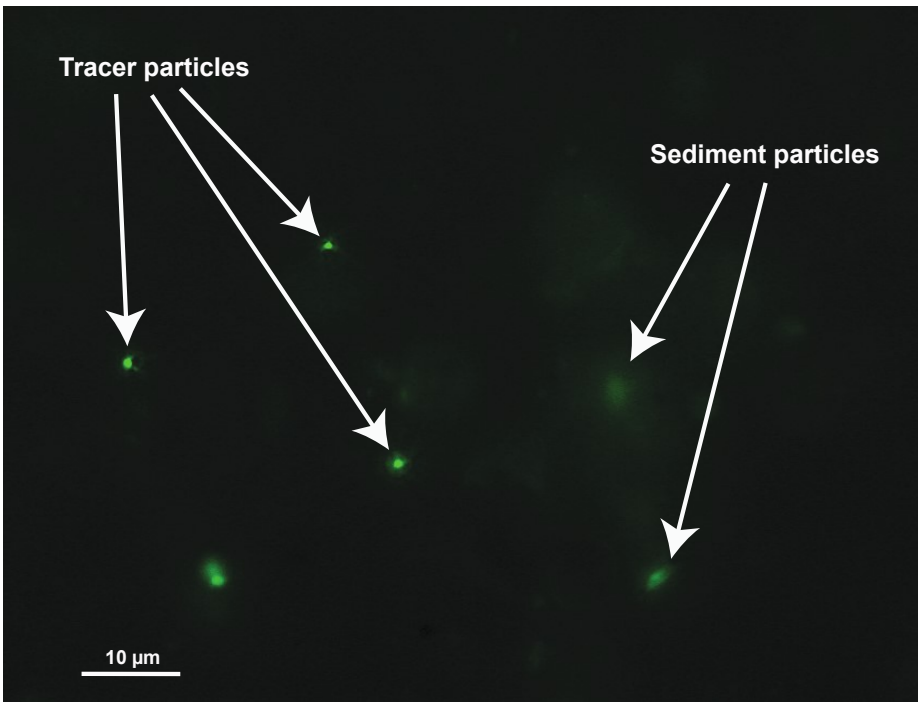

Figure 2.3: *Microscopic image of pigment particles (DayGlo SPL-19N) in a contaminated sediment slurry containing ca. 1 x 10^8 pigment particles per cm^3 sediment. The pigment particles do not adhere on sediment particles, thereby allowing for accurate quantification.*

Photodegradation of particles – Considering the common applications of the pigment particles, we expected them to withstand even excessive exposure to sunlight. To verify this, we performed a long-term experiment by preparing an aqueous suspension of DayGlo SPL-19N with a final concentration of ~10^5 particles per ml. The suspension was stored in a plastic vial on a windowsill and exposed to natural sunlight as well as fluorescent lighting from the room lights. Particles were repeatedly quantified over a period of 220 days. Figure 2.4 shows that the particle concentration did not decrease over this time period. Hence, this tracer remains usable even several months after initial core retrieval, which is a major advantage over fluorescent dyes and Perfluorocarbon tracers.

Thermal degradation of pigment particles – If drilling operations are carried out in areas of hydrothermal or volcanic activity the drilling fluid can heat up extensively during drilling operations. Yanagawa et al. (2013) showed that microsphere particles are thermally degraded under those high-temperature conditions. To address this issue, we prepared an aqueous suspension of DayGlo SPL-19N containing 1 x 10^6 particles per

ml and autoclaved it for 25 minutes at 125 °C and 3 bar (Certoclav Essential 12l, Traun, Austria). No fluorescence could be observed by microscopic analysis, so autoclaving led to a complete degradation of all particles. Therefore, like regular microsphere tracers, our pigment tracer is not applicable for high-temperature drilling operations. As we did not perform a thermal gradient experiment we cannot provide any data on the maximum temperature to which the tracer can be used.

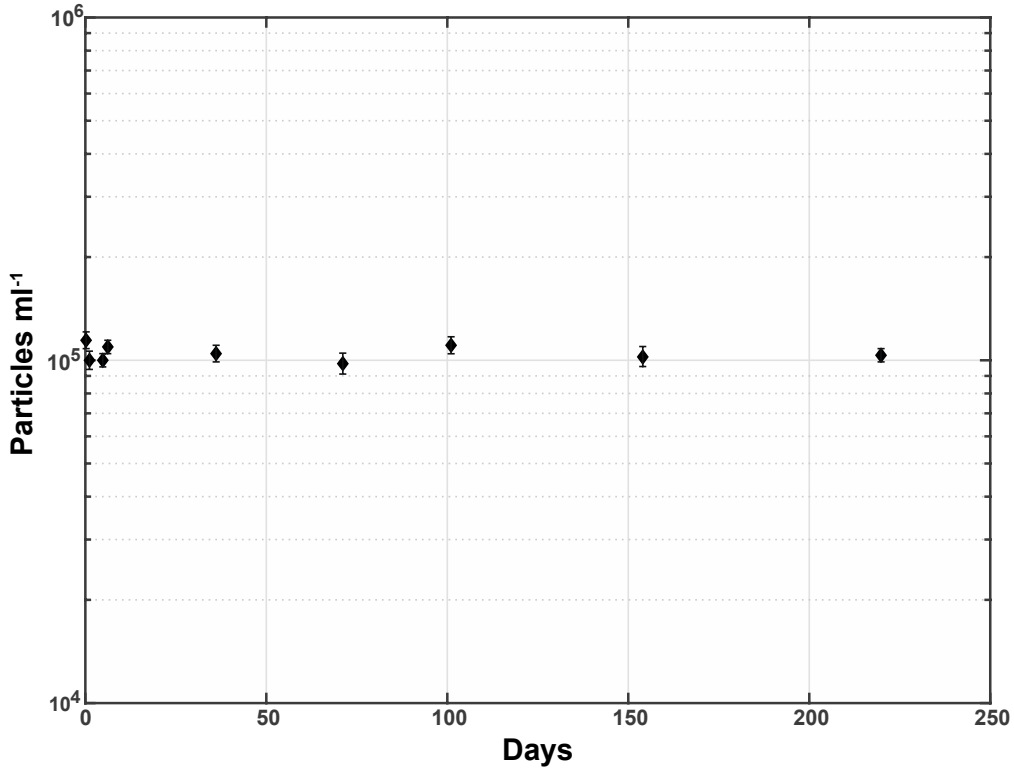

Figure 2.4: *Particle concentrations of a pigment tracer solution with a known concentration of 1 x 10^5 particles per ml over a time span of 220 days. The solution was stored under ambient light conditions over the whole period.*

Applicability for drilling campaigns – To test the applicability of the approach we determined particle concentrations at the rim, at an intermediate position and at the center of each WRC from the Lake Towuti drilling. Almost all samples from the rim contained particles as they were in direct contact with the drilling fluid that flows through the gap between the sediment core and the liner (Fig. 2.5). The number of particles and therefore the infiltration of drilling fluid decreased significantly towards the center of the core, which is in agreement with previous studies (Lever et al., 2006; Smith et al., 2000b).

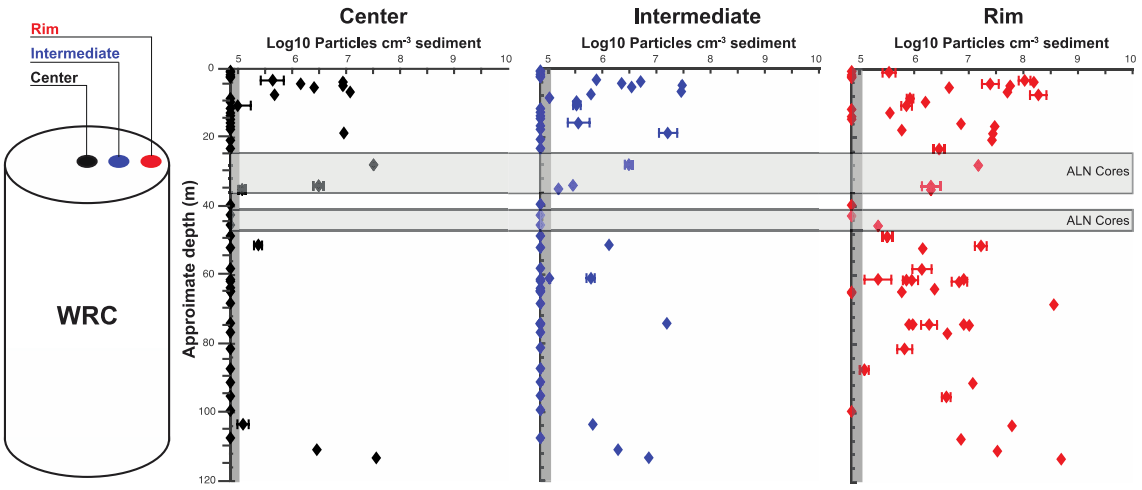

Figure 2.5: *Particle concentrations per cm³ of sediment samples from the rim, the center and the intermediate position of whole round cores (WRC) of the Towuti drilling (DayGlo SPL-19N). Counts are based on fluorescence microscopy and were carried out in duplicates. Error bars represent one standard deviation. Cores retrieved using the ALN tool as well as the limit of detection (LOD) of the particle enumeration method, are indicated in light and dark grey, respectively.*

In two WRC (at 28 and 34 m depth, Fig. 2.5) particle concentrations from the interior of the core exceeded those of the rim. The cores from which these WRC were retrieved were drilled with the ALN tool, where a rotating drill bit cuts the core. This tool is well known to cause disturbances in soft and/or semi-consolidated sediment due to excessive shearing (e.g. Glombitza et al., 2013). Particle concentrations in these samples thus indicate that the sediment was homogenized and reconstituted in a mixture of drilling fluid and sediment, rendering those samples unsuitable for geomicrobiological investigations. It should be noted that the sediment still appeared solid and unaffected upon first inspection. Only during careful sectioning it became obvious that the original sedimentary structure was completely destroyed (Fig. 2.6).

Also, the upper 20 m of the core appear to be generally more contaminated than the lower parts, despite the use of the HPC tool. We presume that the softer sediment in this depth interval is more susceptible to infiltration than the deeper layers.

According to Kallmeyer et al. (2008) the limit of detection (LOD) can be determined using the following equation Eq. 2.1:

$$n = -\frac{T_{fov}}{C_{fov}} \ln (1 - p) \qquad (2.1)$$

where n is the number of particles, C_{fov} is the number of fields counted, T_{fov} is the total number of fields on the filter and p is the confidence level to detect at least 1 particle.

When using a 63x objective the T_{fov} of a 25 mm filter is 7854. When counting 200 fields of view n is 117, meaning that 117 particles are required on the filter to detect at least 1 particle with a 95% probability. For a sample containing 1 x 10^{-3} cm^3 sediment the corresponding detection limit is ~10^5 particles per cm^3 of sediment.

Figure 2.6: *Highly contaminated ALN core. The sediment structure was completely destroyed in the process of drilling, producing cracks and fissures and allowing drilling fluid to infiltrate deeply into the sediment core. Pressure during coring solidified the mixed up material again, producing sedimentary structures that at first glance appear to be original features.*

Infiltration of drilling fluid – It is possible to calculate the amount of liner fluid infiltrating into a sample if the particle concentration in the corresponding drilling fluid is known. The LOD can be calculated by equation Eq. 2.2:

$$LOD = \frac{n}{V_{sed} * C_{LF}} \tag{2.2}$$

where n is the number of particles required in a sample to be able to detect at least one particle with a probability of 95 % (see Eq. 2.1), V_{sed} is the volume of sediment on the filter (cm^3) and C_{LF} is the particle concentration in the drilling fluid at the time the respective core was retrieved. Assuming that the average particle concentration was 1 x 10^9 particles per ml of drilling fluid (Fig. 2.1), the calculated LOD results in ca. 117 nl drilling fluid per cm^3 sediment (Fig. 2.7) if one particle was found in 200 fields of view. This is in the range of already established techniques like PFTs or microsphere tracers

(Kallmeyer et al., 2006; Smith et al., 2000a). For the Lake Towuti drilling surface lake water a cell concentration of ca. 10^6 cells per ml was used as the drilling fluid, resulting in a LOD of ca. 117 nonindigenous cells per cm^3 sediment (Fig. 2.7).

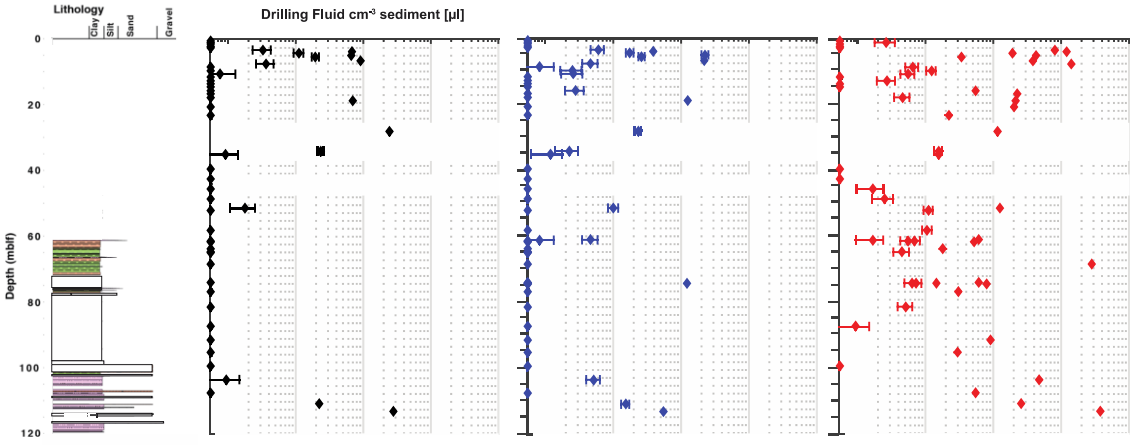

Figure 2.7: *Simplified stratigraphy of the drilled Lake Towuti core (Russell et al., 2016) and amount of drilling fluid (µl) that has infiltrated into one cm^3 of sediment during drilling. Intervals in which the Alien tool (ALN) was used are marked in light grey. The limit of detection (LOD), based on a particle concentration of 1 x 10^9 particles per ml of drilling fluid, is marked in dark grey.*

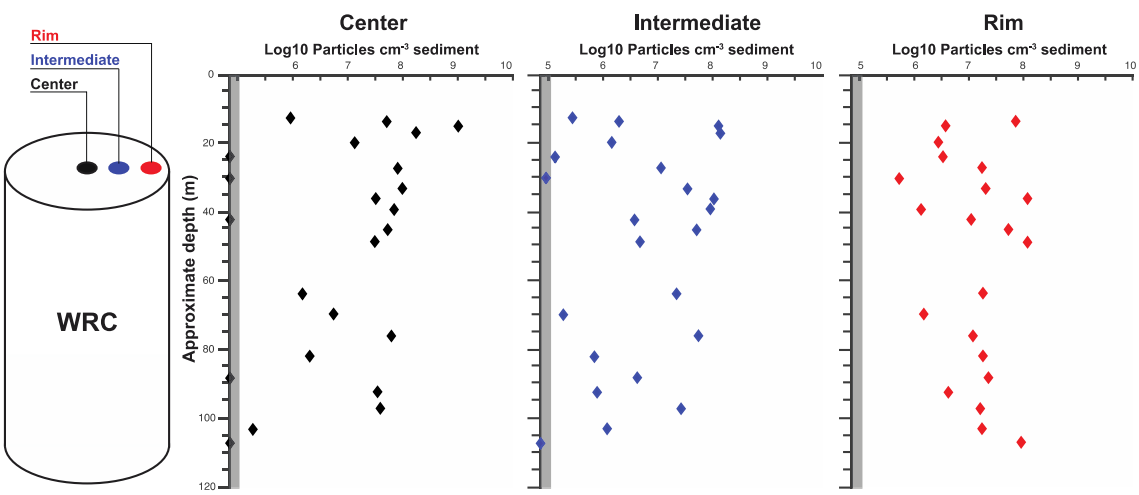

Figure 2.8: *Particle concentrations per cm^3 sediment of drill core samples from Lake Chalco (DayGlo SPL-594N). Severe contamination could be detected at almost all center samples rendering them unsuitable for geomicrobiological investigations.*

For Lake Chalco particle quantification by fluorescence microscopy revealed severe contamination of the upper ~100 m of the drill core (Fig. 2.8). Almost all samples from the center of the drilled core contained high tracer concentrations of up to 10^9 particles per cm^3 sediment, which in some cases exceeded particle concentrations of the rim or intermediate samples (Fig. 2.8). Contamination control of the Lake Chalco

drill core thus revealed that the majority of samples are not suitable for geomicrobiological analysis.

Quantification of pigment particles by flow cytometry – In order to determine the applicability of the flow cytometry approach we prepared three samples for an initial test:

(1) A sediment-free tracer solution containing 1 x 10^6 pigment particles per ml

(2) A tracer-free blank containing 1 x 10^{-3} cm^3 sediment per ml of MilliQ water

(3) A contaminated sediment slurry (1 x 10^{-3} cm^3 sediment per ml of slurry) with a particle concentration of ca. 1 x 10^6 particles per ml.

After analyzing the sediment-free tracer solution of the blue tracer (SPL-19N) it was possible to define the tracer particle populations (Fig. 2.9A). Analysis of the tracer-free sediment suspension of Lake Towuti sediment showed that the sediment particles plot as a distinctly different population outside this group (Fig. 2.9B). The contaminated slurry shows good separation of sediment and tracer particles (Fig. 2.9C). We then quantified the events within the tracer group.

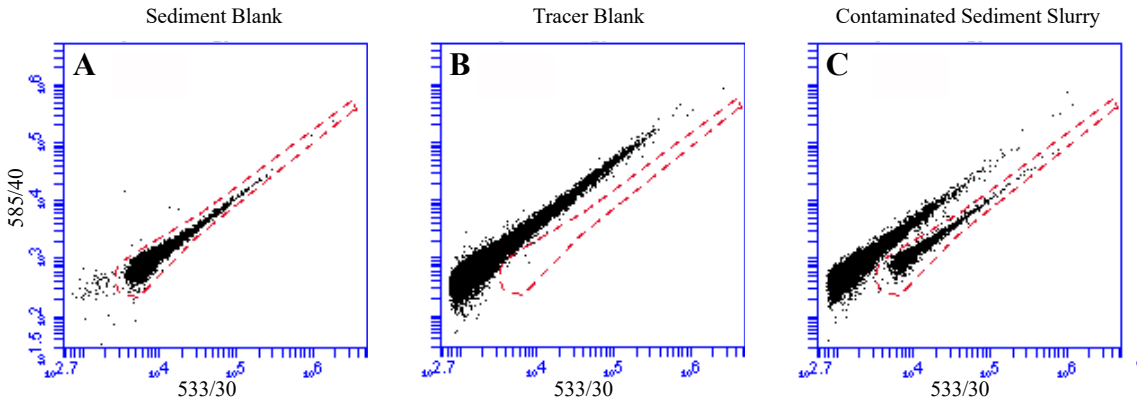

Figure 2.9: *Cytometer dotplots of (A) a sediment-free tracer solution (blue tracer, SPL-19N), (B) a tracer-free sediment suspension blank and (C) a contaminated sediment slurry containing ~1,5 x 10^7 tracer particles per cm^3 sediment.*

For the UV tracer (SPL-594N) the same experiment was performed with sediment samples from Lake Chalco. Here, the sediment particles were plotting in a much wider distribution (Fig. 2.10B), most probably due to the fact that some minerals are fluorescent under UV light. Nevertheless, the dotplot of the contaminated slurry

shows that the tracer particle population is separated from the sediment particle population (Fig. 2.10C).

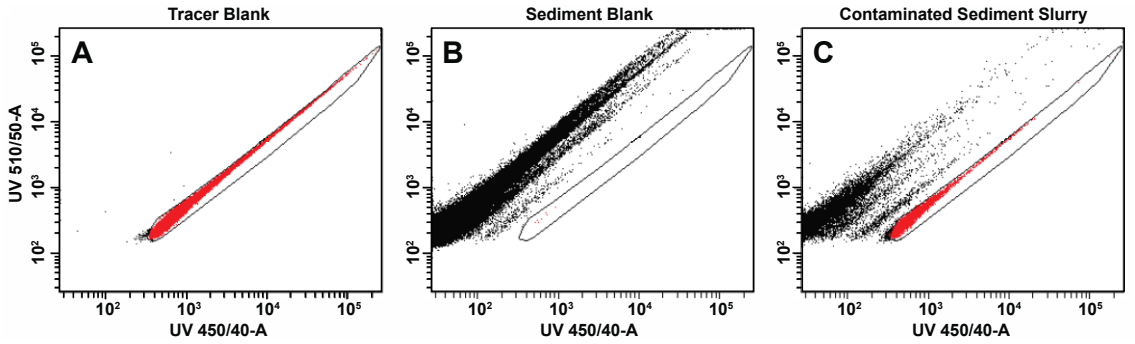

Figure 2.10: *Cytometer dotplots of (A) a sediment-free tracer solution (UV tracer, SPL-594N), (B) a tracer-free sediment suspension blank and (C) a contaminated sediment slurry containing ~ 8 x 10^7 tracer particles per cm^3 sediment.*

To test if the gates were set correctly and the populations only contain sediment or tracer particles, respectively, we performed a particle sorting of the contaminated slurries using a BD FACSAria III cell sorter (BD Biosciences, San Jose, USA). For the SPL-19N tracer the optical parameters were very similar to those used on the Accuri (excitation laser wavelength 488nm, optical filters 616/23 nm and 530/30 nm, threshold 200 for 530/30nm), for the SPL-594N tracer the parameters are given in the Materials and Procedures section. The dotplots of the Towuti samples were very similar to the ones from the Accuri and the gates were set accordingly. Two distinct populations were sorted into separate vials preloaded with 5ml MilliQ water. After sorting, the suspensions were vortexed and filtered onto white polycarbonate membranes, and the particles quantified via fluorescence microscopy using the protocol described above.

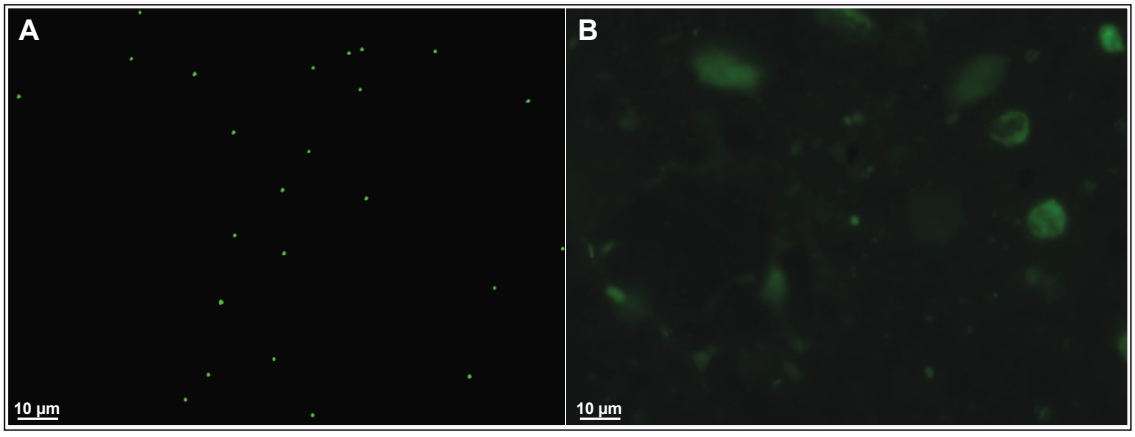

Figure 2.11: *Microscopic image of FACS-sorted (A) tracer particles (SPL-19N) and (B) Towuti sediment particles. The excellent separation of tracer and sediment particles becomes apparent.*

The fraction of sorted tracer contained only tracer particles (Fig. 2.11A), whereas the sorted sediment fraction contained mostly sediment and very few fluorescent particles (Fig. 2.11B). The same observation could be made after sorting the Chalco samples (not shown).

To test whether the values obtained by fluorescence microscopy can be reproduced by flow cytometry over the entire range of particle concentrations found in these samples, we analyzed samples from both Lake Towuti and Lake Chalco.

We chose twenty-three samples from Lake Towuti and twenty samples from Lake Chalco from different depths to cover the widest possible range of particle concentrations. The results were in good agreement with the values obtained by fluorescence microscopy (Fig. 2.12). Thus, it is possible to detect and accurately quantify tracer particles by flow cytometry, which raises the possibility for accurate and rapid contamination control in sediment samples, potentially even directly on-site.

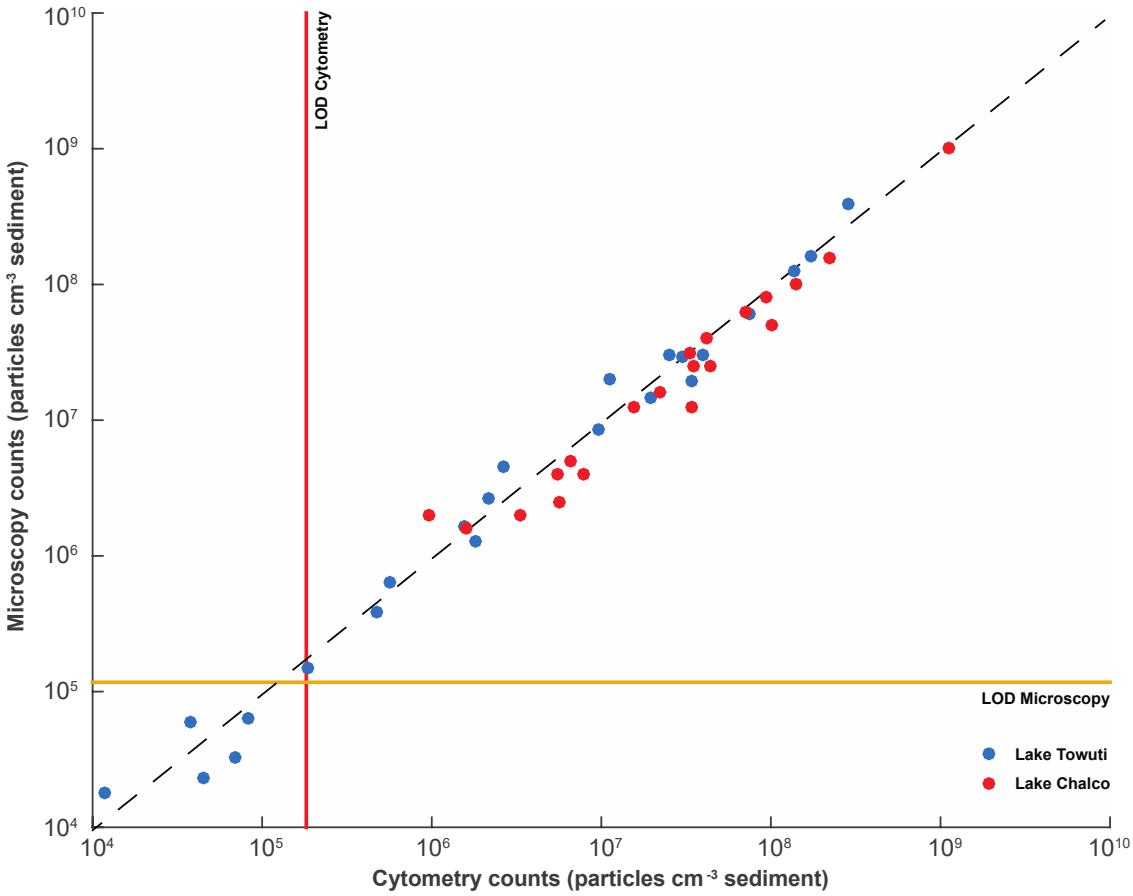

Figure 2.12: *Comparison of tracer particle counts obtained by fluorescence microscopy and flow cytometry for Lake Towuti (blue circles) and Lake Chalco (red circles) samples. The limit of detection of both fluorescence microscopy and flow cytometry is indicated in orange and red, respectively. The dashed line indicates the 1:1 ratio between the two techniques.*

Detection limit of the flow cytometry approach – The sensitivity of the flow cytometry approach depends on the number of non-tracer particles that fall within the population of the tracer, which in turn depends on the volume of sample that was analyzed. After analyzing each 1ml of five tracer-free sediment blanks containing 1 x 10^{-3} cm^3 sediment from Lake Towuti the average number of particles found within the tracer population was 53±29. Based on the approach used by Kallmeyer et al. (2008) and Morono & Kallmeyer (2014) we defined the LOD as the blank plus three times its standard deviation. The LOD thus accounts for 1,4 x 10^5 particles per cm^3 sediment (Fig. 2.12). Assuming a cell concentration of 10^6 cells cm^{-3} and a particle concentration of 1 x 10^9 pigment particles cm^{-3} in the drilling fluid this translates into 140 allochthonous cells per cm^3 of sample. For Lake Chalco four tracer-free sediment blanks containing 1 x 10^{-3} cm^3 sediment were analyzed. The average number of particles within the tracer gate was 87±24 corresponding to a similar LOD of 1,5 x 10^5 particles (150 allochtonous cells per cm^3 of sediment).

2.4 Discussion and Recommendation

Here we present a new tracer method for scientific drilling campaigns that uses an aqueous fluorescent pigment dispersion. Tests confirmed the applicability of our new tracer method for large drilling campaigns with volumes of drilling fluid in the order of tens to hundreds of thousand of liters. The method requires only a minimum of equipment and offers rapid and easy on-site analysis. The sensitivity of the new method is similar to the established microsphere tracer approach but it offers two major improvements. First, the price of the tracer is four orders of magnitude lower and among the lowest of all contamination control tracers. Second, by combining our approach with flow cytometry we decreased processing time per sample by at least a factor of four. It takes about 15 minutes to prepare a set of six filters, and at least 10 minutes per filter to count them (3 seconds per field of view), whereas difficult filters with many mineral particles and/or high background fluorescence might take up to 30 minutes each. For flow cytometry the sample only needs to be diluted and analysis takes about three minutes per sample. Depending on the type of flow cytometer it is possible to use an autosampler, allowing for fully automated rapid on-site analysis. This opens the possibility to select samples of highest quality with respect to contamination and to decide whether changes in drilling techniques are required to optimize core quality.

Like regular microsphere tracers, the pigment tracer is stable to light degradation (Fig. 2.4), which allows for contamination assessment on archived core material even several months after initial core retrieval. This is a major advantage over PFT that, due to its volatility, will not reflect the initial drilling fluid contamination over this time interval and thus will not allow a later contamination assessment.

In contrast, autoclaving tests showed that our tracer particles experience a complete thermal degradation under high temperatures, which is similar to other microsphere particles (Yanagawa et al., 2013). For high-temperature drilling campaigns it is therefore recommended to use other tracers such as PFT, which has a boiling point of 76 °C at atmospheric pressure (Yanagawa et al., 2013) or naphthalene sulfonic acids (NSA) that have been used as a thermally stable tracer for drilling in hydrothermal systems (Gunderson et al., 2002). However, the latter has its limitations concerning handling and environmental regulations. Also, a 16S rRNA gene tracer approach was used successfully for contamination control in hydrothermal drilling operations (Yanagawa et al., 2013).

Chemical tracers (PFTs, fluorescent dyes, etc.) and particulate tracers (microspheres, pigment tracer) differ in their diffusive properties, with chemical compounds diffusing much faster than particulate tracers, which behave more like microbial cells in that their diffusion is extremely slow, being limited to Brownian motion. Particulate tracers thus represent the most suitable, non-biological tracer to trace infiltration of non-indigenous microorganisms in subsurface materials even though their surface characteristics differ substantially from that of microorganisms (Colwell et al., 1992; Harvey et al., 1989). However, particulate tracers have limitations in systems where pore water chemistry is of interest, as drilling fluid may infiltrate into pores that exclude tracer particles. Here, a chemical tracer would be the option, as it would provide more realistic results. To achieve the most accurate contamination assessment with respect to microbial and chemical contamination a combination of particulate and chemical tracers would be recommended.

We consider the sensitivity of the presented approach to be sufficient for contamination assessment in low biomass environments. However, to further increase the sensitivity of the method, a plastic bag filled with undiluted tracer was attached to the core catcher of a hydraulic piston corer prior to deployment (Colwell et al., 1992; Smith et al., 2000a). In principle this would increase the amount of particles in the liner

fluid right at the core, leading to a better LOD of the amount of drilling fluid that has infiltrated into a sample. Using a 3m long liner with a diameter of 66 mm and assuming a 2,5 mm gap between the sediment and the liner this would correspond to a volume of ~1,5 l of drilling fluid that enters the liner during drilling. To reach a particle concentration of ~1 x 10^{10} mL^{-1} (corresponding to a LOD of ~14 nanoliters liner fluid infiltration and thus ~14 allochtonous cells per cm^3 sediment for the flow cytometry approach) we used a plastic bag filled with 20 ml undiluted particle tracer containing in total ~2 x 10^{13} particles.

However, the results from the particle counts of liner and drill fluid show that only in two instances the liner fluid had particle concentrations in the 1 x 10^{10} ml^{-1} range (Fig. 2.1). All other liner fluids had concentrations that were similar to the drilling fluid. We can only speculate why the delivery of additional tracer from the bags did not work out as planned, but we assume that either the bags fell off during tripping of the core through the drill pipe, or the high flow rate of drill fluid flushed the additional tracer out of the liner. However, as the tracer concentration in the drill fluid was in the 1 x 10^9 ml^{-1} range and therefore sufficiently high, we do not think that the malfunctioning of the bags greatly impeded our results.

The presented approach proved to be successful in two different drilling campaigns using different tracers and different drilling techniques. At Lake Chalco it could be shown that tracer amendment into the drilling fluid is unaffected by a suite of polymer additives that are often added to the drilling fluid to stabilize the borehole and to suspend and carry cuttings out of the hole. Also, due to its non-toxic composition the tracer can be used irrespective whether the drilling fluid is discharged or recycled over the course of the drilling. We believe that the approach is likewise applicable for ocean and igneous rock drilling as the similar microsphere tracer approach has already been successfully applied in such operations (Smith et al., 2000b). Our new approach thus offers an inexpensive and rapid alternative approach for assessing contamination in future scientific drilling operations.

2.5 Acknowledgements

This research was carried out with partial support from the International Continental Scientific Drilling Program (ICDP), the U.S. National Science Foundation (NSF), the

German Research Foundation (DFG), the Swiss National Science Foundation (SNSF), PT Vale Indonesia, the Ministry of Research, Education, and Higher Technology of Indonesia (RISTEK), Brown University, the University of Minnesota, the National Autonomous University of Mexico (UNAM), GFZ German Research Centre for Geosciences, the Natural Sciences and Engineering Research Council of Canada (NSERC), and Genome British Columbia. We thank PT Vale Indonesia, the US Continental Scientific Drilling and Coordination Office, and US National Lacustrine Core Repository, and DOSECC Exploration Services for logistical support. The research was carried out with permissions from RISTEK, the Ministry of Trade of the Republic of Indonesia, the Natural Resources Conservation Center (BKSDA), and the Government of Luwu Timur of Sulawesi.

Special thanks are due to Ryan O'Grady from LacCore for expert core handling and curation during both drilling projects as well as for his help with the manuscript.

3 Geomicrobiological Features of Ferruginous Sediments from Lake Towuti, Indonesia

Lake Towuti is a tectonic basin, surrounded by ultramafic rocks. Lateritic soils form through weathering and deliver abundant iron (oxy)hydroxides but very little sulfate to the lake and its sediment. To characterize the sediment biogeochemistry, we collected cores at three sites with increasing water depth and decreasing bottom water oxygen concentrations. Microbial cell densities were highest at the shallow site—a feature we attribute to the availability of labile organic matter (OM) and the higher abundance of electron acceptors due to oxic bottom water conditions. At the two other sites, OM degradation and reduction processes below the oxycline led to partial electron acceptor depletion. Genetic information preserved in the sediment as extracellular DNA (eDNA) provided information on aerobic and anaerobic heterotrophs related to *Nitrospirae*, *Chloroflexi*, and *Thermoplasmatales*. These taxa apparently played a significant role in the degradation of sinking OM. However, eDNA concentrations rapidly decreased with core depth. Despite very low sulfate concentrations, sulfate-reducing bacteria were present and viable in sediments at all three sites, as confirmed by measurement of potential sulfate reduction rates. Microbial community fingerprinting supported the presence of taxa related to *Deltaproteobacteria* and *Firmicutes* with demonstrated capacity for iron and sulfate reduction. Concomitantly, sequences of *Ruminococcaceae*, *Clostridiales*, and *Methanomicrobiales* indicated potential for fermentative hydrogen and methane production. Such first insights into ferruginous sediments showed that microbial populations perform successive metabolisms related to sulfur, iron, and methane. In theory, iron reduction could reoxidize reduced sulfur compounds and desorb OM from iron minerals to allow remineralization to methane. Overall, we found that biogeochemical processes in the sediments can be linked to redox differences in the bottom waters of the three sites, like oxidant concentrations and the supply of labile OM. At the scale of the lacustrine record, our geomicrobiological study should provide a means to link the extant subsurface biosphere to past environments.

3.1 Introduction

Lake Towuti is a tropical 200 m deep tectonic lake seated in ophiolitic rocks and surrounded by lateritic soils (Lehmusluoto et al., 1997; Russell and Bijaksana, 2012). It is part of the Malili Lakes system, comprising several interconnected lakes, including Lake Matano, the 10th-deepest lake in the world (~600 m). Its location on Sulawesi, Indonesia (Fig. 3.1A) renders Lake Towuti's sediments prime recorders of paleoclimatic changes in the tropical Western Pacific warm pool (Russell et al., 2014). The tropical climate and the lateritic weathering of the (ultra)mafic catchment of the Malili Lakes system (Fig. 3.1B) cause a strong flux of iron to the lake. Surrounding lateritic soils are typically related to limonite types, with mostly goethite (α-FeOOH) and ferrihydrite (Fe_2O_3 * 0.5 H_2O) transported to the basin (Crowe et al., 2004; Golightly, 2010) as well as some hematite (Fe_2O_3) and detrital magnetite (Fe_3O_4). High iron fluxes to the lake may exert a decisive constraint on bioavailable phosphorus in the epilimnion as it is scavenged by iron (hydr)oxides, likely driving Lake Towuti's water column towards severely nutrient-limited conditions. However, anoxia in stratified water column can lead to iron reduction and partial release of adsorbed P into the water at the oxycline and below (Zegeye et al., 2012). Biogeochemical and microbiological data gathered from nearby Lake Matano reveal persistent anoxia in the deeper part of Lake Matanos water column (Crowe et al., 2008a; Jones et al., 2011) with organic matter (OM) degradation through methanogenesis (Crowe et al., 2011; Katsev et al., 2010). Although Lake Towuti is anoxic at greater depths as well, it is less deep and can mix periodically (Haffner et al., 2001), presumably causing transient bottom water oxygenation (Costa et al., 2015).

Once buried, ferruginous sediments likely support microbial communities, which can utilize a range of metalliferous substrates (Crowe et al., 2007). Although microbial activity decreases dramatically below the water-sediment interface and with increasing sediment depth, even this low activity can have an appreciable impact on both sediment composition and biogeochemical cycles over long time periods (Berner, 1980; Freudenthal et al., 2001; Horsfield and Kieft, 2007). In addition, iron minerals are also suspected to strongly adsorb DNA (He et al., 2008). Upon cell lysis, nucleic acids are released into the surrounding water and sediment and partitioned between sorption to reactive Fe surfaces (Ceccherini et al., 2009; Pietramellara et al., 2009) and uptake or degradation via microbial metabolisms (Corinaldesi et al., 2008; Corinaldesi et al.,

2007). Binding to metal oxides and colloids (Ceccherini et al., 2009; Cleaves et al., 2011) could result in preservation and persistence of eDNA in the lacustrine record (Pietramellara et al., 2009), providing a valuable archive of genetic information (Corinaldesi et al., 2011). However, since metal-reducing bacteria have the capacity to solubilize structural Fe and utilize adsorbed nutrients (Crowe et al., 2007; Dong et al., 2003), the sediment-bound eDNA should not be totally recalcitrant (Baldwin, 2013, and references therein) and could serve as a labile organic substrate for sedimentary microbes (Corinaldesi et al., 2007). Its concentrations should then depend on the complex interplay between these processes. Altogether, Lake Towuti provides the opportunity to examine microbial populations in an iron-dominated and sulfate-poor ecosystem with dynamic redox conditions and infer sorption and diagenetic processes arising from subsurface microbial activity.

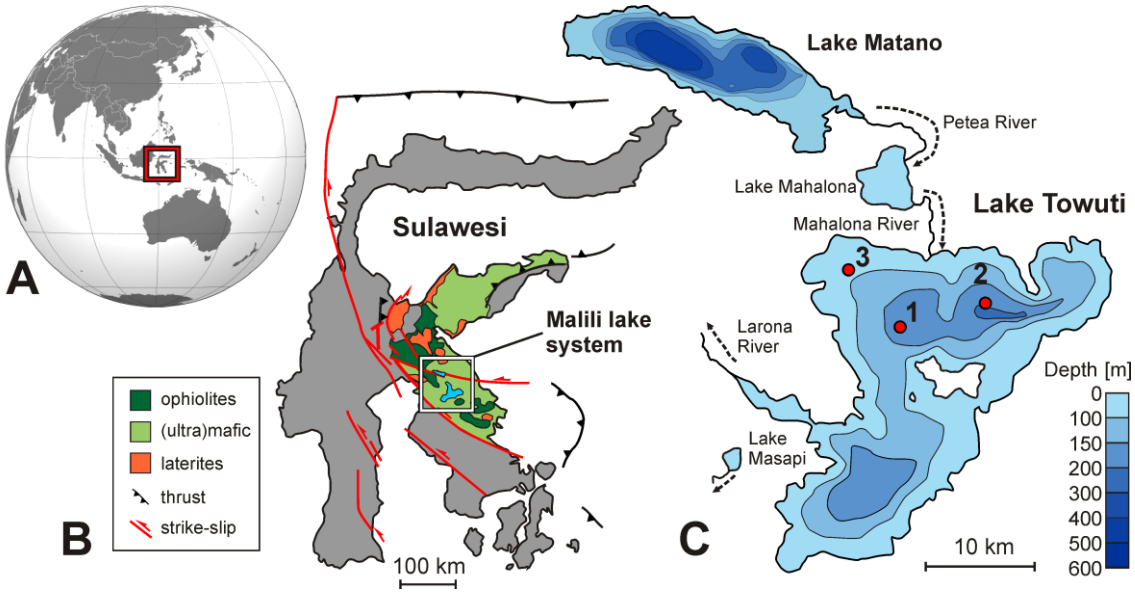

Figure 3.1: *Lake Towuti location and settings. (A) Map of Asia and Oceania displaying the location of Sulawesi Island. (B) Map of Sulawesi illustrating the geological context of the Malili lake system (modified after Calvert and Hall, 2007). (C) Bathymetric map of Lake Matano and Lake Towuti (modified after Herder et al., 2006) displaying the three sites at which gravity cores were retrieved. Sites 1 to 3 correspond respectively to water depths of 153, 200 and 60 m, with oxygenation conditions at the water-sediment interface decreasing with water depth.*

In order to investigate the relationship between biogeochemistry and microbial processes in these iron-rich anoxic sediments, we retrieved short sediment cores from Lake Towuti in 2013 and 2014 at three different depths (Fig. 3.1C). The sediment was analyzed for pore water geochemistry, total cell counts and potential sulfate reduction rates (SRR) as well as extra- and intracellular DNA (iDNA). These data provide a

background for geomicrobiological and biogeochemical analysis of the long (>100 m) drill cores that were retrieved during the ICDP (International Continental Scientific Drilling Program) Towuti drilling campaign in spring/summer 2015.

3.2 Materials and Methods

3.2.1 Site description

Lake Towuti (2.5°S, 121°E) is the largest lake within the Malili Lake System, a chain of five tectonic lakes in Sulawesi, Indonesia (Lehmusluoto et al., 1997). It has a surface area of 560 km^2 and a maximum water depth of 203 m (Haffner et al., 2001). Lake Towuti has a tropical humid climate, with an annual average air temperature of 26 °C and little variations in monthly temperatures. Precipitation averages 2540 mm yr^{-1}, with no distinct dry season (Aldrian and Dwi Susanto, 2003). The Tominanga River, which is the main inflow to the north, drains the extensive catchments of Lakes Matano and Mahalona, while the Larona River constitutes the only outflow to the west (Fig. 3.1C). Lake Towuti is weakly conductive (210 µS cm^{-1}) and circumneutral (pH ~7.8) with a chemistry dominated by Mg and HCO_3^- (Lehmusluoto et al., 1997). Surface water temperatures are commonly 28-29 °C, with weak thermal stratification of the water column (i.e. 28-31°C; Fig. 3.2). Unlike upstream Lake Matano, which is permanently stratified and anoxic below 110 m water depth due to its great depth (600 m) and steep slopes (Crowe et al., 2008a; Katsev et al., 2010), the entire water column of Lake Towuti is reported to mix at least occasionally (Costa et al., 2015; Haffner et al., 2001). Lake Towuti is usually oxygen-depleted below 130 m depth (Fig. 3.2). As a result of sedimentary P trapping due to large amounts of iron oxides derived from lateritic soils being transported into the basin (Zegeye et al., 2012), productivity in the water column is expected to be limited (Bramburger et al., 2008).

3.2.2 Sample Processing

Water temperature, oxygen concentration, light fluorescence reemitted by chlorophyll *a* (Leeuw et al., 2013) and light transmission profiles were collected on site using a submersible conductivity-temperature-depth probe (CTD) (Sea-Bird, SBE-19; Sea-Bird Electronics, Bellevue, WA, USA). Temperature profiles showed that the water column of Lake Towuti is indeed weakly stratified while oxygen concentrations indicated that

the water-sediment interface at the bottom of Lake Towuti is variably oxygenated depending on water depth, with anoxia in waters below 130 m (Fig. 3.2). Several sediment cores (<0.5 m) estimated to cover ca. 1750 years of sedimentation history (Tamuntuan et al., 2015; Vogel et al., 2015) were retrieved at three sites with increasing water depth (60, 153 and 200 m; Fig. 3.1C) and different oxidation states in overlying waters (Fig. 3.2), the intermediate site (153 m depth) was chosen to be the main site of the ICDP Towuti Drilling Project. The cores were sampled for pore water geochemistry, total cell counts, potential SRR and small subunit (16S) rRNA gene fingerprinting analyses.

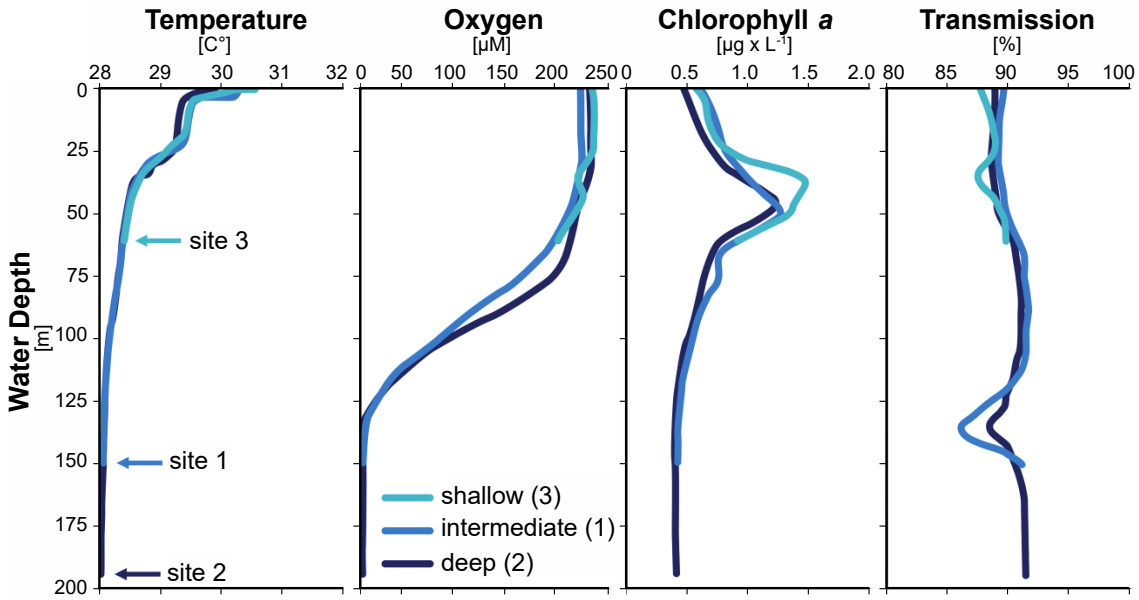

Figure 3.2: *Water column profiles. CTD casts for temperatures [°C], oxygen concentrations [µM], chlorophyll a [µg × L^{-1}] and light transmission [%] measured in the water column of Lake Towuti at each of the three sites. Results show that Lake Towuti is weakly thermally stratified with an oxycline occurring in between 90 and 130 m depth. Chlorophyll a peaks up at 50 m depth, while the presence of suspended particles can be inferred from the transmission decrease at 130 m depth.*

Pore water sampling was carried out on site under anoxic conditions, using a glove bag flushed with nitrogen gas in order to prevent oxidation of the sediment. Using an aseptic spatula, we sectioned the sediment cores in 0.5, 1, and 2 cm resolution for the upper 1 cm, 1 to 10 cm and below 10 cm, respectively. Sediment samples were transferred into 50 mL centrifuge tubes and Rhizon Pore Water Samplers (Rhizon CSS, Rhizosphere research products, Dolderstraat, The Netherlands) were inserted into the sediment through a hole in the lid. For each depth interval, 10 mL of pore water was collected in syringes, filtered through 0.2 µm pore size cellulose acetate membrane

syringe filters (Minisart, Sartorius Stedim Biotech) to remove all particles and most microorganisms, transferred into 2 mL twist top vials and stored at room temperature for analysis in the home lab.

Samples for total cell counts were preserved in a 0.2 µm filtered fixative solution of lake water amended with formalin (final concentration 2 %). For each sample, 2 cm^3 of sediment was retrieved with a sterile 3 mL cut-off syringe, placed in 15 mL centrifuge tube filled with 8 mL of fixative solution and shaken for complete homogenization. The tubes were sealed and stored at 4 °C until analysis in the home lab.

For nucleic acid analyses, entire short cores were sampled inside the nitrogen-filled glove bag. Using an aseptic spatula, we sectioned the cores into 1 cm, 2 cm and 5 cm intervals for the first 10 cm, between 10 and 20 cm and below 20 cm depth, respectively. Samples were packed into gas-tight aluminum foil bags, flushed with nitrogen gas and heat-sealed to keep them under anoxic conditions. Until DNA extraction in the home lab the samples were stored at room temperature. Since lake temperatures are ca. 28°C throughout the year, we considered this storage appropriate to minimize cell lysis or potential shifts in the microbial assemblage due to refrigeration. Freezing was not an option as it would cause cell lysis and therefore artificially increase the eDNA pool.

Samples for potential SRR measurements were collected in triplicate using glass barrels with approximately 5 cm^3 volume. The glass barrels were used to retrieve small sub-cores from the undisturbed inner part of the core, sealed with a butyl rubber stopper and stored in sealed, nitrogen-flushed gas-tight aluminum foil bags at room temperature until incubation in the home lab.

3.2.3 Laboratory procedures

3.2.3.1 Total organic carbon and total nitrogen

Total nitrogen (TN) and total carbon (TC) were measured, using a Vario EL III CHNOS elemental analyzer (Elementar Analysensysteme, Hanau, Germany). Each sample tin cup was loaded with 8 to 9 mg of freeze-dried, powdered sediment plus a spatula tip of tungsten oxide (WO_3) to enhance the combustion, and then combusted at 1150 °C. Detection limit was below 0.1%. TC results were used to calibrate volumes of sample required for total organic carbon (TOC) measurements. For TOC analysis, between 30

and 70 mg of sediment powder were loaded into a crucible and burnt at 580 °C (sensitive carbon T° for non-calcareous samples), 850 °C and 1150 °C (intensive carbon T° for calcareous samples) using a Vario MAX cube elemental macro analyzer (Elementar Analysensysteme), equipped with the soliTIC option for the determination of the total organically bound and inorganic carbon in the sample. Pretreatment of samples with HCl (5 %), as is normally done for standard elemental analyzers (Byers et al., 1978) is not needed with this device. TOC and TN were recalculated to the content of the whole sample to present results in dry mass %. TOC and TN values were then corrected by their respective atomic weights (i.e. 14/12) and used to calculate molar C_{org}/N ratios.

3.2.3.2 Iron spectrophotometry

Dissolved iron concentrations in pore water were measured in the field via spectrophotometry (Viollier et al., 2000). Directly after pore water retrieval, we aliquoted 1 mL of pore water sample to 1.6 mL Rotilabo single-use cells (Carl Roth, Karlsruhe, Germany) and stabilized dissolved Fe^{2+} by adding 100 µL of Ferrozine Iron Reagent (Sigma-Aldrich Chemie, Munich, Germany). To avoid oxidation during handling, all sample handling was carried out inside the nitrogen-filled glove bag. Absorbance of the colored solution was measured at 562 nm with a DR 3900 spectrophotometer (Hach, Düsseldorf, Germany). Detection limit of the method is 0.25 µM.

3.2.3.3 Ion Chromatography

Cation and anion concentrations in pore water samples were analyzed using an ion chromatography (IC) system (Sykam Chromatographie, Fürstenfeldbruck, Germany). Injected sample volume was 50 µL for both anions and cations. For cations, the IC system consisted of a S5300 sample injector (Sykam), a 4.6 × 125 mm ReprosilCAT column (Dr. Maisch HPLC, Ammerbuch-Entringen, Germany) and a S3115 conductivity detector (Sykam). The eluent was 2.5 mM HNO_3. Flow rate was set at 1 mL min^{-1} and column oven temperature at 45°C. A Cation Multi-Element Standard (Carl Roth) was diluted 5 times for calibration. Based on a respective signal-to-noise (S/N) ratio of 3 and 10 (Schibler et al., 2007), the detection and quantification limits were calculated for each ion and are as follows: Li^+ (10.5 µM; 63.5 µM), Na^+ (5.8 µM; 35 µM), K^+ (9.1 µM; 54.7 µM), Mg^{2+} (9.6 µM; 44.6 µM), Ca^{2++}(8.3 µM; 38.5 µM) and NH_4^+ (11.3 µM; 67.6 µM). Samples were measured in triplicates. During each run, nine

standards were measured to check for drift. Reproducibility was always better than 5 % for each ion. Concentrations are given as average values based on triplicates; error bars are one standard deviation.

Anions were analyzed by suppressed ion chromatography using a SeQuant SAMS anion IC suppressor (EMD Millipore, Billerica, Massachusetts), a S5200 sample injector, a 3.0 × 250 mm LCA 14 column and a S3115 conductivity detector (all Sykam). The eluent was 5 mM Na_2CO_3 with 20 mg L^{-1} 4–hydroxibenzonitrile and 0.2 % methanol. Flow rate was set to 1 mL min^{-1} and column oven temperature to 50 °C. A multi-element anion standard (Sykam) containing F^- (263.2 µM), Cl^- (564.1 µM), Br^- (250.3 µM), NO_2^- (434.7 µM), PO_4^{3-} (210.6 µM), NO_3^- (806.4 µM) and SO_4^{2-} (520.5 µM) was diluted 10 times and measured every 10 samples. Respective minimum detection (S/N=3) and quantification limits (S/N=10) are as follows: F^- (2.3 µM; 13.3 µM), Cl^- (5.7 µM; 16.17 µM), NO_2^- (4.1 µM; 14.14 µM), Br^- (3 µM; 10.2 µM), NO_3^- (2.8 µM; 9.3 µM), PO_4^{3-} (4.3 µM; 14.3 µM) and SO_4^{2-} (2 µM; 8.4 µM). The reproducibility was always better than 3 % for each ion.

For ammonium (NH_4^+) concentrations, the cation IC system was converted to a flow injection analysis system (Hall and Aller, 1992) using a second pump and a dialysis cell (Skalar Products, Breda, The Netherlands) instead of a separation column. First, NH_4^+ is quantitatively converted into gaseous ammonia by injecting the sample into an alkaline release solution containing 53.75 g L^{-1} citric acid and 70 g L^{-1} sodium hydroxide. The ammonia diffuses through a Teflon membrane into a capture solution made of 1 g L^{-1} boric acid and reacts to form ammonium borate. The associated change in conductivity is measured with a conductivity detector. The flow rate for release and capture solution was 0.1 mL min^{-1} and 0.3 mL m min^{-1}, respectively. For 100 µL injection volume, the minimum detection (S/N=3) and quantification limits (S/N=10) are 5 and 12.2 µM, respectively. Samples were measured in triplicates; the reproducibility was always below 10 %.

3.2.3.4 Potential sulfate reduction rate quantification

Potential SRR quantification was performed according to (Jørgensen, 1978) and (Kallmeyer et al., 2004). In brief, 3 kBq of $^{35}SO_4^{2-}$ radiotracer were injected into each sediment plug and incubated for 24 hours in the dark close to situ temperatures (ca. 30 °C). Incubated sediments were transferred into 10 mL of 20 % (w/v) zinc acetate and homogenized to precipitate free sulfide as zinc sulfide and stop microbial activity. The

sample slurry was centrifuged (4000 × g, 20 min) and 1 mL of supernatant transferred into a 7 ml scintillation vial with 4 mL of UltimaGold Cocktail (Perkin Elmer, Waltham, United States) for quantification of unreacted $^{35}SO_4^{2-}$. The remaining sediment was flushed out with 20 mL dimethylformamide into a four-neck glass flask. Non-radioactive zinc sulfide was added as a carrier, followed by injection of 8 mL of 6N HCl and 16 mL of 1M $CrCl_2$ solution and stirring of the sample for 2 hours under a constant flow of nitrogen gas. The released H_2S was guided through a trap filled with 7 mL of 0.1 M of a buffered citric acid/Na-citrate solution to trap $^{35}SO_4^{2-}$-containing aerosols. A second trap filled with 7 mL of 5 % (w/v) zinc acetate was used to precipitate H_2S as zinc sulfide. At the end of the distillation, the zinc acetate solution was quantitatively transferred into a scintillation vial with 8 mL of UltimaGold Cocktail (Perkin Elmer). Radioactivity of radiolabelled sulfide was quantified using a Tri Carb 2500 TR liquid scintillation counter (Packard Instruments, Meriden, United States).

3.2.3.5 Total cell counts

Cell counts were performed using a modification of the procedure of (Kallmeyer et al., 2008). In brief, 50 µL of sediment slurry were mixed with 50 µL of detergent mix (i.e. 36.8 g L^{-1} Na_2EDTA × 2 H_2O, 22.3 g L^{-1} Na-pyrophosphate × 10 H_2O and 5 mL TWEEN 80), 50 µL of methanol and 350 µL of ultrapure H_2O. This mixture was vortexed for 30 minutes and sonicated 4 × 1 sec at 10 % amplitude, using a Sonopuls HD 3200 ultrasonic homogenizer equipped with a microtip probe (Bandelin Electronic, Berlin, Germany). 50 µL of this solution were mixed with 5 µL of 1 % HF to dissolve fine mineral particles (Morono et al., 2009). After 10 minutes, the solution was filtered onto black 0.2 µm polycarbonate track-etched membrane filters (Ø 25 mm Cyclopore, Whatman International Ltd, Maidstone, England). Cells were stained with SYBR Green I (Molecular Probes Inc., Eugene, United States), mounted and counted by epifluorescence microscopy (Leica DM2000 microscope, 100 × magnification) with a blue filter set (Leica Filter Cube F1/RH, excitation filter λ = 490/15 to 560/25 nm, suppression filter at λ = 525/20 to 605/30 nm) and non-fluorescent immersion oil (Leica type F oil, $n_e^{23} = 1.518$, $v_e = 46$).

3.2.3.6 Intracellular and extracellular DNA extraction and quantification

The procedure of Alawi et al. (2014) was applied to extract eDNA and iDNA separately from single sediment samples. All extractions were performed in duplicates along with a negative control. In brief, we mixed 1.0 g of fresh sediment with 0.2 g of acid washed

polyvinylpolypyrrolidone (PVPP) and 2.5 mL of 0.1 M sodium phosphate buffer (Na-P-buffer). The sample slurry was centrifuged and the supernatant decanted off twice for a final volume of 7.5 mL. The supernatant was centrifuged for 45 min at 4700 × g to separate the iDNA (i.e. cell pellet, also containing viral particles) from the eDNA (i.e. supernatant). To avoid any DNA adsorption onto the rubber, we used 10 mL syringes without rubber and filtered the supernatant through 0.2 µm cellulose acetate syringe filters (Sartorius, Göttingen, Germany) to remove any residual PVPP. The filtrate was mixed with 3 times its volume of 6 M guanidine hydrochloride. 60 µL of silica particles were added to adsorb eDNA (Boom et al., 1990). After centrifugation, the supernatant was discarded and the eDNA-containing silica pellet rinsed in 150 µL of absolute ethanol and Tris-EDTA in equal amounts and centrifuged twice for complete drying. To desorb the eDNA, 150 µL of Tris-EDTA buffer (1 mM) were added to the silica pellet, vortexed and centrifuged. The final eDNA-containing supernatant was decanted off and stored. The desorption step was repeated to reach a final volume of 300 µL of eDNA extract.

The iDNA extraction was performed using the Mobio PowerSoil DNA extraction and isolation kit. The content of the PowerBead Tube with 60 µL of solution C1 and 500 µL of Na-P-buffer were added to a 15 mL centrifuge tube containing the cell pellet. The mixture was vortexed, sonicated for 6 min, heated twice for 5 min at 70 °C to lyse cells and centrifuged for 15 min at 4700 × g. The supernatant was processed in the same as the eDNA fraction adding 50 µL of silica particles. Final iDNA elution volume was 100 µL.

DNA concentrations of all samples were measured using a Qubit 2.0 fluorometer (Invitrogen, Carlsbad, United States) with 10 µL of DNA template, 1 µL of reagent and 190 µL of buffer solution. The Qubit fluorescent dye targets DNA specifically, as compared to UV absorbance techniques, which measure any compound absorbing at 260 nm (i.e. DNA, RNA, protein, free nucleotide, and excess salt). Measurements were performed in duplicates and the results are given as the average; error bars are one standard deviation.

3.2.3.7 Polymerase chain reaction

DNA extracts were purified following the Mobio PowerSoil experienced user protocol (www.mobio.com/) and eluted in 100 µL for eDNA and 65 µL for iDNA. Purified DNA extracts were diluted 20 times and 10 times for eDNA and iDNA, respectively, and used

as templates in polymerase chain reaction (PCR) amplifications. PCR was performed with 2.5 µL of DNA template, 12.5 µL of MangoMix (Bioline, Life Science Company, London, England), 0.5 µmol L^{-1} of each of the primers, 1 µL of $MgCl_2$ (25 mM) and 8 µL of Ultra-pure 18.2 MΩ PCR Water (Bioline). Negative controls were added to all PCR sets with 2.5 µL of molecular grade water as template. Amplifications of the bacterial small subunit (16S) rRNA gene were performed using the bacterial universal primer pair GC-Uni331F (5'- CGC CCG CCG CGC GCG GCG GGC GGG GCG GGG GCA CGG GGG GTC CTA CGG GAG GCA GCA GT-3') and Eub797R (5'-GGA CTA CCA GGG TAT CTA ATC CTG TT-3') (Brands et al., 2010) . PCR cycles were run as follows: 30 cycles of 95 °C for 1 min, 57 °C for 1 min, and 72 °C for 1 min, with a final extension step of 10 min at 72 °C. Amplifications of the archaeal 16S rRNA gene were performed using the archaeal universal primer pair GC-UA751F (5'- CGC CCG CCG CGC GCG GCG GGC GGG GCG GGG GCA CGG GGG GCC GAC GGT GAG RGR YGA A -3') and UA1204R (5'-TTM GGG GCA TRC IKA CCT-3') (Baker and Cowan, 2004). PCR cycles were run as follows: 35 cycles of 95 °C for 1.5 min, 60 °C for 1.5 min, and 72 °C for 1.5 min, with a final extension step of 10 min at 72 °C. For denaturing gradient gel electrophoresis (DGGE), 120 µL archaeal PCR product were concentrated to 25 µL using the Hi Yield PCR Clean-up and Gel-Extraction Kit (SLG Südlabor, München, Germany).

3.2.3.8 Denaturing gradient gel electrophoresis analysis

8 % polyacrylamide gels were prepared with a linear gradient from 35 to 60 % of the denaturants urea and formamide. The 100 % gradient solution was prepared using 1 mL of TAE (50 ×), 21 g urea, 20 mL of formamide, 10 mL of 40 % acrylamide/bis-acrylamide and molecular grade water for a final volume of 50 mL. The 0 % gradient solution was prepared without urea or formamide. Gels were prepared with 17.5 mL of each solution, plus 50 µL APS and 50 µL TEMED for polymerization. 20 µL of PCR product and 20 µL of blue stain were loaded for each sample. 10 µl of standard (i.e. 13 previously selected bands) with 10 µL of blue stain were loaded in the center and on each side of the gels to reference band positions. Electrophoresis was run at 100 V for 16 h in 1 × TAE buffer at 60 °C. Gels were stained for 30 min in 2.5 µL of SYBRGold nucleic acid gel stain (10,000 time concentrates, Invitrogen) diluted in 25 mL 1 × TAE buffer. Gels were photographed under UV light. The Strati-Signal software (Ndiaye et al., 2012; Vuillemin et al., 2011) was then used to analyze DGGE gel pictures. Band

numbers, intensity values and pattern lengths were extracted (Supplemental material) to calculate Shannon indices. The Shannon index is calculated as follows: Shannon = -∑ (*ni/N*) × log (*ni/N*), where *ni* is the height of each peak and *N* the sum of all peak heights extracted from RGB intensity curves of each sample (Boon et al., 2002; Fromin et al., 2002).

3.2.3.9 Band sequencing and phylogenetic analysis

In total, 131 bands were excised from DGGE gels under UV light. Gel bands were eluted in 20 µL MΩ PCR Water (Bioline) and used as templates in PCR mixtures as described above without GC-clamp on the forward primers. PCR cycles were run as follows: 3 cycles of 95 °C for 1 min, 57 °C for 1 min, and 72 °C for 1 min followed by 27 cycles of 95 °C for 30 sec, 57 °C for 30 sec, and 72 °C for 30 sec with a final extension step of 10 min at 72 °C for *Bacteria*, and 35 cycles of 95 °C for 50 sec, 58 °C for 50 sec, and 72 °C for 50 sec with a final extension step of 10 min at 72 °C for *Archaea*. PCR products were run on 1 % agarose gels and targeted DNA bands excised under UV light to remove residual dimers. DNA bands were purified using the Hi Yield PCR Gel-Extraction Kit (SLG Südlabor) with final elution in 25 µL of Ultra-pure 18.2 MΩ PCR Water (Bioline). DNA concentrations were checked on a NanoPhotometer P330 (Implen, München, Germany) and DNA extracts sent to GATC Biotech AG (European Custom Sequencing Centre, Köln, Germany) for Sanger sequencing using primers Eub797R and UA751F. Sequences were aligned on Sequencher v. 5.1 (Gene Codes Corporation, Ann Arbor, United States) and primers selectively cut off. Chimeras were detected using the online program Bellerophon (Huber et al., 2004). All DGGE sequences have been deposited in the GenBank database under accession numbers KR091588 to KR091718.

The SINA online v.1.2.11 (Pruesse et al., 2012; Pruesse et al., 2007) was used to align, search and classify our sequences. Closest match sequences were downloaded from the SILVA database as taxonomic references, uploaded on the ARB platform and plotted into phylogenetic trees using the Maximum Likelihood method with the RAxML algorithm with advanced bootstrap refinement from 100 replicates (Ludwig et al., 2004). DGGE fragment sequences were added to the RAxML tree using the Bacteria Positional Variability by Parsimony algorithm. Two separate phylogenetic trees were plotted for *Bacteria* and *Archaea* with iDNA and eDNA sequences together

(Supplemental material). Sequences from representative taxa were then selected to build one single tree based on 15 eDNA and 15 iDNA fragments (Fig. 3.4).

3.3 Results

3.3.1 Water column

CTD water column profiles (Fig. 3.2) obtained at each site provided evidence for weak thermal stratification occurring around 25 m water depth with a corresponding drop of 1.5°C. Below this depth, water column temperatures did not vary significantly, with less than 1°C decrease in the subsequent 175 m. Oxygen profiles indicated that the water column is fully oxic (250 µM) down to 60 m depth where oxygen concentration declines gradually over the following 70 m, the deepest part of the water column is anoxic. Thus, the water-sediment interface could be considered oxic at the shallow site (i.e. 60 m depth) and anoxic at the intermediate (i.e. 153 m depth) and deep sites (i.e. 200 m depth). Chlorophyll *a* fluorescence profiles showed that phytoplankton biomass is highest at 50 m water depth. Transmission profiles revealed negative peaks around 50 and 130 m depth indicating higher concentrations of suspended particles in these depth intervals.

3.3.2 Pore water geochemistry

Sodium (Na^+), calcium (Ca^{2+}) and magnesium (Mg^{2+}) were the only cations we were able to detect in the pore water by ion chromatography, only Ca^{2+} and Mg^{2+} were quantified. Ca^{2+} and Mg^{2+} profiles (Fig. 3.3A) did not show much variability with depth, concentrations were around 25 µM and 130 µM for Ca^{2+} and Mg^{2+}, respectively. The intermediate site displays one single significant peak at about 20 cm depth. At the deep site, Mg^{2+} values tend to increase slightly with depth to values around 150 µM. NH_4^+ concentrations in the uppermost pore water sample were similar at all three sites (ca. 22 µM) and showed a general increase with depth, the gradient became increasingly steeper from the shallow to the deep site (Fig. 3.3A), leading to concentrations of 40, 60 and 130 µM at the bottom ends of the cores, respectively. Similarly, dissolved Fe^{2+} concentrations increased from the shallow to the deep site and with sediment depth, with values ranging from 0, 5 and 35 µM in surface sediment to 10, 20 and 50 µM at the bottom of the core, respectively. The Fe^{2+} profile of the deep site exhibits a slight

excursion to lower values in the upper 10 cm of sediment, below this depth values increase constantly like at the other sites.

Chloride (Cl^-) and sulfate (SO_4^{2-}) were the main inorganic anions in the pore water. Nitrate, nitrite and phosphate were below detection limit (5 µM). Profiles for Cl^- (Fig. 3.3A) displayed constant concentrations around 40 to 20 µM with little difference between sites although with a general decrease with increasing water depth. Some minor peaks up to 60 µM could be observed in the upper 15 cm at all sites. SO_4^{2-} concentrations were mainly in the single µM range and often close to the quantification (5 µM) and detection (2 µM) limits. At the shallow site, concentrations were generally higher, with values about 20 µM in the uppermost 4 cm, but decreasing gradually to values between 2 and 5 µM at the base of the core. At the intermediate site, sulfate was detectable at all depths but the measurements were close to or below the quantification limit, except for two peaks of 40 µM and 15 µM at 0.5 and 22.5 cm depth, respectively. At the deep site, all SO_4^{2-} concentrations were around the detection limit.

Respective ion concentrations measured directly above the water-sediment interface in cores from the shallow, intermediate and deep site are given in Table 3.1.

Table 3.1: *Bottom water geochemistry of Lake Towuti. Water samples were retrieved at the water-sediment interface in cores from the shallow, intermediate and deep site and measured by ion chromatography. Values are displayed in [µM] followed by one standard deviation.*

Geochemistry of bottom waters [µM]						
Site	**Depth**	**Ca^{2+}**	**Mg^{2+}**	**Cl^-**	**SO_4^{2-}**	**NH_4^+**
Shallow	60 m	28.6 ± 6.1	145.4 ± 8.9	37.3 ± 0.9	20.2 ± 0.7	< 6
Intermediate	153 m	25.3 ± 0.1	134.8 ± 7.0	38.4 ± 1.9	11.9 ± 0.4	20.3 ± 0.8
Deep	200 m	23.8 ± 2.6	148.7.± 4.3	20.5 ± 0.5	11.8 ± 0.2	13.8 ± 0.2

3.3.3 Potential sulfate reduction rates

Potential rates of sulfate reduction and their depth distribution (Fig. 3.3A) differed significantly between sites. At the shallow site, we found maximum rates of ca. 7 nmol cm^{-3} day^{-1} within the upper 10 cm of sediment. Below this depth, SRR decreased sharply to ca. 2 nmol cm^{-3} day^{-1}. The intermediate site displayed two peaks of elevated SRR of ca. 11 and 8 nmol cm^{-3} day^{-1} at 2 and 22 cm depth which corresponds to anomalous peaks in sulfate concentrations; at all other depths, rates were minimal (< 2

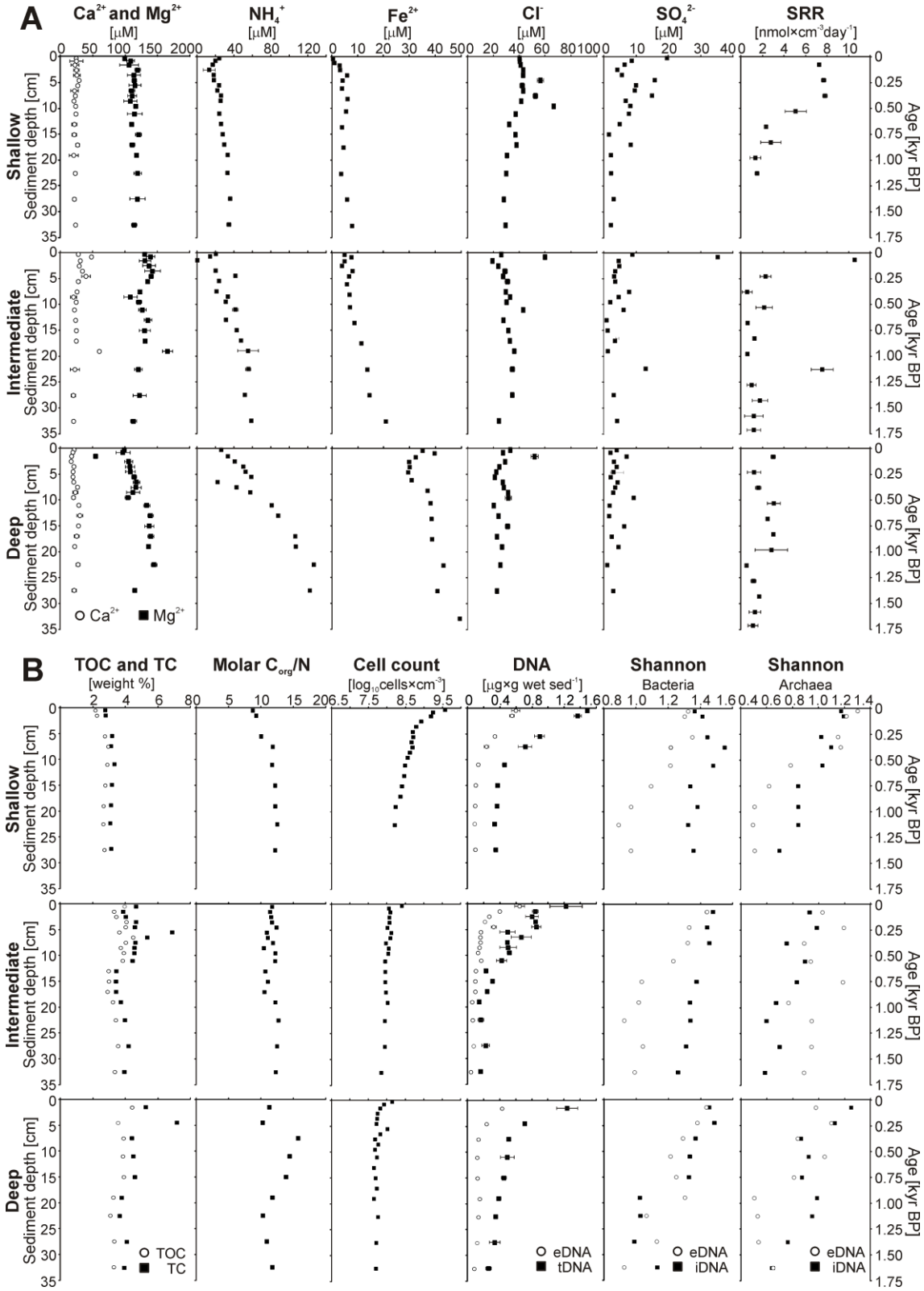

Figure 3.3: *Multiple profiles established on short sediment cores.* ***(A)*** *From left to right: Pore water Ca, Mg, NH_4, Fe, Cl and SO_4^{2-} concentrations [µM] as well as potential sulfate reduction rates [nmol × cm^{-3} day^{-1}]* ***(B)*** *From left to right: Total organic carbon and total carbon [weight %]; molar C_{org}/N ratio measured in bulk sediments; Total cell counts [log_{10} cells × cm^{-3}]; concentrations of extracellular DNA (grey dots) and total DNA (black squares) [µg × g wet sed^{-1}], with distance between the two curves corresponding to intracellular DNA concentrations;*

Shannon index established from bacterial and archaeal DGGE gel features, with eDNA (grey dots) and iDNA (black squares) displayed separately; range-weighted richness index for bacterial DNA (square) and archaeal DNA (dots), with eDNA (grey) and iDNA (black) displayed separately.

nmol cm^{-3} day^{-1}). At the deep site, rates were generally lower than at the other sites (1 to max. 3 nmol cm^{-3} day^{-1}). Altogether, the measurements demonstrated that viable sulfate-reducing bacteria (SRB) were present at all three sites, but were more active at the shallow site. The results also showed a general decrease in SRR with increasing water depth due to decreasing bottom water SO_4^{2-} concentrations and hence lower diffusive fluxes of sulfate into the sediment. Because SO_4^{2-} concentrations were in many cases barely detectable (> 2 µM) and well below the lower limit of quantification (5 µM), the absolute values of the potential SRR have to be carefully considered. However, the data clearly show that the sulfate pool is turned over within days, implying strong internal recycling.

3.3.4 Organic matter

TOC values (Fig. 3.3B) increased from the shallow to the deep site. The shallow site had TOC contents around 2 % in the upper few centimeters with a subsequent increase by about 1 % and constant values over the rest of the core. The intermediate site exhibited oscillating values between 4.5 and 3.5 % in the uppermost 10 cm, continuing with lower and more constant values of ca. 3 to 3.5 % down to the base of the record. At the deep site, TOC concentrations decreased gradually from 4.5 % in the uppermost section to 3 % at the base of the core. In parallel to these results, TC peaks around 5 cm depth at both the intermediate and deep site indicated the likely presence of authigenic carbonates (Fig. 3.3B).

The C_{org}/N ratio profiles resembled those of TOC, with values generally increasing from the shallow site to the deep site. Overall, values increased gradually from 8.5 to 12.5 at the shallow site and varied in between 10.5 and 12.5 at the intermediate site. At the deep site, the ratios ranged from 10.5 to 15.5 in the uppermost samples and gradually decreased to 11.5 in the lower part. Altogether, TOC and C_{org}/N ratio profiles appear to reflect the different bottom water oxygenation conditions at the three sites as values generally increase with water depth.

3.3.5 Total cell counts

Total cell counts (Fig. 3.3B) were much higher at the shallow site than at the other sites. At all three sites, numbers declined steeply in the upper 5 cm, followed by a more gradual decrease over the remainder of the core. Compared to the other two sites, cell concentrations at the shallow site were up to 31 times higher in the 0-1 cm depth interval (i.e. $\log_{10}$ = 9.6, 8.4 and 8.1) and still up to 3 times higher at the base of the cores (i.e. $\log_{10}$ = 8.2, 7.8 and 7.7). The profiles from the intermediate and deep site were very similar, although values were generally lower at the deep site.

3.3.6 Intracellular and extracellular DNA concentrations

Concentrations of eDNA (Fig. 3.3B) were very similar at all three sites, with concentrations around 0.6 µg g^{-1} in the uppermost layer, decreasing to ca. 0.2 µg g^{-1} at 10 cm depth and a final decline to minimum values (< 0.1 µg g^{-1}) at the bottom of the core. Total DNA (tDNA = eDNA + iDNA) concentration profiles mimic those of eDNA, with concentrations of 1.6, 1.2, 1.2□µg g-1 in the surface layer and 0.4, 0.2 and 0.3 µg g^{-1} in the bottom layer for the shallow, intermediate and deep site, respectively. Results showed that concentrations of eDNA and iDNA display similar trends and that iDNA was the dominant fraction in total DNA.

In order to assess the recovery rate of cells and respective amount of extracted iDNA with this procedure, iDNA concentrations were divided by the corresponding cell densities of each sample and results reported in femtogram (fg) of DNA per cell. Averaged values per site were 1.0, 3.7 and 6.5 fg DNA $cell^{-1}$ at the shallow, intermediate and deep site, respectively (data not shown). Published values range from 1.6 to 8.9 fg DNA $cell^{-1}$ (Bakken and Olsen, 1989; Button and Robertson, 2001). In nearby Lake Matano, phosphorus limitation resulted in reduced RNA concentrations per cell (Yao et al., 2015). Similarly in Lake Towuti, the variable sorption capacity of the sediment could influence P availability and DNA concentration per cell. Concerning the presence of viral DNA (Torti et al., 2015), protein capsids are not quantified as DNA with a Qubit 2.0 fluorometer. Moreover, sediment particles also strongly adsorb virions and multiple studies of freshwater sediments showed a low impact of viruses on bacterial mortality (Filippini and Middelboe (2007) and references therein). We acknowledge that viral DNA should be found in our extracts, albeit as a minor fraction

as we did not use a specifically adapted extraction protocol necessary to lyse the capsids (Danovaro and Middelboe, 2010).

3.3.7 Bacterial and archaeal fingerprinting

DGGE provided an assessment of the relative preservation of eDNA at the three sites along with a first fingerprinting of bacterial and archaeal diversity associated with both eDNA and iDNA fractions. In general, eDNA gel features faded with increasing sample depth and led to the transformation of clear bands into smears and further disappearance (Supplemental material). At all three sites, Shannon indices of bacterial eDNA (Fig. 3.3B) decreased almost linearly with depth, whereas those of bacterial iDNA display different trends at each site. Values increased within the upper part of the core before gradually decreasing at the shallow site, decreased linearly at the intermediate site and sharply dropped in the lower half of the core at the deep site. Values of archaeal eDNA (Fig. 3.3B) rapidly declined in the upper 20 cm and stayed minimal below that depth at the shallow site, showed high scatter and little decrease at the intermediate site and dropped at ca. 20 cm followed by constant values at the deep site. Shannon values of archaeal iDNA were similar for each site, with fluctuations in upper sediments and gradual decrease in lower sediments, although the intermediate site generally displayed lower values. Richness indices (Supplemental material) clearly demonstrated the predominance of *Bacteria* over *Archaea*.

3.3.8 Phylogeny of sequenced DNA fragments

Sequences of eDNA were mainly representative of aerobic and anaerobic heterotrophs, with taxa identified as *Actinobacteria*, *Nitrospirae*, *Chloroflexi* and *Thermoplasmatales* (Supplemental material). Taking into account the local conditions of the sediment, these sequences were likely related to microorganisms evolving in the water column and preserved as eDNA in the sediment. We considered eDNA sequences clustering among iDNA-related taxa to derive from cell lysis in the sediment (e.g. *Betaproteobacteria, Deltaproteobacteria, Firmicutes*).

Taxa identified from iDNA fragments were mostly related to *Beta-* and *Deltaproteobacteria*, *Firmicutes* and *Methanomicrobiales* (Fig. 3.4 and Supplemental material)**.** Sequences of *Betaproteobacteria* plotted among *Rhodocyclaceae* with closest cultivated taxa represented by *Thiobacillus* and *Denitratisoma*. Sequences of *Deltaproteobacteria* were closest to *Desulfovibrio*, *Desulfuromonas, Deferrisoma,*

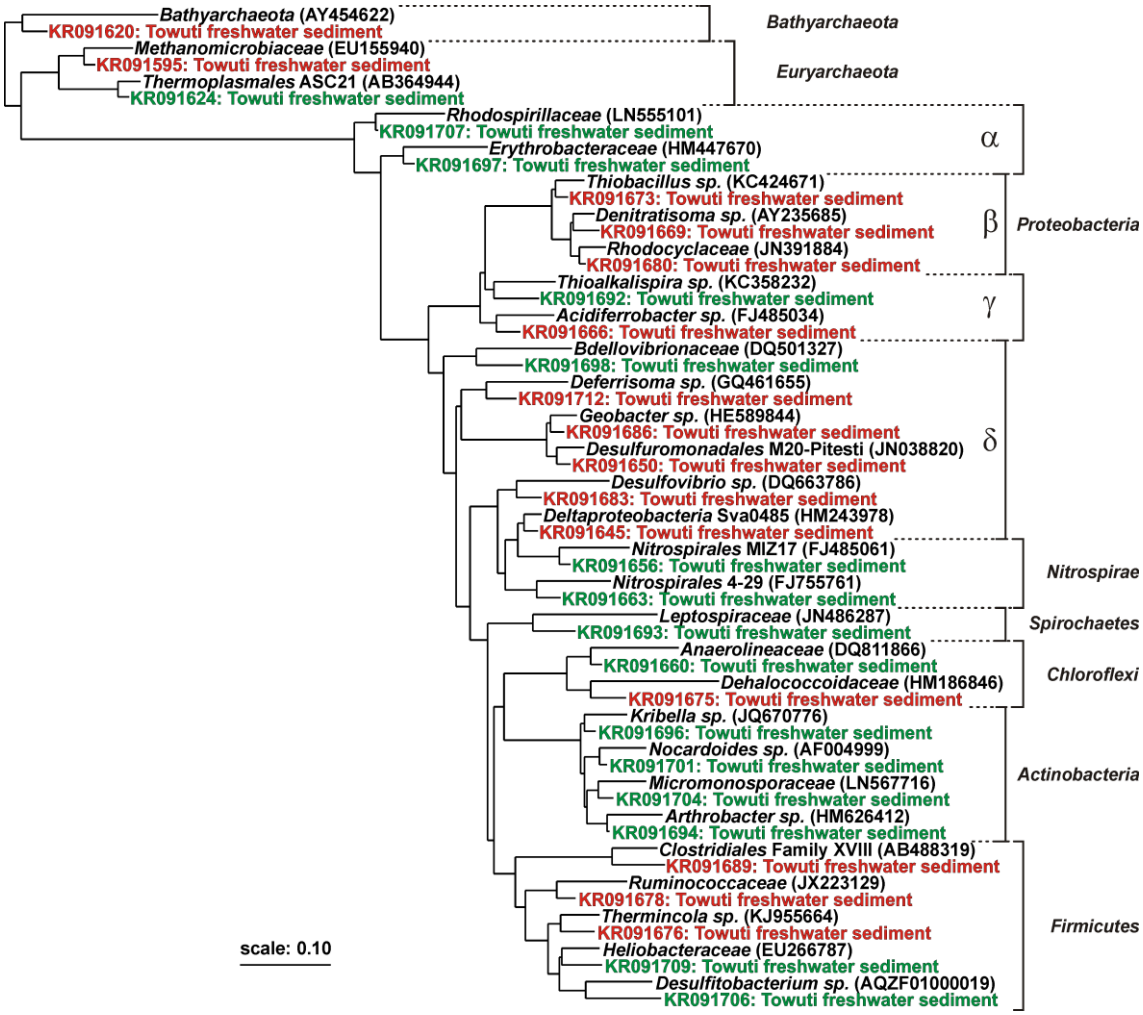

Figure 3.4: *Phylogenetic tree established for intracellular and extracellular DNA fragments obtained from DGGE gels. Among 131 sequences, 30 were selected as representative taxa to build a Maximum Likelihood RAxML tree. Extracellular DNA sequences (green) are indicative of aerobic and anaerobic heterotrophs, among which some can be assigned to the lake oxic (e.g. Nitrospirae, Actinobacteria) and anoxic water column (e.g. Chloroflexi, Firmicutes). Intracellular DNA sequences (red) are closely affiliated with known sulfate and iron reducers (e.g. Deltaproteobacteria, Firmicutes). Concomitant presence of taxa related to Clostridiales and Methanomicrobiales indicates a potential for heterotrophic production of fermentative hydrogen and methane. Boldface types signify database references with sequence accession numbers in parentheses.*

Geobacter and candidate order Sva0485. Together with the potential sulfate reduction rates, these sequences provided evidence for the presence of sedimentary SRB along with microorganisms capable of dissimilatory sulfur and ferric iron reduction at all three sites. Sequences of *Firmicutes* related to *Thermincola* supported the presence of iron reducing bacteria. Finally, taxa among *Ruminococcaceae and Clostridiales* were representative of heterotrophic anaerobes, whose concomitance with

Methanomicrobiales indicated that fermentative hydrogen can be produced via ferredoxin reduction and used during methanogenesis (Hallenbeck, 2009).

3.4 Discussion

3.4.1 Water column conditions and organic matter sedimentation

Varying oxygenation levels in the water column, especially at the water-sediment interface are expected to lead to differences in production, degradation and burial of OM in sediments at the three sites (Katsev and Crowe, 2015, and references therein). Chlorophyll *a* concentrations are highest around 50 m water depth, while transmission profiles indicate suspended matter close to the oxycline at 130 m water depth (Fig. 3.2), pointing towards a redox interface similar to the one observed in the water column of nearby Lake Matano, although less steep (Crowe et al., 2008b). At the intermediate site, a long-term shift in the oxycline was recorded during the mid-Holocene in the form of elevated ferric iron and siderite (i.e. $FeCO_3$) concentrations (Costa et al., 2015). Due to the low sedimentation rates (i.e. 2 mm $year^{-1}$; Vogel et al., 2015), redox fluctuations would be hard to detect at our sampling resolution.

TOC contents indicate increased OM burial from the shallow to the deep site (Fig. 3.3A), associated with a shift towards more recalcitrant OM composition (i.e. higher C_{org}/N ratio). Although degradation processes in an anoxic water column are generally slower (Katsev and Crowe, 2015), iron reduction below the oxycline can foster desorption of labile OM and microbial uptake of nitrogen and phosphorus (Zegeye et al., 2012), thereby increasing carbon burial linked to bacterial production. Remineralization of organic compounds leads to the production of NH_4^+, which can be oxidized or accumulate, depending on the presence of suitable reactants in the water column. NH_4^+ concentrations in bottom waters (Tab. 3.1) indicate that degradation of sinking particulate OM is indeed continuous in the water column, leading to the accumulation of less reactive organic material at the deep site (Amon and Benner, 1996). This interpretation is also consistent with the diverse taxa identified from our eDNA sequences, which corresponded to both aerobic and anaerobic heterotrophs, namely *Actinobacteria, Nitrospirae*, *Chloroflexi* and *Thermoplasmatales,* and secondarily *Alpha-* and *Gammaproteobacteria* (Fig. 3.4 and Supplemental material). Although we did not detect any photoautotrophs, certain elements can still be assigned

to planktonic assemblages coming from the epilimnion (e.g. *Nitrospirales*) and hypolimnion (e.g. *Anaerolineales*).

3.4.2 Pore water geochemistry

High Ca^{2+} and Mg^{2+} concentrations in pore waters (Fig. 3.3A) likely reflect continued weathering of mafic/ultramafic minerals derived from the catchment of the Malili Lake system (Kadarusman et al., 2004). Although fairly constant, variations in these profiles could possibly imply precipitation and/or dissolution of authigenic carbonates (i.e. Ca-Mg-$FeCO_3$) within the sediment. At the intermediate and deep site, the presence of authigenic carbonates can be inferred from peaks in TC profiles. The diagenetic sequence known for freshwater sediments in relation to pore water geochemistry (i.e. Ca-Mg siderite, calcite, ankerite, dolomite) suggests the formation of early diagenetic siderite (Berner, 1980; Matsumoto and Iijima, 1981), which is consistent with the decline in dissolved Fe^{2+} concentrations at the deep site. Lake Matano and Lake Towuti are both iron-rich but also extremely low-sulfate environments, far lower than most aquatic environments studied to date (Crowe et al., 2014). Moreover, microbial reduction processes in the water column likely take place at or directly below the oxycline, as shown for SO_4^{2-} concentrations in Lake Matano, which decrease drastically along with a rapid increase of dissolved Fe^{2+} (Crowe et al., 2008a). In Lake Towuti, SO_4^{2-} concentrations measured at the water/sediment interface decreased from the shallow to the deep site (Tab. 3.1), supporting our assumption that sulfate reduction already takes place in the anoxic bottom water of the intermediate and deep site. As a result pore water SO_4^{2-} concentrations in the uppermost sediment samples decreased towards the deep site and were rapidly depleted with sediment depth at all sites. Pore water Fe^{2+} concentrations show the opposite trend, increasing from the shallow to the deep site and with core depth, showing an increasingly steeper gradient between sites with maximum values around 45 µM (Fig. 3.3A). The production, consumption and dynamics of NH_4^+ in bottom waters seemed to differ between the three sites as indicated by their respective concentrations (i.e. < 6, 20 and 13 µM) and the very similar NH_4^+ concentrations in the uppermost sediment sample at all three sites (ca. 25 µM). The NH_4^+ profile of the deep site is indeed the only one that clearly indicates NH_4^+ diffusion out of the sediment into the bottom waters. Whereas nitrification could take place in the oxic bottom waters of the shallow site, the potential accumulation of NH_4^+ in the anoxic bottom waters of the two other sites remains unclear.

3.4.3 Sediment microorganisms and extracellular DNA remineralization

Several studies showed that bacterial abundance and diversity in lake sediments correlate with environmental parameters such as salinity, pH, OM content, and sediment depth (Borsodi et al., 2013; Nam et al., 2008; Zeng et al., 2009), and can also reflect climatic variations due to forcing of conditions during sediment deposition (Dong et al., 2010; Vuillemin and Ariztegui, 2013; Vuillemin et al., 2014). Lake Towuti's surface sediments are characterized by comparatively high cell densities that decrease from the shallow to the deep site. At all sites, cell counts decrease by one order of magnitude over the uppermost 5 cm below the water-sediment interface and remain more or less constant over the rest of the core (Fig. 3.3B). The corresponding iDNA concentrations follow a similar trend, whereas Shannon indices show more variability between the three sites. Potential SRR measurements with radiotracer (Fig. 3.3A) further demonstrate that SRB are present and viable at all sites, but are more active at the shallow site, showing some correspondence to Shannon indices. We interpret these data as the positive response of bacterial populations to geochemical conditions corresponding with higher bottom water SO_4^{2-} concentrations and increased burial of labile OM and reactive ferric iron into the sediment.

With regard to recording of past lake conditions by eDNA, water temperatures of Lake Towuti are approximately 28 C° throughout the year, which is rather unfavorable for eDNA preservation (Lindahl, 1993; Renshaw et al., 2015). Although sorption capacities in the sediment were expected to vary between the three sampling sites, eDNA distribution patterns are similar, displaying a rapid decrease in the uppermost 5 cm followed by constant but low concentrations over the rest of the cores (Fig. 3.3B). The decline of eDNA Shannon indices also indicates a gradual loss of genetic information associated with the degradation and shortening of eDNA sequences over time (Corinaldesi et al., 2008). Such decrease as a function of sediment depth can be attributed to a combination of sediment sorption capacity, microbial uptake and degradation as well as rates of cell lysis. We argue that the observed lower eDNA concentrations result from an overall decrease in metabolic activity and cell lysis rate coupled with its desorption from Fe (oxy)hydroxides due to iron reduction, followed by immediate degradation (Crowe et al., 2007; Glasauer et al., 2003; Pinchuk et al., 2008). In the long term, eDNA preservation would greatly depend on the stability of ferric

mineral phases and metabolic turnover rates. In this context, preliminary results indicate that reactive ferric iron persist down to 15 m sediment depth at concentrations up to nearly 2 wt% (Simister et al., 2016), suggesting that microbial Fe-reduction might be limited by organic matter rather than reactive iron availability.

3.4.4 Phylogeny of intracellular DNA and presumed metabolic processes

Microbial fingerprinting (Fig. 3.4 and Supplemental material) revealed the presence of microorganisms related to taxa commonly known for iron and sulfate reduction as well as methanogenesis, providing anecdotal support that the autochthonous microbial communities have the metabolic capacity for these processes. Among *Proteobacteria*, certain taxa were affiliated with *Denitratisoma* (Fahrbach et al., 2006), *Thiobacillus* (Haaijer et al., 2006) and *Acidiferrobacter* (Hallberg et al., 2011), indicating putative capacity for both lithotrophic and organotrophic processes driven through use of reduced sulfur and iron as electron donors. However, these *Beta-* and *Gammaproteobacteria* typically exhibit metabolic versatility with the capacity to shift between different modes of facultative metabolisms (Ferguson et al., 1987; Hiraishi and Hoshino, 1984; Masters and Madigan, 1983), making it impossible to assess metabolism from taxonomic information alone.

Interestingly, sequences of *Deltaproteobacteria* at the shallow and intermediate site included taxa assigned to the candidate order Sva0485 and *Desulfovibrio*, which are often reported as part of SRB consortia (Bar-Or et al., 2015; Kleindienst et al., 2014). These sequences were correspondingly identified in sediments with the highest measured SRR. In addition, detection of *Desulfuromonas* M20-Pitesi, *Deferrisoma* and *Geobacter*-related sequences may indicate that the metabolic capacity to reduce sulfur and iron is evenly distributed across all three sites (Greene, 2014; Slobodkina et al., 2012). DGGE fragments affiliated with *Thermincola* also point at a metabolic potential for iron reduction (Zavarzina et al., 2007). In addition, taxa related to *Ruminococcaceae* and *Clostridiales* were representative of heterotrophic anaerobes that can produce fermentative hydrogen via ferredoxin (i.e. Fe_2S_2 protein cluster) reduction (Hallenbeck, 2009). Their concomitance with *Methanomicrobiales* suggests that H_2/CO_2 reduction is a likely pathway for methane production (Kaster et al., 2011; Thauer et al., 2008), although formate and alcohols could also be used (Oren, 2014).

Together, our measurements of potential sulfate reduction and our findings of microbial taxa commonly involved in microbial sulfate and iron reduction suggest that ferruginous sediments support microorganisms that degrade organic matter via sulfate reduction, in spite of the extremely low sulfate concentrations, in collaboration with diverse iron reducing bacteria, fermenters and methanogens. Seemingly, such complementary metabolisms imply desorption of OM following iron reduction and its remineralization to methane. The low pore water SO_4^{2-} concentrations (single µM) and the relatively high potential SRR (single to tens of nmol cm^{-3} d^{-1}) also demonstrate that the sulfate pool is turned over within days. This suggests that reoxidation of reduced sulfur compounds occurs through a cryptic S-cycle driven by iron (Hansel et al., 2015; Norði et al., 2013) in order to maintain these high SRR. Moreover, the persistence of ferric iron in deeper sediment and the potential for methane production could even involve processes of anaerobic oxidation of methane (Hallam et al., 2004).

3.5 Conclusions

Stratification of Lake Towuti's water column gave rise to different biogeochemical conditions in deeper parts of the water column and at the water-sediment interface at the three study sites. Respiration processes led to the gradual depletion of electron acceptors with increasing water depth, with microbial Fe(III) and SO_4^{2-} reduction occurring below the oxycline. As a result, sinking OM was partially desorbed from Fe(oxy)hydroxides, allowing microbial degradation of the labile fraction. Microbial uptake of nitrogen and phosphorus seemed to have fostered bacterial production, thereby increasing carbon burial while NH_4^+ accumulated in anoxic bottom waters. Sequences obtained from sediment eDNA confirmed such microbial degradation with some aerobic and anaerobic heterotrophs, potentially linked to the epilimnion and hypolimnion. Thus, due to different settling times and bottom water redox conditions, sediments at the shallow site exhibit more fresh and labile OM as well as higher pore water SO_4^{2-} concentrations, whereas the deep site had the highest TOC content and most refractory OM along with lowest SO_4^{2-} concentrations. As a consequence, cell densities and potential SRR were highest at the shallow site.

Consistently with these results, iDNA fingerprinting revealed the presence of taxa common in SRB consortia, such as *Desulfovibrio* and candidate order Sva0485,

providing evidence that SRB are present and viable in all samples despite the extremely low SO_4^{2-} concentrations. Likewise, iDNA fragments affiliated with *Deferrisoma*, *Geobacter* and *Thermincola* indicated bacteria related to known iron reducers at all sites. In addition, the identification of *Ruminococcaceae*, *Clostridiales* and *Methanomicrobiales* suggests that fermentative hydrogen can be produced via ferredoxin reduction and used during methanogenesis. These results attest that Lake Towuti's sediments support microorganisms displaying complementary metabolic capabilities related to sulfur, iron and methane cycling. Relatively high SRR could be maintained in these ferruginous sediments through reoxidation of reduced sulfur compounds by iron reduction, which would also lead to OM desorption from reactive iron surfaces and allow its remineralization to methane. We also show that eDNA was substantially degraded in the uppermost sediment layers at all three sites, leading to the gradual loss of genetic information. The possible reasons for this were lower adsorption in the sediment due to anaerobic respiration of ferric iron, uptake as a microbial substrate, and decreased rates of cell lysis with depth. Since reactive ferric iron seems to persist in deeper sediment layers, microbial reduction might be limited by a lack of organic substrates rather than by the availability of reactive iron.

To conclude, changes in redox chemistry, whether they be related to climate or in-lake processes, appear to lead to variable burial of OM, electron acceptors and reactive metal species in the sediments. On the entire lacustrine record, a long-term shift to oxic conditions would result in a persistence of electron acceptors in deeper sediments and could foster the maintenance of a metabolic activity by the subsurface biosphere.

3.6 Acknowledgements

We thank Tri Widiyanto and his staff from the Indonesia Research Center for Limnology for their administrative support in obtaining the Scientific Research Permit. Jan Axel Kitte, Carriayne Jones and Céline C.P. Michiels are thanked for their assistance during sampling at Lake Towuti, and PT Vale Indonesia for field support. Maria Schindler's help in the cell extraction procedure and Dyke Scheidemann's assistance in elemental analysis are kindly acknowledged.

This study was financially and logistically supported by the ICDP priority program of the Deutsche Forschungsgemeinschaft (DFG Schwerpunktprogramm)

through grants to Jens Kallmeyer (KA 2293/8-1) and Aurèle Vuillemin (VU 94/1-1); the Swiss National Science Foundation (SNSF Grant P2GEP2_148621 to Aurèle Vuillemin); the Helmholtz Center Potsdam, German Research Center for Geoscience (GFZ) and an NSERC Discovery grant (0487) to Sean Crowe.

3.7 Supplemental Material

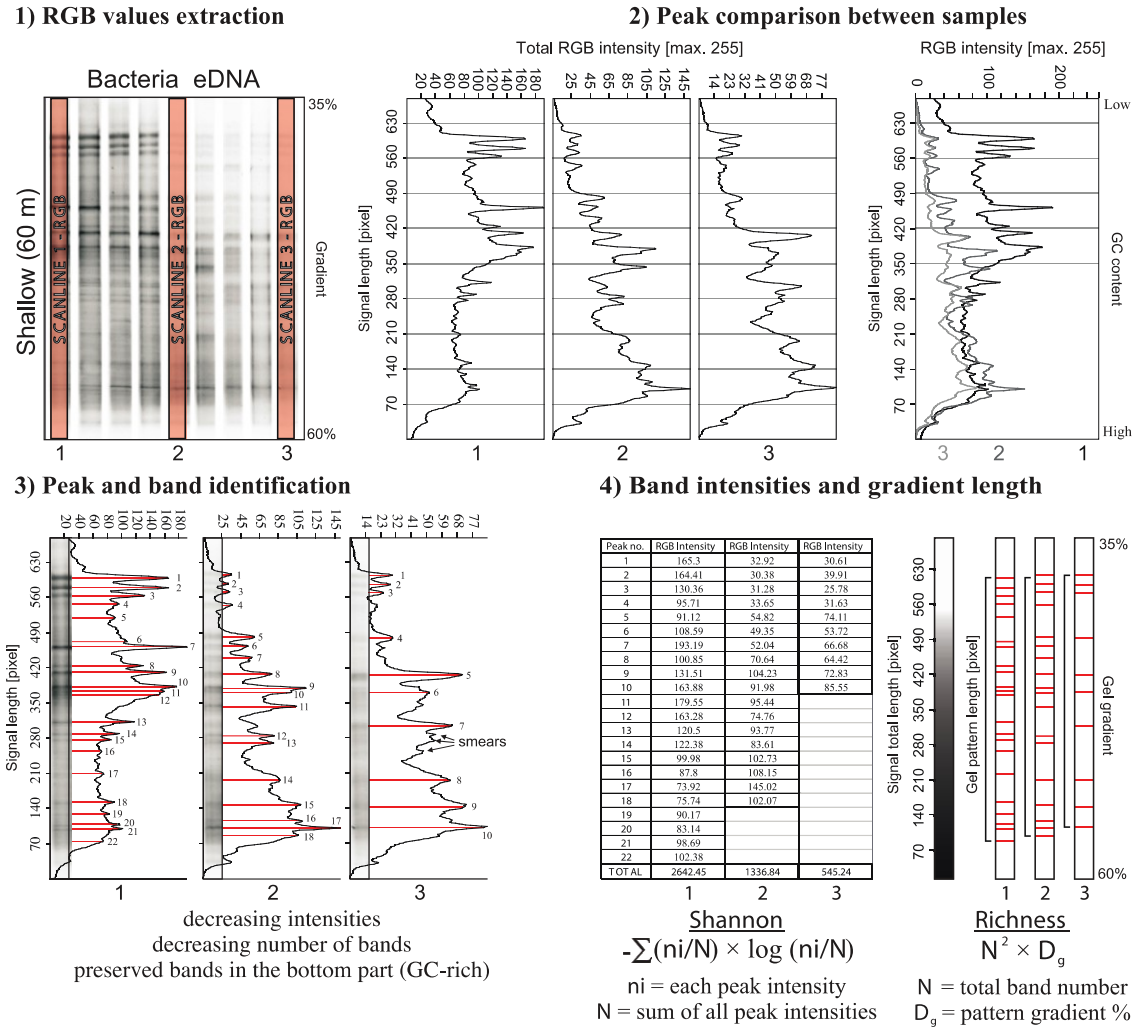

Figure S 3.1: *Signal extraction from DGGE gels using the image software Strati-Signal. Scanlines extract values from selected channels, presently red ®, green (G) and blue (B) simultaneously, transforming image gel patterns into quantitative spectra (1, 2). Peaks corresponding with bands are identified automatically or manually (3). Respective positions and intensities are exported into a .txt file and used for statistical purposes (4). The present example shows that intensity and number of bands decrease in gel patterns with sample depth. Smears in spectra are indicative of residual bands not always visible on gel images.*

Shallow (60 m)				
	Bacteria		*Archaea*	
Depth	**iDNA**	**eDNA**	**iDNA**	**eDNA**
[cm]	[bd nb]	[bd nb]	[bd nb]	[bd nb]
0.5	23	22	16	21
1.5	27	20	17	17
5.5	30	20	11	15
7.5	32	17	13	16
11	31	16	11	7
15	21	12	7	5
19	21	8	7	4
22.5	22	7	7	4
27.5	22	6	5	4

Intermediate (153 m)				
	Bacteria		*Archaea*	
Depth	**iDNA**	**eDNA**	**iDNA**	**eDNA**
[cm]	[bd nb]	[bd nb]	[bd nb]	[bd nb]
1.5	32	29	9	11
4.5	29	23	10	16
7.5	30	23	6	8
11	(16)	19	8	9
15	25	12	7	16
19	23	11	5	6
22.5	23	9	4	9
27.5	23	12	5	9
32.5	19	10	4	8

Deep (200 m)				
	Bacteria		*Archaea*	
Depth	**iDNA**	**eDNA**	**iDNA**	**eDNA**
[cm]	[bd nb]	[bd nb]	[bd nb]	[bd nb]
1.5	30	28	19	10
4.5	32	25	14	13
7.5	24	21	9	7
11	22	18	10	12
15	22	19	9	7
19	11	21	11	4
22.5	11	12	9	4
27.5	10	14	7	4
32.5	14	9	5	5

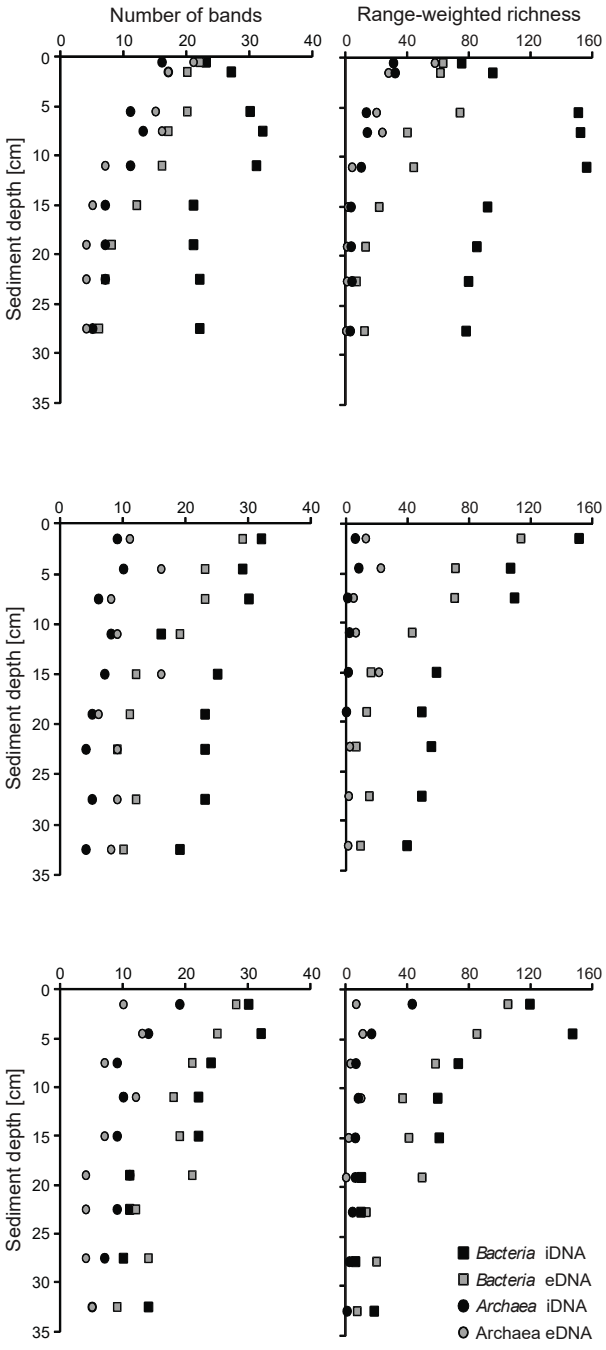

Figure S 3.2: *Summary of the number of bands extracted per sample. Tables list the number of bands counted for each sample based on their respective DGGE gel patterns (left), followed by band numbers plotted against sample depth for the three sites (center) and range-weighted Richness calculated as described in Fig. S 3.1 (right).*

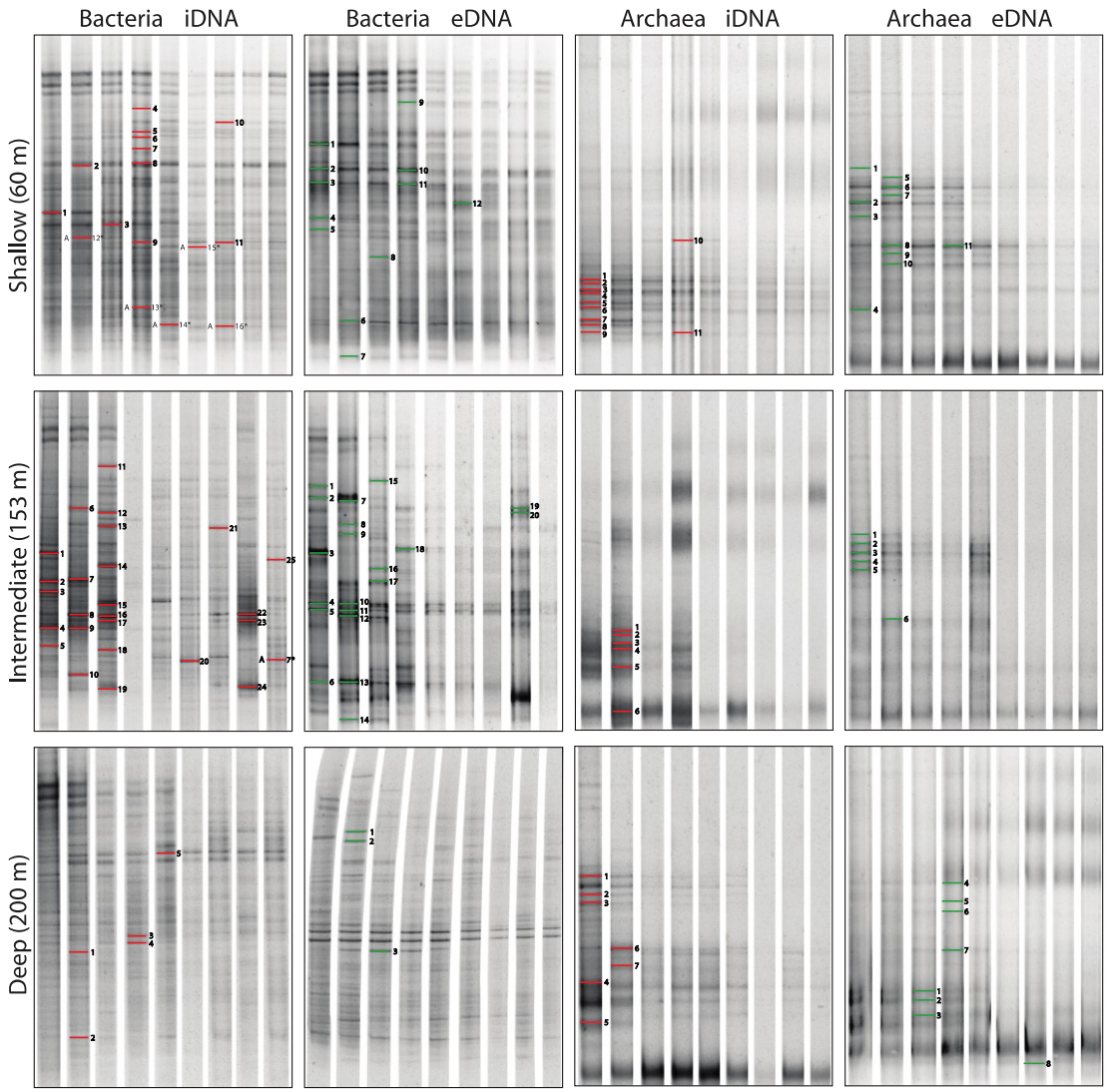

Figure S 3.3: *Pictures of DGGE gels obtained for a gradient from 35 to 60%. Each DGGE gel was processed via image analysis (Fig. S 3.1) and statistical indices calculated for every sample. Red and green bars highlight intracellular and extracellular bands that were picked up and sequenced. Band reference numbers are reported in the bacterial and archaeal phylogenetic trees.*

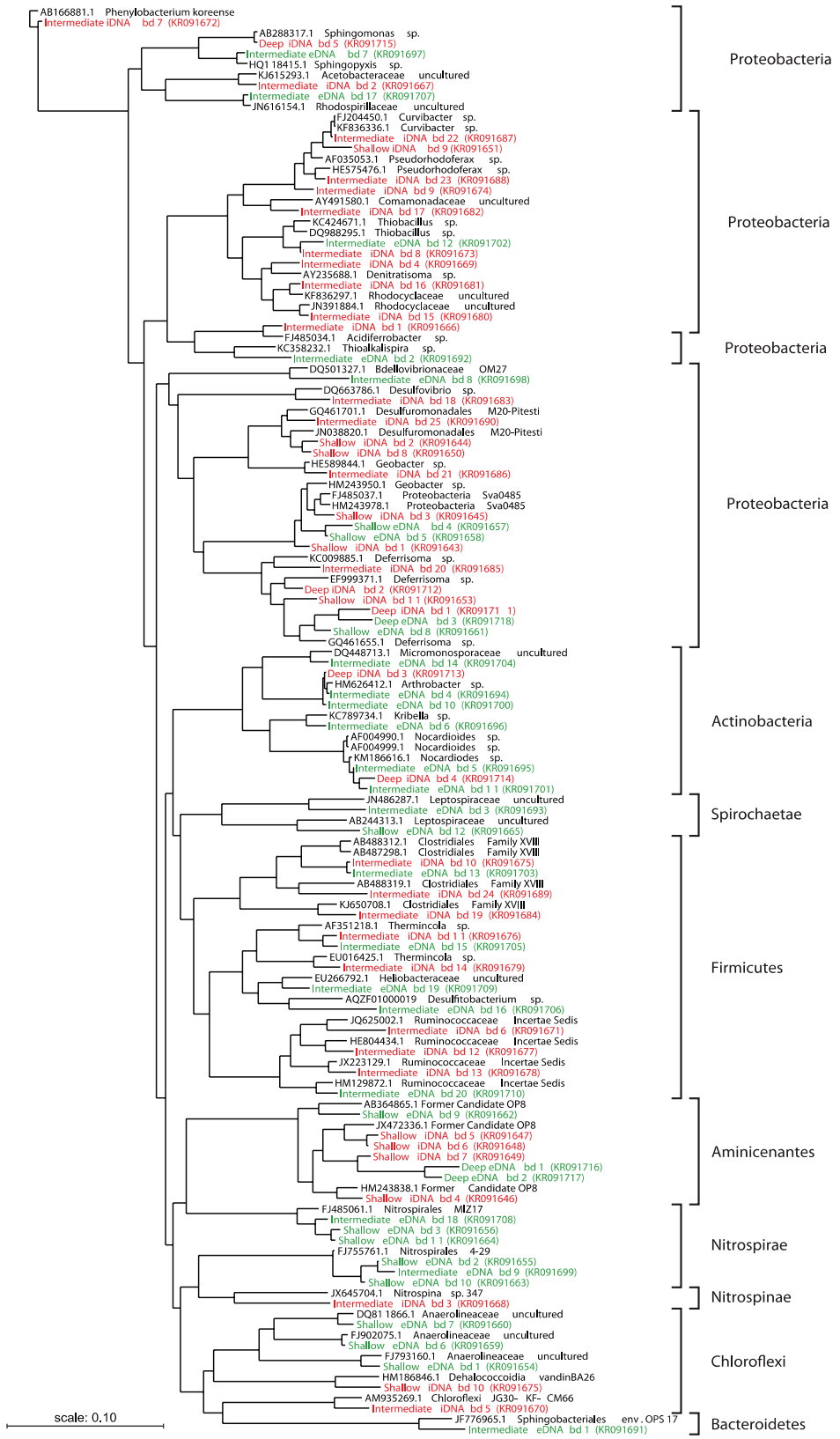

Figure S 3.4: *Phylogenetic tree established for bacterial DNA fragments. (250 to 400 bp) obtained from DGGE gels. Extracellular (green) and intracellular (red) DNA sequences mainly cluster separately. Sequence interfignering may point at cell lysis as an additional source of extracellular DNA. Bolface types signify database references. Accession numbers for Lake Towuti sequences are indicated in parentheses.*

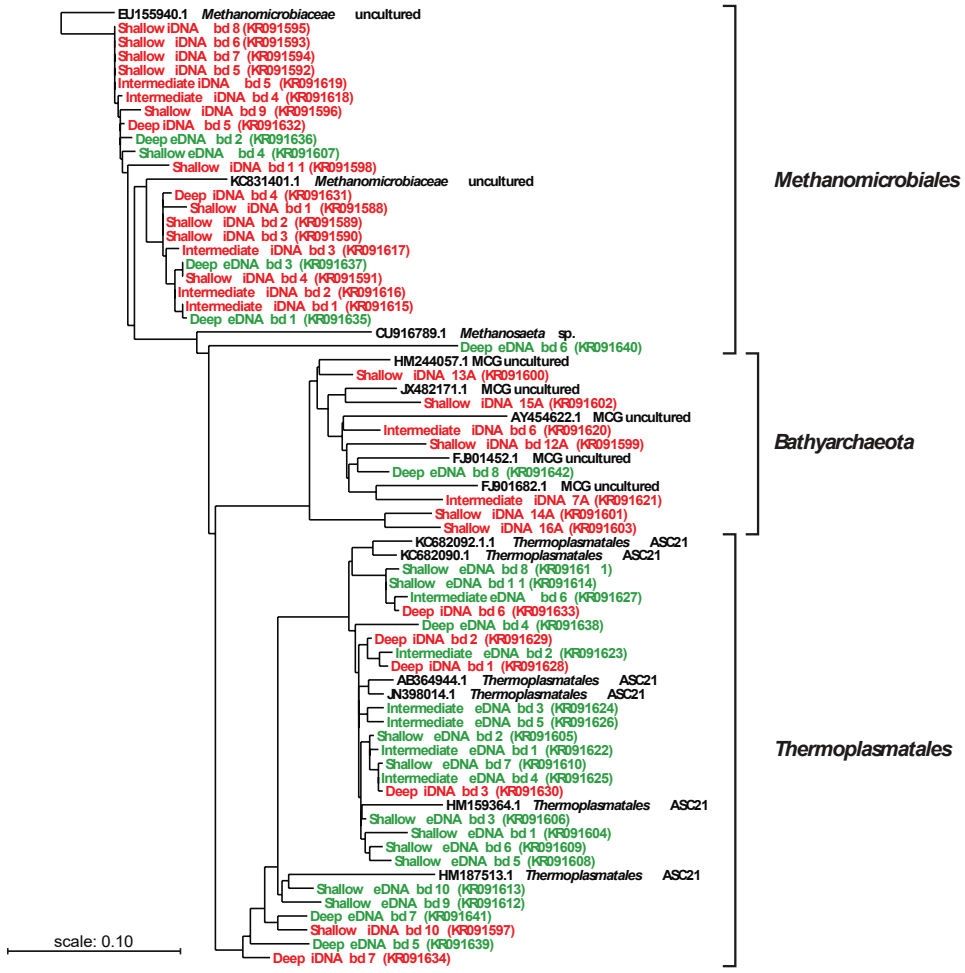

Figure S 3.5: *Phylogenetic tree established for archaeal DNA fragments. (250 to 400 bp) obtained from DGGE gels. Thermoplasmatales and Methanomicrobiales were respectively indentified as eDNA and iDNA sequences, likely indicating that methanogenic populations in the water column differ from those in the sediment. Bolface types signify database references. Genbank accession numbers for Lake Towuti sequences are indicated in parentheses.*

4 Metabolic potential of microbial communities from ferruginous sediments

Ferruginous (Fe-rich, SO_4-poor) environments are relatively rare on Earth today, but were likely widespread during the Archean and Proterozoic Eons. Because ferruginous environments are rarely sampled, the metabolic potential of the microbial communities and related biogeochemical cycling in anoxic, Fe-rich, SO_4-poor sediments are poorly understood. Lake Towuti, Indonesia, is a large ferruginous lake. We combined geochemical measurements (e.g. pore water chemistry, sulfate reduction rates) with metagenomics to assess whether metabolic potential correlated with geochemical processes in the upper 50 cm of sediment. Microbial diversity and quantities of genes for dissimilatory sulfate reduction (*dsrAB*, *aprAB*) and methanogenesis (*mcrA*) decreased with depth, concomitantly with potential sulfate reduction rates. Taxa affiliated with known iron- and sulfate-reducers indicated potential use of ferric iron and sulfate as electron acceptors. Pore water concentrations of acetate suggest fermentation taking place, potentially also leading to the production of hydrogen. Fermentation likely provides substrates for sulfate reducers and methanogens that were detected throughout the core. Presence of ANME-1 16S and *mcrA* genes demonstrates potential for anaerobic oxidation of the resulting methane. Our data suggest that microbial communities in anoxic ferruginous sediments have a potential to markedly influence the Fe and S geochemistry of these unique sedimentary settings.

4.1 Introduction

Ferruginous conditions that are rich in Fe, but poor in sulfate, were widespread during the Archean and Proterozoic Eons (Poulton and Canfield, 2011). However, the diversity and metabolic potential of microbial communities living in anoxic ferruginous sediments remain poorly known. The Malili Lake System of Indonesia (Fig. 4.1A), which comprises five interconnected lakes (Matano, Towuti, Mahalona, Lontoa, Masapi) hosted in ophiolitic and (ultra)mafic rocks (Crowe et al., 2008b; Haffner et al.,

2001), represents a model ferruginous ecosystem. The tropical climate and lateritic weathering of the catchment cause a strong flux of iron (oxy)hydroxides to these lakes but little sulfate. These detrital inputs, which mostly consist of goethite (α-FeOOH) and ferrihydrite ($Fe_2O_3 \cdot 0.5H_2O$) along with some hematite (Fe_2O_3) and magnetite (Fe_3O_4) (Crowe et al., 2004), lead to ferruginous conditions with phosphorus scavenging by iron oxides in the water column (Crowe et al., 2008b; Zegeye et al., 2012). As a result, Lake Matano and by extension Lake Towuti are among the least productive tropical lakes on Earth, the former being considered a ferruginous analogue for the Archean ocean (Crowe et al., 2008a). Under permanent stratification and persistent anoxia, as for instance in the deep basin of Lake Matano, a substantial part of the organic matter (OM) can be desorbed and remineralized through methanogenesis (Crowe et al., 2011).

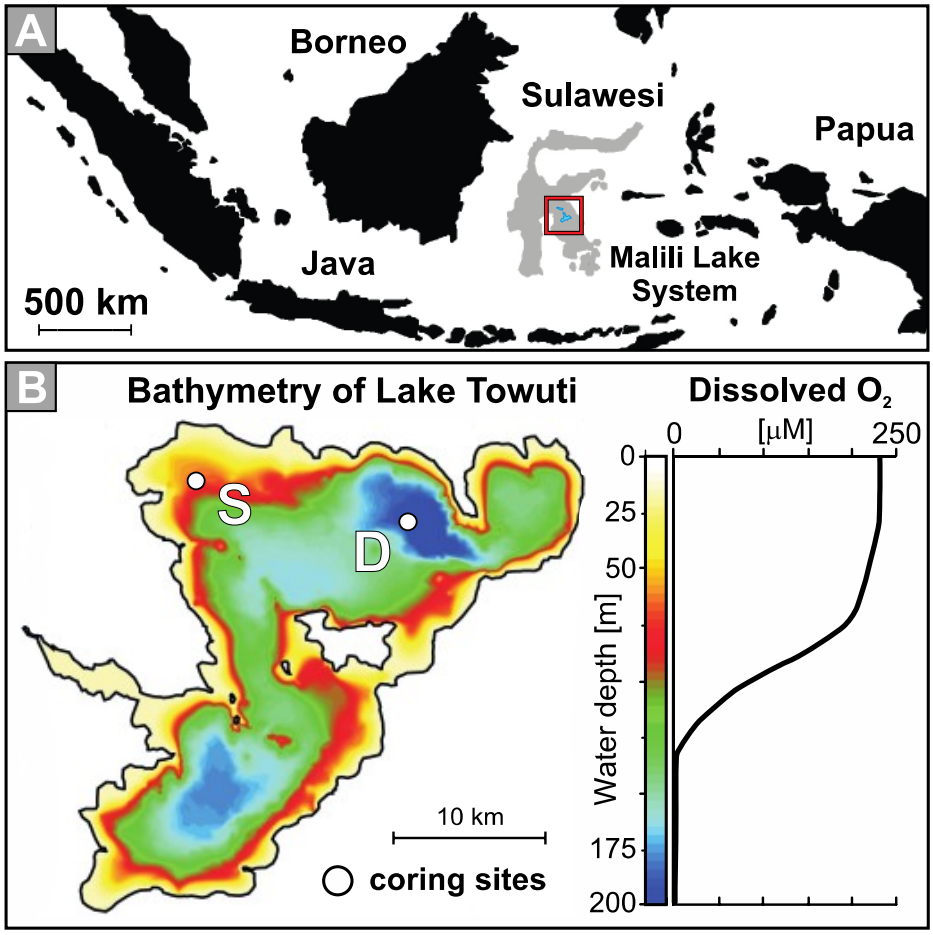

Figure 4.1: *Lake Towuti location, drilling site map and water body conditions. (A) Map of Indonesia displaying the location of Sulawesi Island and the Malili Lake System. (B) Bathymetric map of Lake Towuti (modified after Russell et al., 2016) displaying the shallow (S: 60 m water depth) and deep (D: 200 m water depth) sites at which gravity cores were retrieved, and oxygen profile measured in the water column, with an oxycline occurring in between 90 and 130 m depth.*

Unlike upstream Lake Matano, which is permanently stratified and anoxic below 110 m water depth (Katsev et al., 2010), Lake Towuti (2.5°S, 121°E) has been inferred to mix at least occasionally (Costa et al., 2015), but is presently oxygen-depleted below 130 m depth (Fig. 4.1B). This lake has a maximum water depth of ca. 200 m (Fig. 4.1B), its water column pH is circumneutral (pH ~7.8), weakly conductive (210 μS cm^{-1}) and weakly thermally stratified (i.e. 31-28 °C) (Haffner et al., 2001; Vuillemin et al., 2016). Recent geomicrobiological investigations of Lake Towuti's sediments showed that, despite extremely low sulfate concentrations (<20 μM), biogeochemical processes related to sulfur, iron, and methane transformations can co-occur in the sediment. This led to the hypothesis that cryptic sulfur cycling could be supported through sulfide re-oxidation with ferric iron (Vuillemin et al., 2016). Cryptic sulfur cycling has been extensively studied in the marine (Canfield et al., 2010; Holmkvist et al., 2011) and lacustrine realm (Norði et al., 2013; Hansel et al., 2015) from both geochemical (Thamdrup et al., 1994; Zopfi et al., 2004) and microbiological perspectives (Milucka et al., 2012; Thamdrup et al., 1993). However, the composition and structure of the microbial communities remain largely unknown (Aoki et al., 2015; Meyer and Kuever, 2007; Stewart, 2011). In addition, anaerobic oxidation of methane (AOM) is often reported as a potential sink in ferruginous settings, raising the possibility that alternative electron acceptors like Fe^{3+} may play a role (Beal et al., 2009; Crowe et al., 2011; Ettwig et al., 2016; Norði et al., 2013; Sivan et al., 2011).

Here, we leverage previous biogeochemical analyses of Lake Towuti surface sediment (Vuillemin et al., 2016, 2017) to frame metabolic potential recovered from intracellular DNA (iDNA) extracted from short (<50 cm) sediment cores retrieved from two different sites in Lake Towuti (Fig. 4.1B). Potential sulfate reduction rates (pSRR) were quantified via radiotracer incubations and concentrations of various reduced inorganic sulfur compounds was determined to explore sulfur cycling and its possible connection to iron cycling through re-oxidation of reduced sulfur compounds. We reconstruct microbial diversity using 16S rRNA gene distributions and abundances and examine metabolic potential of microbial communities using functional marker genes. The distribution of microorganisms taxonomically affiliated with known sulfate-reducing (SRB) and iron-reducing bacteria (FeRB) as well as those related to known methanogens and syntrophs involved in hydrogen production and transfer is evaluated.

4.2 Results

4.2.1 Pore Water Chemistry, Sulfate Reduction, Total Reduced Inorganic Sulfur

As expected in ferruginous environments, pore water SO_4^{2-} concentrations (Fig. 4.2) were mainly in the single µM range and often close to the quantification (8.4 µM) and detection (2 µM) limits and H_2S was always below our detection limit (1 µM). At the shallow site, SO_4^{2-} concentrations were higher, with values around 20 µM in the uppermost 4 cm below lake floor (cmblf), decreasing gradually to our detection limit at the base of the core. At the deep site, all SO_4^{2-} concentrations were close to our detection limit. Dissolved Fe^{2+} concentrations at the shallow site fluctuated between 0 and 10 µM with a slight increase below 10 cmblf, whereas at the deep site Fe^{2+} increased from 40 to 50 µM with depth with a slight excursion to lower values (30 µM) in the upper 6 cmblf. Formate concentrations at the shallow site (Fig. 4.2) decreased with depth from 40 to 10 µM within the upper 5 cmblf before increasing again to 20 µM. Acetate concentrations also decreased in the upper 5 cmblf from 70 to 40 µM and, in spite of some scatter, increased again with depth to 70 µM. At the deep site, formate concentrations were all close to quantification and detection limits, with values increasing from 5 to 11 µM with depth. Similarly, acetate concentrations displayed values increasing from 25 to 45 µM with depth.

Potential SRR differed in rates and depth distribution (Fig. 4.2) between the two sites. The shallow site displayed maximum rates (7 nmol cm^{-3} day^{-1}) within the upper 10 cmblf. Below this depth, rates decreased sharply to 2 nmol cm^{-3} day^{-1}. At the deep site, rates were much lower (1 to max. 3 nmol $cm^{-3}day^{-1}$) and did not show any depth trend. Because SO_4^{2-} concentrations were often well below the lower limit of quantification (8.4 µM), the absolute values of the pSRR have to be taken with caution. Distribution of the different fractions comprising the total reduced inorganic sulfur (TRIS) in the sediment was analyzed by sequential extraction. Three fractions were separated: (1) acid volatile sulfur (AVS), consisting mainly of monosulfides and free hydrogen sulfide, (2) chromium reducible sulfide (CRS), consisting mainly of more crystalline disulfides like pyrite (i.e. FeS_2), and (3) elemental sulfur (ES). At both sites CRS was the largest TRIS fraction, although minimal amounts of ES were detected in all but the uppermost samples at both sites (Fig. 4.2). At the shallow site, CRS values increased gradually with depth from 0 to 2.5 µmol × g^{-1}, whereas at the deep site values

were close to 0.1 in the upper half of the core and highest in the lowermost sample, reaching 3 µmol × g^{-1}. AVS was below detection at both sites.

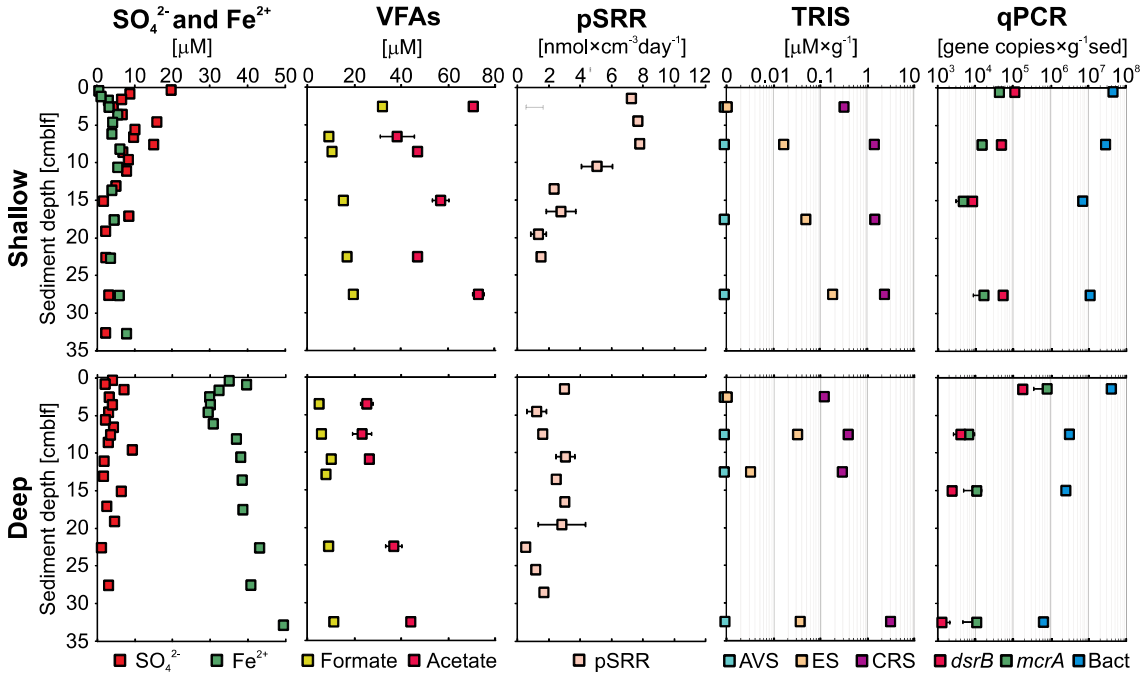

Figure 4.2: *Multiple profiles established on short sediment cores. From left to right: Sulfate and dissolved ferrous iron concentrations [µM] measured in the pore water; formate and acetate concentrations [µM] measured in pore water; potential sulfate reduction rates [nmol × cm^{-3} day^{-1}] obtained after 24 h incubation experiments; total reduced inorganic sulfur (TRIS) compounds [µmol × g^{-1}] in log scale measured in sediments as acid volatile sulfur (AVS) or monosulfides, elemental sulfur (ES) and chromium reducible sulfide (CRS) or disulfides; gene copies per g^{-1} wet sediment based on qPCR assays with primer pairs targeting the bacterial 16S rRNA, dsrB and mcrA gene.*

4.2.2 Quantitative PCR

At the shallow site, the quantity of 16S rRNA, *dsrB*, and *mcrA* gene copies decreased gradually from the surface down to 15 cmblf, then slightly increasing again towards the bottom of the core. At the deep site, values showed a steep drop in the upper 7 cmblf and remained more or less stable throughout the rest of the core (Fig. 4.2). At the shallow site, bacterial 16S rRNA genes in the uppermost sediment corresponded to 4.43 × 10^7 gene copies × g^{-1} (wet sediment) decreasing to 1.11 × 10^7 at the bottom of the core. Similarly, *dsrB* genes decreased from 1.09 × 10^5 to 5.31 × 10^4 gene copies × g^{-1}, while *mcrA* genes displayed overall lower copy numbers decreasing from 4.24 × 10^4 to 1.66 × 10^4 gene copies ×g^{-1} with depth. In comparison to the shallower site, bacterial 16S rRNA genes at the deep site showed lower copy numbers in the uppermost sample

(4.11×10^7 gene copies $\times g^{-1}$), decreasing to 6.64×10^5 gene copies $\times g^{-1}$ at the bottom of the core. Contrary to the shallow site, *dsrB* genes showed higher copy numbers than *mcrA* genes at all depth of the deep site, gradually decreasing from 1.72×10^5 gene copies $\times g^{-1}$ in surface sediment to 1.25×10^3 gene copies $\times g^{-1}$ at the bottom of the core. *McrA* genes gradually decreased from 7.63×10^5 to 1.05×10^4 gene copies $\times g^{-1}$ with depth. The quantity of *mcrA* and *dsrB* genes were generally two to three orders of magnitude lower than 16S rRNA gene copies at all sites and depths.

4.2.3 Relative Abundances of 16S rRNA Gene Operational Taxonomic Units

The sum of 16S rRNA gene OTUs taxonomically affiliated with known SRB decreased with sediment depth from about 35 to less than 10 % of total reads. Their relative abundance clearly dropped in between 1 and 7 cmblf (Fig. 4.3). Because the deltaproteobacterial Candidate Sva0485 clade is commonly found in active sulfate-reducing assemblages and is assumed capable of sulfate reduction (Concheri et al., 2017), it is listed among taxa affiliated with known SRB. Relative abundances of taxa affiliated with FeRB fluctuated between 8 and 15 % of total reads but overall increased with depth at both sites (Fig. 4.3). Bacteriovoracaceae represented ca. 5 % of all reads, but decreased to 1 % with depth at the deep site, whereas Geobacteraceae became gradually more abundant with depth, representing approximately 10 % of all reads in lowermost sediments of the deep site. Only few Firmicutes and Acidobacteria were affiliated with groups known to perform iron reduction including members of the Peptococcaceae (Zavarzina et al., 2007) and Holophagaceae (Nevin and Lovley, 2002). At the shallow site, the relative abundance of OTUs affiliated with known syntrophic bacteria (Sieber et al., 2012) were minor in uppermost and lowermost sediment layers and included Syntrophaceae, Syntrophomonadaceae and Peptococcaceae. Potential syntrophs were also affiliated with Ruminococcaceae and Clostridiales Family XVIII (Thauer et al., 2008), which were only present in the lowermost samples of the deep site where they accounted for up to 12 % of all reads (Fig. 4.3). At both sites, relative abundances of OTUs assigned to methanogens accounted for ca. 4 to 9 % of all reads. Below 7.5 cmblf at the shallow site, values dropped to 3 % and then increased again to 6 %. At the deep site, relative abundances increased gradually with depth from 4 to 8 %.

OTUs of this fraction mainly corresponded to Thermoplasmata, Methanomicrobia, Methanobacteria, as well as Bathyarchaeota, though their capacity of methanogenesis remains unsubstantiated through direct measurements of metabolism. Although the overall relative abundance of bathyarchaeotal OTUs increased with depth from ca. 10 to 50 % at both sites (Supplemental material), we listed only those related to population genomes with inferred metabolic potential for methanogenesis (Evans et al., 2015) which summed up to 5% of all reads. OTUs listed as potential anaerobic methanotrophs were affiliated with Candidate NC10 (He et al., 2015) and ANME-1 (Boetius et al., 2000; Meyerdierks et al., 2010). Their relative abundance remained constant with depth at ca. 4 % of all reads, except in the uppermost part of the deep site with 7 % of NC10 reads. However, methane oxidation via NO-dismutation was only demonstrated for *Candidatus* Methylomirabilis, the only cultivated member of the candidate phylum NC10 (He et al., 2015).

The canonical correspondence analysis (CCA) (Supplemental material) showed that at both sites the differences in communities can be explained by depth or by other factors that also change with depth (e.g. cell counts, SO_4^{2-} and Fe^{2+}concentrations, pSRR). Relative abundances and numbers of representative OTUs are summarized in Table S 3.1 (Supplemental material).

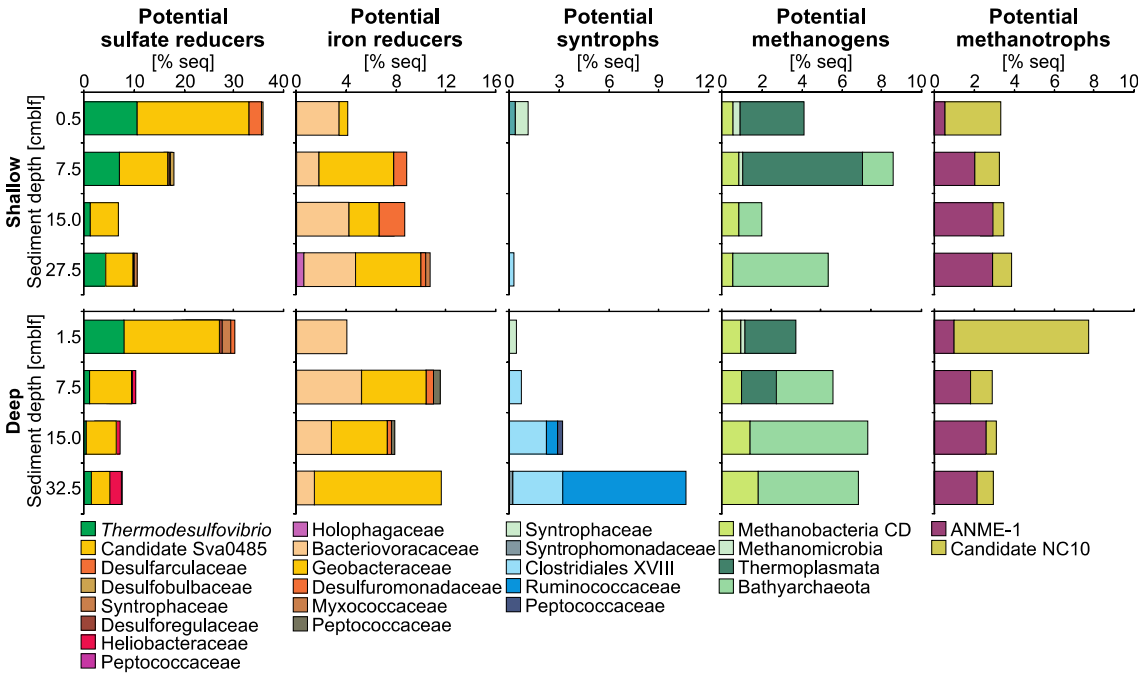

Figure 4.3: *Relative abundances of OTUs related to taxa with proven phenotypes in sulfur, iron, and hydrogen cycling. From left to right: Bar charts displaying relative abundances [% seq] of taxa closely affiliated (>97%) with known sulfate-reducing bacteria, iron-reducing bacteria, hydrogen syntrophs, methanogens and anaerobic methanotrophs.*

4.2.4 Taxonomic Affiliations

Taxa related to known SRB were mainly affiliated with *Thermodesulfovibrio* and *Desulfuromonas*. *Desulfobacca, Desulfurosporosinus,* and *Desulfurispora* were also identified, with the addition of some other minor OTUs (e.g. *Desulforegula*, *Desulfobulbus*, *Desulfatiglans*, *Desulfarculus*). The deltaproteobacterial Candidate Sva0485 clade was also present, but its relatives have only been loosely linked to sulfate reduction and this inference remains speculative. Those taxa related to known FeRB included members of the *Deferrisoma*, *Geobacter*, *Thermincola* and *Geothrix* clades. OTUs affiliated with groups known to act as hydrogen syntrophs included Clostridiales, Ruminococcaceae, *Smithella* and *Pelotomaculum*, to which *Pelospora* and some uncultured Syntrophaceae, and again this inference remains speculative. Taxa related to known methanogens were mainly affiliated with the Incertae Sedis *Methanomassiliicoccus* cluster. Multiple OTUs were identified as *Candidatus* Methanofastidiosum, *Methanolinea* being also present with one single OTU. Among the 136 taxa related to Bathyarchaeota (Supplemental material), 18 OTUs had a close phylogenetic affiliation to population genomes with inferred metabolic potential for methanogenesis (Evans et al., 2015). Taxa listed as anaerobic methanotrophs were related to *Candidatus* Methylomirabilis and ANME-1 only.

4.2.5 Taxonomic Assignment of Functional Genes

Taxonomic assignment of the genes that code for the dissimilatory sulfite reductase subunit alpha and beta (*dsrAB*), the adenylysulfate reductase subunit alpha and beta (*aprAB*), the formate-tetrahydrofolate ligase (*fhs*) and the methyl-coenzyme M reductase subunit alpha (*mcrA*) was based on 128, 70, 328 and 76 predicted protein sequences, respectively. Phylogenetic analyses of these predicted proteins (Fig. 4.5) revealed a correlation between the taxonomic affiliations of the functional markers of sulfate reduction and methanogenesis and the 16S rRNA gene phylogenetic anchor (Fig. 4.3). For example, most *dsrAB* predicted protein sequences derived from sulfate reducing Deltaproteobacteria, Firmicutes and Nitrospirae, though other *dsrAB* predicted proteins also had an affiliation to the Chloroflexi and a number of bacterial candidate phyla. Consistent with this result, most of the *aprAB* genes were also affiliated with the Deltaproteobacteria, Firmicutes and Nitrospirae. Interestingly, many of the *dsrAB* genes were recovered from various uncultivated Deltaproteobacteria (Fig. 4.5A), which

could include the Sva0485 clade presently listed as potential SRB in the 16S rRNA gene dataset (Fig. 4.3).

The *fhs* genes were also mostly affiliated with taxa within the Deltaproteobacteria, Firmicutes and Chloroflexi with a smaller number of sequences affiliating with the Omnitrophica, Aminicenantes, Bathyarchaeota, and Atribacteria (Supplemental material). Thus, relative to the *dsrAB* and *aprAB* genes, the *fhs* gene appeared to be distributed across a broader array of microbial taxa. Sequences of the *mcrA* gene were mostly affiliated to the ANME-1 group, Methanomicrobia, Methanobacteria and the Bathyarchaeota (Fig. 4.5A).

4.3 Discussion

4.3.1 Interactions between Sulfate and Iron Reduction

Measurements of pSRR revealed the physiological capacity for sulfate reduction at both sites, although the potential rates were higher at the shallow site (Fig. 4.2), with rates that imply the sulfate pool is exhausted within days. Decreasing pSRR at the shallow site was correlated with a decline in relative abundances of 16S rRNA sequences affiliated with known SRB (Fig. 4.3) and clear changes in microbial community composition (Fig. 4.4). While it is speculative to infer metabolic potential from 16S rRNA gene sequences alone, our carefully curated phylogenetic analysis (Fig. 4.4) shows that many sequences recovered from these sediments have nearly identical 16S rRNA gene sequences to microorganisms with physiological capacity for sulfate and iron reduction, and methanogenesis. It is generally accepted that, because the 16S rRNA gene sequence is a highly conserved and slow evolving gene, a recovered environmental 16S rRNA gene sequence that is closely related (> 97%) to that of a cultivated strain, with a proven major biochemical phenotype, can be used to infer a similar biogeochemical role from the taxon that the environmental 16S rRNA sequence is derived (Langille et al., 2013). We also note that microorganisms with this level of 16S rRNA gene sequence similarity can be different at the genome level and thus have very different metabolic potential (Louca et al., 2016). Thus, we proceed cautiously with our attempt to connect OTUs with close phylogenetic relationships to taxa with known metabolic phenotypes (e.g. iron reduction, sulfate reduction, methanogenesis).

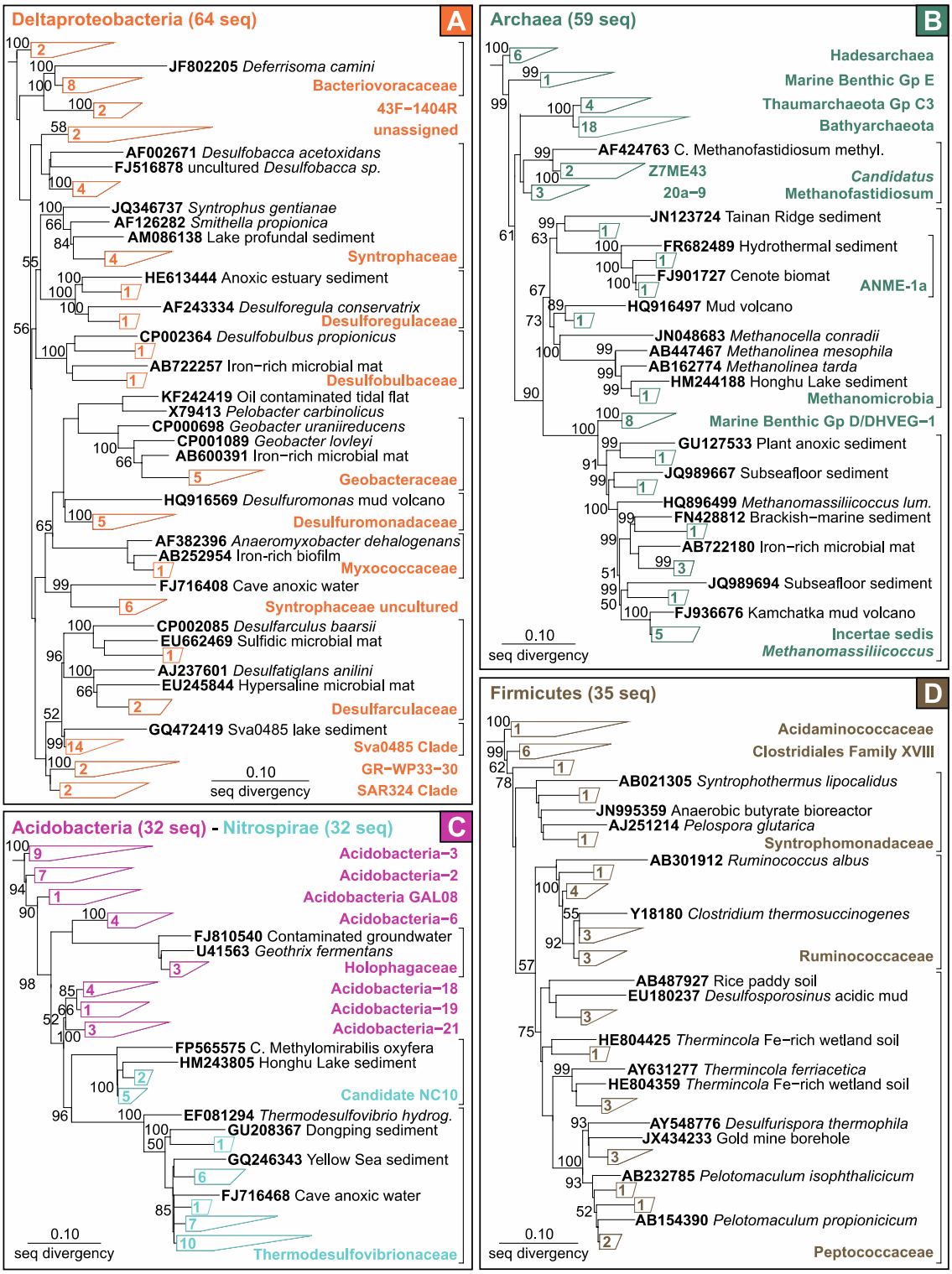

Figure 4.4: *Phylogenetic trees based on partial 16S rRNA gene sequences established for representative OTUs related to sulfur, iron, and hydrogen cycling. (A) Deltaproteobacteria; (B) Archaea; (C) Acidobacteria and Nitrospirae; (D) Firmicutes. Sequences identified as potential SRB are mostly affiliated with Desulfobacca, Thermodesulfovibrio, Desulfurispora and Desulfosporosinus. Those related to potential FeRB are represented by Deferrisoma, Geobacter, Geothrix, and Thermincola. Sequences of potential syntrophs include Smithella, Pelotomaculum, Syntrophothermus, Pelospora, along with candidates among Clostridiales and Ruminococcaceae. Methanogen-related sequences are Methanolinea, Methanomassiliicoccus, Candidatus Methanofastidiosum and Bathyarchaeota. Sequences of anaerobic methanotrophs are represented by the ANME-1a group.*

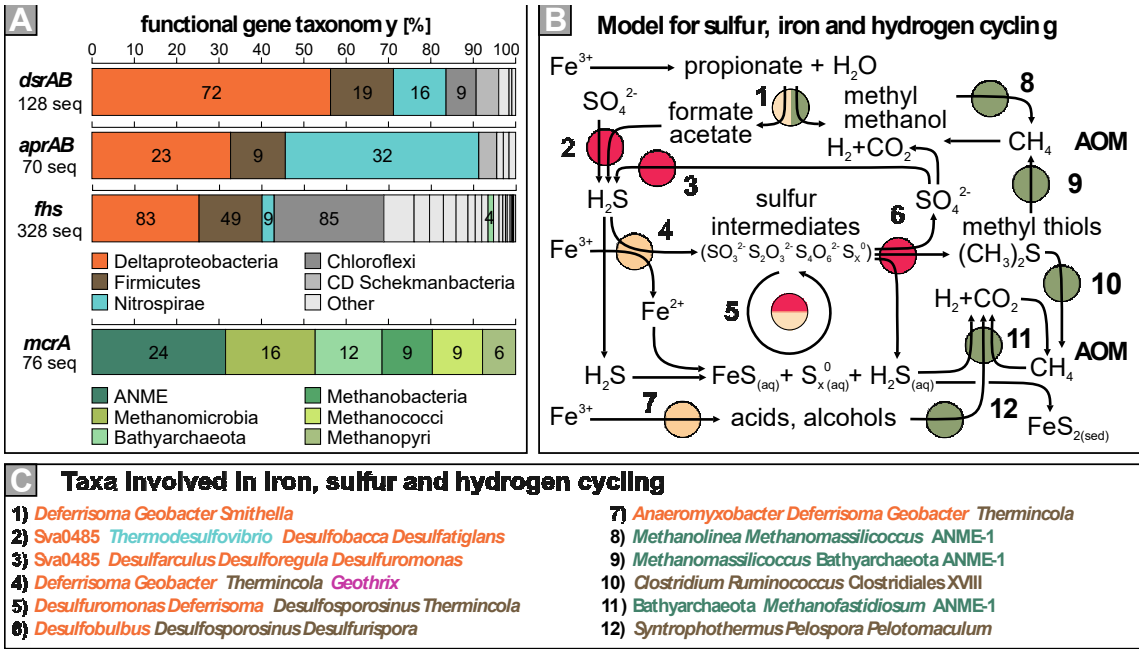

Figure 4.5: *Affiliations of functional genes, reactions involved in sulfur, iron and hydrogen cycling, and 16S rRNA gene taxonomy of taxa driving the corresponding reactions (A) Taxonomic assignment for functional genes corresponding to dissimilatory sulfite reductase subunits (dsrAB), adenylylsulfate reductase subunits (aprAB), formate-tetrahydrofolate ligase (fhs) and methyl-coenzyme M reductase subunits (mcrA). (B) Sketch depicting the expected coupling of iron, sulfur and methane cycles (modified after Holmkvist et al., 2011). Reactions related to iron (light brown circles) and sulfur (red circles) are listed from 1 to 7, whereas methylated compounds and hydrogen conversion to methane (green circles) is listed from 8 to 12. (C) Identified taxa with known metabolic capabilities to drive iron and sulfur cycling (1 to 7) and hydrogen conversion to methane (8 to 12).*

Depths with the highest pSRR also had high relative abundances of *Thermodesulfovibrio* and *Desulfobacca*. In the laboratory, these genera grow through sulfate reduction mainly with formate, pyruvate and lactate as electron donors for the former (Sekiguchi et al., 2000) and only acetate for the latter (Elferink et al., 1999). At the shallow site, transition to low pSRR (ca. 10 cmblf) correlated with the appearance of *Desulfuromonas*, a genus with cultured strains capable of reducing sulfate but also sulfur and iron (Greene, 2014; Pjevac et al., 2014). In sediments of the deep site that exhibited lowest pSRR (Fig. 4.2), *Desulfuromonadales* were also present. Additionally we identified taxa belonging to Firmicutes related to *Desulfurispora* (Kaksonen et al., 2007) and *Desulfosporosinus* (Ramamoorthy et al., 2006), which are known to reduce sulfate, sulfite, thiosulfate, elemental sulfur and iron. We also found taxa affiliated with *Desulfobulbus*, which is related to organisms that in cultures can reduce sulfur and also produce SO_4^{2-} from elemental sulfur in the presence of Fe^{3+}oxides (Castro et al., 2000). Taxonomic affiliation of the *dsrAB* and *aprAB* genes provided additional information

on the taxonomic distribution of metabolic potential for sulfate reduction, which in Lake Towuti sediments includes members of the Deltaproteobacteria (e.g. *Desulfobacca*), Firmicutes (e.g. *Desulfosporosinus*) and Nitrospirae (e.g. *Thermodesulfovibrio*) (Fig. 4.5A). In parallel, the deltaproteobacterial Candidate Sva0485 clade, which is commonly detected in sulfate-reducing consortia (Bar-Or et al., 2015; Kleindienst et al., 2014), was relatively abundant in Lake Towuti sediments (Fig. 4.3 and 4.5A). Although this clade has been found in a variety of environments and was often assumed to be reducing sulfate (Concheri et al., 2017; Hori et al., 2014), it has not been clearly reported to carry functional marker genes of sulfate reduction (Aoki et al., 2015; Meyer and Kuever, 2007; Müller et al., 2015) and it may be limited to fermentation (Kip et al., 2017; Plugge et al., 2011). Nevertheless, many of the *dsrAB* genes were recovered from various uncultivated Deltaproteobacteria (Supplemental material), which could include the Sva0485 clade listed in the 16S rRNA gene dataset (Fig. 4.3).

In parallel to the SO_4^{2-} and Fe^{2+} pore water profiles (Fig. 4.2), the relative abundances of taxa related to bacteria known to reduce Fe in the laboratory (FeRB, Fig. 4.3) tended to exist throughout the sediment cores, successively appearing as *Deferrisoma*, *Geobacter*, *Thermincola, Geothrix*, and *Anaeromyxobacter* (Figs. 4.3 and 4.4). *Deferrisoma* species reduce ferrihydrite, but also elemental sulfur (Slobodkina et al., 2012). *Geobacter* species are capable of Fe reduction in cultures, but are also known to participate as fermenters in syntrophic partnerships (Nagarajan et al., 2013). *Thermincola* reduces ferrihydrite and magnetite, and also has the capacity to reduce sulfonates (Zavarzina et al. 2007). Laboratory strains of *Geothrix* reduce various forms of soluble and insoluble Fe^{3+} via electron shuttles (Nevin and Lovley, 2002). *Anaeromyxobacter* couples the reduction of amorphous Fe^{3+} to the oxidation of acetate, but is also capable of a broad array of metabolic strategies (He and Sanford, 2003). Overall, our 16S rRNA gene sequences and functional marker gene sequences reveal a number of taxa related to microorganisms known to conduct sulfate reduction and Fe reduction in laboratory settings. These organisms and functional genes are broadly distributed throughout these sediments. Many of these organisms differed in relative abundance with depth below the water-sediment interface, implying community structuring that may be linked to the depth distributions of key substrates like sulfate, ferric Fe, and organic matter. Although more detailed studies are needed to connect the metabolic potential of specific taxa to their role in biogeochemical processes, many of

them have theoretically the physiological capability to alternate between reduction of iron, sulfate and sulfur intermediates (i.e. SO_3^{2-}, $S_2O_3^{2-}$, $S_2O_6^{2-}$, S_x^0). The absence of AVS and trace amounts of ES in the sediment (Fig. 4.2) suggested that monosulfides and ES could be re-oxidized in the sediment and transformed to disulfides (i.e. CRS). Under sulfate-poor but iron-rich anoxic conditions, the disproportionation of reduced inorganic sulfur compounds (i.e. S_x^{2-}, HS^-) by ferric iron (Fig. 4.5B) could lead to the co-occurrence of iron and sulfate reduction in the sediment (Wang et al., 2008; Hansel et al., 2015).

4.3.2 Potential for Syntrophy and Methanogenesis

Taxa related to known syntrophs were successively detected in the lower depths of the sediment including *Smithella* (Liu et al., 1999), Syntrophothermus (Sekiguchi et al., 2000), *Pelospora* (Matthies et al., 2000) and *Pelotomaculum* (Imachi et al., 2002). This depth distribution of syntrophic taxa may also reflect substrate availability and notably a likely decrease in the availability of inorganic electron acceptors like SO_4^{2-} or Fe^{3+}. This is consistent with our observation at the deep site that when the relative abundance of 16S rRNA genes related to known SRB dropped below 10 %, those of Ruminococcaceae and Clostridiales increased drastically (Fig. 4.3). Many taxa within these groups are known to interact syntrophically with both SRB and methanogens (Morris et al., 2013; Thauer et al., 2008). The distribution of acetate in pore water implies production of fermentation end products in the deeper sediments, which may also include hydrogen.

In uppermost sediments, taxa related to known methanogens were mainly affiliated with *Methanomassiliicoccus* (Figs. 4.3 and 4.4). The *Methanomassiliicoccus* are known methylotrophs and thus use non-competitive substrates for methane production, notably methylated thiols in sulfidogenic acetogenic associations (Dridi et al., 2012; Kröninger et al., 2016; Plugge et al., 2011). At both sites below 10 cmblf where pSRR were minimal (Fig. 4.2), the relative abundances of taxa affiliated with putative methanogens increased consisting mostly of sequences identified as Bathyarchaeota and *Candidatus* Methanofastidiosum, which were also recently considered to be able to carry out H_2-utilizing methylotrophic methanogenesis, with methane production mainly derived from the reduction of methylated thiols (Evans et al., 2015; Nobu et al., 2016). This suggested that some members of the microbial consortia couple methane production to the recycling of reduced sulfur compounds (Bae

et al., 2015; Kappler and Bryce, 2017; Kiene et al., 1986). Nevertheless, the increasing abundance of hydrogen producers (e.g. Clostridiales and Ruminococcaceae) below 10 cmblf likely indicated that hydrogenotrophic methanogenesis becomes the main pathway for methane production with depth. Taxonomy of the *mcrA* gene (i.e. methanogenesis, anaerobic methane oxidation) pointed to the role of Methanomicrobia and Methanobacteria in producing methane, and also reveal *mcrA* gene sequences affiliated with the Bathyarchaeota and ANME-1 (Fig. 4.5A). However, their degree of activity and the electron acceptor to which AOM processes are coupled remain undetermined.

Altogether, our data suggested that microbial communities in anoxic ferruginous sediments exhibit vertical succession of the putative phenotypes FeRB, SRB, methanogens and methanotrophs (Fig. 4.5B). Metagenomes and biogeochemical rate measurements point to sulfate reduction as a main bioenergetic process in surface sediment directly followed by methanogenesis. The absence of monosulfides but continuous increase of disulfides in the sediment suggested that reduced sulfur compounds could be recycled in parallel to methanogenesis via the reduction of methylated thiols.

4.4 Experimental Procedures

Sampling was carried out at two locations, a shallow (60 m) and deep (200 m) site with oxic and anoxic bottom water conditions, respectively (Fig. 4.1B). Oxygen concentrations in the water column were measured on site using a submersible Conductivity-Temperature-Depth probe (CTD) (SBE-19, Sea-Bird). Additionally, several short sediment cores (<50 cm) were retrieved at each site. To avoid oxidation, all sediment sampling and processing was carried out on site inside a nitrogen-filled glove bag. Pore water was extracted using Rhizon Pore Water Samplers (Rhizon CSS), collected in syringes and filtered (0.2 µm pore size).

4.4.1 Pore Water Chemistry, Sulfate Reduction, Total Reduced Inorganic Sulfur

Dissolved Fe^{2+} concentrations in pore water were measured in the field via spectrophotometry (Viollier et al., 2000) by adding 100 µL of Ferrozine Iron Reagent (Sigma-Aldrich) to 1 mL of pore water and measuring absorbance of the colored

solution at 562 nm with a DR 3900 spectrophotometer (Hach). Detection limit of the method is 0.25 µM. Sulfate, acetate and formate concentrations were analyzed in the home lab by suppressed ion chromatography. The system consisted of a S5200 sample injector, a S3115 conductivity detector and a 4.0 × 150 mm LCA A20 column (all Sykam) and a SeQuant SAMS anion IC suppressor (EMD Millipore). Eluent composition was 1.7 mM $NaHCO_3$ and 1.8 mM Na_2CO_3 and flow rate was set to 1 mL min^{-1} and column temperature to 45°C. Respective minimum detection (Signal to Noise ratio=3) and quantification limits (S/N=10) are: SO_4^{2-} (2 µM; 8.4 µM), formate (2.1 µM; 8 µM) and acetate (8.7 µM; 27.1 µM). Standards were run every ten samples. Reproducibility was always below 3 %.

Potential SRR quantification was performed according to the whole core incubation technique of Jørgensen (1978). In brief, 3 kBq of $^{35}SO_4^{2-}$ radiotracer were injected into each sediment plug and incubated for 24 hours in the dark close to *in situ* temperature (ca. 30 °C) followed by cold chromium distillation (Kallmeyer et al., 2004). Radioactivity was quantified using UltimaGold Scintillation Cocktail (Perkin Elmer) and a Tri Carb 2500 TR liquid scintillation counter (Packard Instruments) with a counting window of 4-167 keV. Detailed protocols are published elsewhere (Vuillemin et al., 2016).

Concentrations of TRIS compounds were determined separately from the pSRR incubations, using approximately 5 g of fresh sediment per sample. Sediment samples were distilled following a modification of the procedure by Canfield et al. (1986) and Kallmeyer et al. (2004). During the three steps of distillation, TRIS was separated into three fractions, namely AVS, CRS, and ES. All three fractions were extracted in three successive 2-hour distillation steps, consecutively adding 8 mL of 6N HCl (AVS), 16 mL of 1M $CrCl_2$ solution (CRS) and 8 mL of dimethylformamide (ES) to the sample (Kallmeyer et al., 2004). Sample slurries were stirred in a glass flask under a continuous stream of nitrogen gas. The liberated hydrogen sulfide was trapped in 7 mL of 5 % (w/v) zinc acetate solution to precipitate as zinc sulfide. After each distillation cycle, the zinc acetate solution was exchanged for a fresh one. The trapping solution was centrifuged, the supernatant discarded and the ZnS pellet suspended in 1 mL of ultrapure H_2O. Sulfide concentrations in the final 1 mL suspensions obtained for each TRIS fraction were measured spectrophotometrically at 667 nm using Cline reagent (Cline, 1969) and a DR 3900 spectrophotometer (Hach). Minimum detection limit of

this method is 5 μg L^{-1}. Samples were processed in duplicates, and concentrations were averaged with error bars corresponding to one standard deviation.

General geochemical data were presented and discussed in detail in a previous study (Vuillemin et al., 2016). The corresponding dataset is archived on the Pangaea® database (www.pangaea.de/) under accession number # 861437.

4.4.2 Intracellular DNA Extraction

The procedure of Alawi et al. (2014) allows for the separate extraction of extracellular DNA (eDNA) and intracellular DNA (iDNA) from the same sample. To specifically analyze the current microbial communities of the sediment, we only used the iDNA fraction in this study. All extractions were performed in duplicates along with a negative control. The first part of the extraction was performed with 1.0 g of fresh sediment, 0.2 g of acid washed polyvinylpolypyrrolidone (PVPP) and 2.5 mL of 0.1 M sodium phosphate buffer (Na-P-buffer). The sediment was washed three times with Na-P-buffer and the supernatant of all washing steps retrieved and pooled, reaching a final volume of 7.5 mL. This supernatant was centrifuged for 45 min at 4700 × g to separate the iDNA (i.e. cell pellet) from the eDNA (i.e. supernatant). The iDNA fraction was extracted from the cell pellet following our previously published protocol (Vuillemin et al., 2017). For further analysis, we selected iDNA samples in duplicates from four different sediment depths at each coring site (shallow site: 0.5, 7.5, 15, 27.5 cmblf; deep site: 1.5, 7.5, 15, 32.5 cmblf). Final extracts were diluted ten times and used as templates in PCR reactions.

4.4.3 Quantitative PCR assays

Quantitative PCR was performed on 8 iDNA extracts using primer pairs specifically targeting the bacterial 16S rRNA gene, methyl coenzyme M reductase alpha subunit (*mcrA*) and dissimilatory sulfite reductase beta subunit (*dsrB*) genes. For each 20 μL reaction unit, PCR mixtures were composed of 10 μL of iTaq SYBR Green Supermix (Bio-Rad), 0.1 μL of each of the primers (100 μM), 7.8 μL of Ultra-pure PCR Water (Bioline) and 2 μL of DNA template diluted 10 times. Samples were processed in triplicate with 6 standards at increasing dilutions from 1 to 1 × 10^6 times. Negative controls were added to all PCR sets with 2 μL of Ultra-pure PCR Water (Bioline) as template to provide a contamination check. Positive controls were also added using 2 μL of *Escherichia coli*, *Methanosarcina barkeri* and *Desulfovibrio vulgaris* (0.1 ng μL^{-}

^{1}), respectively. PCR reactions were run on a CFX Connect Real-Time System thermocycler (Bio-Rad).

For bacterial 16S rRNA gene, we used primer pairs Eub341F (5'- CCT ACG GGA GGC AGC AG -3') with Eub534R (5'- ATT ACC GCG GCT GCT GG -3') with an initial standard concentration of 2.3×10^7 gene copies μL^{-1}. PCR cycles were run as follows: Initial denaturation of 5 min at 98 °C, 40 cycles of 98 °C for 5 sec, 58 °C for 20 sec, 72 °C for 50 sec, with a final melting curve of 95 °C for 10 sec, 65 °C for 5 sec incremented by 0.5 °C per cycle of 5 sec to reach 95 °C. For the *mcrA* gene, the primer pair was msla-F (5'- GGT GGT GTM GGD TTC ACM CAR TA-3') with mcrA-R (5'- CGT TCA TBG CGT AGT TVG GRT AGT -3') with an initial standard concentration of 1.6×10^7 gene copies $\square L^{-1}$. For the *dsrB* gene, we used the primer pair dsrB4-R (5'- GTG TAG CAG TTA CCG CA -3') with dsrB2060-F (5'- CAA CAT CGT YCA YAC CCA GGG-3') with an initial standard concentration of 6.69×10^7 gene copies μL^{-1}. For both primer combinations, PCR cycles were run as follows: Initial denaturation of 3 min at 95 °C, 40 cycles of 95 °C for 3 sec, 60 °C for 20 sec, 72 °C for 30 sec plus 80 °C for 3 sec, with a final melting curve of 65 °C for 5 sec incremented by 0.5 °C per cycle of 5 sec to reach 95 °C.

Run efficiencies for the quantification of the bacterial 16S rRNA gene, *mcrA* and *dsrB* were 97.5, 75.0 and 92.7 %, respectively, with correlation coefficient slope between 0.997 and 0.999. All final products were checked on 1.5 % agarose gels.

4.4.4 PCR Amplification for Next-Generation Sequencing

PCR was performed on 16 iDNA extracts using unique combinations of the tagged universal primer pair 515F (5'- GTG CCA GCM GCC GCG GTA A -3') and 806R (5'- GGA CTA CHV GGG TWT CTA AT -3') to cover 291 bp of the bacterial and archaeal 16S rRNA gene. We acknowledge that this primer pair does not include the adaptation for increased coverage of archaea (Parada et al., 2016). Individual tags composed of 8 nucleotides were attached at each primer 5′-end. A total of 20 different forward and reverse tagged primers (Eurofins Genomics) were designed to enable multiplexing of all PCR products in a unique sequencing library. PCR mixtures were prepared and amplifications performed as previously published (Vuillemin et al., 2017). PCR amplicons were checked on 1.5 % agarose gel. For each sample, 116 µL of PCR product were pooled, purified and eluted in a final volume of 25 µL, using a High Pure

PCR Cleanup Micro Kit (Roche Applied Science). Purified PCR products were quantified by fluorometric method using a QubitHS dsDNA kit (Invitrogen). Concentrations were calculated and normalized for all samples. We pooled 32 ng of each DNA amplicon sample and reduced the volume of the mixture to 120 µL using a Savant SpeedVac High Capacity Concentrator (Thermo Fisher Scientific). We used 60 µL of pooled amplicons, corresponding to an amount of approximately 800 ng of DNA, for the Illumina MiSeq library preparation.

4.4.5 Illumina Library Preparation, Sequencing and Data Analysis

Indexed paired-end libraries of pooled amplicons for consecutive cluster generation and DNA sequencing were constructed using a TruSeq DNA PCR-Free L Kit (Illumina). Libraries were prepared following the manufacturer instructions. PCR-free libraries were validated by qPCR using the KAPA Library Quantification Kit (Kapa Biosystems) following the manufacturer's manual. PCR mixtures were prepared and amplifications performed as previously published (Vuillemin et al., 2017). Final concentration of the library was quantified by a fluorometric method using a Qubit HS dsDNA kit (Invitrogen). A MiSeq Reagent Nano kit v2, with 500 cycles with nano (2 tiles) flow cells was used to run libraries on the Illumina MiSeq Sequencing System. Two 250 cycles were used for an expected output of 500 Mb and an expected number of 7 million reads per library.

Quality of the raw data was checked using FastQC. Demultiplexing was performed using own scripts based on cutadapt (Martin, 2011). No errors in barcodes were allowed with Phred-Score above Q25. Read pairs were merged using PEAR (Zhang et al., 2013). Sequences were trimmed using Trimmomatic (Bolger et al., 2014). Chimeras were detected and removed using usearch61 and the ChimeraSlayer reference database (Edgar, 2010) as it is implemented in the QIIME-pipeline (Caporaso et al., 2010). Script of this pipeline was used to cluster the sequences and assign taxonomies based on the SILVA database at 97 % identity cut-off value (DeSantis et al., 2006). The resulting operational taxonomic unit (OTU) table was filtered by removing all OTUs with abundance below 0.1 % within the sample. Those affiliated with cultivated SRB, FeRB, syntrophs involved in hydrogen production and transfer, methanogens and anaerobic methanotrophs as well as uncultivated clades with the same inferences from single-cell and metagenomic studies were selected to plot bar charts of the corresponding phenotypes (Fig. 4.3). Relative abundances were calculated by dividing

their respective number of reads by the total number of reads per sample. Percentages of relative abundance were summed up by duplicates and averaged.

Sequencing data after demultiplexing were submitted to the European Nucleotide Archive (http://www.ebi.ac.uk/ena) under study accession number PRJEB14484.

4.4.6 Phylogenetic Analysis and Canonical Correspondence Analysis

Representative sequences extracted for the exact same OTUs were aligned to the SILVA database and plotted in four different phylogenetic trees, i.e. Deltaproteobacteria (Fig. 4.4A), Archaea (Fig. 4.4B), Acidobacteria and Nitrospirae including the Candidate NC10 (Fig. 4.4C), and Firmicutes (Fig. 4.4D). The SINA online v.1.2.11 (Pruesse *et al*., 2007, 2012) was used to align our representative sequences. Phylogenetic analysis was performed with ARB software package (Ludwig et al., 2004) based on the upload sequence alignments against the SILVA 16S rRNA SSU NR99 reference database release 12_07_2015 (Quast et al., 2012). Their closest environmental sequences and cultured species were selected as taxonomic references and used to calculate phylogenetic trees with nearly full-length sequences (>1400 bp) using the implemented bacterial and archaeal filter and the Maximum Likelihood algorithm RAxML with advanced bootstrap refinement using 100 tree replicates (Stamatakis, 2006). Partial sequences were added to the tree using the maximum parsimony algorithm without allowing changes of tree topology. Each phylogenetic tree included representative sequences from Lake Towuti and their respective reference sequences for Archaea, Deltaproteobacteria, Firmicutes as well as Acidobacteria together with Nitrospirae. The same procedure was applied to assign all unassigned sequences, which we then incremented in the initial OTU table.

In addition, a CCA was performed with 12 environmental parameters as explanatory variables and all OTUs corresponding to the different selected metabolic pathways (i.e. 204 OTUs). Explanatory variables were standardized prior to computation. The CCA was run using the Past 3.10 software (Hammer et al., 2001). Significance of canonical axes was tested via permutation computed for N = 999. Results are available as Supplemental material.

4.4.7 Metagenomic Libraries and Taxonomic Identification of Functional Genes

Two iDNA samples (S site: 27.5 cmblf; D site: 32.5 cmblf) were sent to the DOE Joint Genome Institute (JGI, University of California) for metagenomic sequencing and assembling (Chin et al., 2013). Samples received accession number I17A3 metaG (project ID: 1107606) and I19B2 metaG (project ID: 1107610) and are included in the Microbial Dark Matter project (proposal ID: 1477). Metagenomic data were obtained via second and third generation high throughput sequencing platforms. Structural and functional annotation was carried out through the JGI's Microbial Genome Annotation Pipeline (MGAP v. 4) as described in (Huntemann et al., 2015). Assembled metagenomic data were screened on the JGI Genome portal IMG/M (http://genome.jgi.doe.gov/) and predicted protein sequences of dissimilatory sulfite reductase alpha and beta subunits (*dsrAB*), adenylylsulfate reductase alpha and beta subunits (*aprAB*), formate-tetrahydrofolate ligase (*fhs*), and methyl coenzyme M reductase alpha to gamma subunits (*mcrA*) were exported for taxonomic identification.

Protein encoding genes and open reading frames (ORFs) were assigned to high-level taxonomic groups (class level and above) using PhymmBL (Brady and Salzberg, 2009). The interpolated Markov model (IMM) bacterial and archaeal database was implemented with genomes available in the NCBI RefSeq database and JGI database, using the customGenomicData.pl script available with the PhymmBL download. Taxonomic identifications were integrated with the functional annotations performing BLASTp searches of ORFs against the SEED database, as described previously (Orsi et al., 2017; Orsi et al., 2013).

4.5 Acknowledgments

This study was financially and logistically supported by the ICDP priority program of the Deutsche Forschungsgemeinschaft (DFG Schwerpunktprogramm) through grants to Jens Kallmeyer (KA 2293/8-1), Aurèle Vuillemin (VU 94/1-1) and William Orsi (OR 417/1-1); the Swiss National Science Foundation (SNSF grant no. P2GEP2_148621 to Aurèle Vuillemin); the Helmholtz Center Potsdam, German Research Center for Geoscience (GFZ); and an NSERC Discovery grant (no. 0487) to Sean A. Crowe.

We thank Tri Widiyanto and his staff from the Indonesia Research Center for Limnology for their administrative support in obtaining the Scientific Research Permit. Jan Axel Kitte, Carriayne Jones, Sulung Nomosatryo and Céline C.P. Michiels are thanked for their assistance during sampling at Lake Towuti, and PT Vale Indonesia for field support. The supervision during Illumina Miseq procedure of Jan Pawlowski, Maria Holzmann, Laure Perret-Gentil, Emanuela Reo and their research partners at the University of Geneva (Switzerland) are kindly acknowledged. Florian Schubert is thanked for processing the samples for total reduced inorganic sulfur analysis.

4.6 Supplemental Material

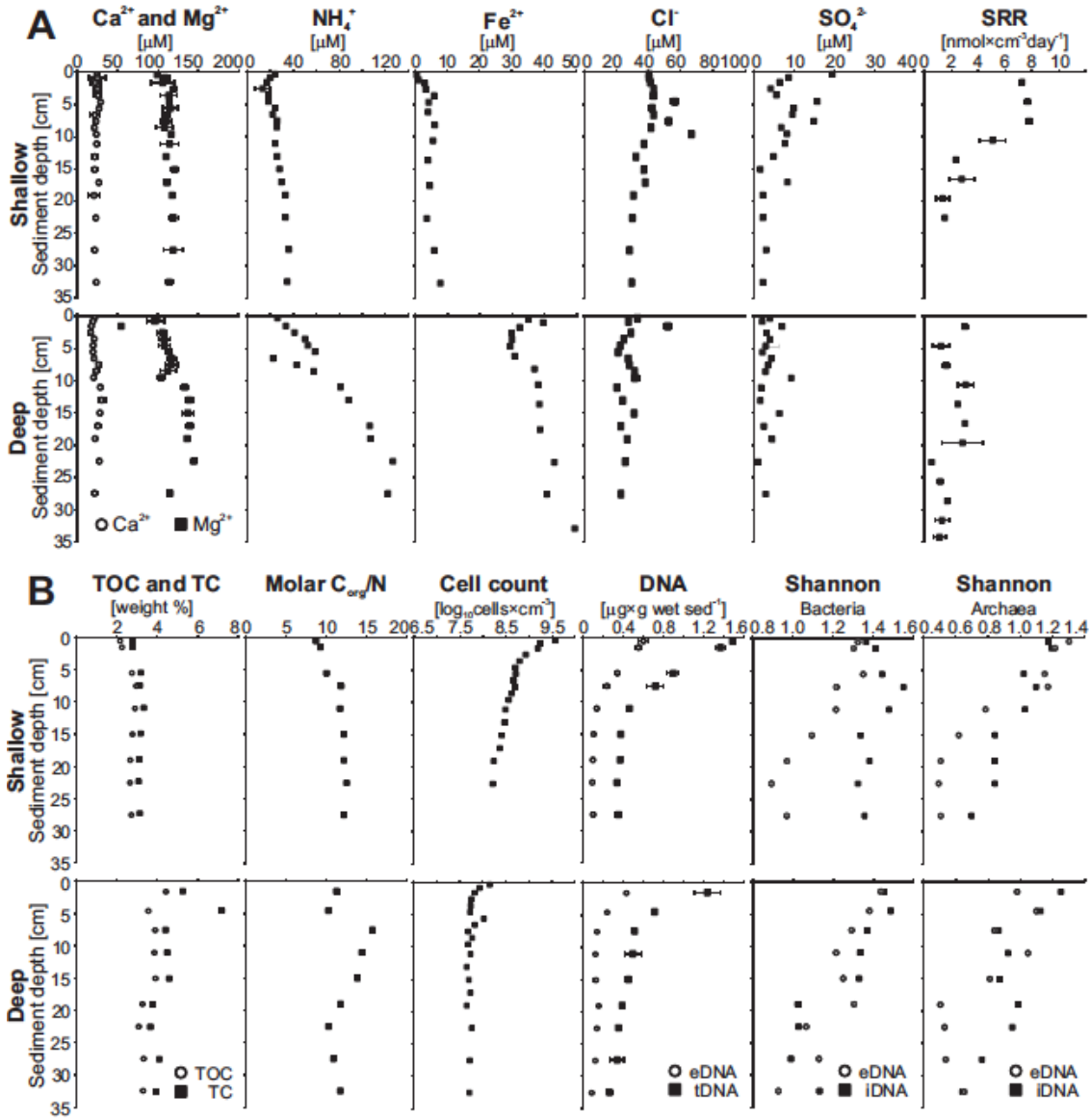

Figure S 4.1: *Multiple sediment downcores obtained for the shallow and deep site. From left to right: (A) Calcium, magnesium, ammonium, dissolved iron, chloride and sulfate concentrations [µM] measured in the pore water; potential sulfate reduction rates [nmol × cm^{-3} day^{-1}]. (B)*

Total organic carbon, total carbon [weight %] and molar C /N ratio measured in bulk sediments; cell counts in log scale [log cells × cm-^{3}]; concentrations of extracellular DNA (grey dots) and total DNA (black squares) [µg × g^{-1} wet sed], with distance between the two curves corresponding to intracellular DNA concentrations; Shannon index established from bacterial and archaeal DGGE gel features, with eDNA (grey dots) and iDNA (black squares) displayed separately (from Vuillemin et al., 2016).

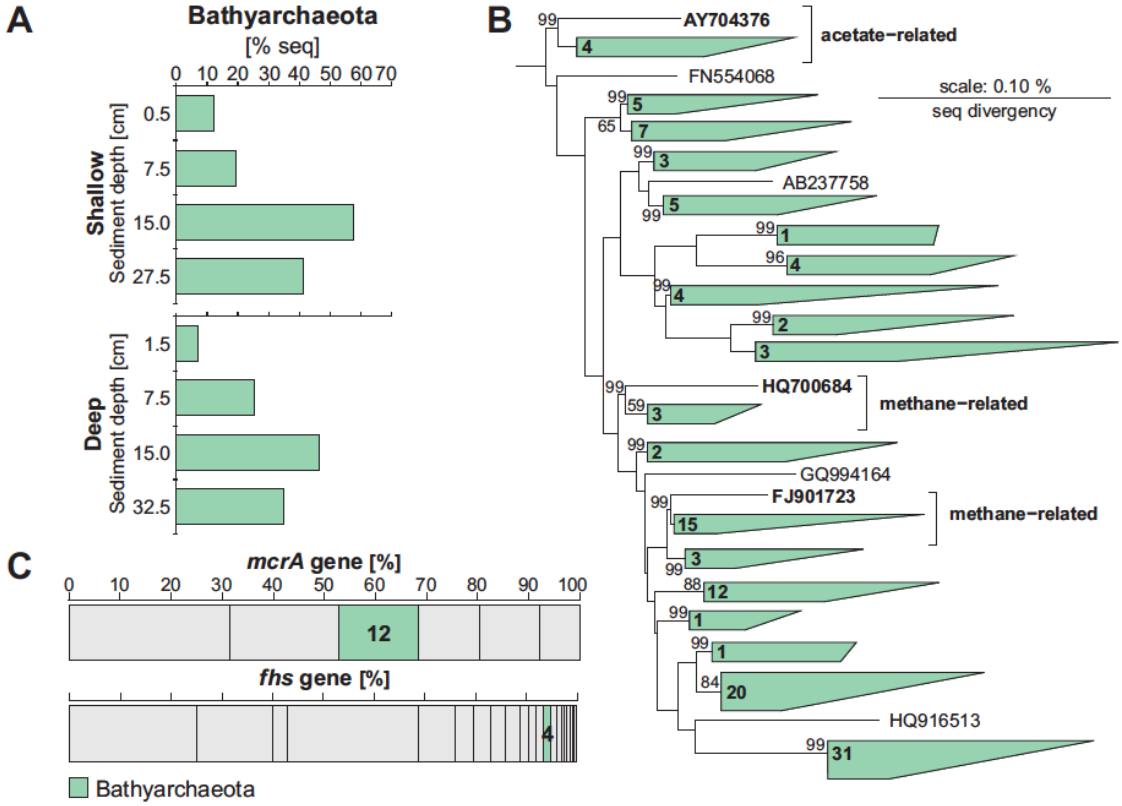

Figure S 4.2: *Relative abundances, phylogenetic tree and functional gene affiliation for Bathyarchaeota sequences. (A) Bar charts displaying the relative abundances of sequences affiliated with Bathyarchaeota. (B) Maximum Likelihood phylogenetic tree based on partial 16S rRNA gene sequences established for Bathyarchaeota representative OTUs. (C) Taxonomic affiliation for the mcrA-G and fhs gene presently including 12 and 4 sequences identified as Bathyarchaeota, respectively.*

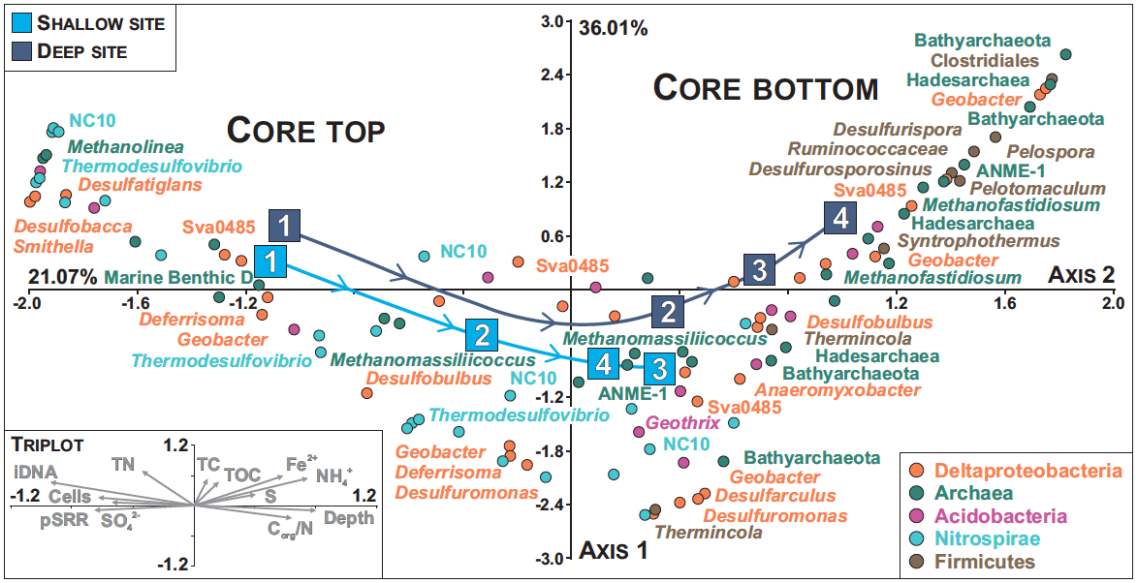

Figure S 4.3: *Canonical correspondence analysis based on 12 environmental parameters with representative operational taxonomic units. The distribution of samples for the shallow and deep site reflects a depth trend as shown by all significant variables of the triplot (insert down left). Taxa can be successively traced from left to right to infer species related to iron, sulfur and hydrogen cycling with sediment depth.*

Table S 4.1: *Table summarizing the number of representative OTUs per phyla and relative abundances for each metabolic category. Relative abundances are listed according to sample depth for the shallow (0.5, 7.5, 15.0, 27.5 cmblf) and deep (1.5, 7.5, 15.0, 32.5 cmblf) sites. Unresolved OTUs correspond to the different candidate divisions plotted in the phylogenetic trees (Figures 4.4A -D).*

	Sulfate reducers				Iron reducers				Hydrogen producers				Methane producers				Methane consumers			
Deltaproteobacteria	**25 OTUs**				**19 OTUs**				**4 OTUs**											
Site S relative %	25.0	10.5	5.5	6.1	4.3	8.7	8.5	9.6	0.7	0	0	0								
Site D relative %	22.2	8.4	6.0	3.8	4.0	10.7	7.5	10.7	0.4	0	0	0								
Archaea									**6 OTUs**				**36 OTUs**				**2 OTUs**			
Site S relative %									0.4	1.5	5.1	5.3	4.2	8.7	2.1	5.4	0.6	2.0	2.9	2.9
Site D relative %									0.3	4.6	3.7	5.1	3.7	5.6	7.3	6.8	1.0	1.8	2.6	2.1
Acidobacteria					**3 OTUs**															
Site S relative %					3.0	3.7	1.3	3.2												
Site D relative %					4.9	3.3	1.5	2.7												
Nitrospirae	**25 OTUs**																**7 OTUs**			
Site S relative %	10.9	7.3	1.3	4.4													2.8	1.2	0.5	0.9
Site D relative %	8.1	1.2	0.5	1.5													6.7	1.1	0.5	0.8
Firmicutes	**6 OTUs**				**4 OTUs**				**23 OTUs**											
Site S relative %	0	0	0	0	0	0	0	0	0	0	0	0.2								
Site D relative %	0	0.6	0.7	2.2	0	0.5	0.3	0	0	0.7	3.1	10.5								
Total % Site S	**35.9**	**17.8**	**6.8**	**10.5**	**7.3**	**12.4**	**9.8**	**12.8**	**1.1**	**1.5**	**5.1**	**5.5**	**4.2**	**7.2**	**0.9**	**0.6**	**3.4**	**3.2**	**3.4**	**3.8**
Total % Site D	**30.3**	**9.8**	**7.2**	**7.5**	**8.9**	**14.0**	**9.0**	**15.4**	**0.7**	**5.3**	**6.8**	**15.6**	**3.7**	**2.8**	**1.4**	**1.8**	**7.7**	**2.9**	**3.1**	**2.9**
Candidate clades	**Deltaproteobacteria: 16 OTUs / Archaea: 15 OTUs / Acidobacteria: 29 OTUs / Nitrospirae: 0 OTUs / Firmicutes: 2 OTUs**																			

5 Iron oxide reactivity controls organic matter mineralization in ferruginous sediments

Organic matter mineralization and diagenesis in ferruginous sediments played a key role in biogeochemical cycling during the Archaean and Proterozoic eons. However, knowledge of organic matter mineralization in ferruginous sediments remains almost entirely conceptual, as analogous modern sediments are extremely rare and largely unstudied. Lake Towuti on Sulawesi Island, Indonesia, is such a rare example. The lake water is poor in sulfate and other electron acceptors and persistently anoxic below 130 m. Due to strong weathering of ultramafic bedrock in the catchment, the lake receives large amounts of iron oxides, leading to sediment with >20 wt% iron content.

We used several biogeochemical analyses to assess rates and pathways of organic matter mineralization in these modern ferruginous sediments. Despite an abundance of ferric iron minerals known to support microbial respiration in laboratory experiments, organic matter degradation proceeds predominantly through methanogenesis. Iron reduction appears to be quantitatively important only in the upper centimeter of the sediment column; below this zone ferric iron minerals are still present in appreciable and relatively constant concentrations. This implies that ferric iron can be buried over geologic timescales, even in the presence of labile organic carbon. Co-existence of abundant methane and ferric iron throughout the sediment further suggests negligible anaerobic methane oxidation coupled to iron respiration. This tendency towards methanogenesis, without anaerobic methane oxidation, implies that methanogenesis would have been important to organic matter mineralization in Precambrian times, leading to high atmospheric CH_4 concentrations, and playing a key role regulating Earth's early climate.

5.1 Main Text

Atmospheric chemistry, and its evolution over geological time, is intrinsically linked to the burial and mineralization of organic matter (Berner, 1989). Burial of organic matter

can be a net source of oxidants (like oxygen) as well as a net sink of CO_2, and its mineralization can result in release of greenhouse gasses like methane (Keil, 2011). In modern marine sediments, overlain by oxygenated bottom waters with abundant sulfate, much of the organic matter mineralization proceeds via a combination of aerobic respiration and sulfate reduction (Jørgensen, 1982). In these sediments, oxygen exposure directly controls sedimentary organic carbon preservation and bottom water anoxia increases carbon burial rates (Hartnett et al., 1998). The Precambrian ocean-atmosphere system was much different than today's—the atmosphere was only weakly oxygenated, seawater was sulfate poor, and the oceans were generally characterized by anoxic ferruginous (Fe-rich) conditions (Crowe et al., 2014b; Poulton and Canfield, 2011). Precipitation of Fe from these oceans resulted in the widespread deposition of ferruginous shales and, in more extreme cases, banded iron formations (BIFs) (Poulton and Canfield, 2011). The fate of organic matter in Precambrian sediments is thus intrinsically linked to coupled C and Fe cycling.

In the complete or near absence of oxygen, nitrate and sulfate, organic matter mineralization in ferruginous sediments would be expected to proceed anaerobically via the energetically most favorable terminal electron acceptors available - in this case ferric iron, followed by CO_2 through methanogenesis (Froelich et al., 1979a). Prior work in freshwater and wetland sediments indeed shows that iron reducing bacteria outcompete methanogens for electron donors (Roden and Wetzel, 2003), even when Fe(III) is supplied in the form of more crystalline oxy(hydr)oxides like goethite (FeOOH), provided surface area is sufficiently high to allow microbial access to Fe(III) surface sites (Roden, 2003). The role of Fe-reduction in organic matter mineralization, however, remains largely untested in Fe(III)-rich modern ferruginous environments analogous to those of the Precambrian oceans. The only study to date investigated the permanently stratified water column of Lake Matano, Indonesia (Crowe et al., 2011). Based on water column methane profiles and mass balance arguments it suggested that, despite abundant iron, methanogenesis is responsible for up to 90% of the total anaerobic organic matter mineralization. Process rates, however, were not measured and the role of methanogenesis both in modern and ancient ferruginous sediments thus remains largely untested through direct measurements. We therefore recovered modern ferruginous sediments from Lake Towuti, Indonesia, and used a suite of biogeochemical analyses to directly determine rates and pathways of organic matter mineralization.

Lake Towuti is situated on Sulawesi Island, has a maximum water depth of 203 m (Fig S5.1) and is weakly thermally stratified with a well-mixed oxygenated surface layer that extends to 70 m depth, and waters below 130 m that are persistently anoxic. Intensive weathering of ophiolitic bedrock from the catchment supplies the lake with a strong influx of iron(oxy)hydroxides and runoff that contains little sulfate, leading to sulfate-poor (< 20 µM) lake water and anoxic ferruginous conditions with Fe^{2+} concentrations up to 40 µM below 130 m (Costa et al., 2015). Such conditions were also reported in nearby Lake Matano, which is considered broadly analogous to Precambrian ferruginous oceans (Crowe et al., 2008a). As part of the Towuti Drilling Project (TDP) of the International Scientific Drilling Program (ICDP), we recovered sediment from a water depth of 153 m (Fig. S5.1), well below the oxycline at the time of sampling (Costa et al., 2015). The drill core was supplemented with short (< 0.4 m) gravity cores that better preserve the sediment-water interface (SWI). Radiocarbon dating revealed a nearly constant sedimentation rate of 19 cm ka^{-1}, yielding an estimated age of ~ 60 ka at 12m depth (Russell et al., 2014).

Lake Towuti's sediment is rich in organic carbon (TOC 0.4-4 wt%) with elemental compositions implying that it is reactive (molar C:N ratio 11-25), readily fermented (Fig. 5.1), and consequently suitable to support microbial life. Given a sedimentation rate of 19 cm ka^{-1} (Russell et al., 2014) and a bulk density of 1.3 g cm^{-3}, these organic carbon concentrations translate to an organic carbon accumulation rate between 220 and 1800 mmol m^{-2} yr^{-1}, and thus place an upper bound on rates of total sedimentary carbon respiration. Fermentation is a key step in organic matter mineralization and its main products are volatile fatty acids (VFA), which are known electron donors for iron reduction (Lovley and Phillips, 1986). We detected formate, acetate, lactate, propionate and butyrate (Fig. 5.2), all showing highest concentrations in the upper 2-6 m. Ammonium, which is also a product of organic matter mineralization (Froelich et al., 1979), reaches peak concentrations around 6 m (Fig. 5.2). Taken together, these results indicate that microbial degradation of organic matter takes place throughout the sediment, with highest rates observed in the upper 6 m below the SWI.

Lake Towuti's sediment has extremely high total Fe concentrations (Fig. 5.1), with maximum values > 2500 µmol Fe cm^{-3} (20 % dry wt.). In most sediments, however, only a fraction of the total Fe pool is geochemically and biologically reactive and has the capacity to participate in redox-reactions associated with organic matter

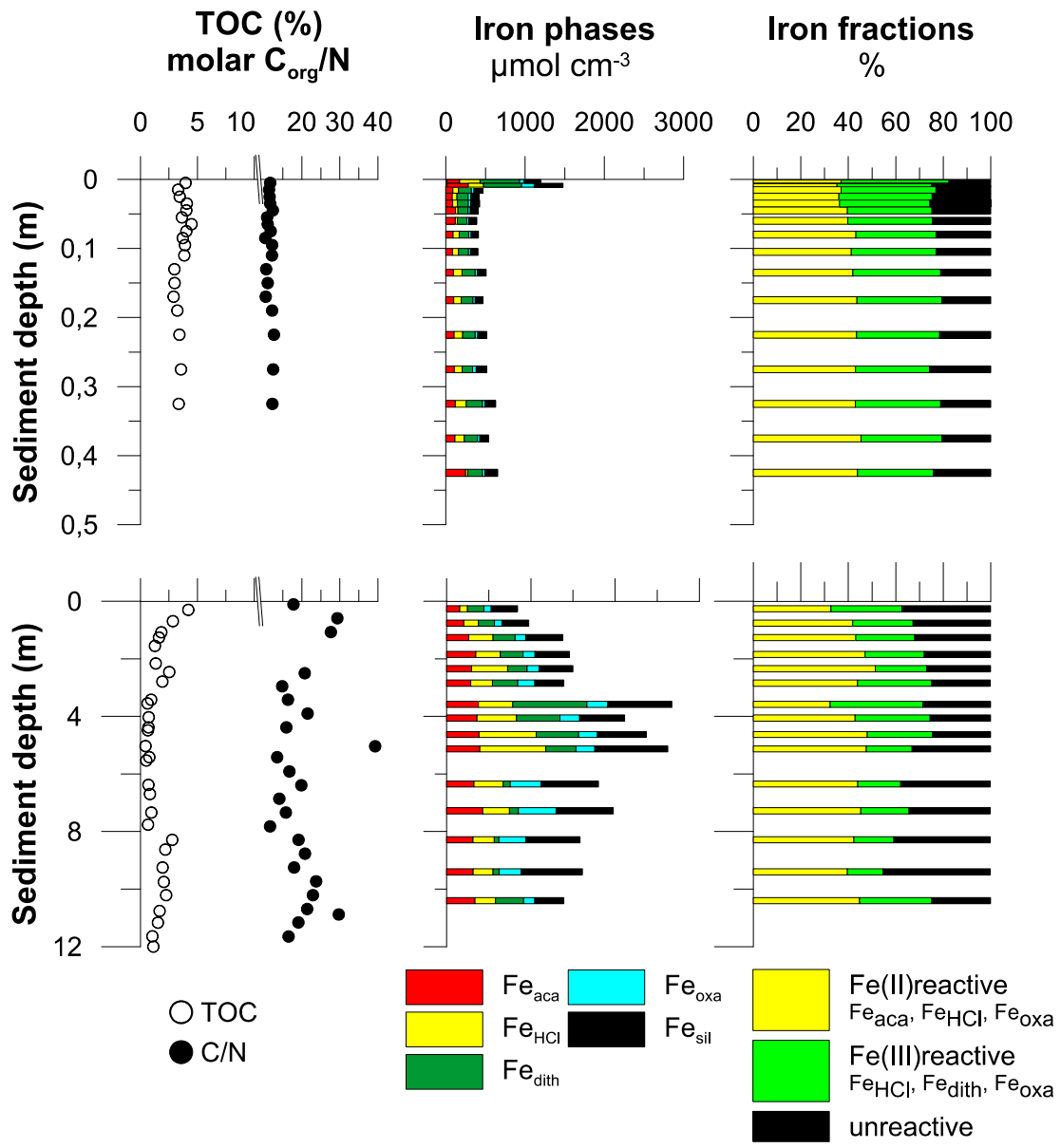

Figure 5.1: *Sediment characteristics. Total organic carbon content in bulk sediment and molar C_{org}/N ratio (left row), sequentially extracted iron phases (center row) and iron fractions (right row) of Lake Towuti sediment of the short (< 0.4 m) gravity core (upper panel) and the 12 m TDP drill core (lower panel). See main text and Supplemental material for detailed description of the iron phases. Total organic carbon content as well as molar C_{org}/N ratios of the short gravity core were taken from Vuillemin et al. (2016).*

mineralization and sediment diagenesis (Canfield, 1997). We thus conducted a suite of selective sequential extractions to determine both the reactive fraction of the sedimentary Fe pool and its transformations during organic matter mineralization and diagenesis in Lake Towuti's sediments (Fig. 5.1). Extraction with 0.5N HCl captures the non- to poorly-crystalline ferric iron (Fe(III)) oxyhydroxides generally considered to be readily available to Fe-respiring microorganisms (Lovley and Phillips, 1986), as well as corresponding respiration products including sorbed ferrous iron (Fe(II)), siderite,

and green rust (Poulton and Canfield, 2005). While 0.5N HCl extractable Fe(II) is abundant at all depths, comprising up to 30 % of the total Fe pool, Fe(III) in this pool is below our limit of detection (10 μmol cm^{-3}) in all samples. So, despite very high total Fe concentrations, Fe(III) phases considered readily available to Fe-respiring microorganisms (Lovley and Phillips, 1986) are virtually absent from Lake Towuti's sediments.

Fe(III) phases not extracted in 0.5N HCl, like goethite, hematite, Fe(III)-bearing crystalline clays like nontronite, can also be respired under some laboratory and environmental conditions (Roden, 2003) and such phases have been shown to react with hydrogen sulfide during diagenesis in marine sediments (Canfield et al., 1992). These phases are thus also considered part of the reactive Fe(III) pool expected to play a role in sediment diagenesis. We therefore targeted these phases using sodium dithionite extractions (Poulton and Canfield, 2005) and found them to be abundant in Lake Towuti's sediments, comprising up to 880 μmol cm^{-3} or 33 % of the total Fe pool (Fig. 5.1). Although this theoretically bioavailable Fe(III) pool (Fe_{HCl}, Fe_{dith}) accounts for up to 39% of the total Fe, it shows little variation with depth. The only exception is a notable decrease in dithionite extractable Fe concentrations in the upper one cm below the SWI (Fig. 5.1).

The apparent lack of Fe(III) reduction in much of the sediment is consistent with the distribution of Fe^{2+} concentrations in pore water. Modeling based on diffusive fluxes of pore water Fe^{2+} indicates very low net rates of background Fe(III) reductive dissolution (~ 1 mmol m^{-2} y^{-1}) in the upper 4 m (Fig. 5.2). Modeling based on solid phases indicates that Fe(III) reduction rates are highest in the upper 1 cm, just below the SWI (53 mmol m^{-2} yr^{-1}), and the depth-integrated Fe(III) reduction rate for the remaining 12 m is 105.4 mmol m^{-2} yr^{-1}, resulting in a total depth-integrated Fe reduction rate of 158 mmol m^{-2} yr^{-1} over the upper 12 m. Assuming a 4:1 stoichiometry of iron reduction coupled to organic carbon oxidation (Canfield et al., 1993), this translates to an organic carbon degradation rate of 39.5 mmol m^{-2} yr^{-1}, which is low compared to total organic carbon accumulation rates at the SWI. These observations thus reveal that microbial Fe reduction is restricted to the uppermost sediment layer in Lake Towuti and imply that Fe(III) phases like goethite are stable throughout the sediment studied and over tens of thousands of years.

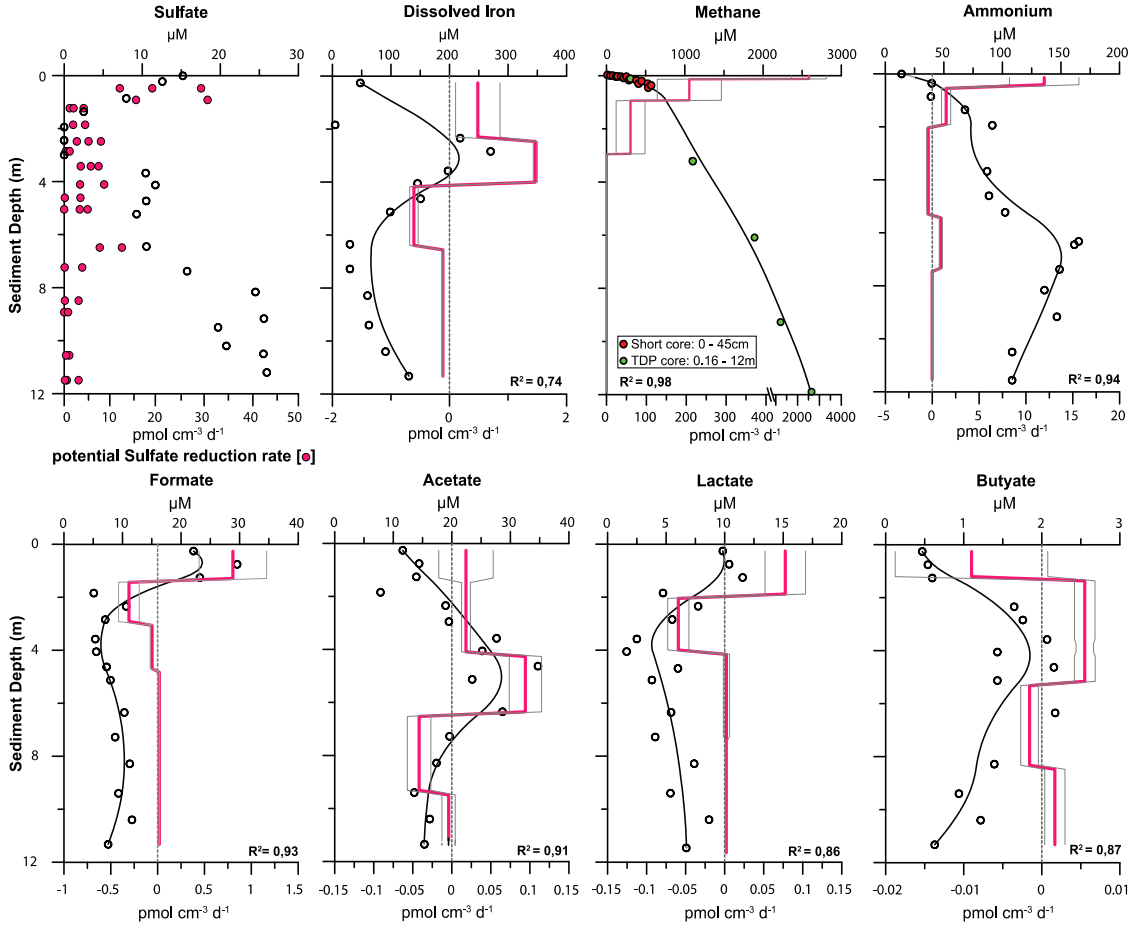

Figure 5.2: *Pore water chemistry of reactants involved in OM mineralization. Open circles show concentrations in sediment pore water, pink circles indicate potential sulfate reduction rates (pSRR), determined by radiotracer experiments. The black lines show the modeled concentration profiles (see Supplemental material, SM), R^2 showing the correlation coefficient of the fit. The pink solid line shows the calculated mean reaction rate profile together with its standard deviation (grey line). Top x-axis shows the concentration, bottom x-axis indicates the reaction rate, positive values indicate net production, negative values net consumption of the respective compound.*

Given the apparently minor role of Fe reduction, in light of the relatively high abundances of canonically reactive Fe(III) and labile organic matter, we explored other pathways of organic matter mineralization. Sulfate reduction commonly follows Fe reduction in order of decreasing free energy yield in marine sediments (Froelich et al., 1979). Pore water sulfate concentrations in Lake Towuti are extremely low and decrease from 15 µM at the SWI to below our detection limit (1 µM) in the upper cm of the sediment (Fig. 5.2). Nevertheless, while geochemical modeling predicts sulfate reduction in the upper 4 m (Fig. S 5.3), radiotracer incubation experiments reveal potential for sulfate reduction over the entire 12 m depth interval (Fig. 5.2). Depth-integrated rates of measured potential sulfate reduction rates (pSRR) are 18 ± 9.5 mmol m^{-2} yr^{-1}, while modeled depth-integrated rates of sulfate reduction are 0.22 ± 0.15 mmol m^{-2} yr^{-1}, which correspond to an organic carbon oxidation rate of 36 ± 19 mmol m^{-2} yr^{-1}

and 0.44 ± 0.3 mmol m^{-2} yr^{-1}, respectively, based on a 1:2 stoichiometry between sulfate reduction and organic carbon oxidation. Assuming that the measured pSRR and the modeled rates represent the respective upper and lower estimate of sulfate reduction (Supplemental material), we conclude that, like iron reduction, sulfate reduction plays only a minor role in organic matter degradation. Nevertheless, the observation that pSRR persists throughout the core confirms microbial reactivity of organic matter in these sediments.

Methanogenesis is commonly referred to as the final step in organic matter mineralization as it has the lowest free energy yield in the canonical cascade of early diagenetic redox reactions. In Lake Towuti, pore water methane concentrations increase continuously from 23 µM at the SWI to 2600 µM at 12 m depth (Fig. 5.2). The accumulation of methane throughout the sediment implies that methanogenesis occurs at all depths. This is further supported by our modeling based on pore water methane concentrations (Fig. 5.2 and S5.4) as well as by incubation-based measurements of potential hydrogenotrophic and acetoclastic methane production (Fig S 5.2). Sediment samples from three depths (0.36 m, 2 m and 7.4 m), reveal the potential for methanogenesis at all depths and by both pathways. The fact that methane concentrations at the SWI are not zero indicates a methane efflux out of the sediment into the water column (Fig. 5.2 and S5.4). These modeling results are supported by the stable isotopic composition of pore water CH_4 and CO_2 (Fig. 5.3): $\delta^{13}C$- and δD-values of methane around -70‰ vs VPDB and -170‰ vs VSMOW, respectively, indicate biogenic methane, and the parallel increase of $\delta^{13}C(CH_4)$ and $\delta^{13}C(CO_2)$ is consistent with the consumption of CO_2 by hydrogenotrophic methanogenesis (Whiticar, 1999). As $\delta^{13}C(CH4)$ and $\delta^{13}C(CO_2)$ rise from -72.7 to -66.7‰ and from -14.5 to -12.3‰ vs VPDB, respectively (Fig. 5.3), the isotope difference between CH_4 and its precursor CO_2 ranges from ~63-54‰ (ε-value according to Friedman and O'Neil, 1977) consistent with the isotopic fractionation reported for methanogens (Conrad, 2005).

The modeled depth-integrated rate of methane production over the upper 12 m was 222 ± 86 mmol m^{-2} yr^{-1}. Assuming a 2:1 stoichiometry for the conversion of organic matter to methane, methanogenesis accounts for the conversion of 444 ± 172 mmol m^{-2} yr^{-1} organic carbon. This rate far exceeds those of all other carbon mineralization processes combined but is still less than, and therefore approximately balanced by, the carbon accumulation rate. Sulfate reduction, iron reduction as well as

methanogenesis combined add up to a total organic carbon mineralization rate of 519 ± 191 mmol m^{-2} yr^{-1}, within the upper 12m of sediment, with methanogenesis being the dominant process (85 - 92%) followed by iron reduction (8 %) and sulfate reduction (<1-7 %).

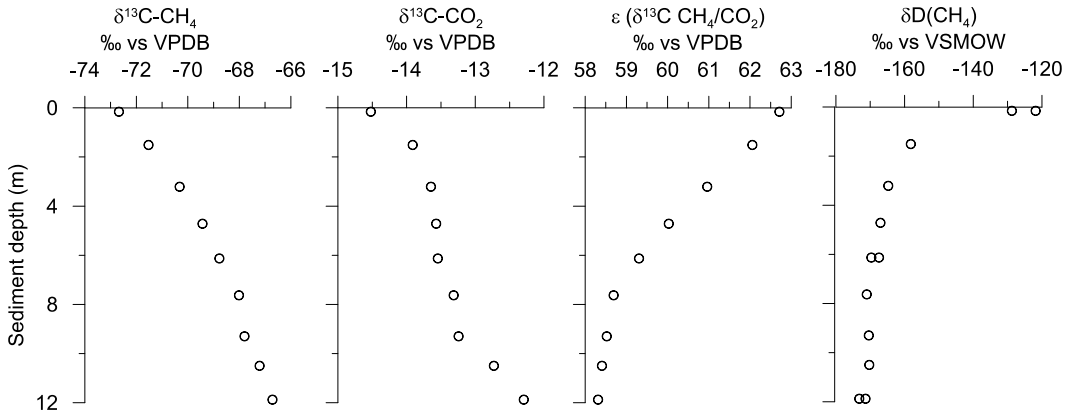

Figure 5.3: *Isotopic composition of methane and carbon dioxide. Isotopic composition of methane and carbon dioxide as well as the isotopic difference between $\delta^{13}C(CO_2)$ and $\delta^{13}C(CH_4)$. See main text and Supplemental material for details*

Microbial methanogenesis produces most of the methane on Earth and marine anaerobic oxidation of methane (AOM) effectively attenuates methane effluxes from marine sediments to the atmosphere (Knittel and Boetius, 2009). AOM coupled to sulfate reduction consumes more than 90% of the total methane produced in seafloor sediments providing a buffer between methane produced in these sediments and the atmosphere (Knittel and Boetius, 2009). In environments where sulfate is scarce, AOM has been linked to the reduction of nitrate (Deutzmann and Schink, 2011) and ferric Fe (Sivan et al., 2011). With nitrate below the limit of detection (4 µM) and very little sulfate, Fe-dependent AOM remains the only pathway with potential to quantitatively consume methane in Lake Towuti's sediment. Pore water profiles, however, show no evidence for net methane consumption and Fe-reduction rates are small, so we thus conclude that AOM coupled to Fe-reduction is negligible in Lake Towuti's sediments.

Our data demonstrate that microbial methanogenesis is the dominant (> 85 %) pathway for carbon mineralization in Lake Towuti sediment and that Fe-reduction plays a relatively minor role in this sedimentary ecosystem despite an abundance of Fe(III)-containing minerals. This has important implications for global biogeochemical cycling in the ferruginous oceans of the Archean and Proterozoic eons. Photosynthesis in the Archean and Proterozoic eons would have led to the production of organic matter, and

under ferruginous ocean conditions, the deposition of Fe(III)-rich sediments, either through direct photosynthetic Fe-oxidation (photoferrotrophy) (Crowe et al., 2008a) or through reaction of Fe(II) with oxygen produced through oxygenic photosynthesis (Canfield, 2005). Rates of organic matter production through photosynthesis during much of the Precambrian Eons were likely between 1 and 10% of modern values, or 40-400 Tmol yr^{-1} (Canfield et al., 2006; Laakso and Schrag, 2019) and if organic carbon burial efficiency was comparable to the modern (1-10%) (Hedges and Keil, 1995; Katsev and Crowe, 2015), this translates to global mineralization rates between 36 and 396 Tmol yr^{-1}. While both Fe-reduction and methanogenesis likely evolved early in the Archean Eon (Ueno et al., 2006; Vargas et al., 1998), we argue that by analogy to Lake Towuti, much of the Fe(III) produced through photosynthesis could have been buried without appreciable respiration and reduction coupled to oxidation of co-deposited organic carbon. Decoupled from Fe-reduction, this organic matter would have accumulated in sediments and supported appreciable methanogenesis. By analogy to Lake Towuti's sediments, breakdown of 85-92 % of organic carbon through methanogenesis would have led to marine CH_4 production of 15-180 Tmol yr^{-1}. In oceans lacking appreciable oxygen and sulfate (Crowe et al., 2014), sedimentary methanogenesis fueled by organic matter would, in the absence of Fe-dependent AOM, have led to equivalent effluxes of CH_4 to the overlying oceans and atmosphere.

Atmospheric CH_4 concentrations can be approximated through new solutions to photochemical models for a given biospheric CH_4 production flux (Ozaki et al., 2018), which imply enormous concentrations from 150 up to 24000 ppmv, depending on biological productivity and organic carbon burial efficiencies. Such strong predicted Precambrian biospheric CH_4 fluxes and atmospheric CH_4 concentrations, versus previous work (Ozaki et al., 2018), are largely the result of the high conversion efficiency of organic carbon to CH_4, as observed in Lake Towuti's sediments. We note, however, that growth of oceanic oxygen and sulfate pools would attenuate CH_4 fluxes and atmospheric concentrations, accordingly. Nevertheless, the atmospheric CH_4 concentrations that are possible when conversion efficiencies from organic carbon are high would have had a strong effect on climate when the oceans existed in ferruginous states.

5.2 Materials and Methods

ICDP drilling campaign and sampling procedure

In 2015 a scientific drilling campaign took place on Lake Towuti within the framework of the International Continental Scientific Drilling Program (ICDP). We retrieved a ~114 m long sediment core dedicated for geomicrobiological investigations from Drill Site 1 at a water depth of 153 m using the ICDP Deep Lakes Drilling System (Cohen et al., 2016). Our study focuses on the upper 12 meters of the drill core, a section equivalent to sediments that have already been subject to comprehensive paleoclimatic investigations, which also supplied sediment ages and estimates of sedimentation rates (Costa et al., 2015). Cores were collected in HQ-size butyrate liners (66 mm core diameter) in 3 m intervals using hydraulic piston coring. After retrieval, sediment cores were cut into two subsections of 1.5 m length. In addition, short (< 0.4 m) sediment cores were retrieved from the same site using a small gravity-coring device that recovered an undisturbed sediment-water interface (SWI) and allowed interrogation of the uppermost sediments in more detail.

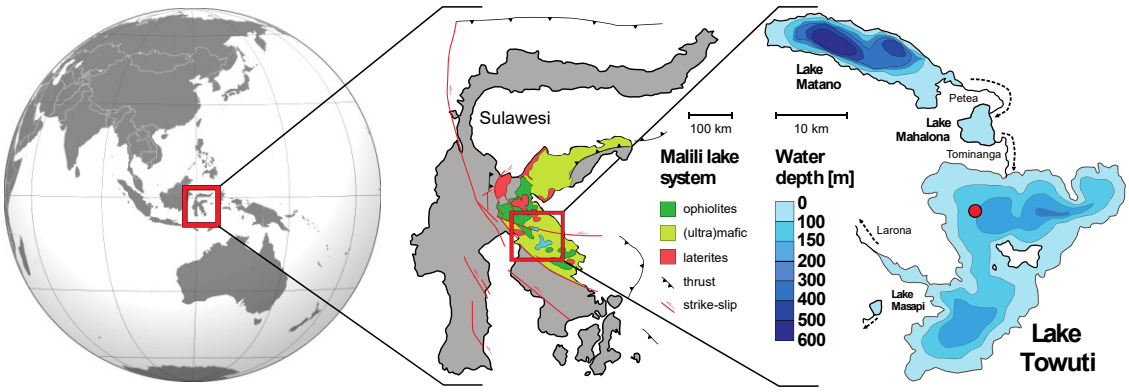

Figure S 5.1: *Lake Towuti location and geological setting. Map of Sulawesi Island illustrating the geological setting of the Malili Lake system, a chain of five tectonic lakes, with Lake Towuti being the largest. The red dot on the bathymetric map marks the location of the drilling site, which is located at a water depth of 153 m, well below the depth of the oxycline (130 m). Figure modified after Vuillemin et al. (2016).*

Pore water sampling and analysis

Whole round cores (WRC, 100 mm long x 66 mm diameter) were cut from the recovered sediment drill core, immediately capped and transferred into a N_2-filled anaerobic chamber that was set up on site. Sediment was transferred under N_2 to an IODP-Style PTFE-titanium pore water extractor (Manheim, 1966) and squeezed using a 22-ton hydraulic press (Carver Inc., Wabash, USA). Pore water samples were filtered

through a sterile 0.2 µm syringe filter and collected in a glass syringe that was pre-flushed with nitrogen. Dissolved Fe concentrations were analyzed on site whereas the remaining pore water samples were preserved for later analysis of dissolved cat- and anions as well as volatile fatty acids (VFAs).

Concentrations of major anions (i.e. Cl^-, SO_4^{2-}, NO_3^-, NO_2^-) in the pore water were measured by suppressed ion chromatography using a SeQuant SAMS anion IC suppressor (EMD Millipore, Billerica, Massachusetts), a S5200 sample injector, a 3.0 × 250 mm LCA 14 column and a S3115 conductivity detector (all Sykam, Fürstenfeldbruck, Germany). The eluent was 5 mM Na_2CO_3 with 20 mg L^{-1} 4–hydroxibenzonitrile and 0.2 % methanol. Flow rate was set to 1 mL min^{-1} and column oven temperature to 50°C. For cations (i.e. Na^+, NH_4^+, K^+, Mg^{2+}, Ca^{2+}), the IC system consisted of a S5300 sample injector (Sykam), a 4.6 × 200 mm ReprosilCAT column (Dr. Maisch HPLC, Ammerbuch-Entringen, Germany) and a S3115 conductivity detector (Sykam). The eluent was 175 mg L^{-1} 18-Crown-6 and 120 µL methanesulfonic acid. Flow rate was set to 1.2 mL min^{-1} and column oven temperature to 30°C. Detection and quantification limits were calculated based on signal-to-noise (S/N) ratios of 3 and 10, respectively. All samples were measured in triplicates and every ten injections a standard was measured to check for drift. Reproducibility was always better than 5 % for each ion. Detection limits for the major an- and cations ranged between 1 – 4 µM and 6 – 11 µM, respectively.

Concentrations of volatile fatty acids (VFAs) in the pore water were measured by 2-dimensional ion chromatography mass spectrometry (2D IC-MS) (Glombitza et al., 2014). This technique allows analysis of the following VFAs: lactate, acetate, propionate, formate, butyrate, pyruvate, valerate (Glombitza et al., 2014). As the method was originally developed for marine pore water samples, some modifications were made, as described below, to account for the low salinity of the pore water of Lake Towuti. The instrument used for 2D IC-MS analysis was a Dionex ICS3000 coupled to a Surveyor MSQ Plus mass spectrometer (both Thermo Scientific). Briefly, in this method the first IC dimension is used to separate the VFAs from other inorganic ions. The VFAs are trapped on a concentrator column and subsequently separated in the second IC dimension. To account for the effect of low salinity, the retention time window of the eluent flow from the first column that is directed to the concentrator column was shifted by one minute to 3.5 - 8.5 min as compared to the marine pore

water analysis protocol (Glombitza et al., 2014). Prior to analysis, the samples were filtered through disposable Acrodisc® 13 mm IC syringe filters (pore size 0.2 µm) that were rinsed with 10 mL Milli-Q® water (Ultrapure Type 1) directly before use. The first 0.5 mL of pore water after filtration was discarded while the second 0.5 mL was used for analysis. Quantification was achieved by a 3-point calibration with external standards containing a mixture of the analyzed VFAs at different concentrations (i.e. 200, 500 and 800 µg L^{-1}) prepared in Milli-Q® water. Blank runs of pure Milli-Q® water were used to correct the peak areas for the small background peaks deriving from accumulation of VFAs from the eluent in the trap column. Detection limits for the individual VFAs were all between 0.1 and 0.5 µM (i.e. formate: 0.37 µM, acetate: 0.19 µM, propionate 0.13 µM, butyrate: 0.09 µM). All core sections were checked for contamination that could potentially be caused during drilling operations (Friese et al., 2017). Samples from contaminated sections were identified by quantification of an artificial tracer compound added to the drilling mud prior to the drilling and were discarded.

Iron speciation

For iron speciation, a sub sample of 500 mg of wet sediment from each core interval of both sediment cores was extracted in the field and immediately leached in 1 ml 0.5 N HCl, and Fe-speciation (Fe(II) and Fe(III)) of the easily extractable Fe-phases was measured spectrophotometrically on site using a ferrozine assay (Thamdrup et al., 1994; Viollier et al., 2000). The complete Fe-speciation protocol was performed on anoxically preserved and freeze-dried sediments milled to fine powders using an agate hand mortar and pestle. Sample masses of 200 mg of sediment were weighed into 15 mL centrifuge tubes, and subjected to the Fe-speciation sequential extraction scheme based on the protocol of Poulton and Canfield (2005):

- Fe in carbonate and poorly crystalline phases were extracted by leaching the sediment with a sodium acetate solution adjusted with acetic acid to pH 4.5 with acetic acid for 48 h (Fe_{aca}). However, easily reducible ferric iron within the Fe_{aca} fraction was always below the limit of detection in all samples, so that this fraction entirely consists of ferrous iron.
- Leaching the sample with 0.5 M HCl for 1 h extracted the highly reactive Fe in hydrous ferric oxides like ferrihydrite or lepidocrocite (Fe_{HCl}).

- Reactive Fe in goethite and hematite was extracted by treating the sediment sample with a sodium dithionite solution (50 g L^{-1}) buffered to pH 4.8 with 0.35 M acetic acid/0.2 M sodium citrate for 2 h (Fe_{dith}).
- Leaching the sediment sample with 0.2 M ammonium oxalate/0.17 M oxalic acid solution (pH 3.2) for 6 h extracted the reactive Fe present in magnetite (Fe_{oxa}).
- Finally, samples were subjected to a near boiling 6 N HCl extraction for 24 h to extract the remaining unreactive Fe in silicates (Fe_{Sil}).

Our reactive Fe pool is defined as carbonate-associated Fe ($Fe_{aca,}$ sodium acetate extractable Fe), hydrous ferric oxides (Fe_{HCl}, 0.5 N HCl extractable Fe), ferric (oxy)hydroxides ($Fe_{dith,}$ dithionite extractable Fe), and magnetite (Fe_{oxa}, oxalate extractable Fe), (Reactive Fe pool = Fe_{aca} + Fe_{HCl} + Fe_{dith}+ Fe_{oxa}). The total reactive ferric Fe pool is defined as ferric iron present within the Fe_{HCl}, Fe_{dith} and within the Fe_{oxa} fraction. The total reactive ferrous iron pool is composed of the ferrous iron within the Fe_{aca}, Fe_{HCl} and Fe_{oxa} fraction. Finally, the total iron pool is defined as the sum of all reactive Fe phases and non-reactive (lithogenic) Fe contained in silicate minerals (Fe_{Sil}). Our extractions dissolved >92% of the Fe from the PACS-2 international reference standard. All Fe concentration measurements were performed using a Flame Atomic Absorption Spectrophotometer (Flame AAS). Precision on triplicate measurements was 1.2 % and our limit of detection was 1500 ug g^{-1} (0.15 wt% or ~10 µmol cm^{-3}).

TOC analysis

The total organic carbon (TOC) was analyzed by Rock-Eval 6 pyrolysis (Vinci Technologies). In the pyrolysis step ~ 60 mg sediment were heated to 650°C in an inert atmosphere. This released free hydrocarbons that were measured by a flame ionization detector (FID). Thermal cracking of long chain carbon compounds and carbonates produced CO and CO_2 that were measured simultaneously by an infrared-cell. The carbonate related peak could be accurately identified allowing the differentiation between mineral and organic carbon. In a second step the material was reheated to 850 °C to quantify the remaining refractory organic matter. TOC (%) was calculated according to (Lafargue et al., 1998).

Methane concentrations and isotopic analysis

For methane analysis, 2 cm^3 of sediment was retrieved with a cutoff syringe immediately after core retrieval and transferred to a 20 mL crimp vial filled with saturated NaCl solution and stored at 4°C without any headspace. Before analysis, 3 mL Helium was introduced as a headspace to all samples followed by equilibration for at least 24 hours. Methane concentrations were determined by injecting 200 µL of the He headspace into a Thermo Finnigan Trace gas chromatograph equipped with a flame ionization detector (Thermo Fisher Scientific). Helium was used as a carrier gas with a constant flow rate of 2 mL min^{-1} and the split ratio was set to 5.

In the 12 m core we analyzed the isotopic composition of the pore water methane. $\delta^{13}C(CH_4)$, $\delta^{13}C(CO_2)$ and $\delta D(CH_4)$ were determined by injecting He headspace to a continuous-flow isotope ratio mass spectrometer (Delta V Plus, Thermo Fisher Scientific) equipped with a Trace GC Ultra (Thermo Fisher Scientific). For $\delta^{13}C(CH_4)$ and $\delta^{13}C(CO_2)$ injection volume was 200 µL. Flow rate of the carrier gas was 3 mL min^{-1} and the split ratio was set to 3. For $\delta D(CH_4)$ 400 µL of He headspace was injected. Flow rate was 2 mL min^{-1} and the split ratio was 5. Results are in δ notation: $\delta^{13}C = ([^{13}C/^{12}C]_{sample}/[^{13}C/^{12}C]_{standard} - 1)*1000$ ‰ referenced against Vienna Pee Dee Belemnite (VPDB, $^{13/12}C$ ratio 0.0112372 ±0.0000090) and $\delta D = ([^{2}H/^{1}H]_{sample}/[^{2}H/^{1}H]_{standard} - 1)*1000$ ‰ referenced against Vienna Standard Mean Ocean water (VSMOW, $^{2/1}H$ ratio 0.00015576 ± 0.00000010).

The isotope difference between $\delta^{13}C\text{-}CH_4$ and $\delta^{13}C\text{-}CO_2$ was calculated according to the following formula (Friedman and O'Neil, 1977):

$$\varepsilon = ((1000+\delta^{13}C[CO_2]/(1000+ \delta^{13}C[CH_4])-1)*1000 ‰$$

where ε is the standard-independent isotope difference between the two components, expressed in ‰.

Potential sulfate reduction rates

Potential sulfate reduction rates were determined by incubation with radioactive $^{35}SO_4^{2-}$ (Jørgensen, 1978). Sterile glass plugs with a syringe plunger fitted into one end were inserted perpendicular to the cut sediment surface of the WRCs, closed with autoclaved butyl rubber stoppers and transferred to an aluminum bag flushed with nitrogen gas. Incubations were carried out at approximately in-situ temperature of 30°C in the dark. The glass plugs were pre-incubated for 24h at 30°C before tracer injection. Each plug

received 15 µL of $^{35}SO_4^{2-}$ tracer (~100 kBq) that contained ~10 µM of non-radioactive SO_4^{2-} in order to avoid complete turnover of the sulfate pool, which would invalidate rate measurements (Fossing, 1995). The samples were incubated for 24h at 30°C in the dark. Transferring the sample to 10 mL of 20 % ZnAc solution terminated all incubations. Terminated incubations were stored at -20°C until analysis. All incubations were done in triplicate.

The microbially produced reduced inorganic sulfur species were separated from the remaining sample and the unreacted sulfate tracer using the cold chromium distillation of (Kallmeyer et al., 2004). We added 8mL 6N HCl, 16 mL of 1 M $CrCl_2$ and 20 mL of dimethylformamide to the distillation flask. Prior to addition of the reagents a small amount of non-radioactive zinc sulfide suspension was added as a sulfide carrier to enhance recovery. The released H_2S was collected in a trap filled with 5 % zinc acetate solution where H_2S was precipitated as zinc sulfide. Fresh traps were used for each fraction. The zinc acetate solution was transferred to a scintillation vial, then 8 mL Ultima Gold Scintillation Cocktail (Perkin Elmer) was added and the mixture homogenized. The radioactivity of recovered sulfide was quantified using a Tri Carb 2500 TR liquid scintillation counter (Packard Instruments, Meriden, CT, USA). Potential sulfate reduction rates were quantified according to Jørgensen (1978) with the following equation:

$$SRR = [SO_4^{2-}] \times P_{SED} \times \frac{a_{TRIS}}{a_{TOT}} \times \frac{1}{t} \times 1.06 \times 10^6 \qquad (1)$$

where SRR is the sulfate reduction rate (pmol $cm^{-3}d^{-1}$); $[SO_4^{2-}]$ the sulfate concentration in the pore water (mmol L^{-1}) plus 0.01mmol L^{-1} non-radioactive sulfate that was added to the radiotracer; P_{SED} is the sediment porosity (mL pore water cm^{-3} sediment); a_{TRIS} is the radioactivity of TRIS (counts per minute); a_{TOT} is the total radioactivity used (counts per minute); 1.06 is the correlation factor for the expected isotopic fractionation (Jørgensen and Fenchel, 1974) and 10^6 is the factor for the change of units from mmol cm^{-3} d^{-1} to pmol cm^{-3} d^{-1}. During incubation, turnover of the injected radiotracer was always below 1 % in all experiments. The depth-integrated potential sulfate reduction rate (mmol m^{-2} yr^{-1}) was calculated as the sum of all measured mean potential sulfate reduction rates from 0 to 12 m. The uncertainty of that rate is the sum of the respective standard deviations.

Geochemical modeling

Net reaction rates of dissolved chemical species linked to select microbial metabolisms (i.e. Fe^{2+}, CH_4, NH_4^+,VFAs) were calculated using the MATLAB script of Wang et al. (2008), assuming that the pore water concentration profiles represent steady-state conditions. We used a measured porosity profile (Tab. S5.1), which the model requires to calculate the formation factor based on the empirical relationship $f = 10.0196\,\phi^{-1.8812}$. The model applied a 5-point Gaussian filter to the respective pore water concentration profile, formation factor and porosity. Diffusion coefficients of the respective compounds were obtained from the compilation of Schulz (2000) and were corrected for in-situ temperature using a temperature profile that was obtained by downhole logging (Tab. S5.1). We used a constant sedimentation rate of 1.9 10^{-4} m yr^{-1} (Russell et al., 2014) and a constant external flow advection velocity near the SWI. A minimum of three measured concentration data points was used to determine each reaction zone. The model quantifies uncertainties in the rate estimates by using a Monte Carlo technique (Wang et al., 2008).

Results of modeled turnover rates in the upper 0.5 m should usually be treated with caution because processes other than molecular diffusion can affect the pore water concentration gradients near the SWI. For example, bioturbation and/or advective transport can enhance the exchange of solutes between sediment and the overlying water (Precht and Huettel, 2004; Ziebis et al., 1996), although we can preclude bioturbation in this particular case because of the anoxic bottom water.

Moreover, disturbances can be caused by the impact of the coring device, especially larger corers like we used for the 12 m core completely destroy the uppermost sediment layer. We thus retrieved a short core (< 0.4 m) with a small gravity corer that recovers an undisturbed SWI. This way we could increase the sampling resolution in the uppermost sediment layers, especially for methane. Due to the very steep gradient and strong curvature we combined the concentration profiles of both cores and used them as a single input for the model. Additionally, we ran a separate model for the short gravity core (Fig. S5.4). Both models are in good agreement to each other.

Summing up all modeled mean reaction rates within the upper 12 m yielded the depth-integrated reaction for the studied depth interval (mmol m^{-2} yr^{-1}). The sum of the respective modeled standard deviations yielded the uncertainty of that rate.

Using the data from our sequential Fe-speciation extraction we calculated depth-integrated rates of microbial Fe reduction by combining sedimentation rates with changes in Fe speciation between depth intervals, assuming steady-state deposition. We focused on sediment intervals in which a decrease in the total Fe(III) pool could be matched to a corresponding increase in the total Fe(II) pool, recognizing that some Fe(II) can be lost to the overlying water column via diffusive transport.

Potential methane production

We performed incubation experiments with sediment samples from three different depths (0.36 m, 1.95 m and 7.4 m) to investigate the potential for methane production in Lake Towuti sediment. Using a sterile cutoff syringe, we retrieved sediment samples of 0.5 cm^3 each from WRCs that were stored in nitrogen-filled aluminum foil bags at room temperature. The respective sediment sample was transferred into an autoclaved 5 mL glass crimp vial together with 1 mL of sulfate-depleted freshwater medium mimicking the pore water concentrations of Lake Towuti sediment (Tab. S5.1). Due to the low pore water sulfate concentrations we substituted the regular sulfur-containing reducing agent (sodium sulfide) with titanium citrate with a final concentration of 1.6 mM in the medium. To check for the potential of hydrogenotrophic methanogenesis, the butyl stoppered glass crimp vial was flushed with a mixture of H_2/CO_2 (80/20 %). A second experiment was set up, in which acetate was added with a final concentration of 100 µM in the medium and N_2/CO_2 (80/20 %) in the headspace. For controls the respective sediment samples were mixed with medium (Tab. S5.2) and the headspace flushed with N_2/CO_2 (80/20 %). Killed controls were not run. All sample handling was done in a nitrogen-filled anaerobic chamber. The vials were constantly shaken in the dark at 100 rpm at a constant temperature of 28°C. Methane production in the experiments was measured by gas chromatography (Agilent Technologies, CA, USA).

After 35 days of incubation, headspace methane concentrations in the hydrogenotrophic incubations reached 17, 5.9 and 2.8 vol.% in sediment from 0.36, 2 and 7.4 m, respectively (Fig. S5.2a). Acetoclastic methane production showed the same depth trend, albeit at a lower rate, never exceeding methane concentrations of 3 vol.% (Fig. S5.2b). This is in line with the distribution of methane production indicated by modeling pore water profiles and methane isotopic compositions (Fig. 5.2 & 5.3). In unamended control experiments methane production could only be observed in the

uppermost sample and did not reach more than 1 vol.%, implying that rates of methane production are limited by H_2 and acetate substrate supply rates.

Methane production and accumulation in the oceans and atmosphere

Solutions to photochemical models (Pavlov et al., 2001) run across a range of biospheric CH_4 fluxes can be approximated by the following equation (Ozaki et al., 2018):

$$f(CH_4) = a \times flux_{CH4}^{b} \quad [1]$$

Where $f(CH_4)$ is the atmospheric CH_4 mixing ratio, a (=1.474 × 10^{-26}) and b (=2.0291) are tunable constants, and $flux_{CH4}$ is the biospheric CH_4 flux (molecules cm^{-2} s^{-1}).

5.3 Acknowledgements

This research was carried out with partial support from the International Continental Scientific Drilling Program (ICDP), the U.S. National Science Foundation (NSF), the German Research Foundation (DFG), the Swiss National Science Foundation (SNSF), PT Vale Indonesia, the Ministry of Research, Education, and Higher Technology of Indonesia (RISTEK), Brown University, the University of Minnesota, the National Autonomous University of Mexico (UNAM), GFZ German Research Centre for Geosciences, the Natural Sciences and Engineering Research Council of Canada (NSERC), and Genome British Columbia. We thank PT Vale Indonesia, the US Continental Scientific Drilling and Coordination Office, and US National Lacustrine Core Repository, and DOSECC Exploration Services for logistical support. The research was carried out with permissions from RISTEK, the Ministry of Trade of the Republic of Indonesia, the Natural Resources Conservation Center (BKSDA), and the Government of Luwu Timur of Sulawesi. We thank Tri Widiyanto and his staff from Research Center for Limnology, Indonesian Institute of Sciences (LIPI) for their administrative support in obtaining the Scientific Research Permit. Special thanks are due to Jenny Wendt and Xavier Prieto for their assistance during methane analysis. Jan Axel Kitte is acknowledged for his support in the field and in the laboratory.

Members of the Towuti Drilling Project Science Team

James M. Russell, Satria Bijaksana, Hendrik Vogel, Martin Melles, Daniel Ariztegui, Kohen W. Bauer, Sean A. Crowe, Alan Deino, Silvia Fajar, André Friese, Doug

Haffner, Abdul Hafidz, Ascelina Hasberg, Cynthia Henny, Imran, Sarah Ivory, Jens Kallmeyer, Christopher Kelly, John King, Kartika Kirana, Ristiyanti Marwoto, Marina Morlock, La Ode Ngkoimani, Sulung Nomosatryo, Anders Noren, Ryan O'Grady, Luis Ordonez, Thomas von Rintelen, La Ode Safiuddin, Rachel L. Simister, Janelle Stevenson, Gerald Tamuntuan, Aurele Vuillemin, Ian Watkinson, Nigel Wattrus, Satrio Wicaksono, Thomas Wonik

5.4 Supplemental Material

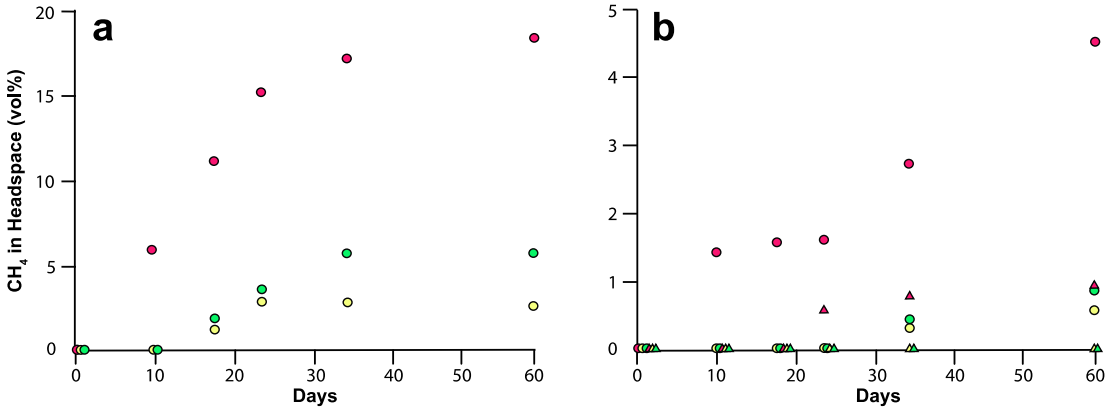

Figure S 5.2: *Potential methane production experiments: Incubation experiments for potential hydrogenotrophic methanogenesis (A) and acetoclastic methanogenesis (B). Samples came from depths of 0.36 m, 1.95 m and 7.4 m, indicated in pink, green and yellow, respectively. Circles are experiments with added substrate H_2/CO_2 (80/20%) in the headspace (A) or 100 µM acetate in the medium (B). Triangles are negative controls with N_2/CO_2 (80/20%) headspace. The negative controls were not amended with substrate, but not killed.*

Table S 5.1: *Input parameters for geochemical modeling: Input parameters for modeling of net turnover rates after the MATLAB script of Wang et al. (2008).*

Depth	Porosity	Depth	Temperature
mblf	%H_2O	mblf	°C
0.035	88.98	0.015	28.19
0.115	84.38	0.065	28.19
0.195	82.01	0.115	28.19
0.275	79.88	0.165	28.19
0.355	79.12	0.215	28.20
0.435	78.40	0.265	28.20
0.515	77.82	0.315	28.20
0.595	77.49	0.365	28.20
0.665	76.70	0.415	28.21
0.745	75.45	0.465	28.21

0.825	75.43	0.515	28.21
0.905	71.97	0.565	28.21
0.985	71.85	0.615	28.22
1.065	69.71	0.665	28.22
1.145	69.26	0.715	28.23
1.225	68.94	0.765	28.23
1.285	66.50	0.815	28.24
1.365	68.06	0.865	28.24
1.445	68.97	0.915	28.24
1.525	70.22	0.965	28.25
1.605	70.53	1.015	28.25
1.685	70.49	1.065	28.26
1.765	72.96	1.115	28.26
1.845	69.26	1.165	28.27
1.925	69.52	1.215	28.27
2.005	70.44	1.265	28.28
2.085	70.73	1.315	28.28
2.165	73.41	1.365	28.29
2.245	69.96	1.415	28.29
2.480	69.86	1.465	28.30
2.965	72.47	1.515	28.30
3.440	64.01	1.565	28.31
3.920	62.99	1.615	28.32
4.400	62.58	1.665	28.32
5.445	62.50	1.715	28.33
5.925	64.50	1.765	28.34
6.405	62.48	1.815	28.35
6.885	67.27	1.865	28.35
7.365	63.36	1.915	28.36
7.845	69.68	1.965	28.36
8.315	67.10	2.015	28.37
8.795	64.70	2.065	28.38
9.275	63.26	2.115	28.39
9.752	60.19	2.165	28.39
10.232	61.41	2.215	28.40
10.707	62.97	2.265	28.41
11.187	63.41	2.315	28.42
11.672	67.80	2.365	28.42
12.152	61.11	2.415	28.43
		2.465	28.44
		2.515	28.45
		2.565	28.46
		2.615	28.47
		2.665	28.48
		2.715	28.49

		2.765	28.49
		2.815	28.50
		2.865	28.51
		2.915	28.52
		2.965	28.53
		3.015	28.53
		3.065	28.54
		3.115	28.55
		3.165	28.55
		3.215	28.56
		3.265	28.56
		3.315	28.57
		3.365	28.58
		3.415	28.58
		3.465	28.59
		3.515	28.60
		3.565	28.60
		3.615	28.61
		3.665	28.61
		3.715	28.62
		3.765	28.63
		3.815	28.63
		3.865	28.64
		3.915	28.65
		3.965	28.65
		4.015	28.66
		4.065	28.66
		4.115	28.67
		4.165	28.68
		4.215	28.68
		4.265	28.69
		4.315	28.69
		4.365	28.70
		4.415	28.70
		4.465	28.71
		4.515	28.71
		4.565	28.71
		4.615	28.72
		4.665	28.72
		4.715	28.73
		4.765	28.73
		4.815	28.74
		4.865	28.74
		4.915	28.74
		4.965	28.75

		5.015	28.75
		5.065	28.75
		5.115	28.76
		5.165	28.76
		5.215	28.76
		5.265	28.77
		5.315	28.77
		5.365	28.77
		5.415	28.78
		5.465	28.78
		5.515	28.78
		5.565	28.79
		5.615	28.79
		5.665	28.79
		5.715	28.80
		5.765	28.80
		5.815	28.80
		5.865	28.80
		5.915	28.80
		5.965	28.81
		6.015	28.81
		6.065	28.81
		6.115	28.81
		6.165	28.82
		6.215	28.82
		6.265	28.82
		6.315	28.82
		6.365	28.82
		6.415	28.82
		6.465	28.83
		6.515	28.83
		6.565	28.83
		6.615	28.83
		6.665	28.83
		6.715	28.84
		6.765	28.84
		6.815	28.84
		6.865	28.84
		6.915	28.84
		6.965	28.84
		7.015	28.84
		7.065	28.84
		7.115	28.84
		7.165	28.85
		7.215	28.85

		7.265	28.85
		7.315	28.85
		7.365	28.85
		7.415	28.85
		7.465	28.85
		7.515	28.85
		7.565	28.86
		7.615	28.86
		7.665	28.86
		7.715	28.86
		7.765	28.86
		7.815	28.86
		7.865	28.86
		7.915	28.86
		7.965	28.86
		8.015	28.86
		8.065	28.86
		8.115	28.86
		8.165	28.87
		8.215	28.87
		8.265	28.87
		8.315	28.87
		8.365	28.87
		8.415	28.87
		8.465	28.87
		8.515	28.87
		8.565	28.87
		8.615	28.88
		8.665	28.88
		8.715	28.88
		8.765	28.88
		8.815	28.88
		8.865	28.88
		8.915	28.88
		8.965	28.88
		9.015	28.88
		9.065	28.88
		9.115	28.88
		9.165	28.89
		9.215	28.89
		9.265	28.89
		9.315	28.89
		9.365	28.89
		9.415	28.89
		9.465	28.89

		9.515	28.89
		9.565	28.89
		9.615	28.89
		9.665	28.89
		9.715	28.90
		9.765	28.90
		9.815	28.90
		9.865	28.90
		9.915	28.90
		9.965	28.90
		10.015	28.90
		10.065	28.90
		10.115	28.90
		10.165	28.90
		10.215	28.90
		10.265	28.90
		10.315	28.90
		10.365	28.91
		10.415	28.91
		10.465	28.91
		10.515	28.91
		10.565	28.91
		10.615	28.91
		10.665	28.91
		10.715	28.91
		10.765	28.91
		10.815	28.92
		10.865	28.92
		10.915	28.92
		10.965	28.92
		11.015	28.92
		11.065	28.92
		11.115	28.92
		11.165	28.92
		11.215	28.92
		11.265	28.93
		11.315	28.93
		11.365	28.93
		11.415	28.93
		11.465	28.93
		11.515	28.93
		11.565	28.93
		11.615	28.93
		11.665	28.93
		11.715	28.94

		11.765	28.94
		11.815	28.94
		11.865	28.94
		11.915	28.94
		11.965	28.94
		12.015	28.94

Table S 5.2: *Medium composition for potential methane production experiments: Medium composition for incubation of methanogens in Lake Towuti sediment.*

Compound	**Concentration (mg L^{-1})**
$MgCl_2*6H_2O$	54
$CaCl_2*2H_2O$	16
NH_4Cl	5
K_2HPO_4	1.7
$NaHCO_3$	500
$FeCl_2$ * $4H_2O$	7.50
$CoCl_2$ * $6H_2O$	0.95
$MnCl_2*4H_2O$	0.50
$ZnCl_2$	0.35
$N_2MoO_4*2H_2O$	0.18
$NiCl_2*6H_2O$	0.12
H_3BO_3	0.03
$CuCl_2*2H_2O$	0.01
4-Aminobenzoate	0.1
Nicotinic acid	0.1
Ca-Pantothenate	0.1
Pyridoxine-Hydrochloride B6	0.1
Riboflavin	0.1
Thyamine-Hydrochloride	0.1
Biotin	0.05
Folic acid	0.05
Lipoic acid	0.05
Vitamine B12	0.05
Titanium citrate	237
Na-Resazurine	0.5

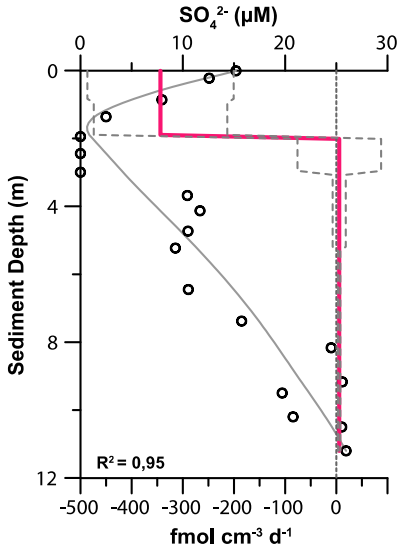

Figure S 5.3: *Geochemical modeling of pore water sulfate: Geochemical modeling of net turnover rates of pore water sulfate for the 12 m drill core. The modeled turnover rates are 10 – 160 times lower than the measured potential sulfate reduction rates, which is consistent with previous observations on Lake Towuti sediments and similar environments (Norði et al., 2013b; Urban et al.; Vuillemin et al., 2016b).*

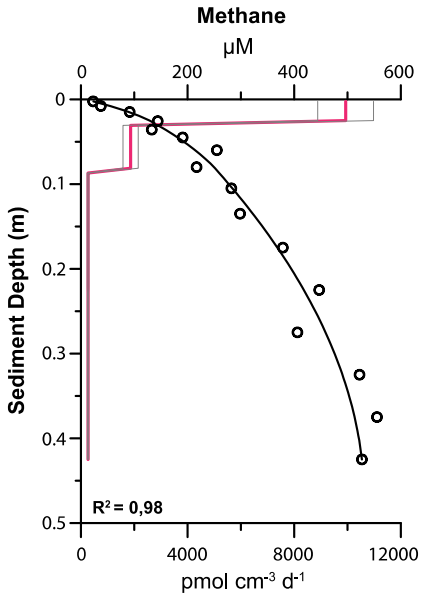

Figure S 5.4: *Geochemical modeling of pore water methane: Geochemical modeling of net turnover rates of pore water methane for the short core (< 0.4 m) that was retrieved with a gravity coring device to better preserve the sediment water interface and thus to increase the accuracy of the modeling results. The net turnover rates show a good fit with those of our model in Figure 5.2 and even predict methane production rates up to 9 µmol cm^{-3} d^{-1} in the upper 3 cm of the sediment core yielding a depth integrated methane production rate of 162 ± 19 mmol m^{-2} yr^{-1} for the upper 0.4 m. Please note that the methane concentration in the uppermost sample (0-0.5 cm) is not zero but around 10 µM, indicating a net flux of methane out of the sediment.*

6 Formation of diagenetic siderite in modern ferruginous sediments

Ferruginous conditions prevailed in the world's deep oceans during the Archean and Proterozoic Eons. Sedimentary iron formations deposited at that time may provide an important record of environmental conditions, yet linking the chemistry and mineralogy of these sedimentary rocks to depositional conditions remains a challenge due to a dearth of information about the processes by which minerals form in analogous modern environments. We identified siderites in ferruginous Lake Towuti, Indonesia, which we characterized using high-resolution microscopic and spectroscopic imaging combined with microchemical and geochemical analyses. We infer early diagenetic growth of siderite crystals as a response to sedimentary organic carbon degradation and the accumulation of dissolved inorganic carbon in pore waters. We suggest that siderite formation proceeds through syntaxial growth on preexisting siderite crystals, or possibly through aging of precursor carbonate green rust. Crystal growth ultimately leads to spar-sized (>50 μm) mosaic single siderite crystals that form twins, bundles, and spheroidal aggregates during burial. Early-formed carbonate was detectable through microchemical zonation and the possible presence of residual phases trapped in siderite interstices. This suggests that such microchemical zonation and mineral inclusions may be used to infer siderite growth histories in ancient sedimentary rocks including sedimentary Iron Formations.

6.1 Introduction

Ancient sedimentary iron formations (IFs) are composed of diverse iron oxides, silicates, and carbonates that are thought to form through diagenesis and subsequent metamorphism of primary ferric-ferrous (Fe^{3+}-Fe^{2+}) iron (oxyhydr)oxide precipitates (Gole, 1980; Raiswell et al., 2011). Yet iron carbonate minerals such as siderite ($FeCO_3$) are also thought to form as primary pelagic precipitates (Canfield et al., 2008; Bekker et al., 2014), and their mineralogy has been used to infer atmospheric and oceanic conditions on early Earth (Holland, 2006). The interpretation of IFs and their depositional conditions depends on our knowledge of their mineral origins and

formation pathways (Ohmoto et al., 2004), which is limited in part due to scarcity of analogous ferruginous environments on Earth today (Konhauser et al., 2005; Posth et al., 58 2014).

Ferruginous sediments are deposited in the Malili Lakes, a chain of five interconnected tectonic lakes in Sulawesi, Indonesia (Haffner et al., 2001). Erosion of ultramafic rocks and lateritic soils in the Malili Lakes catchment supplies considerable amounts of iron (oxyhydr)oxides but little sulfate to the lakes (Crowe et al., 2004; Morlock et al., 2019). Lake Towuti (2°45′0″S, 121°30′0″E) is currently stratified with anoxic conditions below 130 m (Costa et al., 2015; Vuillemin et al., 2016). In nearby Lake Matano (2°29′7″S, 121°20′0″E), carbonate green rust (GR) forms below the chemocline, likely via the reduction of ferrihydrite or via its reaction with dissolved Fe^{2+} and bicarbonate (Zegeye et al., 2012), but the fate of this GR is not known. Although carbonate GR has been proposed as a precursor to other diagenetic mineral phases in banded iron formations (Halevy et al., 2017), its transformation to these phases has not been observed in nature. Prior studies suggested that iron phases in Lake Towuti sediments undergo dissolution during reductive diagenesis, with secondary growth of diagenetic phases such as magnetite and siderite (Tamuntuan et al., 2015). However, siderite was not explicitly documented in that study, nor is it clear where in the lake and sediment these minerals form.

We discovered spar-sized aggregates (>50 μM) of diagenetic siderite crystals in Lake Towuti sediments, and used detailed geochemical and mineralogical information to describe their features and infer pathways of formation. We suggest that this siderite forms during diagenesis through growth on preexisting primary phases, including siderite and possibly carbonate GR. We hypothesize that the chemical and mineralogical features of these siderites, and their irregular distribution down core, reflect changes in redox conditions in the pore water and sediment over time, including non-steady-state diagenesis, which likely results from variability in the burial fluxes of ferric iron and organic matter.

6.2 Methods

Sediments were recovered using the International Continental Scientific Drilling Program Deep Lakes Drilling System (https://www.icdponline.org). Cores from the 114-

m-deep TDP-TOW15- 1A hole (https://csdco.umn.edu/project/lake-towuti-drilling-project-tdp), drilled in 156 m water depth, were split and imaged at the Limnological Research Center LacCore Facility, Minneapolis, Minnesota, USA. This core mainly consists of alternating green and red clays, the latter containing variably distributed siderite concentrations (Russell et al., 2016). Sedimentary organic matter is mainly autochthonous, albeit at low concentrations, with some contribution of fluvial derived material (Hasberg et al., 2019; Morlock et al., 2019).

Here, we focus on material recovered from core catchers. In the field, core catchers were packed into gas-tight aluminum foil bags flushed with nitrogen gas and heat-sealed to keep them under anoxic conditions until mineral extraction. Pore water was retrieved on site using hydraulic squeezers. Alkalinity, pH, and Fe^{2+} concentrations were determined in the field via colorimetric titration, potentiometry, and spectrophotometry, respectively. Major ions were analyzed by ion chromatography. Dissolved inorganic carbon (DIC) was calculated from pH and alkalinity. Siderite crystals were retrieved via density separation and sorted by placing a neodymium magnet under the beaker and rinsing out the non-magnetic fraction with deionized water. Siderite imaging and elemental analysis were performed on a Zeiss Ultra 55 Plus field emission scanning electron microscope (SEM) equipped with an energy-dispersive X-ray spectrometer (EDX). Electron-transparent foils were prepared with a FEI focused ion beam, imaged and analyzed on a FEI Tecnai G2 F20 X-Twin transmission electron microscope (TEM). Structural information was obtained via selected area electron diffraction (SAED) patterns or calculated from high-resolution lattice fringe images (HR-TEM). Freeze-dried powdered bulk sediments and siderite extracts were analyzed in glycerol using a PANalytical Empyrean X-ray diffractometer in a theta-theta configuration. A complete description of all methods is available in the GSA Data Repository.

6.3 Diagenetic Siderites

We identified many discrete siderite-rich layers in the sediment during our initial core description (Russell et al., 2016). TEM imaging and associated diffraction patterns demonstrate that the extracted crystals are indeed siderite (Fig. 6.1 top). These analyses also identified minor quantities of carbonate GR and magnetite within siderite crystals at

6.2 m sediment depth (Fig. 6.1, bottom; Tab. S 6.1 in the Supplemental Material). Our detailed mineralogical analyses show that the siderites are highly ordered, and we did not detect the amorphous carbonate precursors of siderite that are commonly observed in laboratory experiments (Sel et al., 2012; Dideriksen et al., 2015).

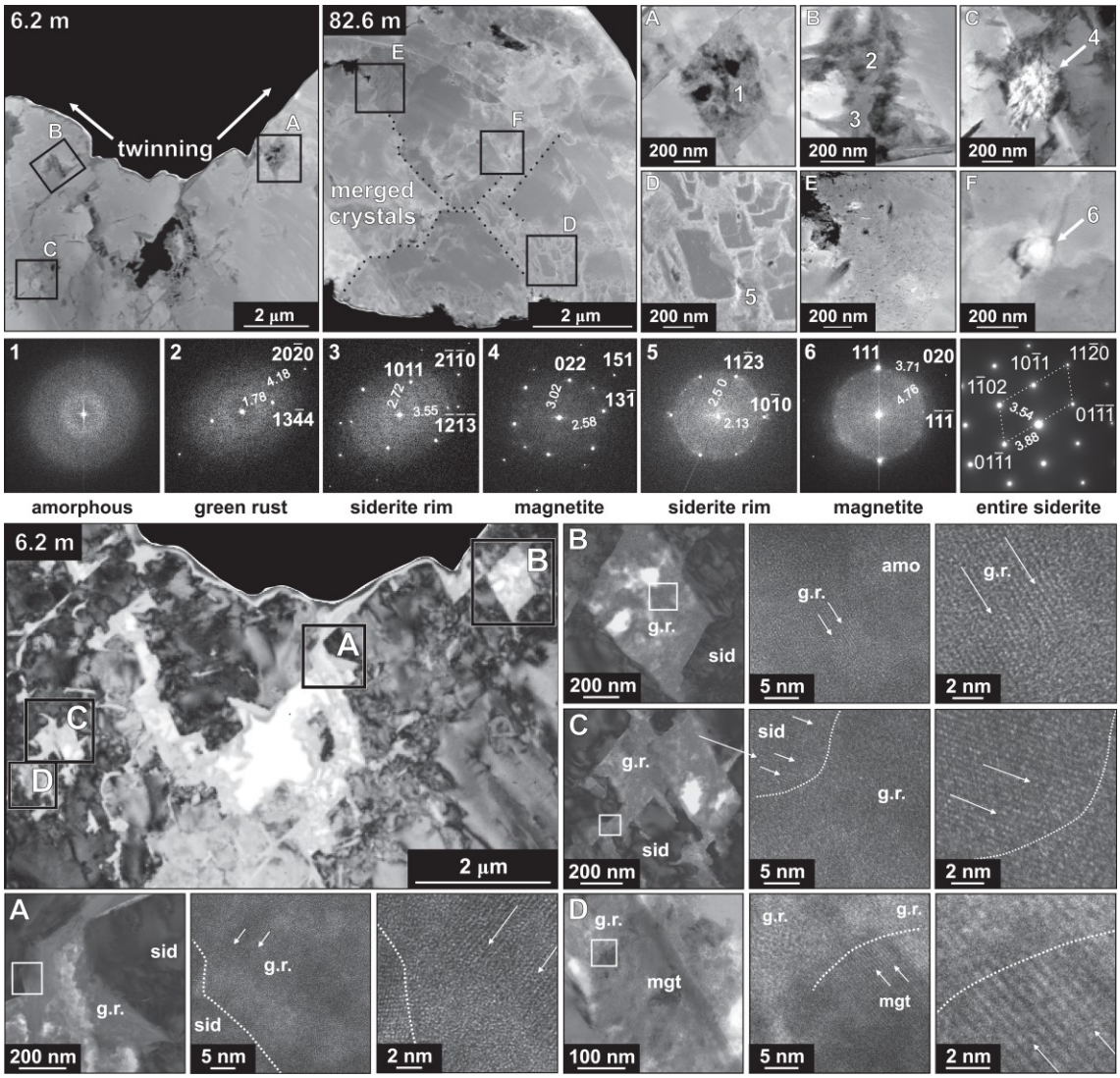

Figure 6.1: ***Top:*** *Scanning transmission electron microscope (TEM) images of siderite crystals from 6.2 m and 82.6 m sediment depth in Lake Towuti Drilling Project hole TDP-TOW15- 1A (https://csdco.umn.edu/project/lake-towuti-drilling-project-tdp) with close-ups of crystal pores (A–F); indexed selected area electron diffraction (SAED) patterns for amorphous iron oxide (1), green rust (2), siderite (3, 5) and magnetite (4, 6), and high-resolution SAED pattern obtained for the entire mosaic monocrystal of siderite from 82.6 m depth.* ***Bottom:*** *Bright-field TEM images of a siderite crystal from 6.2 m depth in scattering intensity after siderite subtraction. Close-ups of crystal pores with the corresponding images of lattice fringes (A–D) illustrate the interface between amorphous iron oxide (amo), green rust (g.r.), siderite (sid) and nano-magnetite (mgt). Arrows point at interphases between phases.*

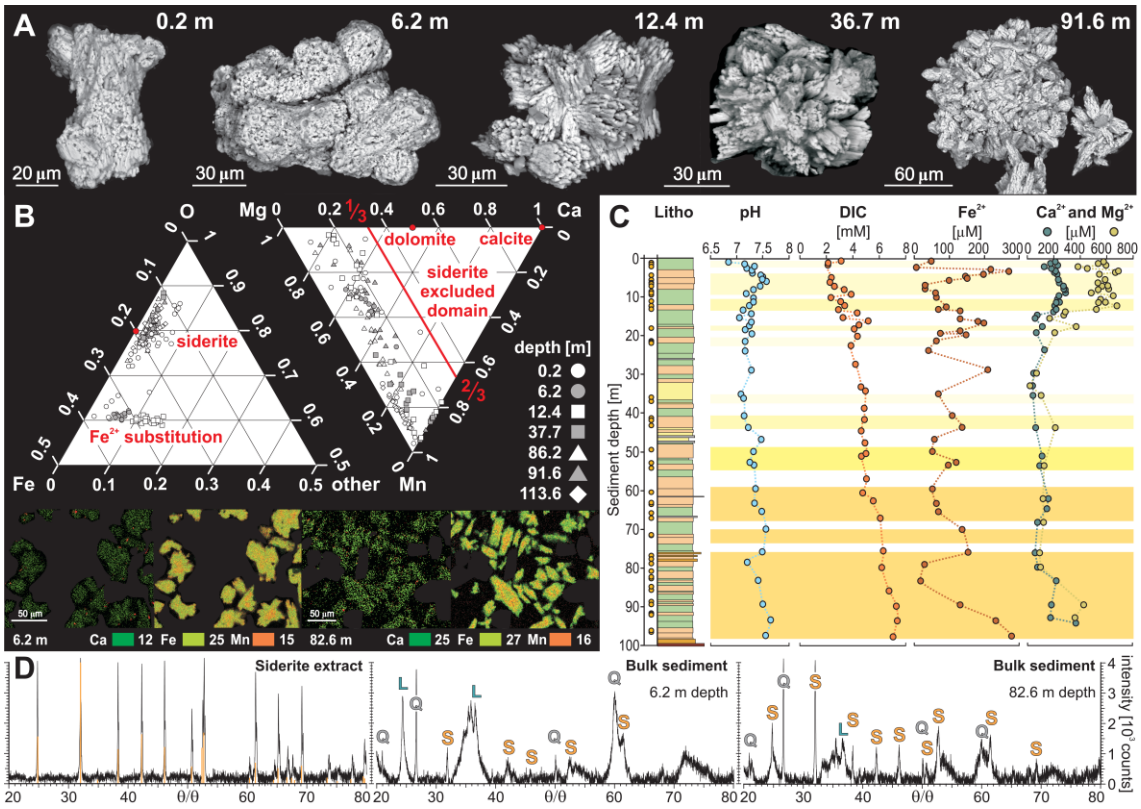

Figure 6.2: ***A:*** *Scanning electron microscope images of siderite crystals at increasing sediment depth in Lake Towuti Drilling Project hole TDP-TOW15- 1A.* ***B:*** *Energy-dispersive X-ray spectrometer point analysis and elemental map of thin section (O, Fe, Mn, Ca, Mg).* ***C:*** *Stratigraphy of Lake Towuti (South Sulawesi, Indonesia) with depths of siderite samples (yellow dots); pore-water profiles for pH, dissolved inorganic carbon (DIC), Fe^{2+}, Ca^{2+} and Mg^{2+} concentrations with siderite concentrations signified by yellow shaded areas.* ***D:*** *X-ray diffraction spectra for siderite (S) extract and bulk sediments from 6.2 and 82.6 m depth. Quartz (Q) and lizardite (L) are of detrital origin, whereas siderite forms in situ.*

SEM imaging and EDX elemental analysis reveal that siderites develop from initial micritic phases into mosaic crystals (Fig. 6.2A; Fig. S 6.1) in the upper 10 m of the sediment, which encompasses ~50 k.y. of depositional history (Costa et al., 2015). Sediment pore waters are saturated with respect to siderite (Tab. 6.1), and we therefore infer that siderite forms and grows during diagenesis and burial (Figs. 6.1 and 6.2A; Figs. S 6.1 and S 6.3). Under these saturated conditions, siderite growth proceeds through twinning and aggregation (Fig. 6.2A; Fig. S 6.1), merging microspar-sized precursor crystals (>20 µM) into larger spar mosaic-type crystals (>60 µM), and further into bundles and spheroidal clusters (Fig. 6.2A) (Fernandez-Diaz et al., 1996). For instance, the siderites observed at 82.6 m depth indicate the complete merger of former crystals with growth structures that connect them into a fully ordered single mosaic crystal (Fig. 6.1D, top), as evidenced by the SAED pattern of the entire crystal, which

displays a single crystallographic orientation (Fig. 6.1, top; Fig. S 6.2). These deeper siderites, found as bundles of twins and spheroidal aggregates in the sediment (Fig. 6.2A; Fig. S 6.1), appear to be dense and have little remaining pore space (Fig. 6.1F, top; Fig. S 6.3). In contrast, siderites at 6 m depth are porous and form multiple twins (Figs. 6.1, bottom and 6.2A; Fig. S 6.1). Diagenetic maturation thus results in an increasing crystallinity of siderites, which is supported by the greater sharpness of siderite reflections in XRD spectra for deeper siderites (Fig. 6.2D). We also observe aggregates of nano-magnetite in Lake Towuti in shallow sediments (Fig. S 6.5) or trapped in siderites (Fig. 6.1). Those found in magnetic separates of deeper samples may derive from multiple origins (e.g., detrital, volcanic, or authigenic) and some display clear features of dissolution (Fig. S 6.5). Given their uncertain origins, we do not discuss them further.

Table 6.1: *Modeled saturation indices.*

5 m depth	Saturation	35 m depth	Saturation
Talc	1.43	**Siderite**	1.00
Siderite	1.29	Quartz	0.71
Quartz	0.71	Vivanite	-0.04
Vivianite	-0.45	Talc	-0.31
Calcite	-0.68	Calcite	-0.83
Dolomite	-0.77	Aragonite	-0.97
Aragonite	-0.82	Dolomite	-1.27

With limited sulfate reduction in Lake Towuti owing to low sulfate concentrations (<20 µM) (Vuillemin et al., 2016), microbial Fe^{3+} reduction is likely to promote formation of mixed-valence iron oxides, like carbonate GR and magnetite, as found in nearby Lake Matano (Zegeye et al., 2012), with almost no formation of sulfide minerals. The presence of carbonate GR and nano-magnetite aggregates in siderite pore spaces is evident from HR-TEM images of crystal lattice fringes (Fig. 6.1, bottom; Fig. S 6.2). We suggest that the carbonate GR and magnetite form in the upper reaches of the sediments or bottom water and become trapped in siderite interstices during its initial formation (Bell et al., 1987). Chemical micro-niches, such as the pore spaces within

siderite, are known to preserve redox-sensitive minerals on geological time scales (Matamoros-Veloza et al., 2018), and trapping in siderite could preserve and shield these mineral grains preventing their further reaction with pore fluids during burial. Fabrics observed in lattice fringes may further suggest epitaxial growth of siderite on carbonate GR (Fig. 6.1, bottom; Figs. S 6.2 and S 6.3), implying that GR may serve as a precursor phase for siderite formation as found in laboratory experiments (Halevy et al., 2017). If the GR we see in siderite interstices is indeed primary, its preservation at ~6 m sediment depth implies GR stability over 30 k.y., based on existing constraints on sedimentation rates (Costa et al., 2015). This stands in contrast to carbonate GR instability in laboratory experiments, even at hourly time scales (Ruby et al., 2010; Guilbaud et al., 2013; Halevy et al., 2017). GR is known to rapidly convert into an amorphous ferric oxyhydroxycarbonate under standard conditions, or to more stable phases such as goethite and lepidocrocite (Legrand et al., 2004). Alternatively, carbonate GR could form through reaction with oxygen during sample exposure to the atmosphere (Tamaura et al., 1984). We acknowledge that both scenarios are possible.

Elemental mapping of siderite crystals revealed Mn/Fe zonation (Fig. 6.2B; Fig. S 6.4), with elevated Mn concentrations at the center of all crystals. We also observed minor substitution of Fe^{2+} by Ca^{2+} (<20 %) at the crystal rims. DIC concentrations gradually increase with depth in Lake Towuti's sediments, likely due to diagenetic organic matter degradation (Vuillemin et al., 2018), which at pH between 7.1 and 7.5 leads to an accumulation of DIC, mainly in the form of HCO_3^- (Fig. 6.2C). The Mn/Fe zonation could thus imply precipitation of siderite in the upper reaches of the sediment where pore water Mn^{2+} can accumulate due to reductive dissolution of Mn(oxyhydr)oxides at relatively low HCO_3^- activities and high Mg^{2+} concentrations (Fig. 6.2C) that may inhibit the initial nucleation of carbonates and result in increased substitution of Fe by Mn in siderite grains (Fig. 6.2B; Fig. S 6.4).

6.4 Siderites in the Precambrian

The morphologies and microchemistry of siderites in Lake Towuti can be compared to siderites from Precambrian rocks to inform on depositional conditions. In Precambrian rocks, pelagic siderites are usually identified as spheroidal crystals that are thought to represent primary precipitates that formed in the water column in response to Fe^{3+}

reduction and organic matter oxidation (Konhauser et al., 2005). These crystals can further transform into rhombohedral and massive siderite in the sediment (Köhler et al., 2013), often with Mg-Ca substitution (Mozley, 1989; Klein, 2005). Fe reduction in the sediment can also lead to formation of similar spheroidal siderite concretions during diagenesis, which can further coalesce into laterally extensive bands of cemented spherules (Coleman, 1993).

In Lake Towuti, we observe laterally continuous siderite-rich layers and the development of spheroidal aggregates of mosaic siderite crystals during burial, but with Ca rather than Mg overgrowth, which instead is often associated with marine or diagenetic fluids (Klein, 2005). In comparison, siderite in marine settings usually displays extensive Mg substitution (Mozley, 1989), as observed in Precambrian rocks. The Mn/Fe and Ca compositions observed in Lake Towuti (Fig. 6.2B) are typical of siderites formed in freshwater depositional environments (Mortimer et al., 1997), and the main carbonates forming in modern marine pore waters (i.e., calcite, aragonite, dolomite) were all undersaturated in Lake Towuti (Tab. 6.1) due to the much lower Ca and Mg ion activities in Lake Towuti pore waters (Fig. 6.2C) than in seawater.

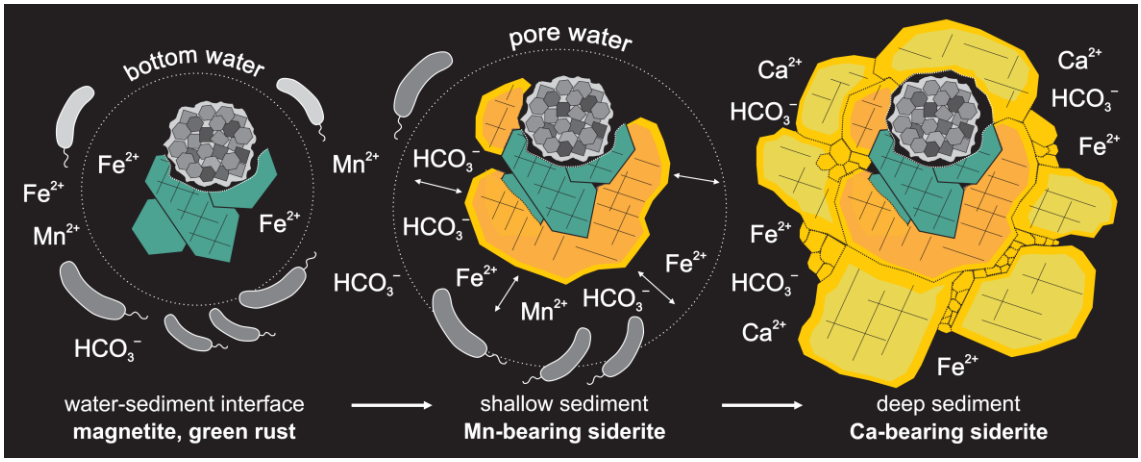

Figure 6.3: *Sketch depicting growth of siderite after carbonate green rust and nano-magnetite. Diagenetic reduction of Mn^{4+} and Fe^{3+} and organic matter degradation lead to pore water saturation with respect to siderite, initially forming Mn-bearing siderites. As pore water remains saturated with respect to siderite in the entire sediment sequence, siderite crystals continue to grow with depth into Ca-bearing mosaic monocrystals forming twins, bundles, and spheroidal aggregates.*

Spheroidal siderite is often inferred to be a water column precipitate and precursor for rhombohedral and cemented diagenetic siderites in Precambrian rocks (Konhauser et al., 2005; Köhler et al., 2013). In contrast, the preservation of residual

phases trapped in spheroidal mosaic siderite crystals in Lake Towuti may, if primary, suggest initial formation of GR, which is subsequently transformed into siderite in the sediment. We suggest that identification of microchemical zoning in ancient siderites, such as we observe in Lake Towuti siderites (Fig. 6.3), may provide clearer insight into water-column and pore-fluid chemistries at the time of IFs deposition. For example, the Mn-rich nuclei of siderite crystals preserved in Lake Towuti sediments likely reflects diagenetic Mn reduction, and if identified in IFs, siderites may signal contemporaneous pelagic or sedimentary Mn cycling with corresponding implications for evolving seawater chemistry and the redox state of the ocean-atmosphere system. Likewise, the possible preservation of mineral inclusions in siderite, like the magnetites and possibly GR we see in Lake Towuti, may assist in reconstruction of diagenetic sequences in IFs. Further exploration of IF mineral microchemistry and mineral inclusions, along with corresponding analyses in modern analogues, holds promise for reconstructing environmental conditions at the time of IF deposition.

6.5 Acknowledgements

Financial and logistical support was provided by the International Continental Scientific Drilling Program (ICDP); U.S. National Science Foundation (NSF); German Research Foundation (DFG); Swiss National Science Foundation (SNSF); PT Vale Indonesia; the Ministry of Research, Education, and Higher Technology of Indonesia (RISTEK); Brown University; University of Minnesota; University of Geneva; GFZ German Research Centre for Geosciences; Natural Sciences and Engineering Research Council of Canada (NSERC); and Genome British Columbia. This study was supported by the DFG through grants to Kallmeyer (KA 2293/8–1) and Vuillemin (VU 94/1–1), an SNSF grant to Vuillemin (P2GEP2_148621) and an NSERC Discovery grant (0487) to Crowe. Benning acknowledges support from the Helmholtz Recruiting Initiative fund. We thank the U.S. Continental Scientific Drilling and Coordination Office, U.S. National Lacustrine Core Repository, and DOSECC Exploration Services for logistical support. Research permits were obtained from RISTEK, Ministry of Trade of the Republic of Indonesia, Natural Resources Conservation Center (BKSDA), and the Luwu Timur Regional Government of South Sulawesi Province, thanks to Tri Widiyanto and his staff from the Indonesian Institute of Sciences (LIPI).

6.6 Supplemental Material

Sample Collection

From May to July 2015, the scientific Towuti Drilling Project (TDP) was carried out on Lake Towuti using the International Continental Scientific Drilling Program (ICDP) Deep Lakes Drilling System (Russell et al., 2016). In February 2016, the cores from TDP-TOW15-1A (hereafter TDP-1A) were scanned at the Limnological Research Center LacCore Facility, University of Minnesota, using a multisensor core logger MSCL-S to obtain p wave velocity, gamma density, loop magnetic susceptibility (MS), electrical resistivity, and natural gamma radiation data at intervals of 2–4 cm. After splitting, cores were logged using an MSCL-XYZ to obtain high-resolution MS and color reflectance spectrophotometry at 0.5 cm resolution. Split cores were cleaned and scanned with a Geotek Single Track Core Imaging System (MSCL-CIS) digital linescan imager. Visual core description and smear slide analyses were carried out and described macroscopically and microscopically to determine their stratigraphy and composition and classify the sediment into major lithological units (Russell et al., 2016). Additional sampling was performed on split core surfaces from intervals with high siderite concentrations.

In the field, core catchers from the 114 m deep TDP-1A hole (156 m water depth) were packed into gas-tight aluminum foil bags flushed with nitrogen gas and heat-sealed to keep them under anoxic conditions until mineral extraction in the home lab. We separated siderites by homogenizing 50 mL of sediment in deionized water and performing density separation on the slurry. The non-magnetic fraction was retrieved using a neodymium magnet placed under the beaker and rinsing out the dense non-magnetic mineral extract with deionized water. This fraction was dried with acetone and checked under a binocular microscope (Nikon SMZ800) to ensure a minimum of 80 % siderite in the final sample. Siderite crystals were handpicked for further analyses.

Pore water chemistry and modeling

We obtained pH in the field with a portable pH meter, respectively, after homogenizing 2 mL of sediment in 2 mL of deionized water and measuring the supernatant after 2 min. We extracted pore water from TDP-1A on site from whole round core sections (5 cm Å~ 6.6 cm) in an anaerobic chamber flushed with nitrogen to avoid oxidation during sample handling. We used rhizon samplers inserted into soft sediments or, for more

dense sediment, transferred the sediments to a titanium cylinder and squeezed them using a hydraulic press (Mannheim, 1966). Pore water was filtered through a sterile 0.2 µm syringe filter and collected in a glass syringe pre-flushed with nitrogen. Fe^{2+} concentrations were measured in the field via spectrophotometry by using 1 mL of pore water stabilized with 100 µL of Ferrozine Iron Reagent and measuring absorbance of the solution at 562 nm with a DR 3900 spectrophotometer (Viollier et al., 2000). Alkalinity was determined via colorimetric titration. Major cations (Na^+, NH_4^+, K^+, Mg^{2+}, Ca^{2+}, Si^{4+}) and anions (Cl^-, SO_4^{2-}, NO_3^-, PO_4^{3-}) were analyzed by normal or suppressed ion chromatography (IC). Multi-element standards were used for calibration, with detection and quantification limits based on a respective signal-to-noise ratio of 3 and 10. All samples were measured in triplicates, with reproducibility better than 5 % for each ion (Vuillemin et al., 2016). Dissolved inorganic carbon (DIC) concentrations were calculated by solving the carbonate system using the pH and alkalinity profiles. The complete pore water dataset was used to calculate mineral saturation indices with the PHREEQC v.3 software (Parkhurst and Appelo, 2013). Additionally, we measured pore water chemistry via inductively coupled plasma optic emission spectrometry (ICP-OES) on five samples to provide an assessment of the evolution Mn^{2+} concentrations in pore water with depth.

Microscopic imaging, spectroscopic and mineralogical analyses

Separated siderite crystals were mounted on aluminum stubs (Ø 12.7 mm) and carbon coated, then imaged and analyzed on a Zeiss Ultra 55 Plus field emission scanning electron microscope (FESEM) equipped with an energy-dispersive X-ray (EDX) spectrometer and a silicon-drift detector (SDD UltraDry; Thermo Fisher Scientific). The SEM was operated at 20 kV and both secondary electron (SE) and back-scattering electron (BSE) images and maps were acquired. Quantitative element analyses were normalized to 100 % atomic weight displayed as oxides according to the matrix correction method of the Noran System Seven software.

Electron-transparent siderite films (15Å~10Å~0.1 µm) were prepared with a FEI focused ion beam (FEI FIB200) and gallium ion source. These FIB-cut foils were imaged and analyzed using a FEI Tecnai G2 F20 X-Twin transmission electron microscope (TEM) equipped with a Schottky field emitter electron source and a Fishione high-angle annular dark-field (HAADF) detector, and a Gatan imaging filter. The TEM was operated at 200 kV using a beam size of 1 to 2 nm to collect bright-field,

dark-field and HAADF images in both scanning transmission and analytical electron microscopy mode. All HAADF images were acquired with a camera length of 330 mm imaging simultaneous Z and diffraction contrast. Semi-quantitative analyses were obtained from an EDAX ultra-thin window EDX spectrometer with 60-120 s acquisition times. Structural information of mineral phases was either obtained through selected area electron diffraction (SAED) patterns recorded on image plates for high precision, or by calculating diffraction patterns with a fast Fourier transform from high-resolution lattice fringe (HR-TEM) images for fast data acquisition using the Digital Micrograph Gatan software (Wirth, 2009).

Freeze-dried bulk powders from 6 different depths and one concentrated extract of siderite were ground and analyzed in glycerol for their mineralogical assemblage using a PANalytical Empyrean X-ray diffractometer (XRD) operated in a theta-theta configuration. We used a CuKα source and acquired diffraction patterns between 5 and 85° 2θ at a count time of 1 min per step and at 40 kV and 40 mA. Data were collected on a PIXcel 3D detector and processed using Bruker AXS DIFFRACplus EVA and AXS Topas v. 4.2 softwares.

Table S 6.1: *Calculated d-spacing and assignments from diffraction patterns collected from high-resolution images of lattice fringes.*

Green rust - Fougèrite			Magnetite		
observed	reference	d(hkl)	observed	reference	d(hkl)
1.75	1.7573	(13$\underline{4}$4)	0.92	0.9164	(420)
1.88	1.8934	(32$\underline{5}$0)	1.45	1.4847	(404)
2.18	2.1853	(22$\underline{4}$2)	2.07	2.0996	(004)
2.31	2.3282	(22$\underline{4}$1)	2.62	2.5322	(131)
2.64	2.6684	(03$\underline{3}$1)	Ferrihydrite		
2.78	2.7511	(03$\underline{3}$0)	-	1.7323	(10$\underline{1}$4)
4.18	4.1266	(20$\underline{2}$0)	-	1.8800	(0005)

Table S 6.2: *Saturation indices modeled with PHREEQC v.3 based on pH, alkalinity, pore water concentrations of major ions and borehole temperatures. Siderite appears to be oversaturated throughout the sedimentary sequence, whereas vivianite remains close to but slightly below saturation. Serpentine/talc becomes undersaturated with depth.*

5 m: zone 1	Saturation	10 m: zone 2	Saturation	35 m: zone 4	Saturation
talc	1.43	**siderite**	**1.00**	siderite	**1.00**
siderite	**1.29**	quartz	0.71	quartz	0.71
quartz	0.71	chalcedony	0.29	chalcedony	0.29
chalcedony	0.29	**vivianite**	**-0.04**	**vivianite**	**-0.04**
vivianite	**-0.45**	talc	-0.31	talc	-0.31
α SiO_2	-0.54	α SiO_2	-0.54	α SiO_2	-0.54
calcite	-0.68	calcite	-0.83	calcite	-0.83
dolomite	-0.77	aragonite	-0.97	aragonite	-0.97
aragonite	-0.82	dolomite	-1.27	dolomite	-1.27

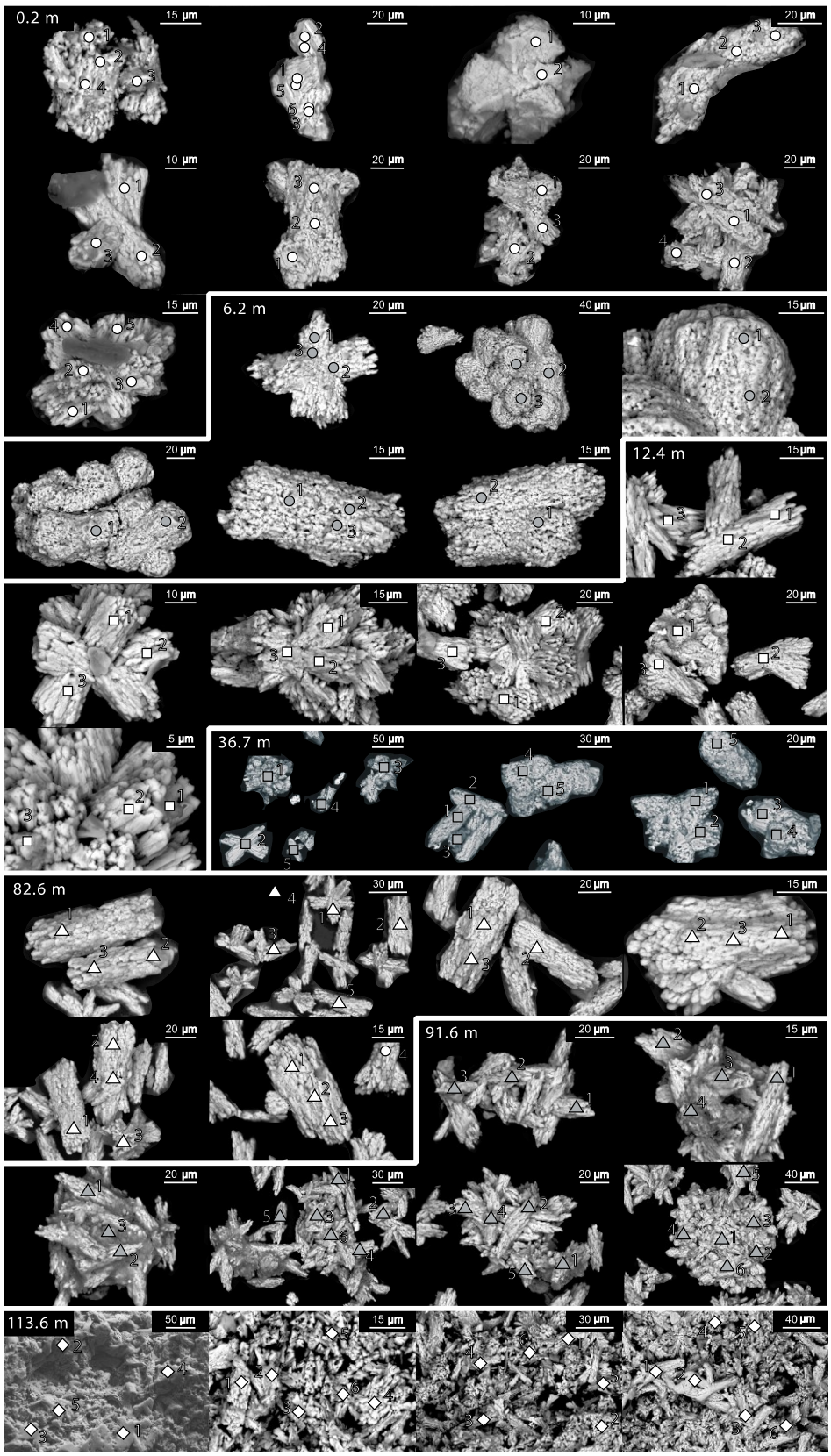

Figure S 6.1: *SEM images in back-scatter mode indicating all points of EDX analysis (Squares, triangles, diamonds). The sample at 113.6 m depth belongs to a different stratigraphic unit mainly consisting of fluvial and lacustrine sediment (Russell et al., 2016). Elemental compositions are plotted in the triangular diagrams in figure 6.3B. See digital version for more details.*

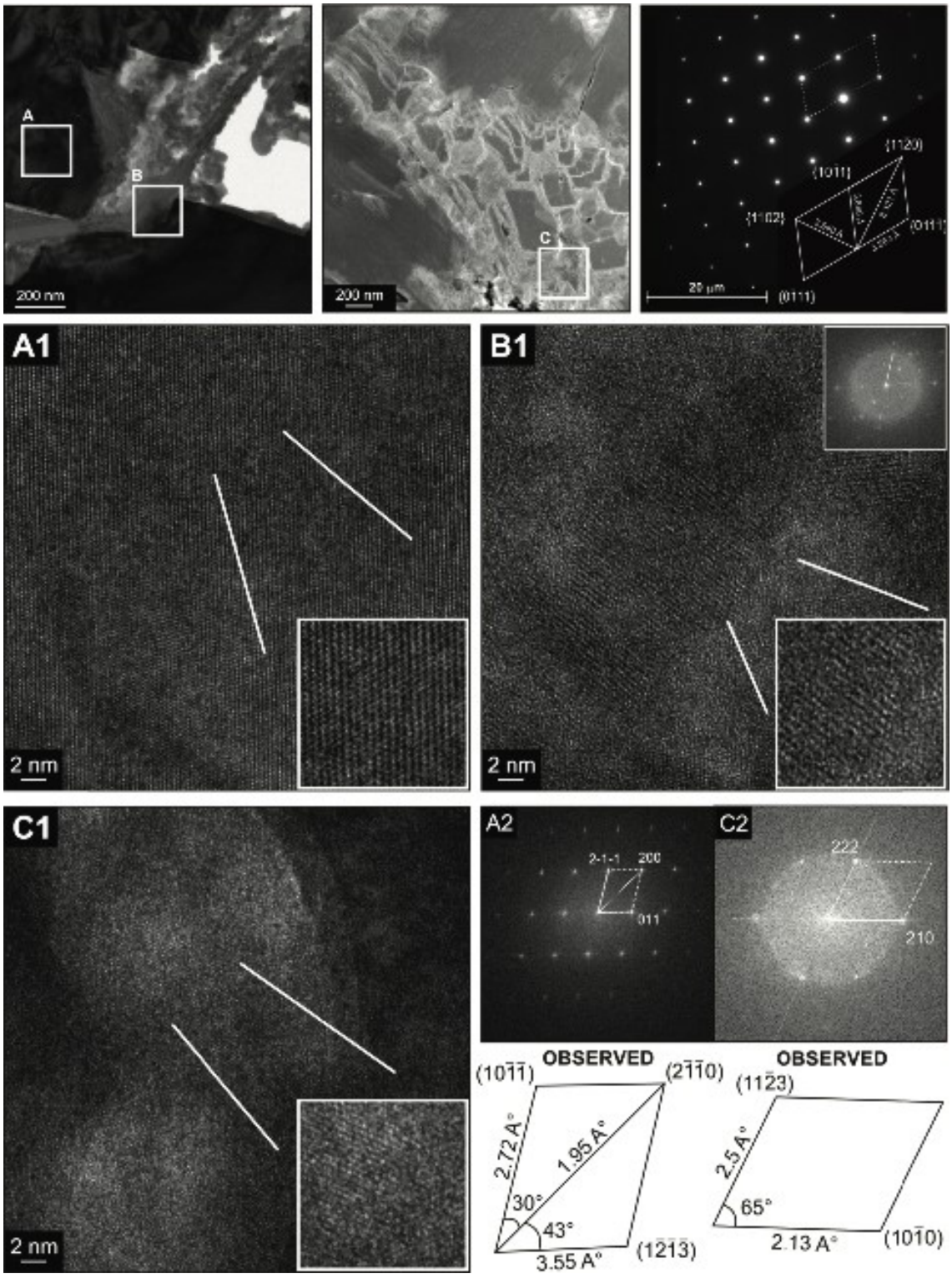

Figure S 6.2 (part 1, siderite): ***(Top left)*** *TEM images of siderite from 6.2and 82.6 m depth with areas (A, B, C) selected for high-resolution episcopic TEM imaging (HR-TEM) and electron diffraction (SAED) patterns.* ***(Top right)*** *High-resolution SAED pattern obtained for the entire siderite crystal lattice fringes (A2, C2) and their SAED patterns with the corresponding interatomic distances and annotations of* d_{hkl} *indices.*

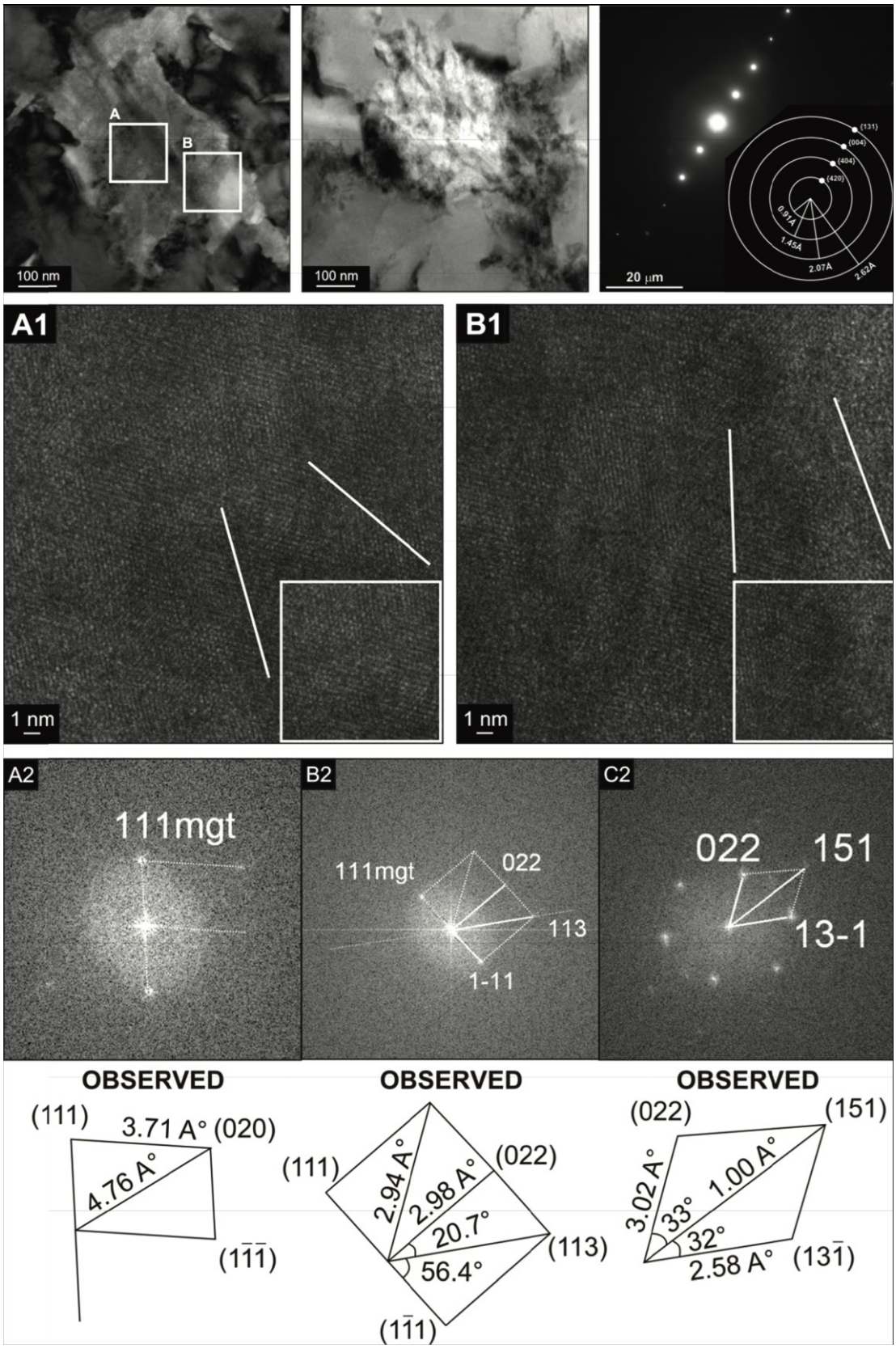

Figure S 6.2 (part 2, magnetite): ***(Top left)*** *TEM images of magnetites from 6.2 m depth with areas (A, B) selected for episcopic high-resolution TEM imaging (HR-TEM) and electron diffraction (SAED) patterns.* ***(Top right)*** *High-resolution SAED pattern obtained for magnetite. (A1, B1) HR-TEM images of crystal lattice fringes; (A2, B2, C2) and their SAED patterns with the corresponding interatomic distances and annotations of d_{hkl} indices.*

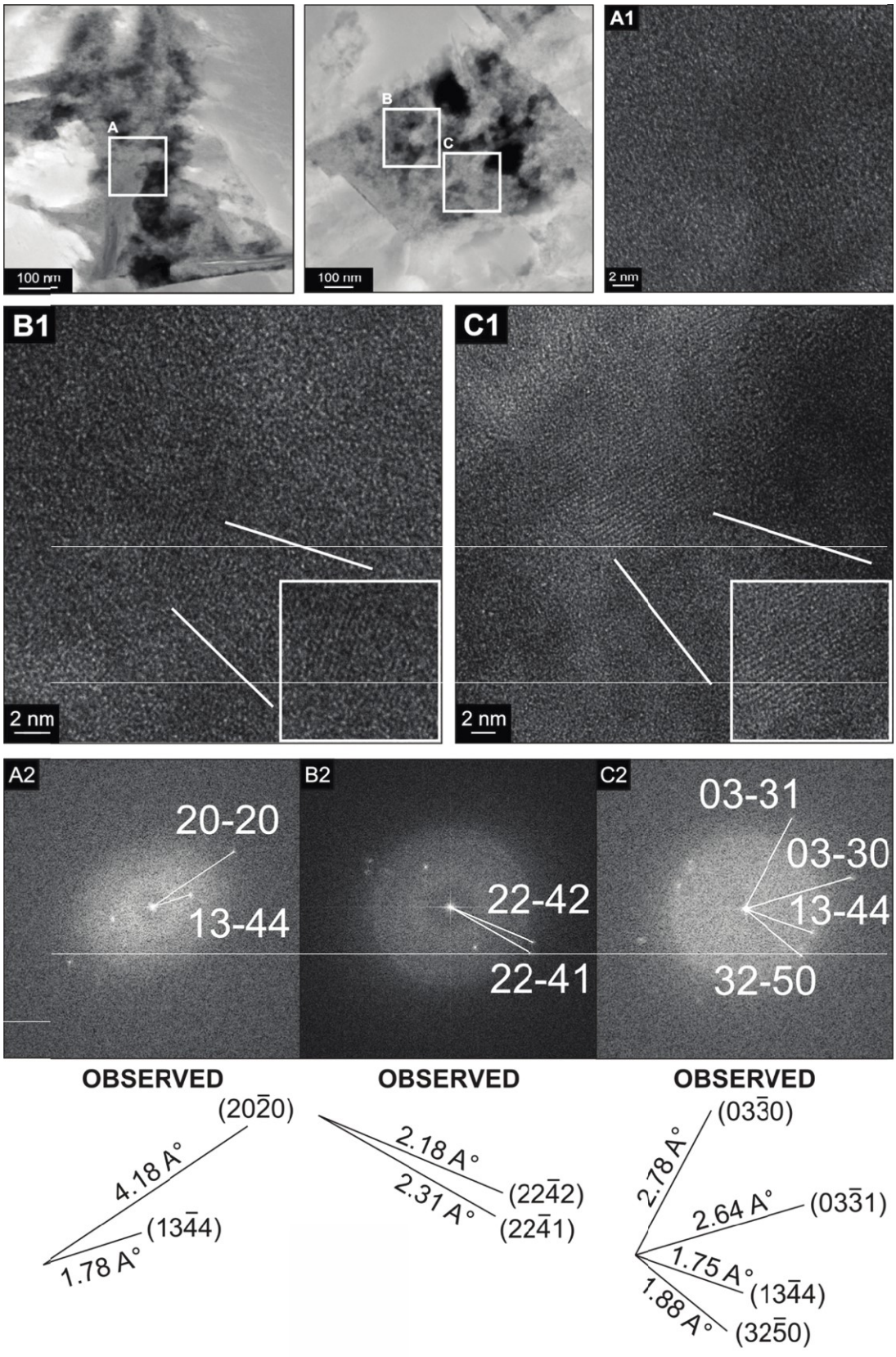

Figure S 6.2 (part 3, green rust): ***(Top left)*** *TEM images of magnetites from 6.2 m depth with areas (A, B, C) selected for high-resolution episcopic TEM imaging (HR-TEM) and electron diffraction (SAED) patterns. (A1, B1, C1) HR-TEM images of crystal lattice fringes; (A2, B2, C2) and their SAED patterns with the corresponding interatomic distances and annotations of* d_{hkl} *indices.*

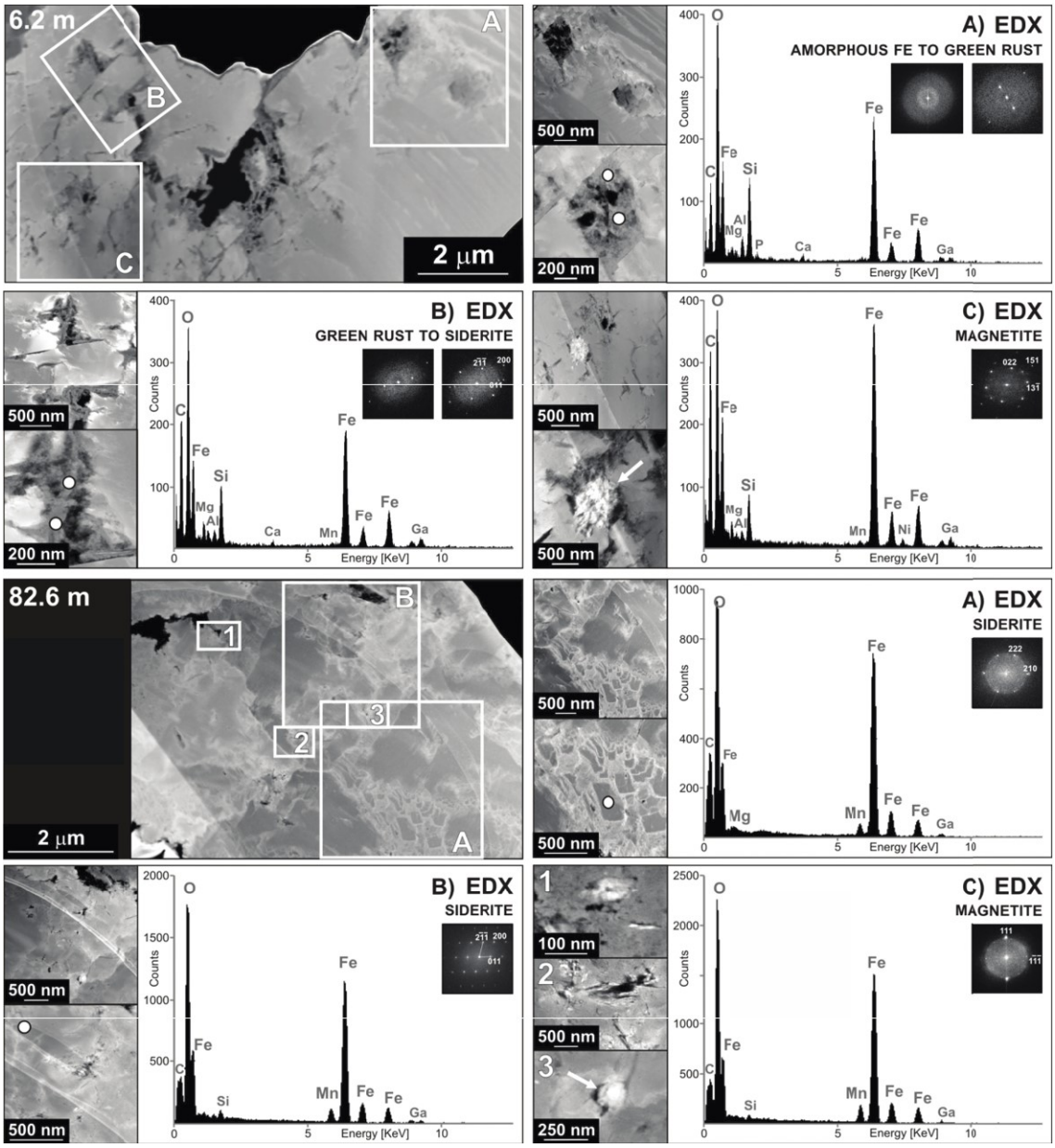

Figure S 6.3: ***(Top)*** *Scanning TEM images of siderite crystals from 6.2 m depth with focus on phase inclusions (white frames) and points of energy-dispersive X-ray (EDX) and electron real diffraction analysis (SAED) (white dots). Although the semi-quantitative composition of the different analyzed phases are rather constant, results of the selected SAED show that the observed phases become more crystalline, likely transiting from amorphous iron to carbonate green rust (A), and from carbonate green rust to either siderite (B) or magnetite (C).* ***(Bottom)*** *Scanning TEM images of a siderite crystal from 82.6 m depth with focus on phase inclusions (white frames) and points of EDX and SAED analysis (white dots). Rims of the siderite crystal appear porous, although filled spaces between former crystals are part of a single mosaic crystal. SAED patterns in the rims (A) are blurry but specific to siderite. In contrast, denser parts of the crystal (B) show fully organized lattice diffraction. Nano-magnetites can be found trapped in residual voids within the siderite (1-3) yet with a total lack of green rust, contrasting with the sample from 6.2 m depth.*

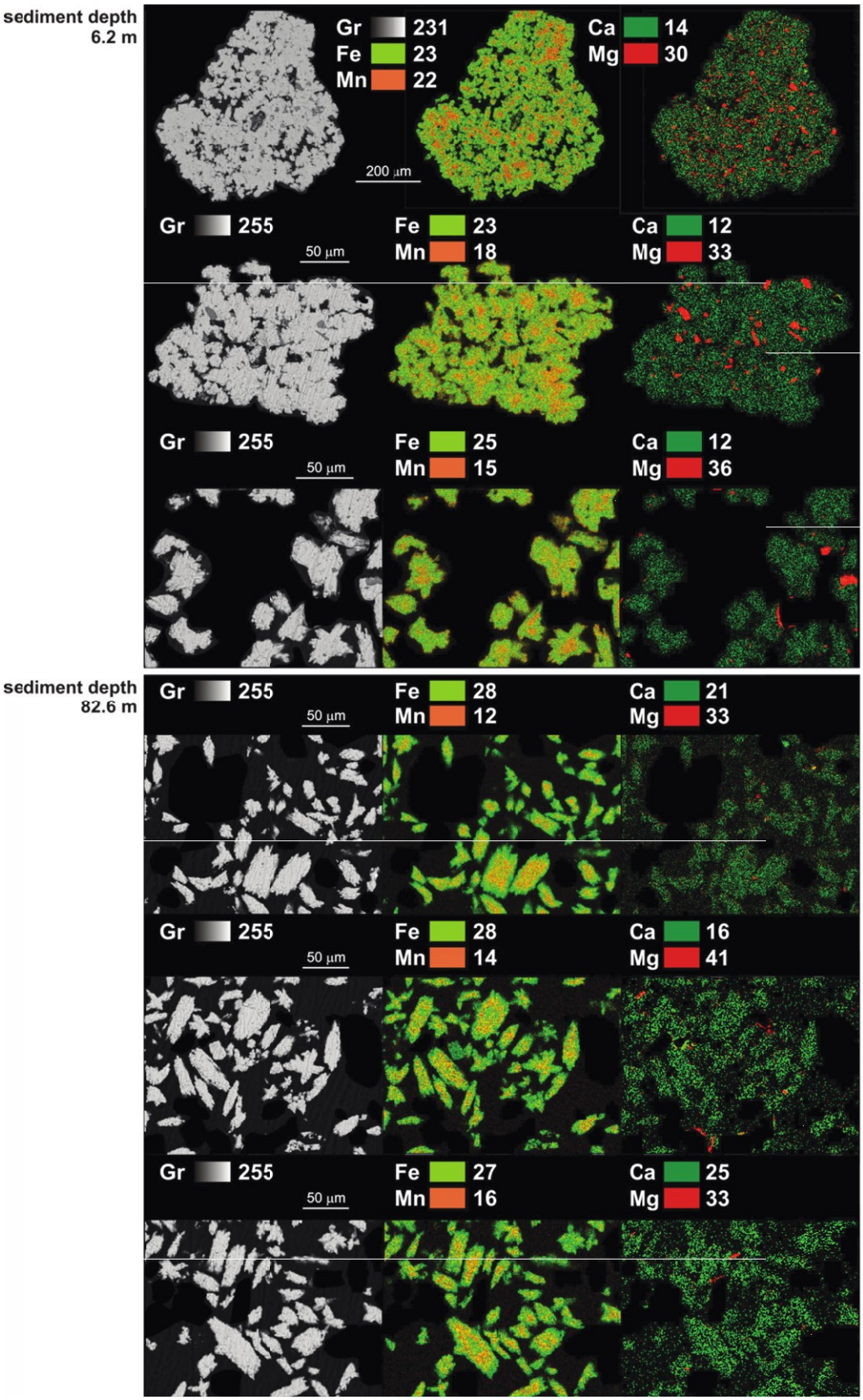

Figure S 6.4: *SEM back-scatter images with EDX elemental mapping of thin sections prepared with siderite separates from 6.2 and 82.6 m sediment depth. Stacked intensity images for Fe and Mn indicate that Fe substitution by Mn occurs preferentially in the center of siderite crystals. Ca and Mg images indicate a limited but increased substitution by Ca in siderites from 82.6 m depth. Mg is only observed in residual detrital silicates.*

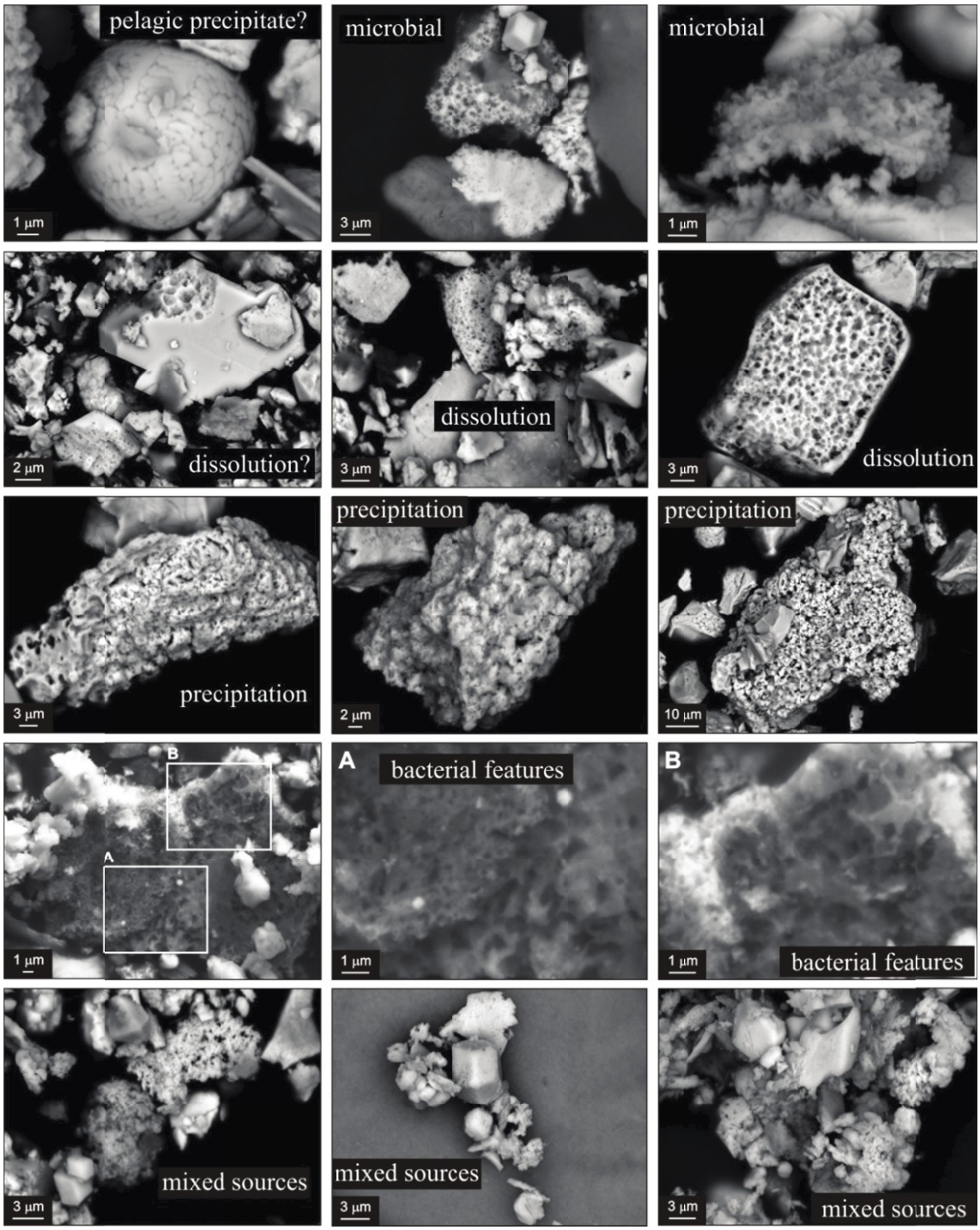

Figure S 6.5: *SEM back-scatter images of magnetite extracts.* ***(1st row)*** *Magnetite spherule potentially representing water column precipitate, and nano-magnetite aggregates interpreted as microbially mediated.* ***(2nd row)*** *Features of dissolution commonly observed on detrital magnetites.* ***(3rd row)*** *Iron precipitates observed in deep sediments.* ***(4th row)*** *Diagenetic dissolution of iron with reprecipitation at the vicinity. The 1-2 µm long dissolution features clearly mimic microbial cells.* ***(5th row)*** *Images illustrating the multiple sources of magnetite e.g. detrital, volcanic, authigenic. Although potentially present in our extracts, magnetosomes from magnetotactic bacteria were not formally identified.*

7 Conclusions and outlook

Anoxic, ferruginous sediments were prevalent throughout much of the Earth's history and microbial organic matter mineralization within those sediments likely played a key role in global biogeochemical cycling throughout much of the Precambrian Eons. However, knowledge of organic matter mineralization in ferruginous sediments remains poorly understood, as modern analogue environments are extremely rare. The aim of this thesis was to investigate the biogeochemistry of modern ferruginous sediments of Lake Towuti, Indonesia that are partly analogous to those that likely deposited throughout the Precambrian Eons. It is the first biogeochemical characterization of an anoxic, iron-rich and sulfate-poor sedimentary subsurface environment. To investigate organic matter mineralization in Lake Towuti's sediments geochemical and microbiological analyses were applied. First, geomicrobiological investigations were done at sediment samples from short (< 35 cm) sediment cores that experienced different redox conditions at the sediment-water interface from oxic to anoxic. Then, a suite of biogeochemical analyses were done on sediment samples from the upper 12 m of a sediment core that was retrieved during the ICDP drilling campaign in spring 2015.

In order to get a true signal, geochemical and microbiological analyses depend on uncontaminated samples. However, exploration of subsurface environments relies on drilling, which inevitably causes infiltration of drilling fluids into the sediment core. Several techniques have been used in past drilling operations; each with their specific strengths and weaknesses. However, none of the established techniques were suitable for the Towuti Drilling project as they were either logistically not applicable (e.g. Perfluorocarbon tracers), interfered with the high iron concentrations of Lake Towuti's sediment (fluorescent dyes) or were exceptionally expensive not allowing for a high-resolution contamination assessment (microspheres). Thus, a simple and inexpensive technique for assessing contamination during drilling operations was developed. Here, aqueous fluorescent pigment dispersions, commonly used in the paint industry, were used as a particulate tracer. The physical properties of these dispersions were similar to those of commonly used particulate tracers (i.e. microspheres). However, the price was nearly four orders of magnitude lower. One major advantage over fluorescent dyes and

chemical tracers was the long-term stability of the dispersions, allowing for a contamination assessment on archived core material several months and potentially even years after core retrieval. While the approach requires only a minimum of equipment, the sensitivity was in the range of already established techniques (117 nanoliters drilling fluid cm^{-3} sediment). To allow for a rapid and automatic detection of contamination on site even in remote locations, combination with flow cytometry was proposed and successfully tested. The approach was applied at the Towuti drilling campaign and showed that more than 75 % of the sediment samples retrieved for geomicrobiological investigations were not contaminated. Contaminated samples were identified and not used for further geochemical and microbiological analyses.

In order to obtain a first picture of the biogeochemical processes in the ferruginous sediments of Lake Towuti and the microbial community inhabiting this environment, geomicrobiological investigations were done on sediment samples from short sediment cores (< 35 cm). They showed that the electron acceptors commonly used in organic matter mineralization, i.e. oxygen, nitrate and sulfate are absent (oxygen, nitrate) or scarce (sulfate) in Lake Towuti's sediment. Still, the sediments harbor high microbial cell densities. It could be shown that the microbial cell densities as well as the biogeochemical processes are a function of redox differences of Lake Towuti's bottom water. Bottom water oxygenation at the sediment-water interface leads to a higher input of labile organic matter and electron acceptors like sulfate and iron, which promotes a higher microbial abundance. Despite the low sulfate concentrations (< 25 μM), sulfate-reducing bacteria were viable and active throughout the upper 35 cm and rapidly turn over the available sulfate pool in the order of days. Microbial analyses could show that Lake Towuti's surface sediments is inhabited by a microbial community with a potential to perform metabolisms related to iron and sulfate reduction, fermentation as well as methanogenesis. How extracellular DNA is preserved in Towuti's sediment and the extent to which it can be used as an archive for genetic information has been briefly studied. From a rapid decrease in extracellular DNA concentrations in the upper reaches of the sediment it has been inferred that the ferruginous sediments of Lake Towuti may loose its genetic information with time. However, intracellular DNA can also be a major source of preserved DNA, being preserved in pollen or spores or through adsorption on the abundant metal oxides, and thus might be misinterpreted as part of the living and active microbial community. Also,

the timing at which a cell has died and lysed and thereby contributed to the extracellular DNA pool is not known. Thus, Lake Towuti's sediment might still record genetic information over longer timescales despite a rapid decrease of extracellular DNA concentrations in the upper sediments. Extraction of DNA from Towuti's sediment is ongoing work and – if successful – will allow reconstructing past environmental conditions.

Biogeochemical studies made in Towuti's short cores were extended to the upper 12 m of the sediment core that was retrieved during the Towuti drilling campaign. Total microbial organic matter mineralization was investigated using a suite of biogeochemical analyses. We performed potential sulfate reduction rate experiments, extracted the different iron phases, analyzed the pore water chemistry and applied geochemical modeling to the measured pore water concentration profiles. These analyses revealed that Lake Towuti's sediments are extremely rich in iron with total concentrations up to 2500 μmol cm^{-3} (20 wt. %), which makes it the natural sedimentary environment with the highest total iron concentrations studied to date. In absence of oxygen and nitrate together with the scarcity of sulfate, organic matter would be expected to proceed via the most abundant and energetically most favorable electron acceptor, in this case iron(oxy)hydroxides. However, this thesis could show that microbial organic matter mineralization is almost exclusively channeled via methanogenesis (> 85 %) even though reactive iron was present and readily available for microbial iron reduction throughout the upper 12 m. Reactive iron(oxy)hydroxides theoretically available for microbial respiration thus remained stable for at least 60.000 years.

A process that can efficiently decrease the methane efflux to the atmosphere is the anaerobic oxidation of methane. In marine environments this process has been shown to effectively consume the produced methane by being coupled to sulfate reduction. Anaerobic oxidation of methane has further been shown to be coupled to nitrate or iron reduction in environments where sulfate is scarce. The absence of nitrate and scarcity of sulfate in ferruginous sediments would leave behind iron reduction as the only process to effectively reduce the methane efflux to the water body and eventually the atmosphere. In this thesis it was suggested that due to the poor reactivity of iron, anaerobic oxidation of methane is not expected to be an appreciable process in the modern ferruginous sediments of Lake Towuti and indeed the geochemical data

point towards a methane efflux from the sediment into the water column. This would have important implications for global biogeochemical cycling in the ferruginous sediments of the Archean and Proterozoic eons. Breakdown of more than 85% of organic carbon through methanogenesis would have led to significant marine methane production (15 – 180 Tmol yr^{-1}). In oceans largely devoid of oxygen and sulfate, sedimentary methanogenesis fueled by methanogenesis would, in the absence of iron dependent anaerobic oxidation of methane, have led to equivalent effluxes of methane to the overlying oceans and atmosphere. Methane as an important greenhouse gas likely played a key role as a regulator of Earth's early climate and contributed to warming under a faint young sun. To prove this hypothesis, it is essential to investigate the role of anaerobic oxidation of methane in the modern ferruginous sediments of Lake Towuti. This can either be done via radiotracer incubation experiments using ^{14}C-labeled methane or by microbiological studies that may identify the potential of the microbial community to perform metabolisms related to the anaerobic oxidation of methane.

In this study it could be shown that iron(oxy)hydroxides, which have been shown to be reactive towards microbial iron reduction in laboratory experiments, remained stable over at least 60.000 years. These findings should be extended to the 114 m long sedimentary record that spans approximately the last 600.000 years. This should be supplemented by studies on the reason why the microbially available ferric iron phases in their high abundance are so poorly reactive. If this is a general feature and not only exclusive for Lake Towuti's sediments, it would underline the extrapolation of the findings made in this study to the ancient sediments of Earth's early oceans. Finally, to support the geochemical data, microbiological studies are needed. Microbiological studies on the 114 m long sediment core will elucidate the microbial community composition, its diversity, its metabolic potential as well as the adaptations made to this unique environment.

In the ferruginous sediments of Lake Towuti diagenetic siderites could be identified throughout the 114 m long sediment core. Their formation is a function of changes in redox conditions in the pore water and sediment over time leading to microchemical zoning of siderite crystals. It is thus suggested in this thesis that identification of microchemical zoning in ancient siderites, such as it is observed in Lake Towuti siderites, may provide insight into water column and pore fluid chemistries at the time of their deposition. Also, mineral inclusions in siderites,

especially magnetite and green rust, could be observed in siderite crystals. Likewise, the preservation of those mineral inclusions may help to reconstruct diagenetic sequences in ancient sedimentary iron formations. Thus, further exploration of the microchemistry and phase inclusions of minerals in modern analogue systems may hold promise for reconstructing environmental conditions at the time of deposition of ancient sedimentary iron formations.

8 References

Alawi, M., Schneider, B., Kallmeyer, J., 2014. A procedure for separate recovery of extra-and intracellular DNA from a single marine sediment sample. Journal of microbiological methods 104, 36-42.

Aldrian, E., Dwi Susanto, R., 2003. Identification of three dominant rainfall regions within Indonesia and their relationship to sea surface temperature. International Journal of Climatology 23, 1435-1452.

Alin, S.R., Johnson, T.C., 2007. Carbon cycling in large lakes of the world: A synthesis of production, burial, and lake-atmosphere exchange estimates. Global Biogeochemical Cycles 21, GB3002.

Amon, R.M., Benner, R., 1996. Bacterial utilization of different size classes of dissolved organic matter. Limnology and Oceanography 41, 41-51.

Aoki, M., Kakiuchi, R., Yamaguchi, T., Takai, K., Inagaki, F., Imachi, H., 2015. Phylogenetic diversity of aprA genes in subseafloor sediments on the northwestern Pacific margin off Japan. Microbes and environments 30, 276-280.

Bae, H.-S., Holmes, M.E., Chanton, J.P., Reddy, K.R., Ogram, A., 2015. Distribution, activities, and interactions of methanogens and sulfate-reducing prokaryotes in the Florida Everglades. Applied Environmental Microbiology 81, 7431-7442.

Baker, G., Cowan, D.A., 2004. 16 S rDNA primers and the unbiased assessment of thermophile diversity. Portland Press Limited.

Bakken, L.R., Olsen, R.A., 1989. DNA-content of soil bacteria of different cell size. Soil Biology and Biochemistry 21, 789-793.

Baldwin, D.S., 2013. Organic phosphorus in the aquatic environment. Environmental Chemistry 10, 439-454.

Bar-Or, I., Ben-Dov, E., Kushmaro, A., Eckert, W., Sivan, O., 2015. Methane-related changes in prokaryotes along geochemical profiles in sediments of Lake Kinneret (Israel). Biogeosciences 12, 2847.

Bauer, K.W., Gueguen, B., Cole, D.B., Francois, R., Kallmeyer, J., Planavsky, N., Crowe, S.A., 2017. Chromium isotope fractionation in ferruginous sediments. Geochimica et Cosmochimica Acta 223, 198-215.

Beal, E.J., House, C.H., Orphan, V.J., 2009. Manganese-and iron-dependent marine methane oxidation. Science 325, 184-187.

Bekker, A., Planavsky, N.J., Krapež, B., Rasmussen, B., Hofmann, A., Slack, J.F., Rouxel, O.J., and Konhauser, K.O., 2014. Iron formations: Their origins and implications for ancient seawater chemistry, *in* Mackenzie F.T., et al., eds., Treatise in Geochemistry, Volume 9: Elsevier, Amsterdam, p. 561- 628.

Bell, P.E., Mills, A.L., and Herman, J.S., 1987. Biogeochemical conditions favoring magnetite formation during anaerobic iron reduction: Applied and Environmental Microbiology, v. 53, p. 2610–2616.

Berner, R.A., 1980. Early diagenesis: A theoretical approach. Princeton University Press.

Berner, R.A., 1989. Biogeochemical cycles of carbon and sulfur and their effect on atmospheric oxygen over phanerozoic time. Palaeogeography and Palaeoclimatology 75, 97-122.

Biddle, J.F., Jungbluth, S.P., Lever, M.A., Rappe, M., 2014. Life in the Oceanic Crust, in: Kallmeyer, J., Wagner, D. (Eds.), Microbial Life in the Deep Biosphere. DeGruyter, pp. 29 - 62.

Boetius, A., Ravenschlag, K., Schubert, C.J., Rickert, D., Widdel, F., Gieseke, A., Amann, R., Jørgensen, B.B., Witte, U., Pfannkuche, O., 2000. A marine microbial consortium apparently mediating anaerobic oxidation of methane. Nature 407, 623-626.

Bolger, A.M., Lohse, M., Usadel, B., 2014. Trimmomatic: a flexible trimmer for Illumina sequence data. Bioinformatics 30, 2114-2120.

Boom, R., Sol, C., Salimans, M., Jansen, C., Wertheim-van Dillen, P., Van der Noordaa, J., 1990. Rapid and simple method for purification of nucleic acids. Journal of clinical microbiology 28, 495-503.

Boon, N., Windt, W., Verstraete, W., Top, E.M., 2002. Evaluation of nested PCR–DGGE (denaturing gradient gel electrophoresis) with group-specific 16S rRNA primers for the analysis of bacterial communities from different wastewater treatment plants. FEMS Microbiology Ecology 39, 101-112.

Borsodi, A.K., Felföldi, T., Máthé, I., Bognár, V., Knáb, M., Krett, G., Jurecska, L., Tóth, E.M., Márialigeti, K., 2013. Phylogenetic diversity of bacterial and archaeal communities inhabiting the saline Lake Red located in Sovata, Romania. Extremophiles 17, 87-98.

Bramburger, A.J., Hamilton, P.B., Hehanussa, P.E., Haffner, G.D., 2008. Processes regulating the community composition and relative abundance of taxa in the

diatom communities of the Malili Lakes, Sulawesi Island, Indonesia. Hydrobiologia 615, 215-224.

Brands, B., Vianna, M.E., Seyfarth, I., Conrads, G., Horz, H.P., 2010. Complementary retrieval of 16S rRNA gene sequences using broad-range primers with inosine at the 3′-terminus: implications for the study of microbial diversity. FEMS Microbiology Ecology 71, 157-167.

Button, D., Robertson, B.R., 2001. Determination of DNA content of aquatic bacteria by flow cytometry. Applied Environmental Microbiology 67, 1636-1645.

Byers, S.C., Mills, E.L., Stewart, P.L., 1978. A comparison of methods of determining organic carbon in marine sediments, with suggestions for a standard method. Hydrobiologia 58, 43-47.

Canfield, D.E., 1997. The geochemistry of river particulates from the continental USA: Major elements. Geochimica et Cosmochimica Acta 61, 3349-3365.

Canfield, D.E., 2005. The early history of atmospheric oxygen: Homage to Robert M. Garrels. Annual Review of Earth and Planetary Sciences 33, 1-36.

Canfield, D.E., Poulton, S.W., Knoll, A.H., Narbonne, G.M., Ross, G., Goldberg, T., and Strauss, H., 2008. Ferruginous conditions dominated later Neoproterozoic deep-water chemistry: Science, v. 321, p. 949–952.

Canfield, D.E., Raiswell, R., Bottrell, S., 1992. The reactivity of sedimentary iron minerals towards sulfide. American Journal of Science 292, 659-683.

Canfield, D.E., Raiswell, R., Westrich, J.T., Reaves, C.M., Berner, R.A., 1986. The use of chromium reduction in the analysis of reduced inorganic sulfur in sediments and shales. Chemical Geology 54, 149-155.

Canfield, D.E., Rosing, M.T., Bjerrum, C., 2006. Early anaerobic metabolisms. Philosophical transactions of the Royal Society of London. Series B, Biological sciences 361, 1819-1836.

Canfield, D.E., Stewart, F.J., Thamdrup, B., De Brabandere, L., Dalsgaard, T., Delong, E.F., Revsbech, N.P., Ulloa, O., 2010. A cryptic sulfur cycle in oxygen-minimum–zone waters off the Chilean coast. Science 330, 1375-1378.

Canfield, D.E., Thamdrup, B., Hansen, J.W., 1993. The anaerobic degradation of organic matter in Danish coastal sediments: Iron reduction, manganese reduction, and sulfate reduction. Geochimica et Cosmochimica Acta 57, 3867-3883.

Caporaso, J.G., Kuczynski, J., Stombaugh, J., Bittinger, K., Bushman, F.D., Costello, E.K., Fierer, N., Pena, A.G., Goodrich, J.K., Gordon, J.I., 2010. QIIME allows analysis of high-throughput community sequencing data. Nature methods 7, 335.

Castro, H.F., Williams, N.H., Ogram, A., 2000. Phylogeny of sulfate-reducing bacteria. FEMS Microbiology Ecology 31, 1-9.

Ceccherini, M.T., Ascher, J., Agnelli, A., Borgogni, F., Pantani, O.L., Pietramellara, G., 2009. Experimental discrimination and molecular characterization of the extracellular soil DNA fraction. Antonie Van Leeuwenhoek 96, 653-657.

Chiang, J.C.H., 2009. The Tropics in Paleoclimate. Annual Review of Earth and Planetary Sciences 37, 263-297.

Chin, C.-S., Alexander, D.H., Marks, P., Klammer, A.A., Drake, J., Heiner, C., Clum, A., Copeland, A., Huddleston, J., Eichler, E.E., 2013. Nonhybrid, finished microbial genome assemblies from long-read SMRT sequencing data. Nature methods 10, 563.

Cleaves, H.J., Crapster-Pregont, E., Jonsson, C.M., Jonsson, C.L., Sverjensky, D.A., Hazen, R.A., 2011. The adsorption of short single-stranded DNA oligomers to mineral surfaces. Chemosphere 83, 1560-1567.

Cohen, A., Campisano, C., Arrowsmith, R., Asrat, A., Behrensmeyer, A.K., Deino, A., Feibel, C., Hill, A., Johnson, R., Kingston, J., Lamb, H., Lowenstein, T., Noren, A., Olago, D., Owen, R.B., Potts, R., Reed, K., Renaut, R., Schäbitz, F., Tiercelin, J.J., Trauth, M.H., Wynn, J., Ivory, S., Brady, K., O'Grady, R., Rodysill, J., Githiri, J., Russell, J., Foerster, V., Dommain, R., Rucina, S., Deocampo, D., Russell, J., Billingsley, A., Beck, C., Dorenbeck, G., Dullo, L., Feary, D., Garello, D., Gromig, R., Johnson, T., Junginger, A., Karanja, M., Kimburi, E., Mbuthia, A., McCartney, T., McNulty, E., Muiruri, V., Nambiro, E., Negash, E.W., Njagi, D., Wilson, J.N., Rabideaux, N., Raub, T., Sier, M.J., Smith, P., Urban, J., Warren, M., Yadeta, M., Yost, C., Zinaye, B., 2016. The Hominin Sites and Paleolakes Drilling Project: inferring the environmental context of human evolution from eastern African rift lake deposits. Scientific Drilling 21, 1-16.

Coleman, M.L., 1993. Microbial processes: Controls on the shape and composition of carbonate concretions: Marine Geology, v. 113, p. 127–140.

Colwell, F.S., Stormberg, G.J., Phelps, T.J., Birnbaum, S.A., McKinley, J., Rawson, S.A., Veverka, C., Goodwin, S., Long, P.E., Russell, B.F., Garland, T.,

Thompson, D., Skinner, P., Grover, S., 1992. Innovative techniques for collection of saturated and unsaturated subsurface basalts and sediments for microbiological characterization. Journal of Microbiological Methods 15, 279-292.

Concheri, G., Stevanato, P., Zaccone, C., Shotyk, W., D'orazio, V., Miano, T., Piffanelli, P., Rizzi, V., Ferrandi, C., Squartini, A., 2017. Rapid peat accumulation favours the occurrence of both fen and bog microbial communities within a Mediterranean, free-floating peat island. Scientific reports 7, 8511.

Conrad, R., 2005. Quantification of methanogenic pathways using stable carbon isotopic signatures: a review and a proposal. . Organic Geochemistry 36, 739-752.

Corinaldesi, C., Barucca, M., Luna, G.M., DELL'ANNO, A., 2011. Preservation, origin and genetic imprint of extracellular DNA in permanently anoxic deep-sea sediments. Molecular Ecology 20, 642-654.

Corinaldesi, C., Beolchini, F., Dell'Anno, A., 2008. Damage and degradation rates of extracellular DNA in marine sediments: implications for the preservation of gene sequences. Molecular Ecology 17, 3939-3951.

Corinaldesi, C., Dell'Anno, A., Danovaro, R., 2007. Early diagenesis and trophic role of extracellular DNA in different benthic ecosystems. Limnology and Oceanography 52, 1710-1717.

Costa, K., Russell, J., Vogel, H., Bijaksana, S., 2015. Hydrological connectivity and mixing of Lake Towuti, Indonesia in response to paleoclimatic changes over the last 60,000 years. Palaeogeography and Palaeoclimatology 417, 467-475.

Cragg, B.A., Parkes, R.J., Fry, J.C., Herbert, R.A., Wimpenny, J.W.T., Getliff, J.M., 1990. Bacterial biomass and activity profiles within deep sediment layers, in: Suess, E., von Huene, R. (Eds.), Proceedings of the Ocean Drilling Program, Scientific Results. Ocean Drilling Program, College Station, TX, pp. 607-619.

Crowe, S., Pannalal, S., Fowle, D., Cioppa, M., Symons, D., Haffner, G., Fryer, B., McNeely, R., Sundby, B., Hehanussa, P., 2004. Biogeochemical cycling in Fe-rich sediments from Lake Matano, Indonesia, 11th International symposium on Water-Rock Interaction, Saratoga Springs, pp. 1185-1189.

Crowe, S.A., Jones, C., Katsev, S., Magen, C., O'Neill, A.H., Sturm, A., Canfield, D.E., Haffner, G.D., Mucci, A., Sundby, B., Fowle, D.A., 2008a. Photoferrotrophs

thrive in an Archean Ocean analogue. Proceedings of the National Academy of Sciences of the United States of America 105, 15938-15943.

Crowe, S.A., Katsev, S., Leslie, K., Sturm, A., Magen, C., Nomosatryo, S., Pack, M.A., Kessler, J.D., Reeburgh, W.S., Roberts, J.A., Gonzalez, L., Douglas Haffner, G., Mucci, A., Sundby, B., Fowle, D.A., 2011. The methane cycle in ferruginous Lake Matano. Geobiology 9, 61-78.

Crowe, S.A., O'Neill, A.H., Katsev, S., Hehanussa, P., Haffner, G.D., Sundby, B., Mucci, A., Fowle, D.A., 2008b. The biogeochemistry of tropical lakes: A case study from Lake Matano, Indonesia. Limnology and Oceanography 53, 319 - 331.

Crowe, S.A., Paris, G., Katsev, S., Jones, C., Kim, S.-T., Zerkle, A.L., Nomosatryo, S., Fowle, D.A., Adkins, J.F., Sessions, A.L., Farquhar, J., Canfield, D.E., 2014. Sulfate was a trace constituent of Archean seawater. Science 346, 735-739.

Crowe, S.A., Roberts, J.A., Weisener, C.G., Fowle, D.A., 2007. Alteration of iron-rich lacustrine sediments by dissimilatory iron-reducing bacteria. Geobiology 5, 63-73.

D'Hondt, S., Inagaki, F., Zarikian, C.A., Abrams, L.J., Dubois, N., Engelhardt, T., Evans, H., Ferdelman, T., Gribsholt, B., Harris, R.N., Hoppie, B.W., Hyun, J.H., Kallmeyer, J., Kim, J., Lynch, J.E., McKinley, C.C., Mitsunobu, S., Morono, Y., Murray, R.W., Pockalny, R., Sauvage, J., Shimono, T., Shiraishi, F., Smith, D.C., Smith-Duque, C.E., Spivack, A.J., Steinsbu, B.O., Suzuki, Y., Szpak, M., Toffin, L., Uramoto, G., Yamaguchi, Y.T., Zhang, G.L., Zhang, X.H., Ziebis, W., 2015. Presence of oxygen and aerobic communities from sea floor to basement in deep-sea sediments. Nature Geoscience 8, 299-304.

D'Hondt, S., Jørgensen, B., Miller, D.J., Batzke, A., Blake, R., Cragg, B.A., Cypionka, H., Dickens, G.R., Ferdelman, T., Hinrichs, K.-U., Holm, N.G., Mitterer, R., Spivack, A.J., Wang, A., Bekins, B., Engelen, B., Ford, K., Gettemy, G., Rutherford, S., Sass, H., Skilbeck, C.G., Aiello, I.W., Guèrin, G., House, C.H., Inagaki, F., Meister, P., Naehr, T., Niitsuma, S., Parkes, R.J., Schippers, A., Smith, D.C., Teske, A., Wiegel, J., Padilla, C.N., Acosta, J.L.S., 2004. Distributions of microbial activities in deep subseafloor sediments. Science 306, 2216-2221.

Daniels, L., Sparling, R., Sprott, G.D., 1984. The bioenergetics of methanogenesis. Biochimica et Biophysica Acta (BBA)-Reviews on Bioenergetics 768, 113-163.

Danovaro, R., Middelboe, M., 2010. Separation of free virus particles from sediments in aquatic systems. Manual of Aquatic Viral Ecology. ASLO, 74-81.

DeSantis, T.Z., Hugenholtz, P., Larsen, N., Rojas, M., Brodie, E.L., Keller, K., Huber, T., Dalevi, D., Hu, P., Andersen, G.L., 2006. Greengenes, a chimera-checked 16S rRNA gene database and workbench compatible with ARB. Applied Environmental Microbiology 72, 5069-5072.

Deutzmann, J.S., Schink, B., 2011. Anaerobic oxidation of methane in sediments of Lake Constance, an oligotrophic freshwater lake. Applied Environmental Microbiology 77, 4429-4436.

Dideriksen, K., Frandsen, C., Bovet, N., Wallace, A.F., Sel, O., Arbour, T., Navrotsky, A., De Yoreo, J.J., and Banfield, J.F., 2015. Formation and transformation of a short range ordered iron carbonate precursor: Geochimica et Cosmochimica Acta, v. 164, p. 94–109.

Diehl, H., Horchak-Morris, N., 1987. Studies on fluorescein-V The absorbance of fluorescein in the ultraviolet, as a function of pH. Talanta 34, 739-741.

DLDS, 2010. New drilling platform expands climate studies in lakes. Scientific Drilling 10, 64.

Dong, H., Jiang, H., Yu, B., Liu, X., Zhang, C., 2010. Impacts of environmental change and human activity on microbial ecosystems on the Tibetan Plateau, NW China. GSA Today 20, 4-10.

Dong, H., Kukkadapu, R.K., Fredrickson, J.K., Zachara, J.M., Kennedy, D.W., Kostandarithes, H.M., 2003. Microbial Reduction of Structural Fe(III) in Illite and Goethite. Environmental Science and Technology 37, 1268-1276.

Dridi, B., Fardeau, M.-L., Ollivier, B., Raoult, D., Drancourt, M., 2012. Methanomassiliicoccus luminyensis gen. nov., sp. nov., a methanogenic archaeon isolated from human faeces. International Journal of Systematic and Evolutionary Microbiology 62, 1902-1907.

Edgar, R.C., 2010. Search and clustering orders of magnitude faster than BLAST. Bioinformatics 26, 2460-2461.

Elferink, S.J.O., Akkermans-van Vliet, W., Bogte, J.J., Stams, A.J., 1999. Desulfobacca acetoxidans gen. nov., sp. nov., a novel acetate-degrading sulfate reducer isolated from sulfidogenic granular sludge. International Journal of Systematic and Evolutionary Microbiology 49, 345-350.

Ettwig, K.F., Zhu, B., Speth, D., Keltjens, J.T., Jetten, M.S., Kartal, B., 2016. Archaea catalyze iron-dependent anaerobic oxidation of methane. Proceedings of the National Academy of Sciences U.S.A. 113, 12792-12796.

Evans, P.N., Parks, D.H., Chadwick, G.L., Robbins, S.J., Orphan, V.J., Golding, S.D., Tyson, G.W., 2015. Methane metabolism in the archaeal phylum Bathyarchaeota revealed by genome-centric metagenomics. Science 350, 434-438.

Fahrbach, M., Kuever, J., Meinke, R., Kämpfer, P., Hollender, J., 2006. Denitratisoma oestradiolicum gen. nov., sp. nov., a 17β-oestradiol-degrading, denitrifying betaproteobacterium. International Journal of Systematic and Evolutionary Microbiology 56, 1547-1552.

Fenchel, T., Blackburn, H., King, G.M., 1998. Bacterial biogeochemistry: the ecophysiology of mineral cycling. Academic Press.

Ferguson, S.J., Jackson, J.B., McEwan, A.G., 1987. Anaerobic respiration in the Rhodospirillaceae: characterisation of pathways and evaluation of roles in redox balancing during photosynthesis. FEMS Microbiology Reviews 3, 117-143.

Fernandez-Diaz, L., Putnis, A., Prieto, M., & Putnis, C. V. (1996). The role of magnesium in the crystallization of calcite and aragonite in a porous medium. Journal of sedimentary research 66(3), 482-491.

Filippini, M., Middelboe, M., 2007. Viral abundance and genome size distribution in the sediment and water column of marine and freshwater ecosystems. FEMS Microbiology Ecology 60, 397-410.

Fossing, H., 1995. ^{35}S-Radiolabeling to probe biogeochemical cycling of sulfur, in: Vairavamurthy, M.A., Schoonen, M.A.A. (Eds.), Geochemical Transformations of Sedimentary Sulfur. American Chemical Society, Washington, DC.

Freudenthal, T., Wagner, T., Wenzhöfer, F., Zabel, M., Wefer, G., 2001. Early diagenesis of organic matter from sediments of the eastern subtropical Atlantic: evidence from stable nitrogen and carbon isotopes. Geochimica et Cosmochimica Acta 65, 1795-1808.

Friedman, I., O'Neil, J.R., 1977. Compilation of stable isotope fractionation factors of geochemical interest, USGS Professional Paper, - ed.

Friese, A., Kallmeyer, J., Kitte, J.A., Martinez, I.M., Bijaksana, S., Wagner, D., International Lake Chalco Drilling Science Team, International Lake Towuti Drilling Science Team 2017. A simple and inexpensive technique for assessing

contamination during drilling operations. Limnology and Oceanography: Methods 15, 200-211.

Froelich, P.N., Klinkhammer, G.P., Bender, M.L., Luedtke, N.A., Heath, G.R., Cullen, D., Dauphin, P., Hammond, D., Hartman, B., Maynard, V., 1979. Early oxidation of organic matter in pelagic sediments of the eastern equatorial Atlantic: suboxic diagenesis. Geochimica et Cosmochimica Acta 43, 1075-1090.

Fromin, N., Hamelin, J., Tarnawski, S., Roesti, D., Jourdain-Miserez, K., Forestier, N., Teyssier-Cuvelle, S., Gillet, F., Aragno, M., Rossi, P., 2002. Statistical analysis of denaturing gel electrophoresis (DGE) fingerprinting patterns. Environmental Microbiology 4, 634-643.

Fry, J.C., 1988. Determination of Biomass, in: Austin, B. (Ed.), Methods in Aquatic Bacteriology. John Wiley & Sons Ltd.

Glasauer, S., Weidler, P.G., Langley, S., Beveridge, T.J., 2003. Controls on Fe reduction and mineral formation by a subsurface bacterium. Geochimica et Cosmochimica Acta 67, 1277-1288.

Glombitza, C., Pedersen, J., Røy, H., Jørgensen, B.B., 2014. Direct analysis of volatile fatty acids in marine sediment porewater by two-dimensional ion chromatography-mass spectrometry. Limnology and Oceanography: Methods 12, 455-468.

Glombitza, C., Stockhecke, M., Schubert, C.J., Vetter, A., Kallmeyer, J., 2013. Sulfate reduction controlled by organic matter availability in deep sediment cores from the saline, alkaline Lake Van (Eastern Anatolia, Turkey). Frontiers in Microbiology 4.

Gole, M.J., 1980. Mineralogy and petrology of very-low-metamorphic grade Archean banded-iron formations, Weld Range, Western Australia: American Mineralogist, v. 65, p. 8–25.

Golightly, J., 2010. Progress in understanding the evolution of nickel laterites. The Challenge of Finding New Mineral Resources: Global Metallogeny, Innovative Exploration, and New Discoveries 2, 451-475.

Greene, A.C., 2014. The family desulfuromonadaceae, The Prokaryotes. Springer, pp. 143-155.

Guilbaud, R., White, M.L., and Poulton, S.W., 2013. Surface charge and growth of sulphate and carbonate green rust in aqueous media: Geochimica et Cosmochimica Acta, v. 108, p. 141–153.

Gunderson, R., Parini, M., Sirad-Azwar, L., 2002. Fluorescein and naphthalene sulfonate liquid tracer results at the Awibengkok geothermal field, West Java, Indonesia, Proceedings, 27th Workshop on Geothermal Reservoir Engineering, Stanford, California, January 28.

Haaijer, S., Van der Welle, M.E., Schmid, M.C., Lamers, L.P., Jetten, M.S., Op den Camp, H.J., 2006. Evidence for the involvement of betaproteobacterial Thiobacilli in the nitrate-dependent oxidation of iron sulfide minerals. FEMS Microbiology Ecology 58, 439-448.

Haffner, G., Hehanussa, P., Hartoto, D., 2001. The biology and physical processes of large lakes of Indonesia: Lakes Matano and Towuti. The Great Lakes of the World. Food-web, Health and Integrity. Backhuys Publishers, Leiden, 183-192.

Hafuka, A., Ding, Q., Yamamura, H., Yamada, K., Satoh, H., 2015. Interactions of dissolved humic substances with oppositely charged fluorescent dyes for tracer techniques. Water Research 85, 193-198.

Halevy, I., Alesker, M., Schuster, E.M., Popovitz-Biro, R., and Feldman, Y., 2017. A key role for green rust in the Precambrian oceans and the genesis of iron formations: Nature Geoscience, v. 10, p. 135–139.

Hall, P., Aller, R.C., 1992. Rapid, small-volume, flow injection analysis for SCO2, and NH4+ in marine and freshwaters. Limnology and Oceanography 37, 1113-1119.

Hallam, S.J., Putnam, N., Preston, C.M., Detter, J.C., Rokhsar, D., Richardson, P.M., DeLong, E.F., 2004. Reverse methanogenesis: testing the hypothesis with environmental genomics. Science 305, 1457-1462.

Hallberg, K.B., Hedrich, S., Johnson, D.B., 2011. Acidiferrobacter thiooxydans, gen. nov. sp. nov.; an acidophilic, thermo-tolerant, facultatively anaerobic iron-and sulfur-oxidizer of the family Ectothiorhodospiraceae. Extremophiles 15, 271-279.

Hallenbeck, P.C., 2009. Fermentative hydrogen production: principles, progress, and prognosis. International Journal of Hydrogen Energy 34, 7379-7389.

Hammer, Ø., Harper, D., Ryan, P., 2001. PAST-Palaeontological statistics. www. uv. es/~ pardomv/pe/2001_1/past/pastprog/past. pdf, acessado em 25, 2009.

Hansel, C.M., Lentini, C.J., Tang, Y., Johnston, D.T., Wankel, S.D., Jardine, P.M., 2015. Dominance of sulfur-fueled iron oxide reduction in low-sulfate freshwater sediments. ISME Journal 9, 2400-2412.

Hartnett, H.E., Keil, R.G., Hedges, J.I., Devol, A.H., 1998. Influence of oxygen exposure time on organic carbon preservation in continental margin sediments. Nature 391, 572-574.

Harvey, R.W., George, L.H., Smith, R.L., LeBlanc, D.R., 1989. Transport of microspheres and indigenous bacteria through a sandy aquifer: results of natural- and forced-gradient tracer experiments. Environmental Science and Technology 23, 51-56.

Hasberg, A.K.M., Bijaksana, S., Held, P., Just, J., Melles, M., Morlock, M.A., Opitz, S., Russell, J.M., Vogel, H., and Wennrich, V., 2019. Modern sedimentation processes in Lake Towuti, Indonesia, revealed by the composition of surface sediments: Sedimentology, v. 66, p. 675–698.

He, J., Zhang, L., Jin, S., Zhu, Y., Liu, F., 2008. Bacterial communities inside and surrounding soil iron-manganese nodules. Geomicrobiology J. 25, 14-24.

He, Q., Sanford, R.A., 2003. Characterization of Fe (III) reduction by chlororespiring Anaeromxyobacter dehalogenans. Applied Environmental Microbiology 69, 2712-2718.

He, Z., Geng, S., Cai, C., Liu, S., Liu, Y., Pan, Y., Lou, L., Zheng, P., Xu, X., Hu, B., 2015. Anaerobic oxidation of methane coupled to nitrite reduction by halophilic marine NC10 bacteria. Applied Environmental Microbiology 81, 5538-5545.

Hedges, J.I., Keil, R.G., 1995. Sedimentary organic matter preservation: an assessment and speculative synthesis. Marine Chemistry 49, 137-139.

Hiraishi, A., Hoshino, Y., 1984. Distribution of rhodoquinone in Rhodospirillaceae and its taxonomic implications. The Journal of General and Applied Microbiology 30, 435-448.

Holland, H.D., 2006. The oxygenation of the atmosphere and oceans: Philosophical Transactions of the Royal Society of London. Series B, Biological Sciences, v. 361, p. 903–915.

Holmkvist, L., Ferdelman, T.G., Jørgensen, B.B., 2011. A cryptic sulfur cycle driven by iron in the methane zone of marine sediment (Aarhus Bay, Denmark). Geochimica et Cosmochimica Acta 75, 3581-3599.

Hope, G., 2001. Environmental change in the late Pleistocene and later Holocene at Wanda site, Soroako, South Sulawesi, Indonesia. Palaeogeography and Palaeoclimatology 171, 129-145.

Hori, T., Kimura, M., Aoyagi, T., Navarro, R.R., Ogata, A., Sakoda, A., Katayama, Y., Takasaki, M., 2014. Biodegradation potential of organically enriched sediments under sulfate-and iron-reducing conditions as revealed by the 16S rRNA deep sequencing. Journal of Water and Environment Technology 12, 357-366.

Horsfield, B., Kieft, T.L., 2007. The geobiosphere, Continental Scientific Drilling. Springer, pp. 163-211.

House, C.H., B.A., C., Teske, A., Party, a.t.L.S., 2003. Drilling contamination tests during ODP Leg 201 using chemical and particulate tracers. Proc. ODP Initial Reports. 201, 1 - 19.

Huber, T., Faulkner, G., Hugenholtz, P., 2004. Bellerophon: a program to detect chimeric sequences in multiple sequence alignments. Bioinformatics 20, 2317-2319.

Huntemann, M., Ivanova, N.N., Mavromatis, K., Tripp, H.J., Paez-Espino, D., Palaniappan, K., Szeto, E., Pillay, M., Chen, I.-M.A., Pati, A., 2015. The standard operating procedure of the DOE-JGI microbial genome annotation pipeline (MGAP v. 4). Standards in genomic sciences 10, 86.

Imachi, H., Sekiguchi, Y., Kamagata, Y., Hanada, S., Ohashi, A., Harada, H., 2002. Pelotomaculum thermopropionicum gen. nov., sp. nov., an anaerobic, thermophilic, syntrophic propionate-oxidizing bacterium. International journal of systematic and evolutionary microbiology 52, 1729-1735.

Jones, C., Crowe, S.A., Sturm, A., Leslie, K.L., MacLean, L.C.W., Katsev, S., Henny, C., Fowle, D.A., Canfield, D.E., 2011. Biogeochemistry of manganese in ferruginous Lake Matano, Indonesia. Biogeosciences 8, 2977-2991.

Jørgensen, B.B., 1978. A Comparison of Methods for the Quantification of Bacterial Sulfate Reduction in Coastal Marine Sediments 1. Measurement with radiotracer techniques. Geomicrobiology J. 1, 11-27.

Jørgensen, B.B., 1982. Mineralization of organic matter in the sea bed-the role of sulphate reduction. Nature 296, 643-644.

Jørgensen, B.B., 2006. Bacteria and Marine Geochemistry, Schulz, H.D., Zabel, M. (Eds.): Marine Geochemistry (2nd edition), Springer Science, Berlin. Schulz, H.D., Zabel, M., pp. 169 - 206.

Jørgensen, B.B., 2012. Shrinking majority of the deep biosphere. Proceedings of the National Academy of Sciences of the United States of America 109, 15976-15977.

Jørgensen, B.B., Fenchel, T., 1974. The Sulfur Cycle of a Marine Sediment Model System. Marine Biology 24, 189-201.

Kadarusman, A., Miyashita, S., Maruyama, S., Parkinson, C.D., Ishikawa, A., 2004. Petrology, geochemistry and paleogeographic reconstruction of the East Sulawesi Ophiolite, Indonesia. Tectonophysics 392, 55-83.

Kaksonen, A.H., Spring, S., Schumann, P., Kroppenstedt, R.M., Puhakka, J.A., 2007. Desulfurispora thermophila gen. nov., sp. nov., a thermophilic, spore-forming sulfate-reducer isolated from a sulfidogenic fluidized-bed reactor. International Journal of Systematic and Evolutionary Microbiology 57, 1089-1094.

Kallmeyer, J., 2011. Chapter 3 - Detection and Quantification of Microbial Cells in Subsurface Sediments, in: Allen I. Laskin, S.S., Geoffrey, M.G. (Eds.), Advances in applied microbiology. Academic Press, pp. 79-103.

Kallmeyer, J., 2017. Contamination Control for Scientific Drilling Operations. Advances in applied microbiology 98, 61-91.

Kallmeyer, J., Ferdelman, T.G., Weber, A., Fossing, H., Jørgensen, B.B., 2004. A cold chromium distillation procedure for radiolabeled sulfide applied to sulfate reduction measurements. Limnology and Oceanography: Methods 2, 171-180.

Kallmeyer, J., Mangelsdorf, K., Cragg, B., Horsfield, B., 2006. Techniques for contamination assessment during drilling for terrestrial subsurface sediments. Geomicrobiology J. 23, 227-239.

Kallmeyer, J., Pockalny, R., Adhikari, R.R., Smith, D.C., D'Hondt, S., 2012. Global distribution of microbial abundance and biomass in subseafloor sediment. Proceedings of the National Academy of Sciences of the United States of America 109, 16213-16216.

Kallmeyer, J., Smith, D.C., Spivack, A.J., D'Hondt, S., 2008. New cell extraction procedure applied to deep subsurface sediments. Limnology and Oceanography: Methods 6, 236-245.

Kappler, A., Bryce, C., 2017. Cryptic biogeochemical cycles: unravelling hidden redox reactions. Environmental Microbiology 19, 842-846.

Kaster, A.-K., Moll, J., Parey, K., Thauer, R.K., 2011. Coupling of ferredoxin and heterodisulfide reduction via electron bifurcation in hydrogenotrophic methanogenic archaea. Proceedings of the National Academy of Sciences of the United States of America 108, 2981-2986.

Katili, J.A., 1971. A review of the geotectonic theories and tectonic maps of Indonesia. Earth-Science Reviews 7, 143-163.

Katsev, S., Crowe, S.A., 2015. Organic carbon burial efficiencies in sediments: The power law of mineralization revisited. Geology 43, 607-610.

Katsev, S., Crowe, S.A., Mucci, A., Sundby, B., Nomosatryo, S., Haffner, G.D., Fowle, D.A., 2010. Mixing and its effects on biogeochemistry in the persistently stratified, deep, tropical Lake Matano, Indonesia. Limnology and Oceanography 55, 763-776.

Keil, R.G., 2011. Terrestrial influences on carbon burial at sea. Proceedings of the National Academy of Sciences of the United States of America 108, 9729-9730.

Kiene, R.P., Oremland, R.S., Catena, A., Miller, L.G., Capone, D.G., 1986. Metabolism of reduced methylated sulfur compounds in anaerobic sediments and by a pure culture of an estuarine methanogen. Applied Environmental Microbiology 52, 1037-1045.

Kip, N., Jansen, S., Leite, M.F., Hollander, M., Afanasyev, M., Kuramae, E.E., Van Veen, J.A., 2017. Methanogens predominate in natural corrosion protective layers on metal sheet piles. Scientific reports 7, 11899.

Klein, C., 2005. Some Precambrian banded iron-formations (BIFs) from around the world: Their age, geologic setting, mineralogy, metamorphism, geochemistry, and origin: The American Mineralogist, v. 90, p. 1473–1499.

Kleindienst, S., Herbst, F.-A., Stagars, M., Von Netzer, F., Von Bergen, M., Seifert, J., Peplies, J., Amann, R., Musat, F., Lueders, T., 2014. Diverse sulfate-reducing bacteria of the Desulfosarcina/Desulfococcus clade are the key alkane degraders at marine seeps. ISME Journal 8, 2029-2044.

Knittel, K., Boetius, A., 2009b. Anaerobic oxidation of methane: progress with an unknown process. Annual review of microbiology 63, 311-334.

Köhler, I., Konhauser, K.O., Papineau, D., Bekker, A., and Kappler, A., 2013. Biological carbon precursor to diagenetic siderite with spherical structures in iron formations: Nature Communications, v. 4, p. 1741.

Konhauser, K., Newman, D.K., and Kappler, A., 2005. The potential significance of microbial Fe(III) reduction during deposition of Precambrian banded iron formations: Geobiology, v. 3, p. 167–177.

Konecky, B., Russell, J., Bijaksana, S., 2016. Glacial aridity in central Indonesia coeval with intensified monsoon circulation. Earth and Planetary Science Letters 437, 15-24.

Konhauser, K.O., 2009. Introduction to geomicrobiology. John Wiley & Sons.

Krause, C., Ozkan, H., Zhu, H., Derksen, R., Fox, R., Brazee, R., 2005. Fluorescent intensity of dye solutions under different pH conditions. Journal of ASTM international 2, 1-7.

Kröninger, L., Berger, S., Welte, C., Deppenmeier, U., 2016. Evidence for the involvement of two heterodisulfide reductases in the energy-conserving system of Methanomassiliicoccus luminyensis. The FEBS journal 283, 472-483.

Laakso, T.A., Schrag, D.P., 2019. A small marine biosphere in the Proterozoic. Geobiology 17, 161-171.

Lafargue, E., Marquis, F., Pillot, D., 1998. Rock-Eval 6 applications in hydrocarbon exploration, production, and soil contamination studies. Revue de l'institut français du pétrole 53.

Langille, M.G., Zaneveld, J., Caporaso, J.G., McDonald, D., Knights, D., Reyes, J.A., Clemente, J.C., Burkepile, D.E., Thurber, R.L.V., Knight, R., 2013. Predictive functional profiling of microbial communities using 16S rRNA marker gene sequences. Nature biotechnology 31, 814.

Leeuw, T., Boss, E.S., Wright, D.L., 2013. In situ measurements of phytoplankton fluorescence using low cost electronics. Sensors 13, 7872-7883.

Legrand, L., Mazerolles, L., and Chaussé, A., 2004. The oxidation of carbonate green rust into ferric phases: solid-state reaction or transformation via solution: Geochimica et Cosmochimica Acta, v. 68, p. 3497–3507.

Lehmusluoto, P., Machbub, B., Terangna, N., Rusmiputro, S., Achmad, F., Boer, L., Brahmana, S., Priadi, B., Setiadji, B., Sayuman, O., 1997. National inventory of the major lakes and reservoirs in Indonesia. Expedition Indodanau Technical Report, Edita Oy.

Lever, M.A., Alperin, M., Engelen, B., Inagaki, F., Nakagawa, S., Steinsbu, B.r.O., Teske, A., 2006. Trends in basalt and sediment core contamination during IODP Expedition 301. Geomicrobiology J. 23, 517-530.

Lever, M.A., Rouxel, O., Alt, J.C., Shimizu, N., Ono, S., Coggon, R.M., Shanks, W.C., Lapham, L., Elvert, M., Prieto-Mollar, X., 2013. Evidence for microbial carbon and sulfur cycling in deeply buried ridge flank basalt. Science 339, 1305-1308.

Lindahl, T., 1993. Instability and decay of the primary structure of DNA. Nature 362, 709-715.

Liu, Y., Balkwill, D.L., Aldrich, H.C., Drake, G.R., Boone, D.R., 1999. Characterization of the anaerobic propionate-degrading syntrophs Smithella propionica gen. nov., sp. nov. and Syntrophobacter wolinii. International Journal of Systematic and Evolutionary Microbiology 49, 545-556.

Louca, S., Parfrey, L.W., Doebeli, M., 2016. Decoupling function and taxonomy in the global ocean microbiome. Science 353, 1272-1277.

Lovley, D.R., 1991. Dissimilatory Fe (III) and Mn (IV) reduction. microbiological reviews 55, 259.

Lovley, D.R., Phillips, E.J., 1986b. Organic matter mineralization with reduction of ferric iron in anaerobic sediments. Applied Environmental Microbiology 51, 683-689.

Ludwig, W., Strunk, O., Westram, R., Richter, L., Meier, H., Buchner, A., Lai, T., Steppi, S., Jobb, G., Förster, W., 2004. ARB: a software environment for sequence data. Nucleic acids research 32, 1363-1371.

Magal, E., Weisbrod, N., Yakirevich, A., Yechieli, Y., 2008. The use of fluorescent dyes as tracers in highly saline groundwater. Journal of Hydrology 358, 124-133.

Manheim, F.T., 1966. A hydraulic squeezer for obtaining interstitial water from consolidated and unconsolidated sediments. USGS Reference Paper 550, 171–174.

Martin, M., 2011. Cutadapt removes adapter sequences from high-throughput sequencing reads. EMBnet. journal 17, pp. 10-12.

Masters, R.A., Madigan, M., 1983. Nitrogen metabolism in the phototrophic bacteria Rhodocyclus purpureus and Rhodospirillum tenue. Journal of bacteriology 155, 222-227.

Matamoros-Veloza, A., Cespedes, O., Johnson, B.R.G., Stawski, T.M., Terranova, U., de Leeuw, N.H., and Benning, L.G., 2018. A highly reactive precursor in the iron sulfide system: Nature Communications, v. 9, p. 1–7.

Matsumoto, R., Iijima, A., 1981. Origin and diagenetic evolution of Ca–Mg–Fe carbonates in some coalfields of Japan. Sedimentology 28, 239-259.

Matthies, C., Springer, N., Ludwig, W., Schink, B., 2000. Pelospora glutarica gen. nov., sp. nov., a glutarate-fermenting, strictly anaerobic, spore-forming bacterium. International Journal of Systematic and Evolutionary Microbiology 50, 645-648.

Meyer, B., Kuever, J., 2007. Molecular analysis of the diversity of sulfate-reducing and sulfur-oxidizing prokaryotes in the environment, using aprA as functional marker gene. Applied Environmental Microbiology 73, 7664-7679.

Meyerdierks, A., Kube, M., Kostadinov, I., Teeling, H., Glöckner, F.O., Reinhardt, R., Amann, R., 2010. Metagenome and mRNA expression analyses of anaerobic methanotrophic archaea of the ANME-1 group. Environmental Microbiology 12, 422-439.

Milsom, J., Thurow, J., Roques, D., 2000. Sulawesi dispersal and the evolution of the Northern Banda Arc. Proceedings Indonesia Petroleum Association, 27th Annual Convention, IPA999-G-023, 1 - 11.

Milucka, J., Ferdelman, T.G., Polerecky, L., Franzke, D., Wegener, G., Schmid, M., Lieberwirth, I., Wagner, M., Widdel, F., Kuypers, M.M., 2012. Zero-valent sulphur is a key intermediate in marine methane oxidation. Nature 491, 541.

Morlock, M.A., Vogel, H., Nigg, V., Ordoñez, L., Hasberg, A.K.M., Melles, M., Russell, J.M., and Bijaksana, S., and the TDP Science Team, 2019. Climatic and tectonic controls on source-to-sink processes in the tropical, ultramafic catchment of Lake Towuti, Indonesia: Journal of Paleolimnology, v. 61, p. 279–295.

Morono, Y., Terada, T., Masui, N., Inagaki, F., 2009. Discriminative detection and enumeration of microbial life in marine subsurface sediments. ISME Journal 3, 503-511.

Morris, B.E., Henneberger, R., Huber, H., Moissl-Eichinger, C., 2013. Microbial syntrophy: interaction for the common good. FEMS Microbiology Reviews 37, 384-406.

Mortimer, R.J.G., Coleman, M.L., and Rae, J.E., 1997. Effect of bacteria on the elemental composition of early diagenetic siderite: Implications for palaeoenvironmental interpretations: Sedimentology, v. 44, p. 759–765.

Mozley, P.S., 1989. Complex compositional zonation in concretionary siderite: Implications for geochemical studies: Journal of Sedimentary Petrology, v. 59, p. 815–818.

Müller, A.L., Kjeldsen, K.U., Rattei, T., Pester, M., Loy, A., 2015. Phylogenetic and environmental diversity of DsrAB-type dissimilatory (bi) sulfite reductases. ISME Journal 9, 1152.

Nagarajan, H., Embree, M., Rotaru, A.-E., Shrestha, P.M., Feist, A.M., Palsson, B.Ø., Lovley, D.R., Zengler, K., 2013. Characterization and modelling of interspecies electron transfer mechanisms and microbial community dynamics of a syntrophic association. Nature communications 4, ncomms3809.

Nam, Y.-D., Sung, Y., Chang, H.-W., Roh, S.W., Kim, K.-H., Rhee, S.-K., Kim, J.-C., Kim, J.-Y., Yoon, J.-H., Bae, J.-W., 2008. Characterization of the depth-related changes in the microbial communities in Lake Hovsgol sediment by 16S rRNA gene-based approaches. The Journal of Microbiology 46, 125-136.

Ndiaye, M., Davaud, E., Ariztegui, D., Fall, M., 2012. A semi automated method for laminated sediments analysis. International Journal of Geosciences 3, 206.

Nelson, D.M., Ohene-Adjei, S., Hu, F.S., Cann, I.K., Mackie, R.I., 2007. Bacterial diversity and distribution in the Holocene sediments of a northern temperate lake. Microbial ecology 54, 252-263.

Nevin, K.P., Lovley, D.R., 2002. Mechanisms for accessing insoluble Fe (III) oxide during dissimilatory Fe (III) reduction by Geothrix fermentans. Applied Environmental Microbiology 68, 2294-2299.

Nobu, M.K., Narihiro, T., Kuroda, K., Mei, R., Liu, W.-T., 2016. Chasing the elusive Euryarchaeota class WSA2: genomes reveal a uniquely fastidious methyl-reducing methanogen. ISME Journal.

Norði, K.A., Thamdrup, B., Schubert, C.J., 2013. Anaerobic oxidation of methane in an iron-rich Danish freshwater lake sediment. Limnology and Oceanography 58, 546-554.

Nunoura, T., Oida, H., Nakaseama, M., Kosaka, A., Ohkubo, S.B., Kikuchi, T., Kazama, H., Hosoi-Tanabe, S., Nakamura, K.-i., Kinoshita, M., 2010. Archaeal diversity and distribution along thermal and geochemical gradients in hydrothermal sediments at the Yonaguni Knoll IV hydrothermal field in the Southern Okinawa Trough. Applied Environmental Microbiology 76, 1198-1211.

Ohmoto, H., Watanabe, Y., and Kumazawa, K., 2004. Evidence from massive siderite beds for a CO2-rich atmosphere before approximately 1.8 billion years ago: Nature, v. 429, p. 395–399.

Oren, A., 2014. The family methanomicrobiaceae, The Prokaryotes. Springer, pp. 231-246.

Orsi, W.D., Coolen, M.J., Wuchter, C., He, L., More, K.D., Irigoien, X., Chust, G., Johnson, C., Hemingway, J.D., Lee, M., 2017. Climate oscillations reflected within the microbiome of Arabian Sea sediments. Scientific Reports 7, 6040.

Orsi, W.D., Edgcomb, V.P., Christman, G.D., Biddle, J.F., 2013. Gene expression in the deep biosphere. Nature 499, 205.

Ozaki, K., Tajika, E., Hong, P.K., Nakagawa, Y., Reinhard, C.T., 2018. Effects of primitive photosynthesis on Earth's early climate system. Nature Geoscience 11, 55.

Parada, A.E., Needham, D.M., Fuhrman, J.A., 2016. Every base matters: assessing small subunit rRNA primers for marine microbiomes with mock communities, time series and global field samples. Environmental Microbiology 18, 1403-1414.

Parkes, R.J., Cragg, B.A., Wellsbury, P., 2000. Recent studies on bacterial populations and processes in subseafloor sediments: a review. Hydrogeology J. 8, 11-28.

Parkes, R.J., Webster, G., Cragg, B.A., Weightman, A.J., Newberry, C.J., Ferdelman, T.G., Kallmeyer, J., Jorgensen, B.B., Aiello, I.W., Fry, J.C., 2005. Deep sub-seafloor prokaryotes stimulated at interfaces over geological time. Nature 436, 390-394.

Parkhurst, D.L., and Appelo, C.A.J., 2013. Description of input and examples for PHREEQC version 3 - A computer program for speciation, batch-reaction, one-dimensional transport, and inverse geochemical calculations: U.S. Geological Survey Techniques and Methods, Book 6, Chapter A43, p. 497.

Pavlov, A.A., Brown, L.L., Kasting, J.F., 2001. UV shielding of NH3 and O2 by organic hazes in the Archean atmosphere. Journal of Geophysical Research: Planets 106(E10), 23267-23287.

Pedersen, K., Hallbeck, L., Arlinger, J., Erlandson, A.-C., Jahromi, N., 1997. Investigation of the potential for microbial contamination of deep granitic aquifers during drilling using 16S rRNA gene sequencing and culturing methods. Journal of Microbiological Methods 30, 179-192.

Pellizzari, L., Neumann, D., Alawi, M., Voigt, D., Norden, B., Würdemann, H., 2013. The use of tracers to assess drill-mud penetration depth into sandstone cores

during deep drilling: method development and application. Environmental Earth Sciences 70, 3727-3738.

Phelps, T.J., Fliermans, C.B., Garland, T.R., Pfiffner, S.M., White, D.C., 1989. Methods for recovery of deep terrestrial subsurface sediments for microbiological studies. Journal of Microbiological Methods 9, 267-279.

Pierrehumbert, R.T., 1999. Subtropical water vapor as a mediator of rapid global climate change. Geophysical Monograph Series 112, 339-361.

Pietramellara, G., Ascher, J., Borgogni, F., Ceccherini, M., Guerri, G., Nannipieri, P., 2009. Extracellular DNA in soil and sediment: fate and ecological relevance. Biology and Fertility of Soils 45, 219-235.

Pinchuk, G.E., Ammons, C., Culley, D.E., Li, S.-M.W., McLean, J.S., Romine, M.F., Nealson, K.H., Fredrickson, J.K., Beliaev, A.S., 2008. Utilization of DNA as a sole source of phosphorus, carbon, and energy by Shewanella spp.: ecological and physiological implications for dissimilatory metal reduction. Applied Environmental Microbiology 74, 1198-1208.

Pjevac, P., Kamyshny, A., Dyksma, S., Mußmann, M., 2014. Microbial consumption of zero-valence sulfur in marine benthic habitats. Environmental Microbiology 16, 3416-3430.

Plugge, C.M., Zhang, W., Scholten, J., Stams, A.J., 2011. Metabolic flexibility of sulfate-reducing bacteria. Frontiers in Microbiology 2, 81.

Posth, N.R., Canfield, D.E., and Kappler, A., 2014. Biogenic Fe (III) minerals: From formation to diagenesis and preservation in the rock record: Earth-Science Reviews, v. 135, p. 103–121.

Poulton, S.W., Canfield, D.E., 2005. Development of a Sequential Extraction Procedure for Iron: Implications for Iron Partitioning in Continentally Derived Particulates. Chemical Geology 214, 209–221.

Poulton, S.W., Canfield, D.E., 2011. Ferruginous conditions: a dominant feature of the ocean through Earth's history. Elements 7, 107-112.

Precht, E., Huettel, M., 2004. Rapid wave-driven advective pore water exchange in a permeab le coastal sediment. Journal of Sea Research 51, 93-107.

Pruesse, E., Peplies, J., Glöckner, F.O., 2012. SINA: accurate high-throughput multiple sequence alignment of ribosomal RNA genes. Bioinformatics 28, 1823-1829.

Pruesse, E., Quast, C., Knittel, K., Fuchs, B.M., Ludwig, W., Peplies, J., Glöckner, F.O., 2007. SILVA: a comprehensive online resource for quality checked and

aligned ribosomal RNA sequence data compatible with ARB. Nucleic acids research 35, 7188-7196.

Quast, C., Pruesse, E., Yilmaz, P., Gerken, J., Schweer, T., Yarza, P., Peplies, J., Glöckner, F.O., 2012. The SILVA ribosomal RNA gene database project: improved data processing and web-based tools. Nucleic acids research 41, D590-D596.

Raiswell, R., Reinhard, C.T., Derkowski, A., Owens, J., Bottrell, S.H., Anbar, A.D., and Lyons, T.W., 2011. Formation of syngenetic and early diagenetic iron minerals in the late Archaean Mt. McRae Shale, Hamersley Basin, Australia: New insights on the patterns, controls and paleoenvironmental implications of authigenic mineral formation: Geochimica et Cosmochimica Acta, v. 75, p. 1072–1087.

Ramamoorthy, S., Sass, H., Langner, H., Schumann, P., Kroppenstedt, R., Spring, S., Overmann, J., Rosenzweig, R., 2006. Desulfosporosinus lacus sp. nov., a sulfate-reducing bacterium isolated from pristine freshwater lake sediments. International Journal of Systematic and Evolutionary Microbiology 56, 2729-2736.

Renshaw, M.A., Olds, B.P., Jerde, C.L., McVeigh, M.M., Lodge, D.M., 2015. The room temperature preservation of filtered environmental DNA samples and assimilation into a phenol–chloroform–isoamyl alcohol DNA extraction. Molecular ecology resources 15, 168-176.

Roden, E.E., 2003. Diversion of electron flow from methanogenesis to crystalline Fe (III) oxide reduction in carbon-limited cultures of wetland sediment microorganisms. Applied Environmental Microbiology 69, 5701-5706.

Roden, E.E., Wetzel, R.G., 2003. Competition between Fe (III)-reducing and methanogenic bacteria for acetate in iron-rich freshwater sediments. Microbial Ecology 45, 252-258.

Roussel, E.G., Bonavita, M.-A.C., Querellou, J., Cragg, B.A., Webster, G., Prieur, D., Parkes, R.J., 2008. Extending the sub-sea-floor biosphere. Science 320, 1046-1046.

Ruby, C., Abdelmoula, M., Naille, S., Renard, A., Kahre, V., Ona-Nguema, G., Morin, G., and Génin, J.-M.R., 2010. Oxidation modes and thermodynamics of FeII-III oxyhydroxycarbonate green rust: Dissolution-precipitation versus in-situ deprotonation: Geochimica et Cosmochimica Acta, v. 74, p. 953–966.

Russell, B.F., Phelps, T.J., Griffin, W.T., Sargent, K.A., 1992. Procedures for Sampling Deep Subsurface Microbial Communities in Unconsolidated Sediments. Ground Water Monitoring & Remediation 12, 96-104.

Russell, J., Bijaksana, S., 2012. The Towuti drilling project: paleoenvironments, biological evolution, and geomicrobiology of a tropical Pacific lake. Scientific Drilling 14, 68-71.

Russell, J.M., Bijaksana, S., Vogel, H., Melles, M., Kallmeyer, J., Ariztegui, D., Crowe, S., Fajar, S., Hafidz, A., Haffner, D., Hasberg, A., Ivory, S., Kelly, C., King, J., Kirana, K., Morlock, M., Noren, A., O'Grady, R., Ordonez, L., Stevenson, J., von Rintelen, T., Vuillemin, A., Watkinson, I., Wattrus, N., Wicaksono, S., Wonik, T., Bauer, K., Deino, A., Friese, A., Henny, C., Imran, Marwoto, R., Ngkoimani, L.O., Nomosatryo, S., Safiuddin, L.O., Simister, R., Tamuntuan, G., 2016. The Towuti Drilling Project: paleoenvironments, biological evolution, and geomicrobiology of a tropical Pacific lake. Scientific Drilling 21, 29-40.

Russell, J.M., Vogel, H., Konecky, B.L., Bijaksana, S., Huang, Y.S., Melles, M., Wattrus, N., Costa, K., King, J.W., 2014. Glacial forcing of central Indonesian hydroclimate since 60,000 y BP. Proceedings of the National Academy of Sciences of the United States of America 111, 5100-5105.

Schibler, J., Moore, D., De Borba, B., 2007. Setting Meaningful Detection and Quantitation Limits for Chromatography Methods. Sunnyvale, CA: PITTCON.

Schippers, A., Neretin, L.N., Kallmeyer, J., Ferdelman, T.G., Cragg, B.A., John Parkes, R., Jorgensen, B.B., 2005. Prokaryotic cells of the deep sub-seafloor biosphere identified as living bacteria. Nature 433, 861-864.

Schulz, H.D., 2000. Quantification of Early Diagenesis: Dissolved Constitutents in Marine Pore Water, in: Schulz, H.D., Zabel, M. (Eds.), Marine Geochemistry. Springer, Berlin.

Sekiguchi, Y., Kamagata, Y., Nakamura, K., Ohashi, A., Harada, H., 2000. Syntrophothermus lipocalidus gen. nov., sp. nov., a novel thermophilic, syntrophic, fatty-acid-oxidizing anaerobe which utilizes isobutyrate. International Journal of Systematic and Evolutionary Microbiology 50, 771-779.

Sel, O., Radha, A.V., Dideriksen, K., and Navrotsky, A., 2012. Amorphous iron (II) carbonate: Crystallization energetics and comparison to other carbonate minerals related to CO_2 sequestration: Geochimica et Cosmochimica Acta, v. 87, p. 61–68.

Senum, G., Dietz, R., 1991. Perfluorocarbon tracer tagging of drilling muds for the assessment of sample contamination. Brookhaven National Lab., Upton, NY (USA).

Sieber, J.R., McInerney, M.J., Gunsalus, R.P., 2012. Genomic insights into syntrophy: the paradigm for anaerobic metabolic cooperation. Annual review of microbiology 66, 429-452.

Sivan, O., Adler, M., Pearson, A., Gelman, F., Bar-Or, I., John, S.G., Eckert, W., 2011. Geochemical evidence for iron-mediated anaerobic oxidation of methane. Limnology and Oceanography 56, 1536-1544.

Slobodkina, G.B., Reysenbach, A.-L., Panteleeva, A., Kostrikina, N., Wagner, I., Bonch-Osmolovskaya, E., Slobodkin, A.I., 2012. Deferrisoma camini gen. nov., sp. nov., a moderately thermophilic, dissimilatory iron (III)-reducing bacterium from a deep-sea hydrothermal vent that forms a distinct phylogenetic branch in the Deltaproteobacteria. International Journal of Systematic and Evolutionary Microbiology 62, 2463-2468.

Smart, P., Laidlaw, I., 1977. An evaluation of some fluorescent dyes for water tracing. Water Resources Research 13, 15-33.

Smith, D. C., Simon, M., Alldredge, A.L., Azam, F., 1992. Intense hydrolytic enzyme activity on marine aggregates in aquatic ecosystems. Aquatic microbial ecology 18, 119-130.

Smith, D.C., Spivack, A.J., Fisk, M.R., Haveman, S.A., Staudigel, H., 2000a. Methods for quantifying potential microbial contamination during deep ocean coring. Ocean Drilling Program Technical Note.

Smith, D.C., Spivack, A.J., Fisk, M.R., Haveman, S.A., Staudigel, H., 2000b. Tracer-based estimates of drilling-induced microbial contamination of deep sea crust. Geomicrobiology J. 17, 207-219.

Stamatakis, A., 2006. RAxML-VI-HPC: maximum likelihood-based phylogenetic analyses with thousands of taxa and mixed models. Bioinformatics 22, 2688-2690.

Stewart, F.J., 2011. Dissimilatory sulfur cycling in oxygen minimum zones: an emerging metagenomics perspective. Portland Press Limited.

Tamaura, Y., Yoshida, T., and Katsura, T., 1984. The synthesis of green rust II (Fe^{III}_1-Fe^{II}_2) and its spontaneous transformation into Fe3O4: Bulletin of the Society of Japan, v. 57, p. 2411–2416.

Tamuntuan, G., Bijaksana, S., King, J., Russell, J., Fauzi, U., Maryunani, K., Aufa, N., 2015. Variation of magnetic properties in sediments from Lake Towuti, Indonesia, and its paleoclimatic significance. Palaeogeography and Palaeoclimatology 420, 163-172.

Thamdrup, B., Finster, K., Hansen, J.W., Bak, F., 1993. Bacterial disproportionation of elemental sulfur coupled to chemical reduction of iron or manganese. Applied Environmental Microbiology 59, 101-108.

Thamdrup, B., Fossing, H., Jørgensen, B.B., 1994. Manganese, iron and sulfur cycling in a coastal marine sediment, Aarhus Bay, Denmark. Geochimica et Cosmochimica Acta 58, 5115-5129.

Thamdrup, B., Rosselló-Mora, R., Amann, R., 2000. Microbial manganese and sulfate reduction in Black Sea shelf sediments. Applied Environmental Microbiology 66, 2888-2897.

Thauer, R.K., Kaster, A.-K., Seedorf, H., Buckel, W., Hedderich, R., 2008. Methanogenic archaea: ecologically relevant differences in energy conservation. Nature Reviews Microbiology 6, 579-591.

Tierney, J.E., Russell, J.M., 2009. Distributions of branched GDGTs in a tropical lake system: implications for lacustrine application of the MBT/CBT paleoproxy. Organic Geochemistry 40, 1032-1036.

Torti, A., Lever, M.A., Jørgensen, B.B., 2015. Origin, dynamics, and implications of extracellular DNA pools in marine sediments. Marine genomics 24, 185-196.

Ueno, Y., Yamada, K., Yoshida, N., Maruyama, S., Isozaki, Y., 2006. Evidence from fluid inclusions for microbial methanogenesis in the early Archaean era. Nature 440, 516-519.

Urban, N., Brezonik, P., Baker, L., Sherman, L., Sulfate reduction and diffusion in sediments of Little Rock Lake, Wisconsi. Limnology and Oceanography 39, 797-815.

Vaillant, J.J., Haffner, G.D., Cristescu, M.E., 2011. The ancient lakes of Indonesia: towards integrated research on speciation. Integrative and Comparative Biology 51, 634-643.

Vargas, M., Kashefi, K., Blunt-Harris, E.L., Lovley, D.R., 1998. Microbiological evidence for Fe(III) reduction on early Earth. Nature 395, 65-67.

Viollier, E., Inglett, P.W., Hunter, K., Roychoudhury, A.N., Van Cappellen, P., 2000. The ferrozine method revisited: Fe(II)/Fe(III) determination in natural waters. Applied Geochemistry 15, 785-790.

Vogel, H., Russell, J.M., Cahyarini, S.Y., Bijaksana, S., Wattrus, N., Rethemeyer, J., Melles, M., 2015. Depositional modes and lake-level variability at Lake Towuti, Indonesia, during the past~ 29 kyr BP. Journal of paleolimnology 54, 359-377.

Vuillemin, A., Ariztegui, D., 2013. Geomicrobiological investigations in subsaline maar lake sediments over the last 1500 years. Quaternary Science Reviews 71, 119-130.

Vuillemin, A., Ariztegui, D., Lücke, A., Mayr, C., 2014. Paleoenvironmental conditions define current sustainability of microbial populations in Laguna Potrok Aike sediments, Argentina. Aquatic Sciences 76, 101-114.

Vuillemin, A., Friese, A., Alawi, M., Henny, C., Nomosatryo, S., Wagner, D., Crowe, S.A., Kallmeyer, J., 2016b. Geomicrobiological features of ferruginous sediments from Lake Towuti, Indonesia. Frontiers in Microbiology 7.

Vuillemin, A., Horn, F., Alawi, M., Henny, C., Wagner, D., Crowe, S.A., Kallmeyer, J., 2017. Preservation and Significance of Extracellular DNA in Ferruginous Sediments from Lake Towuti, Indonesia. Frontiers in Microbiology 8, 1440.

Vuillemin, A., Ndiaye, M., Martini, R., Davaud, E., 2011. Cement stratigraphy: image probes of cathodoluminescent facies. Swiss Journal of Geosciences 104, 55-66.

Wang, G., Spivack, A.J., Rutherford, S., Manor, U., D'Hondt, S., 2008. Quantification of co-occurring reaction rates in deep subseafloor sediments. Geochimica et Cosmochimica Acta 72, 3479-3488.

Webster, G., Blazejak, A., Cragg, B., Schippers, A., Sass, H., Rinna, J., Tang, X., Mathes, F., Ferdelman, T., Fry, J., Weightman, A., Parkes, R., 2009. Subsurface microbiology and biogeochemistry of a deep, cold-water carbonate mound. - Environmental Microbiology11(1), 239-57.

Weiss, M., Abele, U., Weckesser, J., Welte, W.u., Schiltz, E., Schulz, G., 1991. Molecular architecture and electrostatic properties of a bacterial porin. Science 254, 1627-1630.

Whiticar, M.J., 1999. Carbon and hydrogen isotope systematics of bacterial formation and oxidation of methane. Chemical Geology 161, 291-314.

Wirth, R., 2009. Focused Ion Beam (FIB) combined with SEM and TEM: Advanced analytical tools for studies of chemical composition, microstructure and crystal

structure in geomaterials on a nanometre scale: Chemical Geology, v. 261, p. 217-229.

Yanagawa, K., Nunoura, T., McAllister, S., Hirai, M., Breuker, A., Brandt, L., House, C., Moyer, C.L., Birrien, J.-L., Aoike, K., Sunamura, M., Urabe, T., Mottl, M., Takai, K., 2013. The first microbiological contamination assessment by deep-sea drilling and coring by the D/V Chikyu at the Iheya North hydrothermal field in the Mid-Okinawa Trough (IODP Expedition 331). Frontiers in Microbiology 4.

Yao, M., Elling, F.J., Jones, C., Nomosatryo, S., Long, C.P., Crowe, S.A., Antoniewicz, M.R., Hinrichs, K.U., Maresca, J.A., 2015. Heterotrophic bacteria from an extremely phosphate-poor lake have conditionally reduced phosphorus demand and utilize diverse sources of phosphorus. Environmental Microbiology

Zavarzina, D.G., Sokolova, T.G., Tourova, T.P., Chernyh, N.A., Kostrikina, N.A., Bonch-Osmolovskaya, E.A., 2007. Thermincola ferriacetica sp. nov., a new anaerobic, thermophilic, facultatively chemolithoautotrophic bacterium capable of dissimilatory Fe (III) reduction. Extremophiles 11, 1-7.

Zegeye, A., Bonneville, S., Benning, L.G., Sturm, A., Fowle, D.A., Jones, C., Canfield, D.E., Ruby, C., MacLean, L.C., Nomosatryo, S., Crowe, S.A., Poulton, S.W., 2012. Green rust formation controls nutrient availability in a ferruginous water column. Geology 40, 599-602.

Zeng, J., Yang, L., Li, J., Liang, Y., Xiao, L., Jiang, L., Zhao, D., 2009. Vertical distribution of bacterial community structure in the sediments of two eutrophic lakes revealed by denaturing gradient gel electrophoresis (DGGE) and multivariate analysis techniques. World Journal of Microbiology and Biotechnology 25, 225-233.

Zhang, J., Kobert, K., Flouri, T., Stamatakis, A., 2013. PEAR: a fast and accurate Illumina Paired-End reAd mergeR. Bioinformatics 30, 614-620.

Ziebis, W., Forster, S., Huettel, M., Jorgensen, B.B., 1996. Complex burrows of the mud shrimp Callianassa truncata and their geochemical impact in the sea bed. Nature 382, 619-622.

Zopfi, J., Ferdelman, T.G., Fossing, H., 2004. Distribution and fate of sulfur intermediates—sulfite, tetrathionate, thiosulfate, and elemental sulfur—in marine sediments, in: Amend, J.P., Edwards, K.J., Lyons, T.W. (Eds.), Sulfur Biogeochemistry - Past and Present. Geological Society of America.

9 Appendix

Additional manuscript I (Published in Scientific Drilling, 2016, 21, 29-40, doi:10.5194/sd-21-29-2016).

The Towuti Drilling Project: Paleoenvironments, Biological Evolution, and Geomicrobiology of a Tropical Pacific Lake

James M. Russell[1], Satria Bijaksana[2], Hendrik Vogel[3], Martin Melles[4], Jens Kallmeyer[5], Daniel Ariztegui[6], Sean Crowe[7], Silvia Fajar[2], Abdul Hafidz[2], Doug Haffner[8], Ascelina Hasberg[4], Sarah Ivory[1], Christopher Kelly[1], John King[9], Kartika Kirana[2], Marina Morlock[3], Anders Noren[10], Ryan O'Grady[10], Luis Ordonez[6], Janelle Stevenson[11], Thomas von Rintelen[12], Aurele Vuillemin[5], Ian Watkinson[13], Nigel Wattrus[14], Satrio Wicaksono[1], Thomas Wonik[15], Kohen Bauer[8], Alan Deino[16], André Friese[5], Cynthia Henny[17], Imran[18], Ristiyanti Marwoto[17], La Ode Ngkoimani[19], Sulung Nomosatryo[5], La Ode Safiuddin[19], Rachel Simister[7], Gerald Tamuntuan[20]

[1] Department of Earth, Environmental, and Planetary Sciences, Brown University, 324 Brook St., Providence, RI, 02912, USA
[2] Faculty of Mining and Petroleum Engineering, Institut Teknologi Bandung, Jalan Ganesa 10, Bandung, 50132, Indonesia
[3] Institut of Geological Science & Oeschger Center for Climate Change Research, University of Bern, Baltzerstrasse 1+3, 3012, Bern, Switzerland
[4] Institute for Geology and Mineralogy, University of Cologne, Zülpicher Str. 49a/b, 50674, Cologne, Germany
[5] Helmholtz Centre Potsdam, GFZ German Research Center for Geosciences, Telegrafenberg, Building C, 14473, Potsdam, Germany
[6] Department of Earth Sciences, University of Geneva, rue des Maraichers 13, 1205 Geneva, Switzerland
[7] Department of Microbiology and Immunology, University of British Columbia, Vancouver, BC, Canada
[8] Great Lakes Institute for Environmental Research, University of Windsor, Windsor, Ontario, N9B 3P4, Canada
[9] Graduate School of Oceanography, University of Rhode Island, Narragansett, RI, 02882, USA
[10] LacCore, Dept. of Earth Science, University of Minnesota, Minneapolis, MN, 55455, USA
[11] School of Culture, History and Language, Australia National University, Acton, ACT 2601, Australia
[12] Museum für Naturkunde, Leibniz Institute for Evolution and Biodiversity Science, Invalidenstr. 43, 10115 Berlin, Germany
[13] Dept. of Earth Sciences, Royal Holloway University of London, Egham, Surrey TW20 0EX, United Kingdom

[14] Large Lakes Observatory, University of Minnesota Duluth, Duluth, MN, 55812, USA
[15] Liebniz Institute for Applied Geophysics, Stilleweg 2, 30655 Hannover, Germany
[16] Berkeley Geochronology Center, Berkeley, CA, 94709, USA
[17] Research Center for Limnology, Indonesian Insitute of Sciences (LIPI), Jl. Raya Bogor m 46, Cibinong, West Java, Indonesia
[18] Geological Department, Universitas Hasanuddin, Kampus UNHAS Tamalanrea, Makassar, 90245, Indonesia
[19] Faculty of Earth Sciences and Technology, Haluoleo University, Kampus Baru Unhalu Anduoonoho, Kendari, 93232, Indonesia
[20] Department of Physics, Faculty of Mathematics and Natural Sciences, Sam Ratulangi University, Jl. Kampus Unsrat Manado 95114, Indonesia

Abstract:

The Towuti Drilling Project (TDP) is an international research program whose goal is to understand long-term environmental and climatic change in the tropical western Pacific, the impacts of geological and environmental changes on the biological evolution of aquatic taxa, and the geomicrobiology and biogeochemistry of metal-rich, ultramafic-hosted lake sediments through scientific drilling of Lake Towuti, South Sulawesi, Indonesia. Lake Towuti is a large tectonic lake at the downstream end of the Malili lake system, a chain of five highly biodiverse lakes that are among the oldest lakes in southeast Asia. In 2015 we carried out a scientific drilling program on Lake Towuti using the Deep Lake Drilling System of the International Continental Scientific Drilling Program (ICDP). We recovered a total of ~1018 m of core from 11 drilling sites with water depths ranging from 156 to 200 m. Recovery averaged 91.7%, and the maximum drilling depth was 175 m below the lake floor, penetrating the entire sedimentary infill of the basin. Initial data from core and borehole logging indicate that these cores record the evolution of a highly dynamic tectonic and limnological system, with clear indications of orbital-scale climate variability during the mid- to late Pleistocene.

Introduction

The Towuti Drilling Project (TDP) is an international research program whose objective is to understand long-term environmental and climatic change in the tropical western Pacific, the impacts of geological and environmental changes on the biological evolution of aquatic taxa, and the geomicrobiology and biogeochemistry of metal-rich, ultramafic-hosted lake sediment. To accomplish this goal, TDP recovered over 1,000

meters of sediment core from the floor of Lake Towuti, the largest tectonic lake in Southeast Asia. Analysis of these cores is just beginning, but will provide a new long, high-resolution record of tropical western Pacific paleohydrology during the Pleistocene, information on the age and history of the lake and the limnological conditions that gave rise to Towuti's endemic fauna and flora, and new insight into the microbial processes operating at depth in Towuti's sediments and their effects on sediment mineralogy and biogeochemistry.

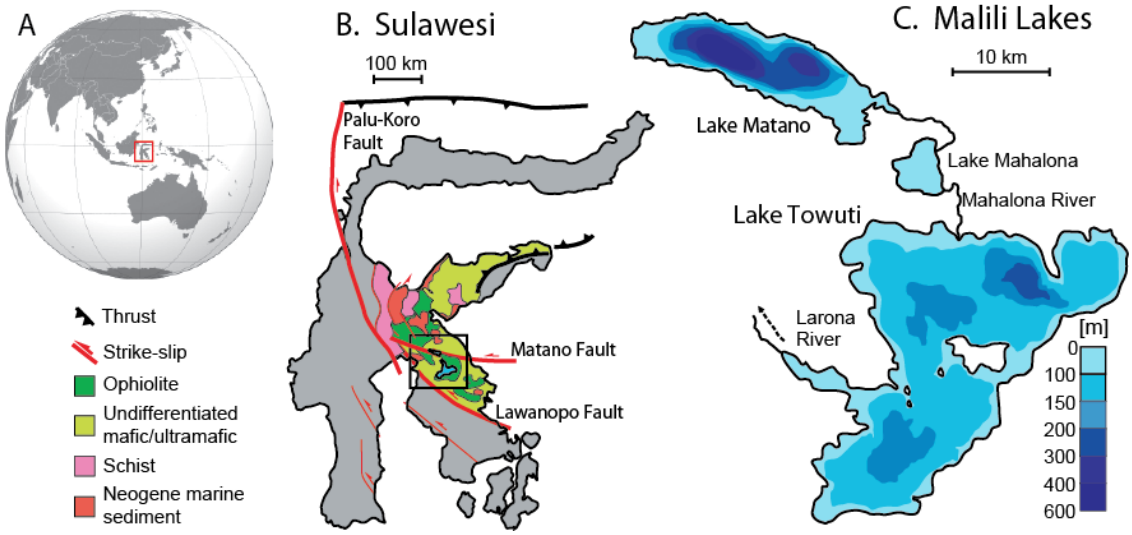

Figure 9.1: *Overview map of the study area showing A) the location of Sulawesi in the Indo-Pacific region, B) the regional geology of Sulawesi (modified after Kadarusman et al., 2004), and C) the configuration of the Malili Lake system.*

Lake Towuti is a large tectonic lake at the downstream end of the Malili lake system (Fig. 9.1), a set of five ancient, tectonic lakes that formed over the past ~1.5 million years on the island of Sulawesi, Indonesia (Haffner et al., 2001; Lehmusluoto et al., 1995; Russell et al., 2012). These are the oldest lakes in Indonesia and are thought to contain the longest continuous terrestrial records of climate in the Indo-Pacific Warm Pool (IPWP), a vast pool of warm surface waters in the western tropical Pacific. The IPWP exerts enormous influence on global climate through its interactions with the El Niño-Southern Oscillation (ENSO), the Austral-Asian monsoons, and the Intertropical Convergence Zone (ITCZ) (Chiang, 2009; Clement et al., 2001; Seager and Battisti, 2007) and through its influence on the concentration of atmospheric water vapor – the Earth's most important greenhouse gas (Pierrehumbert, 1999, 2000). Our ability to make accurate predictions about future climate, and in particular future precipitation, thus rests on our understanding of the tropical Pacific climate under different climate

boundary conditions than today. Global climate models exhibit significant inter-model differences in their simulations of recent and future precipitation change over the IPWP (Kumar et al., 2013; Meehl et al., 2007), as do simulations of IPWP precipitation under glacial boundary conditions (DiNezio et al., 2011; DiNezio and Tierney, 2013), motivating scientific drilling at Lake Towuti.

In recent years the global lakes drilling program under the auspices of the International Continental Scientific Drilling Program (ICDP) has made substantial contributions to understanding Plio-Pleistocene climate variability, including multiple paleoclimate records from the northern and southern tropics. These records, together with many long speleothem datasets, have highlighted the importance of 21,000-year cycles in subtropical rainfall, indicating strong forcing of the strength of the monsoons by orbital precession (e.g. Fritz et al., 2007; Hodell et al., 2007; Scholz et al., 2007; Wang et al., 2008). Despite these advances, we lack long records of terrestrial paleoclimate from equatorial regions and particularly the Indo-Pacific. Previous sedimentary records from Lake Towuti span the last ~60 kyr BP, and contain an intriguing record of past climate that differs markedly from that of the subtropics (Russell et al., 2014). In particular, we observed grassland expansion, lowered lake levels, and strong drying during the last glacial maximum (LGM) relative to both Marine Isotope Stage 3 (~30-60 kyr BP) and the Holocene (Costa et al., 2015; Konecky et al., 2016; Russell et al., 2014; Vogel et al., 2015). The strong glacial-interglacial signal at Lake Towuti challenge the hypothesis that tropical hydroclimate is predominantly controlled by precessional orbital forcing, with little influence of glacial-interglacial changes in climate boundary conditions (Carolin et al., 2013; Meckler et al., 2012). A critical goal of TDP is, therefore, to obtain a continuous sedimentary record to document orbital-scale patterns of climate change spanning as many glacial-interglacial cycles as possible to test and differentiate the forcings that govern Indo-Pacific rainfall variations.

Lake Towuti is not simply a repository of information on past climate. The lake is situated within the East Sulawesi Ophiolite (Fig. 9.1, Kadarusman et al., 2004; Monnier et al., 1995), the third largest ophiolite in the world, which releases iron, chromium, and other metals that catalyze biogeochemical activity by a unique and diverse microbial community in the lake and its sediments (Crowe et al., 2008b). Lake Towuti's sediments are extremely Fe-rich and thus stand out as an end-member

microbial habitat. The prevalence of Fe-rich sedimentary rock units in the Precambrian suggests that ferruginous conditions were a prominent feature of the deep ocean throughout the Earth's history (Poulton and Canfield, 2011), and with mounting evidence for Fe-rich Martian soils and lake sediments dominated by ultramafic weathering products (e.g. Ehlmann et al., 2008), the study of an active biosphere in environments such as Towuti is timely and critical. Moreover, Towuti's pelagic microbial ecology, biogeochemistry, and sediment mineralogy are tightly linked to climate variations through varying lake mixing regimes, soil erosion, and weathering (Costa et al., 2015; Tamuntuan et al., 2015). These processes are directly or indirectly responsible for the production and deposition of many paleoclimate proxies, and postdepositional alteration of those proxies is often linked to the activity of sedimentary microorganisms. In light of these issues, a critical component of the TDP is to investigate the microbial community at depth and its effects on iron mineralogy, carbon, and metal cycling using a variety of state-of-the-art geochemical, molecular genetic, and isotopic tools.

Towuti is surrounded by one of the most diverse tropical rainforests on Earth, and harbors endemic species flocks of fish, snails, shrimp, crabs, and other organisms. Identifying the role of past environmental change in governing the evolution and biogeographical range of these organisms will be crucial for identifying conservation priorities and strategies to cope with anthropogenic climate change and land use. In terms of its flora, Sulawesi lies within one of the world's most biologically complex and diverse regions and is home to fundamentally important faunal and floristic boundaries such as the famed Wallace Line (which separates fauna of Australian and Asian origin). The regional phytogeography is controlled by these diverse geological origins and by subsequent modification by climate variations, particularly the glacial-interglacial cycles, which have influenced the connectivity between adjacent islands as well as drought tolerance and resilience of the regional flora (Cannon et al., 2009, van Welzen et al., 2011). Understanding the past dynamics of these forest communities therefore is critical for our understanding of their response to future change. Faunally, the Malili Lakes offer by far the most outstanding example of lacustrine biological evolution in Southeast Asia, with parallel adaptive radiations of gastropods (Rintelen et al., 2004), crabs (Schubart et al., 2008), shrimps (Rintelen et al., 2010), and fishes (Herder et al., 2006). Genetic and morphological data indicate multiple colonizations of the lakes in

several of these groups; a high level of endemism within each lake, suggesting allopatric speciation despite the presence of riverine connections among the lakes; and intralacustrine diversification through shifting trophic structure suggesting ecological speciation (Rintelen et al., 2012). These faunal data thus have strong links to the climatic, limnological, and geological evolution of Lake Towuti. Drilling in Lake Towuti will document the environmental and climatic context that shaped the evolution of these unique lacustrine and terrestrial ecosystems, and their resilience to long-term environmental change.

These outstanding characteristics motivated the TDP, under the auspices of the ICDP. Through continuous coring of the entire sedimentary sequence of Lake Towuti, the project aims to:

1) Reconstruct long-term hydrologic change in central Indonesia in order to understand the processes controlling long-term climate change in the tropical western Pacific,

2) Discover the microorganisms living in Towuti's metal-rich sediments, and determine their impacts on the lake's sediments and biogeochemistry,

3) Evaluate the history and stability of Sulawesi's lush rainforests, and the impacts of past climate change on these ecosystems,

4) Document the age of Lake Towuti, its long-term limnological history, and the environmental background shaping the diversification of Towuti's endemic flora and fauna.

Study Site

Lake Towuti is located near the equator (2.75° S, 121.5° E; Fig. 9.1 and 9.2) at 318 m above sea level in central Sulawesi, Indonesia. The island of Sulawesi has a complex tectonic history. At the large scale, a complex zone of deformation extends across central Sulawesi and absorbs the collision of Australia with Asia (Sundaland). Three major sinistral strike-slip fault systems accommodate this motion: the Palu-Koro, Matano, and Lawanopo faults. Lake Towuti and neighbouring lakes occupy small transtensional basins along the Matano Fault. Northeast of Sulawesi, the Molucca Sea subduction zone accommodates convergence between the Philippine Sea Plate and Sundaland, giving rise to extensive volcanic fields in North Sulawesi (Hamilton, 1988).

Sulawesi is composed of four elongate ‘arms’, which broadly correspond to lithotectonic units (Hamilton 1979). The southeast arm, which houses Lake Towuti, is dominated by the highly tectonized East Sulawesi Ophiolite, which is inter-thrust with Mesozoic and Cenozoic sediments. These rocks are comprised of ultramafic mantle peridotites (lherzolites and harzburgites), cumulate gabbros, and basalts of normal mid-ocean ridge composition (Kadarusman et al., 2004; Monnier et al., 1995). The ophiolites have sourced large lateritic nickel deposits that attracted the mining industry beginning in the 1970s, with active operations and extensive infrastructure in the region currently operated by PT Vale Indonesia (a subsidiary of Vale SA).

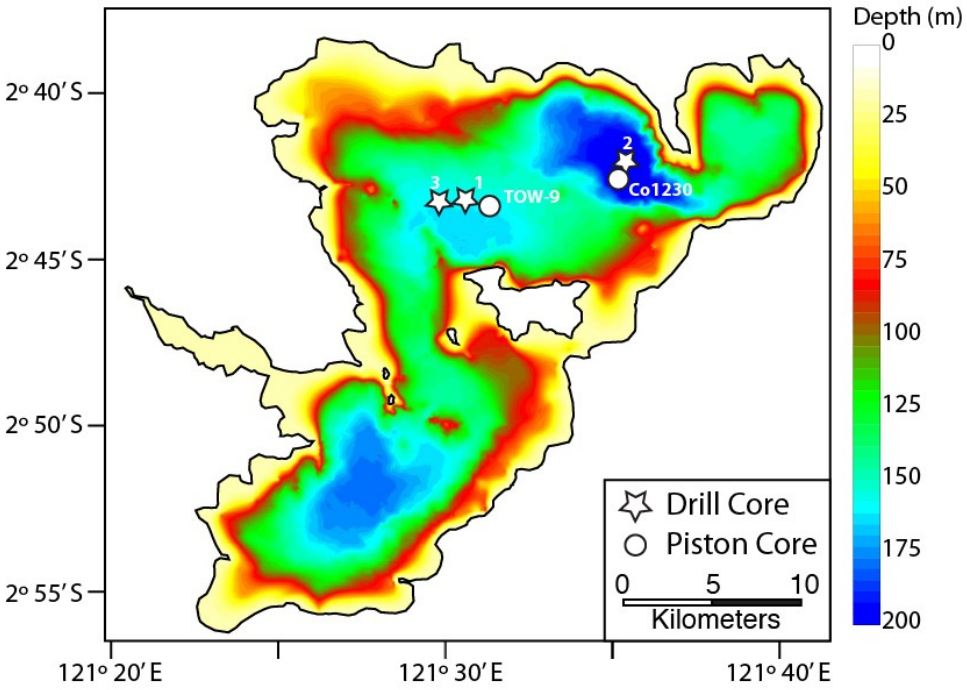

Figure 9.2: *A bathymetric map of Lake Towuti showing the location of core sites discussed in the text.*

The three largest of the Malili lakes, Matano, Mahalona, and Towuti are connected with surface outflow from Matano to Mahalona to Towuti via the Mahalona River, the largest river inflow to the lake (Fig. 9.2). Lake Towuti is the largest of the Malili lakes, with a surface area of 560 km^2 and a maximum water depth of 200 m (Haffner et al., 2001; Lehmusluoto et al., 1995). A chain of islands divides the lake into two basins: a larger northern basin that contains the deepest part of the lake, and a smaller southern basin. Lake Towuti is presently hydrologically open with outflow to the southwest through the Larona River, which flows to the Bay of Bone.

Lake Towuti experiences a tropical humid climate. The region receives ~2,700 mm/yr of precipitation, with a wet season from Dec-May, during which strong northeasterly flow, warm SSTs, and local convective activity (Hendon, 2003) maintain precipitation at >250 mm/month. Precipitation falls below 150 mm/month from Aug-Oct, when southeasterly flow and cool SSTs suppress regional convection. This circulation and precipitation seasonality is characteristic of much of southern Sumatra, southern Borneo (Kalimantan), Java, and the Moluccas (Hendon, 2003), suggesting our record should represent climate change across a broad swath of central and southern Indonesia (Aldrian and Susanto, 2003; Konecky et al., 2016).

Towuti's surface water temperatures vary between ~29 and 31° C. The lake water column is thermally stratified, with seasonal mixing to a depth of ~100 m (Costa et al., 2015). Lake Towuti is relatively dilute (210 µS/cm) and circumneutral (pH ~7.8) with a chemistry dominated by Mg and HCO_3^- (Haffner et al., 2001, Lehmusluoto et al. 1995). The lake is among the least productive tropical lakes on Earth (ultraoligotrophic), likely due to low nutrient delivery from intensely weather soils and sedimentary PO_4^{3-} trapping by very high Fe concentrations. The surface waters are well-oxygenated, but hypoxic to anoxic conditions exist below ~120 m depth allowing for the development of ferruginous conditions with very low concentrations of dissolved sulfur.

Core Site Selection

Site selection for the TDP was guided by three surveys carried out between 2007 and 2013 that collected over 1000 km of seismic reflection data and piston cores that document the nature of the upper 10-20 meters of Towuti's sediment column. Seismic data include "CHIRP" data acquired with an Edgetech™216s towfish with a topside 3200XS collection system, and both single channel and multichannel data collected using a Bolt™5 in^3 airgun and a 150-m-long Geometrics™GeoEel solid digital streamer with 24 channels.

The seismic data reveal two major sedimentary units in Lake Towuti (Fig. 9.3) (Russell et al., 2012). Unit 1 consists of a well-stratified sequence that extends from the lake floor down to ~100 m sub-bottom, and is characterized by parallel acoustic reflectors that can be traced across most of the basin. These reflectors do not exhibit obvious geometric relationships such as angular contacts that would indicate large lake

level changes, suggesting stable, continuous, fine-grained sediment deposition in Towuti's deep basins. Some of the thickest Unit 1 accumulations are found in the deepest basin of Lake Towuti, located near the northern shore of the lake. This basin receives distal deltaic sediments derived from the Mahalona River, which drains the upstream Lakes Matano and Mahalona.

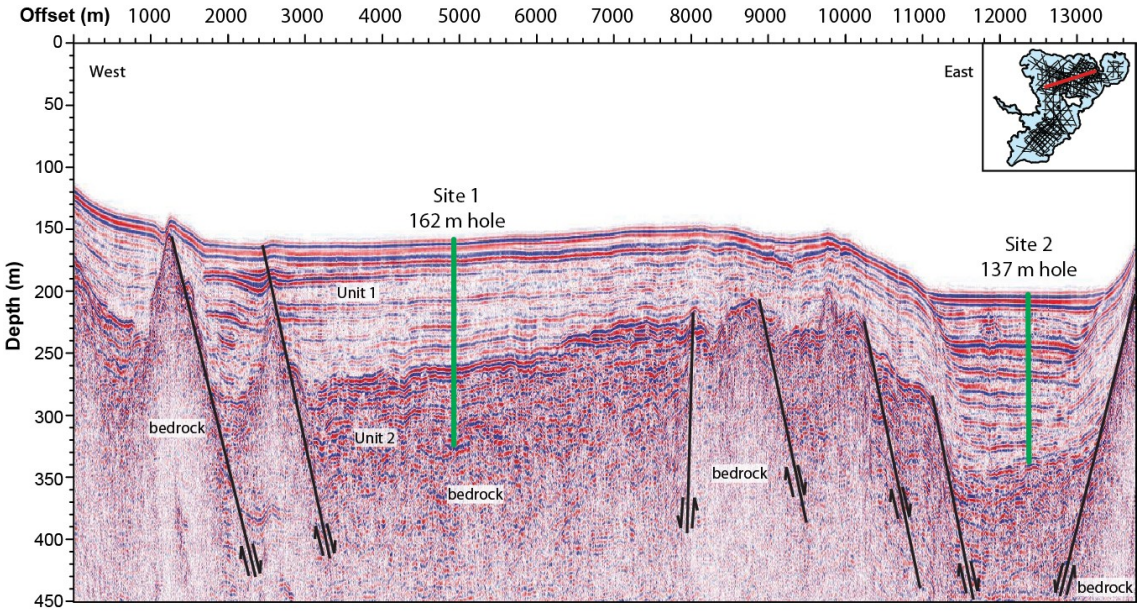

Figure 9.3: *Seismic reflection profile oriented WSW-ENE over Lake Towuti's northern basin (see inset for line position) crossing TDP Sites 1 and 2. Thick green lines show the borehole depths for TDP-TOW15-1B and TDP-TOW15-2A. Seismic Units 1, 2, and bedrock are labeled, and major faults are indicated by thin black lines.*

Our piston coring survey sampled only the uppermost sediments of Unit 1, but confirmed the observations from our seismic reflection data. A core collected at site TOW-9 (Fig. 9.2) documented continuous, fine-grained sedimentation in the central part of Towuti's northern basin, with sedimentation rates of ~5.5 kyr/meter during the past ~60 kyr BP (Russell et al., 2014). We found very frequent distal deltaic turbidites in the deepest part of the lake (Site Co1230, Fig. 9.2), particularly during lake level low-stands that remobilize delta topset beds and force deltaic progradation (Vogel et al., 2015). Elsewhere, the piston cores generally consisted of fine-grained clays interbedded with more or less frequent turbidites. Turbidites increased in frequency and thickness with proximity to the Mahalona River Delta, but were also common near shorelines or in the deepest parts of sub-basins within the lake, perhaps originating from seismically induced failure of poorly consolidated sediments in this tectonically active basin.

Unit 1 is underlain by Unit 2, a more poorly stratified unit that varies between a few tens to ~150 m in thickness. Unit 2 is characterized by a range of sediment types,

from continuous, sub-parallel reflectors to short, discontinuous reflectors. Prior to drilling, Unit 2 was interpreted to reflect alternating fluvial and lacustrine sedimentation that occurred during the initial stages of formation of Lake Towuti. Drilling Unit 2 could provide insight into Lake Towutis age, processes of basin formation, and the early lake stages, information critical to understanding the biological evolution of Towuti's endemic fauna.

Based upon these data, we selected three primary drilling sites, between 156 and 200 m water depth, and with drilling targets between ~130 and ~175 m sub-bottom. Our primary goals in selecting drilling sites were to recover:

1) High-quality continuous sections with as few turbidites as possible through Unit 1 for paleoclimate, paleolimnological, and geomicrobiological studies
2) A distal record of the Mahalona River system to monitor changes in deltaic sedimentation forced by lake level changes and possible changes in the river system itself signaling changes in the hydrological connectivity of Lakes Towuti, Mahalona, and Matano.
3) As long a section as possible through Unit 2, preferably at sites containing more lacustrine than fluvial sedimentation (fine-grained deposits).

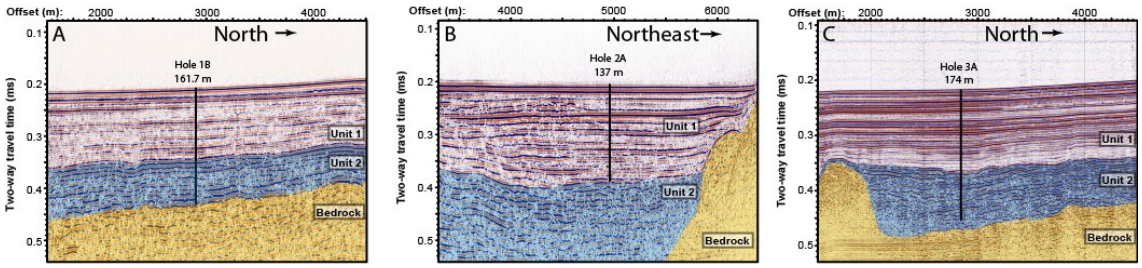

Figure 9.4: *Expanded seismic reflection sections over the TDP core Sites 1 (a), 2 (b), and 3 (c), with seismic units 1 and 2, and bedrock labeled. Black lines show the positions and depths of TDP-TOW15-1B, TDP-TOW15-2A, and TDP-TOW15-3A.*

Site 1 is TDP's primary drilling target, located in the central part of Towuti's northern basin in ~156 m water depth (Fig. 9.4A). This 'master site' is located close to our piston coring site TOW-9, which has yielded high quality paleoclimatic and paleolimnologic reconstructions. The site is located upslope of slightly deeper areas of the lake on the northern edge of the Loeha Island, and south of a large WNW-ESE trending intrabasin fault that limits sediment inputs from the Mahalona River, and thus contains few turbidites. Site 1 is well-suited to address most of our key studies in

paleoclimate, paleolimnology, paleoecology, and geomicrobiology. Seismic data over site 1 show that Unit 1 is approximately 100 m thick, and piston cores suggest the site is undisturbed by turbidites or other event deposits. Seismic data also imaged approximately at least 75 m of sediment in Unit 2, including two intervals marked by roughly parallel acoustic reflectors centered at ~115 m and ~160 m depth, indicating relatively well-stratified sediments. Our primary goals at Site 1 were to obtain overlapping triplicated cores through the upper ~100 m, to obtain 100% recovery of Unit 1, and to recover as complete a section as possible of Unit 2 including cores to bedrock if possible.

Site 2 is located in the deepest part of Lake Towuti at 200 m water depth (Fig. 9.4b). Piston core Co1230 indicates that this site receives distal deltaic sediments derived from the Mahalona River, and seismic reflection data indicated a major change in the acoustic character of the sediments at ~65 meters depth that could reflect the beginning of distal deltaic sedimentation from the Mahalona River. The principle objectives of drilling this location were therefore to provide a record of lake level changes and/or major changes in the hydrological connection between Lakes Towuti, Mahalona, and Matano through study of these distal deltaic deposits. Changes in the amount and style of clastic sedimentation, together with sediment provenance studies, at Site 2 may provide relatively direct insight into the history of hydrological connectivity between the Malili Lakes, with important implications for the biological, hydrological, and geological evolution of Lake Towuti. Seismic reflection data suggested ~130 m of well-stratified lacustrine sediment at this site, so our goal was to recover duplicate overlapping cores to the Unit 1/Unit 2 boundary.

Site 3 was originally proposed for Towuti's southern basin to provide a sedimentary sequence unaffected by sedimentological changes associated with the evolution of the Mahalona River, in order to test the reproducibility of our reconstructions of terrestrial weathering and sediment supply obtained from Site 1. The long transit times to Towuti's southern basin, combined with equipment failures, forced us to relocate Site 3. An alternate site was selected to the west of Site 1 in 159 m water depth (Fig. 9.4C). Seismic data suggested that this site could have the most continuous lacustrine sedimentation through the time period represented by Unit 2, as the site is located in a small structural sag that may have allowed for continuous lacustrine conditions while other sites in the basin were dry. Our goal at this site was to obtain

overlapping duplicated cores as deeply as possible.

Drilling, logging, and on-site geomicrobiological operations

Drilling in a remote part of central Indonesia was a difficult logistical undertaking. Major logistical activities began in September 2014, when we shipped 14 containers of drilling equipment and supplies from the United States of America to the town of Sorowako, Sulawesi Selatan, Indonesia; initiated research permit applications and paperwork; began on-site construction of a dock and crane pad from which we could launch the drilling barge; and developed agreements with PT Vale Indonesia for local logistical support including the use of cranes, housing, and assistance with environmental, health, and safety planning. We shipped the GFZ "Buglab" to Sorowako to support on-site sample processing for geomicrobiological investigations, as well as borehole logging equipment from the Leibniz Institute for Applied Geophysics (LIAG), Hannover, Germany. Logistical preparations were completed in May 2015, when the drilling team arrived and set up on-site analytical facilities and the drilling barge on Lake Towuti's shore.

Drilling commenced at Site 1 on 23 May 2015 using the ICDP Deep Lakes Drilling System (DLDS) operated by DOSECC Exploration Services. Boreholes were drilled using PQ (122.6 mm hole, 66 mm core) diameter drill string using the hydraulic piston corer (HPC) for soft sediment and the "Alien" rotating corer to recover more resistant lithologies; attempts to recover more resistant lithologies with the Extended Nose Corer (EXN) resulted in poor core recovery and quality. All cores were recovered into standard IODP butyrate liners. Geophysical downhole logging data including natural gamma radiation, magnetic susceptibility (MS), electrical resistivity, temperature, acoustic velocity, vertical seismic profiles, and borehole diameter and dip were measured at varying depth resolutions in a subset of holes.

A multisensor core logger (MSCL, Geotek Ltd.) was used to collect magnetic susceptibility (MS) and p-wave velocity data on whole cores in an on-site laboratory immediately after drilling, though the p-wave velocity data was of low-quality due to gas expansion in most cores. At hole 1A, also known as the "bughole", a fluid contamination tracer was used to aid geomicrobiological sampling. Samples were collected from cores from hole 1A immediately upon recovery on the drilling barge to measure trace and redox-sensitive gas concentrations (such as methane), and over 450

samples were subsequently processed in the BugLab for analyses of pore-water chemistry, cell counting and microbial fingerprinting, experiments on microbial turnover and processes, and organic geochemistry.

Upon conclusion of drilling operations, cores were shipped via air freight to LacCore, the National Lacustrine Core Facility at the University of Minnesota, USA, for full processing, description, scanning, and subsampling. There, physical properties for whole cores were analyzed via MSCL-S to obtain *p*-wave velocity, gamma density, loop MS, electrical resistivity, and natural gamma radiation data at intervals of 2-4 cm. After splitting, cores were logged using an MSCL-XYZ to obtain high-resolution MS and color reflectance spectrophotometry at 0.5 cm resolution. Split cores were cleaned and scanned with a Geotek™ MSCL-CIS digital linescan imager. Visual core description and smear slide analyses were carried out to classify the sediment into major compositional units, and subsamples were extracted at intervals coordinated to obtain stratigraphically equivalent samples for sedimentological, geochemical, and paleoecological parameters. All cores received identical treatment except cores from hole 1C, which were left in Indonesia to aid in educational and outreach activities, and cores from hole 1A, many of which were completely sampled in the field leaving no material for logging nor core description.

Initial coring and core description results

TDP drilled 11 boreholes in total (Tab. 9.1), although several of these were relatively short due to twist offs that broke drilling rods, or other equipment malfunctions. In total we drilled ~1228 m of sediment and recovered ~1018 m of core within the intervals where coring was attempted, resulting in a recovery of 91.7% (Fig. 9.5). Recovery was generally very high through the upper ~100 m of sediment (Unit 1), but much lower in Unit 2 due to the presence of coarse-grained unconsolidated lithologies. We acquired borehole logging data from three holes, though not all parameters were logged at all depths due to borehole collapse in shallow unconsolidated sediment. Attempts to collect vertical seismic profiles at Site 1 were unsuccessful due to equipment malfunction, and were not repeated at other sites.

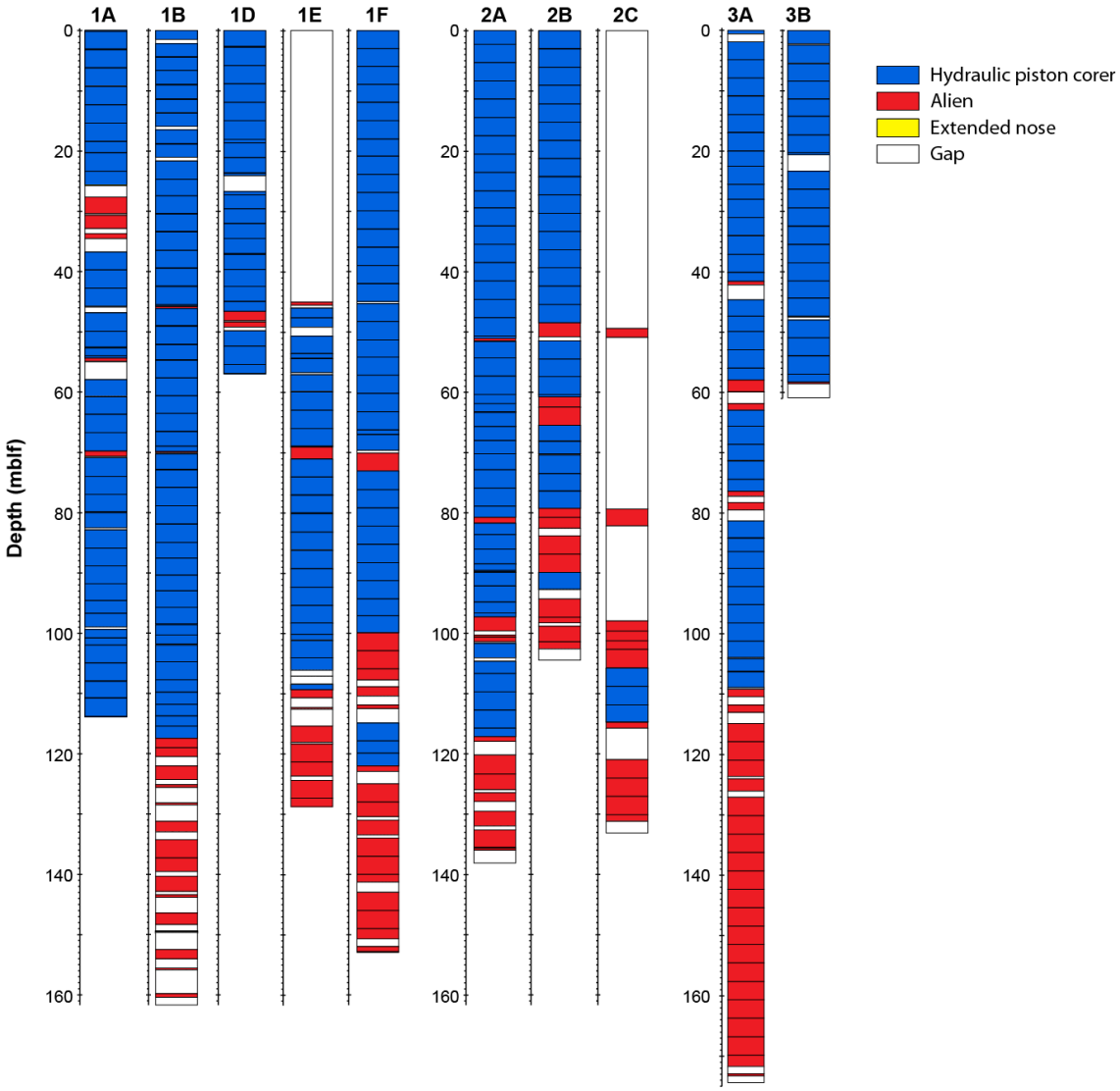

Figure 9.5*: Core recovery from the TDP drill sites in Lake Towuti. Colors indicate the various tools used to recover cores from all TDP sites except 1C. White boxes indicate intervals that were not recovered.*

Six boreholes were drilled at Site 1 yielding approximately 524 m of core. Drilling commenced at Site 1A on 23 May 2015, and penetrated ~115 m reaching ~10 meter below the Unit 1/Unit 2 boundary. Our geomicrobiology team did extensive sampling of this core in the field. The majority of the core consists of relatively soft clays that were cored with the HPC; however, we encountered four relatively hard beds between ~25 and 70 m sub-bottom that required drilling with the Alien tool. These hard beds were later determined to be tephras, which, despite their deposition as airfall, were frequently semi-lithified. Drilling the soft sediments surrounding these tephras with the Alien tool resulted in significant homogenization and contamination of these cores, as revealed by our contamination tracer, results from which are in preparation for publication (Friese et al., 2017). We subsequently adjusted our drilling strategy to

maximize recovery of the tephras while minimizing disturbance of the soft clays. Drilling was terminated in this hole upon encountering the first resistant sand bed, in order to start a new hole to ensure duplication of the upper 100 m of the sediment column.

Table 9.1: *Summary information about TDP drill sites. Drilled depth indicates the bottom depth of each hole. %Recovery indicates the meters of core recovered within the depth intervals where coring was attempted, and thus excludes intervals drilled with a non-coring assembly.*

Labels	Water depth (m)	Core length (m)	Drilled depth (mblf)	Recovery (%)	Borehole Logging	Remarks
Site 1						
TDP-TOW15-1A	156	105.837	113.58	93.2	N	Geomicrobio Site
TDP-TOW15-1B	156	137.871	161.7	85.3	Y	
TDP-TOW15-1C	156	4.455	5.64	79.0	N	Rig failure
TDP-TOW15-1D	156	53.21	53.91	98.7	N	Ended in twist off
TDP-TOW15-1E	156	76.19	128.72	91.0	N	Continuation of 1D
TDP-TOW15-1F	156	145.965	154.06	94.7	Y	
Site 2						
TDP-TOW15-2A	201	134.515	137.58	97.8	Y	
TDP-TOW15-2B	201	103.918	104.55	99.4	N	Ended in twist off
TDP-TOW15-2C	201	34.175	133.21	82.9	N	Continuation of 2B
Site 3						
TDP-TOW15-3A	159	166.08	174.09	95.4	N	
TDP-TOW15-3B	159	55.3	60.88	90.8	N	Ended in twist off
TOTAL		**1017.5**	**1227.9**			

Our second hole, 1B, was our deepest hole at Site 1, extending to 162 m below lake floor (mblf). The upper ~115 mblf was very similar to hole 1A, but the lower ~46 mblf consisted of a variety of coarser grained lithologies that resulted in relatively low recovery. Coring was terminated at ~162 mblf after coring ~0.40 m of bedrock, which consisted of a lithified mafic conglomerate that appears similar to Eocene-aged deposits that occasionally outcrop in the region.

While drilling hole 1B, we began to experience problems with the hydraulic power system of the drilling rig, and after completing hole 1B, we completely lost rig function. Drilling operations had to be shut down for 18 days in order to replace the

main hydraulic pumps of the rig. We then repositioned the drill rig and cored a short hole, 1C, which extended only ~5.5 mblf. After correcting additional hydraulic problems identified while drilling this hole, we drilled three additional holes at Site 1 (1D, 1E, and 1F). Hole 1D extends ~54 mblf with excellent recovery, and was terminated due to a stuck tool. We repositioned and reamed to ~45 mblf with a non-coring assembly (NCA) at hole 1E, and then cored the interval from 45 to ~129 mblf with 91% recovery. In light of the various equipment issues and difficulties recovering sediments around tephras in Unit 1 and coarse sediments in Unit 2, we drilled a sixth and final hole, 1F. This hole extends to ~154 mblf, with nearly 95% recovery, and was terminated when we encountered gravels that, based on 1B, cap a bedrock-soil-fluvial sequence. Holes 1B and 1F were successfully logged for various geophysical parameters, though barge movement and borehole collapse prevented logging of the upper ~20 meters of sediment.

Core 1F is the most complete section from Site 1 and its lithology is representative of the section recovered from this site (Fig. 9.6). The basal sediments consist of a variety of lithologies including alternating gravels, poorly to well-sorted sands, silts, clayey silts, and peats. This unit is capped by a ~2.5 m thick woody peat at ~100 mblf, which correlates to the transition from Unit 2 to Unit 1 in seismic reflection data. The upper 100 m of sediments consist largely of alternating thinly bedded to massive dark reddish-gray to dark-green gray clays. Normally-graded silts (turbidites) are relatively rare but more common in the lower ~50 m of this interval, and we discovered ~14 light gray tephras that range from ~1 to ~40 cm thickness and are scattered through the upper ~95 meters. The source of these tephras is currently under investigation, but they likely derive from the Tondano caldera system in North Sulawesi, which is the closest tephra source to Lake Towuti. We also observed two 3 – 5 meter thick intervals of laminated to medium bedded diatomaceous ooze. Diatoms are not a significant part of the pelagic phytoplankton in the present-day lake (Haffner et al., 2001; Lehmusluoto et al., 1995), suggesting that these intervals mark major changes in the biogeochemical functioning of Lake Towuti.

Three holes were drilled at Site 2 to obtain a record of the evolution of the Mahalona River delta. Hole 2A reached ~134 mblf with ~98% recovery, though there was significantly more gas expansion at Site 2 than at Site 1, which contributed significantly to the high apparent recovery. Coring was terminated when we reached

sandy gravel, interpreted to correspond to the Unit 1/Unit 2 boundary observed in seismic reflection data (Fig. 9.4B). Hole 2B extended to ~105 mblf, and ended in a twist off of the drilling rod. We repositioned and in hole 1C reamed down to 100 m using a NCA, with spot coring to close coring gaps in 2A and 2B. We then cored from ~100 to ~133 m with 83% recovery.

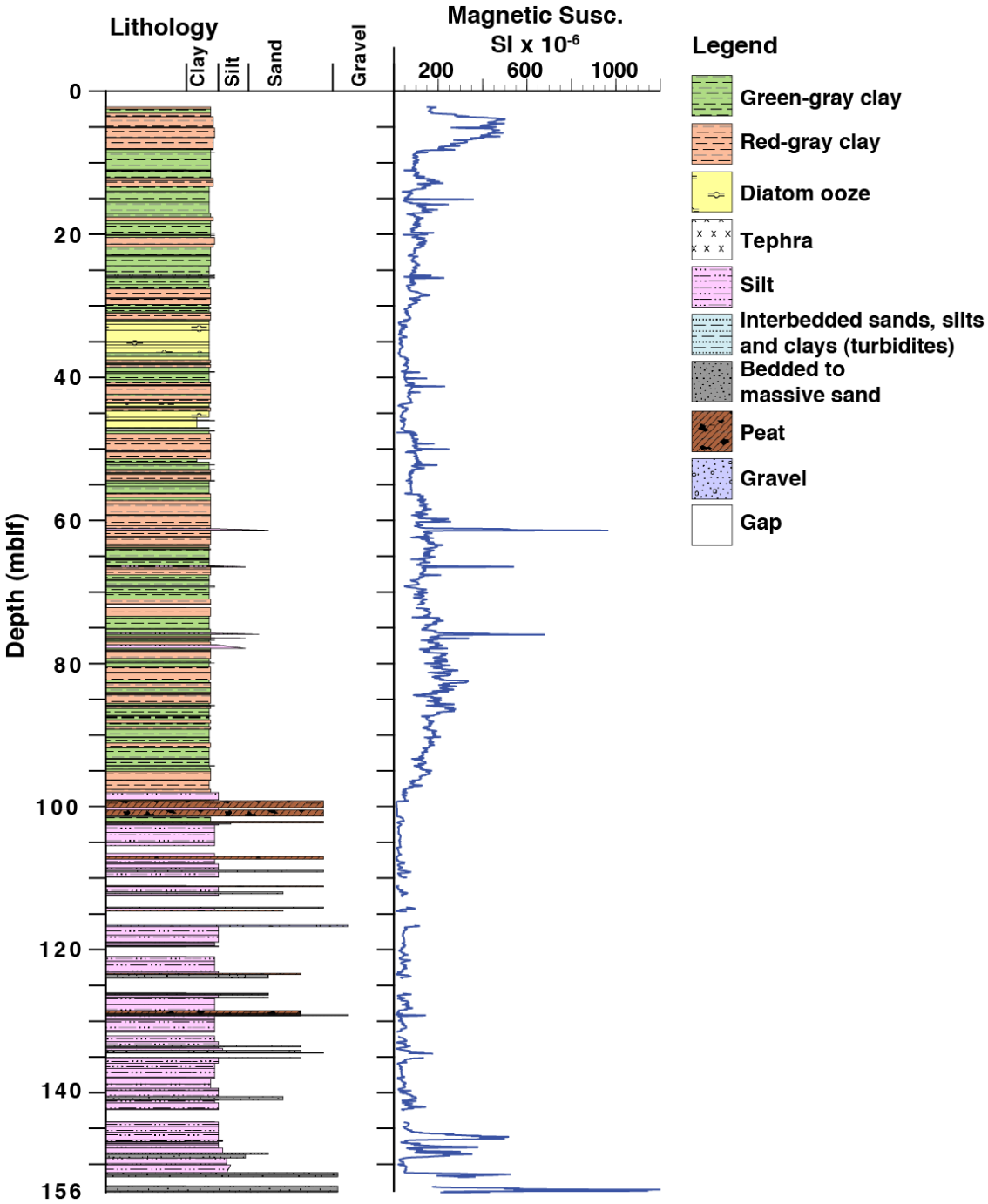

Figure 9.6: *Summary stratigraphy of core TDP-TOW15-1F, based on initial core descriptions. Lithology data are based upon visual and smear slide descriptions, and are rendered in PSICAT. Magnetic susceptibility data measured on the whole (unsplit) core from the Geotek MSCL are shown in the central panel, and at far right is the key to the lithologic symbols. Blank (white) areas indicate zones with no recovery.*

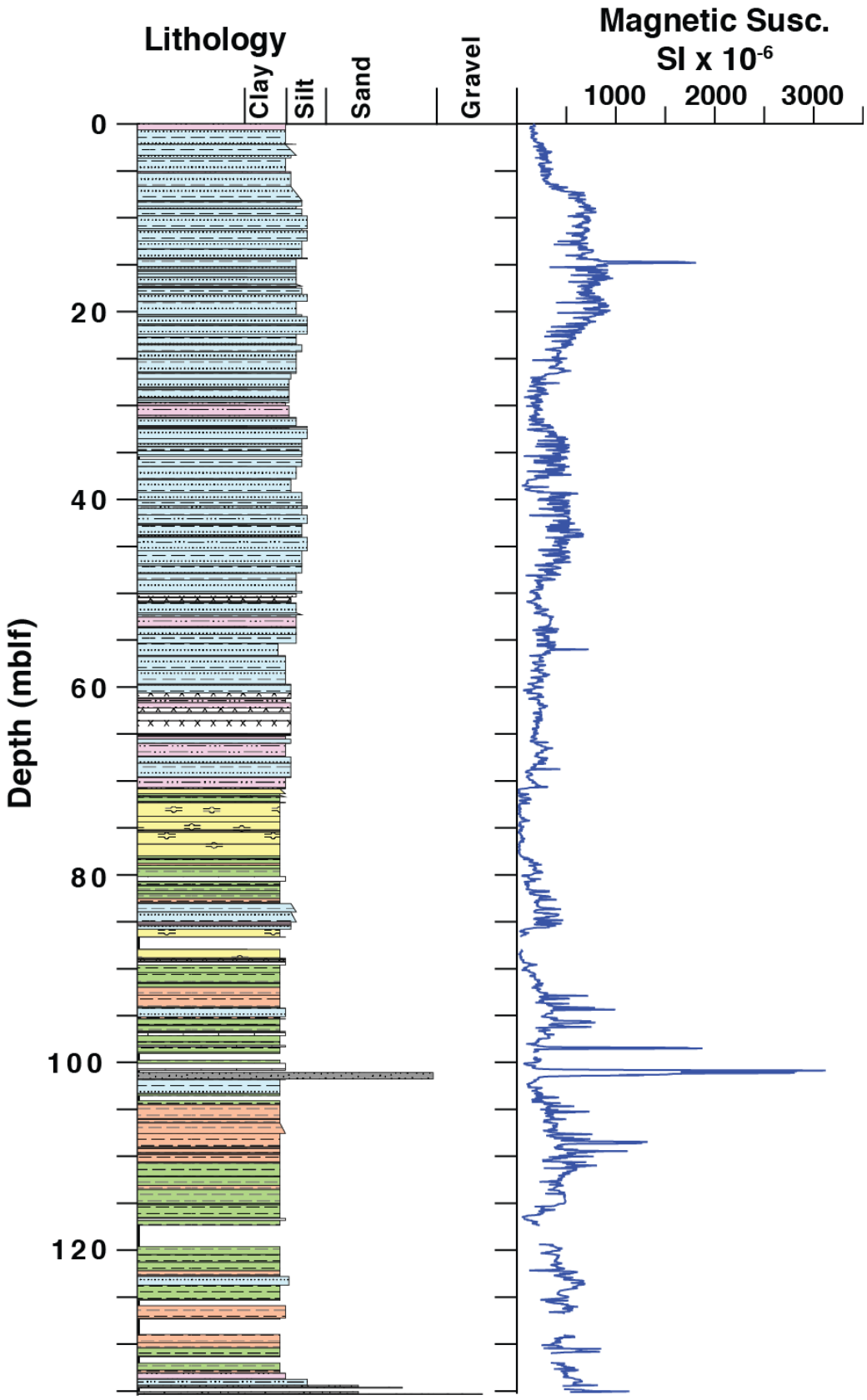

Figure 9.7: *Summary stratigraphy of core TDP-TOW15-2A, based on initial core descriptions, and magnetic susceptibility data measured on the whole (unsplit) core from the Geotek MSCL. The key to the lithologic symbols is given in Figure 9.6.*

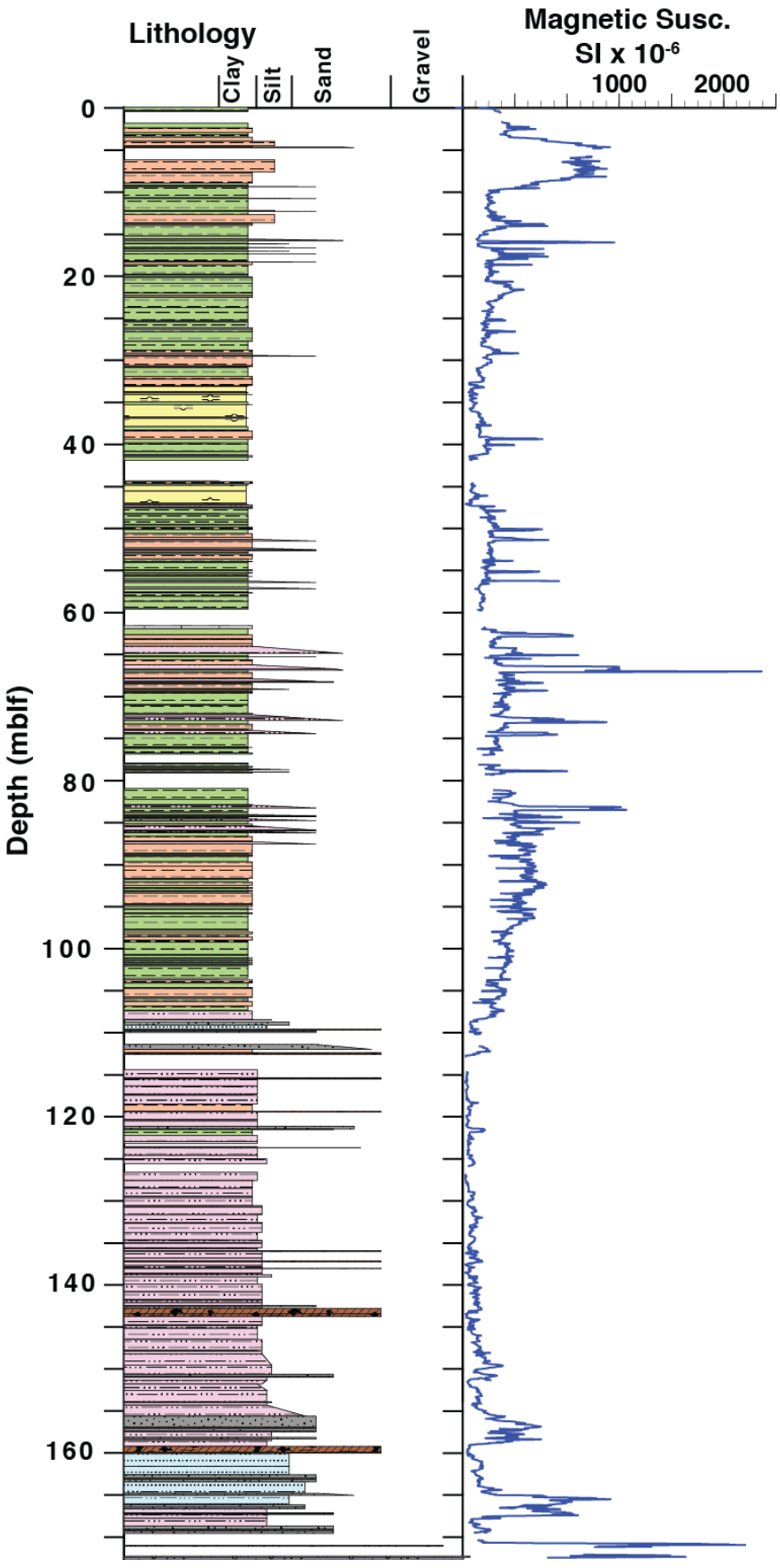

Figure 9.8: *Summary stratigraphy of core TDP-TOW15-3A based on initial core descriptions, and magnetic susceptibility data measured on the whole (unsplit) core from the Geotek MSCL. The key to the lithologic symbols is given in Figure 9.6.*

Hole 2A provides the most complete and representative stratigraphy from Site 2. The upper ~71 m of this core consist of 1-80 cm thick normally graded silts (Fig. 9.7), reflecting deposition by turbidity currents, interbedded with dark reddish to greenish-gray silty clay, whereas the lower 64 m consists largely of alternating thinly bedded to massive dark reddish-gray to dark-green gray clays similar to Site 1. We observe multiple tephra beds as well as two intervals of diatomaceous ooze, similar to Site 1. The tephras are much thicker than observed at Site 1, likely reflecting enhanced reworking of tephra from the Mahalona Delta and steep slopes bordering the basin.

We drilled our deepest hole of the project at Site 3, where hole 3A reached ~174 mblf with over 95% core recovery. Drilling at 3A was terminated when we encountered gravel near the contact with bedrock (Fig. 9.8). We began a second hole, 3B, which ended in a twist-off while trying to drill through a tephra at ~61 m depth. Due to time and budgetary constraints, we were not able to drill a third hole at Site 3 and concluded the project. Hole 3A, however, contains an excellent record of sedimentation at this site. Unit 1 at Site 3 is similar to that of Site 1, but is slightly expanded (~10% thicker) and contains much more frequent turbidites, particularly in the lower ~50 m. Peats are less common in Unit 2 of Site 3 than at Site 1, and the sediments are generally finer grained, resulting in better recovery. These observations are consistent with our interpretation of the seismic reflection data that places Site 3 in a small structural basin that supported more continuous lacustrine sedimentation during the early stages of formation of the Lake Towuti basin.

Conclusions

The TDP cores record the evolution of a highly dynamic tectonic and limnological system. Sediments in Unit 2 represent a mixture of lacustrine, fluvial, and terrestrial sediments deposited during the initial stages of extension and subsidence of the Lake Towuti basin. Comparison of Unit 2 sediments between Sites 1 and 3, or even between different holes drilled at Site 1, suggest Unit 2 is highly spatially variable over short distances, perhaps reflecting a variety of lake, swamp, and riverine environments that existed simultaneously in a large, slowly subsiding swampy plain. The rapid transition from Unit 2, which represents sedimentation near base level, to Unit 1, which represents sedimentation permanently below base level, suggests rapid fault movement and creation of accommodation space.

We interpret Unit 1 to represent sedimentation in a generally deep lake, with red/green alternations reflecting climate-driven transitions in lake level and mixing (Costa et al., 2015). Unit 1 sediments are quite similar at Sites 1 and 3, but differ substantially at Site 2, where the upper ~70 m of sediment predominantly consists of distal deltaic sedimentation. This supports our interpretation of the seismic reflection data and could indicate relatively recent establishment of the Mahalona River.

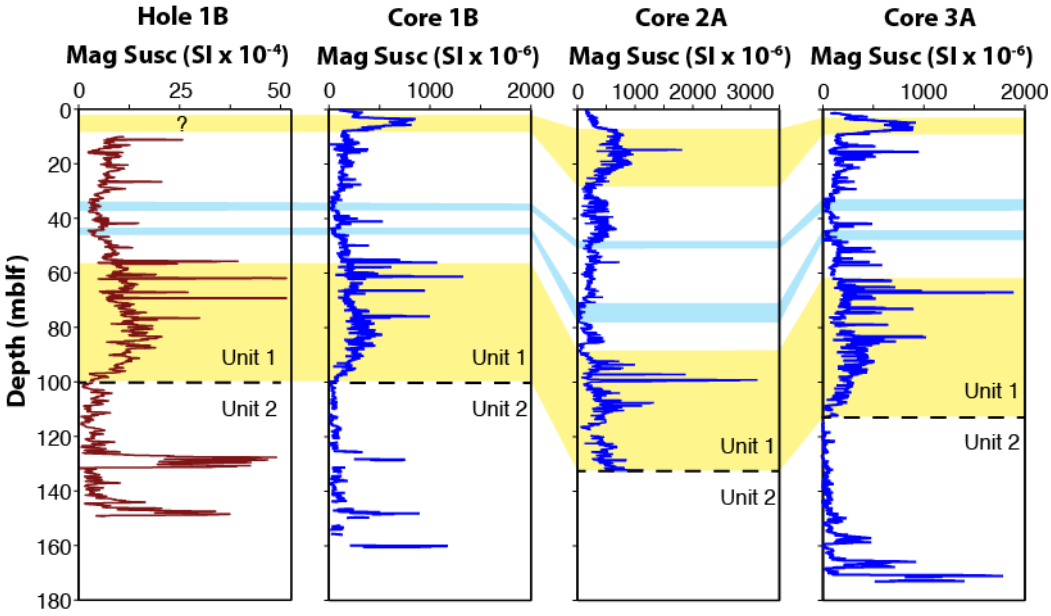

Figure 9.9: *Magnetic susceptibility data from borehole logging of Hole 1B as well as MS data of cores 1B, 2A, and 3A. Yellow shading indicates correlative high magnetic susceptibility features in each site, whereas blue shading indicates correlative low susceptibility features. The dashed line marks the interpreted boundary between Seismic Unit 1 and 2; note that this boundary appears younger in core 2A than at sites 1 and 3.*

Magnetic susceptibility profiles from Lake Towuti show very similar patterns at all three sites, and show generally excellent correlation to borehole profiles (Fig. 9.9). These data, together with tephras, biogenic opal beds, and other distinct beds, allow a preliminary correlation of cores from the three holes. This correlation highlights the relatively rapid influx of sediment to the upper 70 m of Site 2 relative to Sites 1 and 3, likely reflecting the rapid influx of sediment from the Mahalona River to the core site during this time. Interestingly, the basal sediments of Site 2 appear to be younger than those at Sites 1 and 3, despite the fact that Site 2 currently lies in deeper water than the other sites. This could suggest relatively fast subsidence of the northernmost part of the lake relative to the central part of the basin, perhaps reflecting recent changes in fault motion.

Our analysis of these cores is just beginning and includes an array of geochronological, sedimentological, geochemical, geophysical, and biological methods. The geochronology is being assembled through a combination of $^{40}Ar/^{39}Ar$ ages on tephras, paleomagnetic, luminescence, and ^{14}C dating. State of the art isotopic, organic geochemical, and elemental methods are being applied to understand the climate history of the tropical western Pacific and the evolving biogeochemistry of the basin. Analyses of the pore fluid chemistry, Fe-mineralogy, and microbial communities in the sediments will reveal the nature of the deep biosphere that inhabits these iron-rich sediments, and fossil pollen and fossil diatoms will reveal the dynamics of the evolving terrestrial and aquatic biota in central Sulawesi. Ultimately, through interactions between these groups we will try to unravel the coupled tectonic, biologic, and climatic evolution of this unique system.

Acknowledgements

This research was carried out with partial support from the International Continental Scientific Drilling Program (ICDP), the U.S. National Science Foundation (NSF), the German Research Foundation (DFG) the Swiss National Science Foundation (SNSF), PT Vale Indonesia, the Ministry of Research, Education, and Higher Technology of Indonesia (RISTEK), Brown University, the GFZ German Research Centre for Geosciences, the Natural Sciences and Engineering Research Council of Canada (NSERC), and Genome British Columbia. We thank PT Vale Indonesia, the US Continental Scientific Drilling and Coordination Office, and US National Lacustrine Core Repository, and DOSECC Exploration Services for logistical support. The research was carried out with permissions from RISTEK, the Ministry of Trade of the Republic of Indonesia, the Natural Resources Conservation Center (BKSDA), and the Government of Luwu Timur of Sulawesi. Cores and project data are archived at the National Lacustrine Core Repository, USA. We thank Andy Cohen and Christine Lane for helpful comments on a previous version of this paper.

References

Aldrian, E., and Susanto, R. D., 2003, Identification of three dominant rainfall regions within Indonesia and their relationship to sea surface temperature: International Journal of Climatology, v. 23, p. 1435-1452.

Cannon, C.H., Morley, R.J., and Bush, A.B.G., 2009. The current rainforests of Sundaland are unrepresentative of their biogeographic past and highly vulnerable to disturbance. Proceedings of the National Academy of Sciences, USA 106: 11188–11193.

Carolin, S. A., Cobb, K. M., Adkins, J. F., Clark, B., Conroy, J. L., Lejau, S., Malang, J., and Tuen, A. A., 2013, Varied response of western Pacific hydrology to climate forcings over the last glacial period: Science, v. 340, p. 1564-1566.

Chiang, J. C. H., 2009, The tropics in paleoclimate: Annual Review of Earth and Planetary Sciences, v. 37, p. 20.21-20.35.

Clement, A. C., Cane, M. A., and Seager, R., 2001, An orbitally-driven tropical source for abrupt climate change: Journal of Climate, v. 14, p. 2369-2375.

Costa, K., Russell, J. M., Vogel, H., and Bijaksana, S., 2015, Hydrologial connectivity and mixing of Lake Towuti, Indonesia in response to paleoclimatic change over the last 60,000 years: Palaeogeography, Palaeoclimatology, Palaeoecology, v. 417, p. 467-475.

Crowe, S. A., O'Neill, A. H., Katsev, S., Hehanussa, P. E., Haffner, G. D., Sundby, B., Mucci, A., and Fowle, D. A., 2008, The biogeochemistry of tropical lakes: a case study from Lake Matano, Indonesia: Limnology and Oceanography, v. 53, p. 319-331.

DiNezio, P. N., Clement, A. C., Vecchi, G. A., Soden, B. J., Broccoli, A. J., Otto-Bliesner, B., and Braconnot, P., 2011, The response of the Walker Circulation to LGM forcing: Impilcations for detection in proxies: Paleoceanography, v. 26, p. PA3217.

DiNezio, P. N., and Tierney, J. E., 2013, The effect of sea level on glacial Indo-Pacific climate: Nature Geoscience, v. 6, p. 485-491.

Friese, A., Kallmeyer, J., Kitte, J.A., Martinez, I.M., Bijaksana, S., Wagner, D., Team, I.L.C.D.S., Team, I.T.D.S., 2017. A simple and inexpensive technique for assessing contamination during drilling operations. Limnology and Oceanography: Methods 15, 200-211.

Fritz, S. C., Baker, P. A., Seltzer, G. O., Ballantyne, A., Tapia, P. M., Cheng, H., and Edwards, R. L., 2007, Quaternary glaciation and hydrologic variation in the South American tropics as reconstructed from the Lake Titicaca drilling project: Quaternary Research, v. 68, p. 410-420.

Haffner, G. D., Hehanussa, P. E., and Hartoto, D., 2001, The biology and physical processes of large lakes of Indonesia: Lakes Matano and Towuti, *in* Munawar, M., and Hecky, R. E., eds., The Great Lakes of the World (GLOW): Food-Web, Health, and Integrity: Leiden, The Netherlands, Blackhuys, p. 129-155.

Hamilton, W. B., 1988, Plate tectonics and island arcs: Geologic Society of America Bulletin, v. 100, p. 1503-1327.

Hendon, H. H., 2003, Indonesian rainfall variability: impacts of ENSO and local air-sea interaction: Journal of Climate, v. 16, p. 1775-1790.

Herder, F., Nolte, A.W., Pfänder, J., Schwarzer, J., Hadiaty, R.K., and Schliewen, U.K., 2006, Adaptive radiation and hybridization in Wallace's dreamponds: evidence from sailfin silversides in the Malili lakes: Proceedings of the Royal Society of London B, v. 273, p. 2209-2217.

Hodell, D. A., Anselmetti, F. S., Ariztegui, D., Brenner, M., Curtis, J. H., Gilli, A., Grzesik, D., Guilderson, T. J., Müller, A. D., Bush, M. B., Correa-Metrio, A., Escobar, J., and Kutterolf, S., 2007, An 85-ka record of climate change in lowland central America: Quaternary Science Reviews, v. 27, p. 1152-1165.

Kadarusman, A., Miyashita, S., Maruyama, S., Parkinson, C. D., and Ishikawa, A., 2004, Petrology, geochemistry, and paleogeographic reconstruction of the East Sulawesi ophiolite, Indonesia: Tectonophysics, v. 392, p. 55-83.

Konecky, B. L., Russell, J. M., and Bijaksana, S., 2016, Glacial aridity in central Indonesia coeval with intensified monsoon circulation: Earth and Planetary Science Letters, v. 437, p. 15-24.

Kumar, S., Merwade, V., Kinter, J. L., and Niyogi, D., 2013, Evaluation of temperature and precipitation trends and long-term persistence in CMIP5 Twentieth-Century Climate Simulations: Journal of Climate, v. 26, p. 4168-4185.

Lehmusluoto, P., Machbub, B., Terangna, N., Rusmiputro, S., Achmad, F., Boer, L., Brahmana, S. S., Priadi, B., Setiadji, B., Sayuman, O., and Margana, A., 1995, National inventory of the major lakes and reservoirs in Indonesia. General limnology.: FAO-FINNIDA.

Meckler, A. N., Clarkson, M. O., Cobb, K. M., Sodemann, H., and Adkins, J., 2012, Interglacial hydroclimate in the tropical west Pacific through the late Pleistocene: Science, v. 336, p. 1301-1304.

Meehl, G. A., Stocker, T., Collins, W. D., Friedlingstein, P., Gaye, A. T., Gregory, J. M., Kitoh, A., Knutti, R., Murphy, J. M., Noda, A., Raper, S. C. B., Watterson,

I. G., Weaver, A. J., and Zhao, Z.-C., 2007, Global Climate Projections, *in* Solomon, S., Qin, D., Manning, M., Chen, Z., Marquis, M., Averyt, K. B., Tignor, M., and Miller, D. J., eds., Climate Change 2007: The Physical Science Basis. Contribution of Working Group I to the Fourth Assessment of the Intergovernmental Panel on Climate Change: New York, USA, Cambridge University Press, p. 747-845.

Monnier, C., Girardeau, J., Maury, R. C., and Cotten, J., 1995, Back-arc basin origin for the East Sulawesi ophiolite (eastern Indonesia): Geology, v. 23, p. 851-854.

Pierrehumbert, R. T., 1999, Subtropical water vapor as a mediator of rapid global climate changes, *in* Clark, P. U., Webb, R. S., and Keigwin, L. D., eds., Mechanisms of global climate change at millennial time scales. Geophysical monograph series v. 112.: Washington DC, American Geophysical Union, p. 339-361.

Pierrehumbert, R. T., 2000, Climate change and the tropical Pacific: the sleeping dragon wakes: Proceedings of the National Academy of Science U.S.A., v. 97, p. 1355-1358.

Rintelen, T. v., Rintelen, K. v., Glaubrecht, M., Schubart, C., and Herder, F., 2012, Aquatic biodiversity hotspots in Wallacea – the species flocks in the ancient lakes of Sulawesi, Indonesia, *in* Gower, D. J., Johnson, K. G., Richardson, J. E., Rosen, B. R., Rüber, L., and Williams, S. T., eds., Biotic evolution and environmental change in southeast Asia Cambridge, Cambridge University Press.

Rintelen, T.v., Wilson, A.B., Meyer, A., and Glaubrecht, M., 2004, Escalation and trophic specialization drive adaptive radiation of viviparous freshwater gastropods in the ancient lakes on Sulawesi, Indonesia.: Proceedings of the Royal Society of London B, v. 271, p. 2541-2549.

Russell, J. M., Bijaksana, S., and Members, T. P., 2012, The Towuti Drilling Project: Paleoenvironments, Biological Evolution, and Geomicrobiology of a Tropical Pacific Lake: Scientific Drilling, v. 14, 68-71

Russell, J. M., Vogel, H., Konecky, B. L., Bijaksana, S., Huang, Y., Melles, M., Wattrus, N., Costa, K., and King, J. W., 2014, Glacial forcing of central Indonesian hydrolclimate since 60,000 yr B.P.: Proceedings of the National Academic of Science U.S.A., v. 111, p. 5100-5105.

Scholz, C., Johnson, T. C., Cohen, A. S., King, J. W., Peck, J. A., Overpeck, J. T., Talbot, M. R., Brown, E. T., Kalindekafe, L., Amoako, P. Y. O., Lyons, R. P., Shanahan, T., Castañeda, I. S., Heil, C. W., Forman, S. L., McHargue, L. R., Beuning, K. R. M., Gomez, J., and Pierson, J., 2007, East African megadroughts between 135 and 75 thousand years ago and bearings on early-modern human origins: Proceedings of the National Academic of Science U.S.A., v. 42, p. 16416-16421.

Schubart, C. D., Santl, T., and Koller, P., 2008, Mitochondrial patterns of intra- and interspecific differentiation among endemic freshwater crabs of ancient lakes in Sulawesi: Contributions to Zoology, v. 77, p. 83-90.

Seager, R., and Battisti, D. S., 2007, Challenges to our understanding of the general circulation: abrupt climate change, *in* Schneider, R. R., and Sobel, A. H., eds., Global Circulation of the Atmosphere: Princeton, Princeton University Press, p. 331-371.

Tamuntuan, G., Bijaksana, S., King, J. W., Russell, J. M., Fauzi, U., Maryuanani, K., Aufa, N., and Safiuddin, L. O., 2015, Variation of magnetic properties in sediments from Lake Towuti, Indonesia, and its paleoclimatic significance: Palaeogeography, Palaeoclimatology, Palaeoecology, v. 420, p. 163-172.

van Welzen, P. C., Parnell, J. A. N., Slik, J. W. F., 2011. Wallace's line and plant distributions: two or three phytogeographical areas and where to group Java? *Biological Journal of the Linnaen Society* 103: 541-545.

Vogel, H., Russell, J. M., Cahyarini, S. Y., Bijaksana, S., Wattrus, N., Rethemeyer, J., and Melles, M., 2015, Depositional modes and lake-level variability at Lake Towuti, Indonesia during the past ~29 kyr BP: Journal of Paleolimnology, v. 54, p. 359-377.

Wang, Y., Cheng, H., Edwards, R. L., Kong, X., Shao, X., Chen, S., Wu, J., Jiang, X., Wang, X., and An, Z., 2008, Millennial- and orbital-scale chanes in the East Asian monsoon over the past 224,000 years: Nature, v. 451, p. 1909-1093.

Additional manuscript II (Published in Organic Geochemistry, 2019, 134, 32 - 44, doi:10.1016/j.orggeochem.2019.05.002).

Empowering conventional Rock-Eval pyrolysis for organic matter characterization of the siderite-rich sediments of Lake Towuti (Indonesia) using End-Member Analysis

Luis Ordoñez[1], Hendrik Vogel[2], David Sebag[3-4], Daniel Ariztegui[1], Thierry Adatte[5], James M. Russell[6], Jens Kallmeyer[7], Aurèle Vuillemin[1, 8], André Friese[7], Sean A. Crowe[9], Kohen W. Bauer[9], Rachel Simister[9], Cynthia Henny[10], Sulung Nomosatryo[10], Satria Bijaksana[11] and the Towuti Drilling Project Scientific Team

[1] Department of Earth Sciences, University of Geneva, 1205 Geneva, Switzerland
[2] Institute of Geological Sciences and Oeschger Centre for Climate Change Research, University of Bern, 3012 Bern, Switzerland
[3] Normandie Univ, UNIROUEN, UNICAEN, CNRS, M2C, 76000 Rouen, France
[4] Institute of Earth Surface Dynamics, Geopolis, University of Lausanne, Lausanne, Switzerland
[5] Institut des Sciences de la Terre (ISTE), Université de Lausanne, GEOPOLIS, CH-1015 Lausanne, Switzerland
[6] Department of Earth, Environmental, and Planetary Sciences, Brown University, Providence RI 02912, USA
[7] GFZ German Research Centre For Geosciences, Section 5.3. Geomicrobiology, D-14473 Potsdam, Germany
[8] Ludwig-Maximilians-Universität München, Department of Earth & Environmental Sciences, Paleontology & Geobiology, 80333 Munich, Germany
[9] Department of Microbiology and Immunology and Department of Earth, Ocean, and Atmospheric Sciences, University of British Columbia, Vancouver, Canada
[10] Research Center for Limnology, Indonesian Institute of Sciences (LIPI), Jl. Raya Bogor, Cibinong, Bogor, West Java 16911, Indonesia
[11] Faculty of Mining and Petroleum Engineering, Institut Teknologi Bandung, Bandung 40132, Indonesia

Abstract

Qualitative and quantitative changes of organic and carbonate carbon in sedimentary records are frequently used to reconstruct past environments, paleoproductivity and sediment provenance. Amongst the most commonly used proxies are Total organic carbon (TOC), Mineral carbon (MinC), as well as Hydrogen (HI) and Oxygen Indices (OI) of organic matter (OM). Rock-Eval pyrolysis enables the assessment of these quantitative and qualitative parameters with a single analysis. This is achieved through transient pyrolysis of the samples up to 650°C followed by combustion up to 850°C,

with hydrocarbons, CO and CO_2 measured during the thermal decomposition of both OM and carbonate minerals.

Carbonate minerals with low thermal cracking temperatures such as siderite (< 400°C) can induce significant matrix effects, which bias the TOC, MinC and OI Rock-Eval parameters. Here we assess the applicability of End-Member Analysis (EMA) as a means to correct Rock-Eval thermograms for siderite matrix effects. For this, we performed Rock-Eval pyrolysis on sideritic sediments of Lake Towuti (Indonesia). New thermal boundaries were constrained in Rock-Eval thermograms using EMA to limit siderite matrix effects and improve TOC, MinC, and OI calculations. Our approach allowed us to: 1) evaluate the influence of siderite matrix effects on Rock-Eval thermograms; 2) properly exploit a Rock-Eval dataset to characterize the type and sources of OM in siderite-rich sediments; and 3) identify the OM behind degradation and mineralization processes. The Rock-Eval dataset revealed sediments with a substantial amount of refractory OM, especially in those where TOC is high and HI characteristic of autochthonous biomass. These results, associated to alternative indices used to assess OM preservation, suggest that refractory OM is residually enriched following strong degradation of labile compounds. Finally, relatively labile and refractory organic fractions may be consumed in the formation of siderite during this sequential process of OM mineralization.

Introduction

Sedimentary organic matter (OM) in marine and lacustrine sedimentary records is widely used as an indicator of changes in past depositional environments. Changes in OM quality and amount can indicate the sources (aquatic/terrestrial) of sedimentary OM, the paleoecology (e.g. productivity) of aquatic systems, and help to identify the external drivers (climate, anthropogenic) leading to these changes (Dean et al., 1997; Meyers, 1997; Meyers and Lallier-Vergès, 1999; Ariztegui et al., 2001). Fresh OM can be easily degraded by oxidation, respiration, and anoxic microbially-mediated decomposition in the water column and within the sediment. The most labile organic fraction, such as microbial biomass or water-soluble OM, will be mineralized into CO_2 and CH_4, and contribute to the precipitation of other mineral phases such as carbonates (Henrichs, 1993), potentially leaving behind the most recalcitrant OM. A better understanding of the underlying processes that convert total organic carbon (TOC – in

wt%) to mineral carbon (MinC – in wt%) is therefore crucial for accurate reconstructions of depositional and post-depositional environments.

Thermal analyses are especially useful since specific temperature thresholds enable the distinction between TOC and MinC. Among the most common techniques, Rock-Eval pyrolysis (Espitalié et al., 1985) provides measurements of both TOC and MinC as well as indices that can be used towards disentangling OM sourcing: the Oxygen Index (OI) and Hydrogen Index (HI), or the g CO_2 and g HC per g of TOC, respectively. These indices have widely been used to discriminate between sources of OM in previous studies (e.g. Tyson, 1995; Meyers, 1997; Meyers and Lallier-Vergès, 1999) and enabled, for example, the reconstruction of variations in authigenic biomass as a result of climate change (Ariztegui et al., 2001; Steinmann et al., 2003) and erosional patterns in subalpine sediments due to anthropogenic impact (Giguet-Covex et al., 2011; Bajard et al., 2017).

To achieve these results, the Rock-Eval analyser (Vinci, France) performs a pyrolysis of the samples to 650°C, followed by combustion to 850°C, with hydrocarbons, CO and CO_2 measured during the thermal decomposition of OM and carbonate minerals. The main advantage of the Rock-Eval method lies in the simple and fast sample preparation, and the simultaneous determination of TOC, MinC, and indices enabling the qualitative (OM sourcing & degradation) characterization of OM. However, the presence of siderite ($FeCO_3$) in samples is known to impact the accuracy of standard Rock-Eval parameters (Lafargue et al., 1998). The siderite-matrix effect, first mentioned by Espitalié et al. (1980), is due to the low cracking temperature of pure siderite (515°C-519°C; Pillot et al., 2014) compared to other carbonates (i.e. Rhodochrosite, 647°C-652°C; Calcite, 776°C-850°C; Aragonite, 762°C-841°C; Pillot et al., 2014), thus overlapping the cracking temperature of OM (Carrie et al. 2012). Siderite can therefore also contribute carbon during combustion of sideritic sediments and induce a significant bias for Rock-Eval analysis in such samples. This prevents the accurate measurement of MinC and TOC, while also leading to over- and underestimations of the OI and HI indices, respectively. Previous studies (Pillot et al., 2014; Milesi et al., 2016; Sebag et al., 2018) have shown that siderite matrix effects can be corrected processing Rock-Eval thermograms (evolved gas versus temperature). Milesi et al. (2016) suggested a siderite-matrix effect correction derived from Rock-Eval for Paleozoic sediments, which assumes that OM has a constant CO/CO_2 ratio with

the excess CO_2 originating from siderite. However, siderite also releases variable amounts of CO during pyrolysis, with the result that the CO/CO_2 ratio cannot be satisfactorily assumed. A more recent study proposed a correction protocol based on thermogram analysis by means of quantifying CO and CO_2 released during the thermal decomposition of siderite in Holocene tropical lake sediments (Sebag et al., 2018). Nevertheless, the deposits Sebag et al. (2018) analyzed are homogeneous in lithology and characterized by low MinC (0.2-1.9%wt). Thus, an alternative approach needs to be developed for more complex lithologies, with variations in the nature and quantity of carbon fractions to evaluate the applicability of the Rock-Eval correction method.

The Towuti Drilling Project (TDP), carried out through the International Continental Scientific Drilling Program (ICDP), aims to understand the climatic, biological, and geomicrobiological evolution of Lake Towuti, a part of the Malili lakes system in Indonesia, during the Pleistocene (Russell et al., 2016). Here, we used Rock-Eval analysis to study sediments acquired by the TDP, which have variable lithologies and abundant siderite (Russell et al., 2016). Rock-Eval data show different OM characteristics in samples where MinC values (> 0.3 – 0.5%) indicate the presence of carbonates inducing potential matrix effects. Therefore, we used a novel End-Member Analysis (EMA) approach to deconvolve Rock-Eval thermograms and defined accurate thermal boundaries for organic and inorganic carbon. Following this step, we estimated siderite abundance and calculated matrix effect-free Rock-Eval parameters. Finally, we utilized our dataset for qualitative OM characterization, i.e. determination of sources and identification of degradation processes preceding the formation of siderite.

Local setting, sampling and lithology

Lake Towuti (2.75°S, 121.5°E, 318 m a.s.l.) is a tectonic lake located in central Sulawesi, Indonesia (Fig. 9.10). With a surface area of ~560 km^2 and a maximum water depth of 203 m, it is the largest of a set of five basins forming the Malili lake system. Lying within the East Sulawesi Ophiolite complex, Lake Towuti has a catchment composed primarily of ultramafic rocks (Monnier et al., 1995; Kadarusman et al., 2004). The tropical and humid climate conditions, with precipitation averaging 2700 mm yr^{-1} (Konecky et al., 2016), leads to erosion and extensive lateritic soil formation (Morlock et al., 2018). Most of the lake is surrounded by a dense rainforest, however, a recent increase in agricultural activity, particularly in the northern part of the catchment,

has led to substantial deforestation (Vuillemin et al., 2017; Morlock et al., 2018). Water chemistry is dominated by Mg^{2+} and HCO^{3-} and has low sulfate concentrations (1.5-2 ppm) with circumneutral pH (7.3-7.8). Nutrient concentrations are close to or below the detection limit making Lake Towuti one of the least productive lakes on Earth (Lehmusluoto et al., 1997; Haffner et al., 2001). The water column is weakly thermally stratified, with anoxic conditions below 130 m allowing for an enrichment of dissolved Fe^{2+} (0.12 ppm) (Costa et al., 2015; Vuillemin et al., 2016). OM in modern sediments seems to be mainly sourced from authigenic production as shown by a C/N ratio averaging 10.8 (Meyers and Lallier-Vergès, 1999; Hasberg et al., 2018). Higher ratios, located in front of the main inlets and steep slopes, support fluvial OM supply from terrestrial sources in near shore areas.

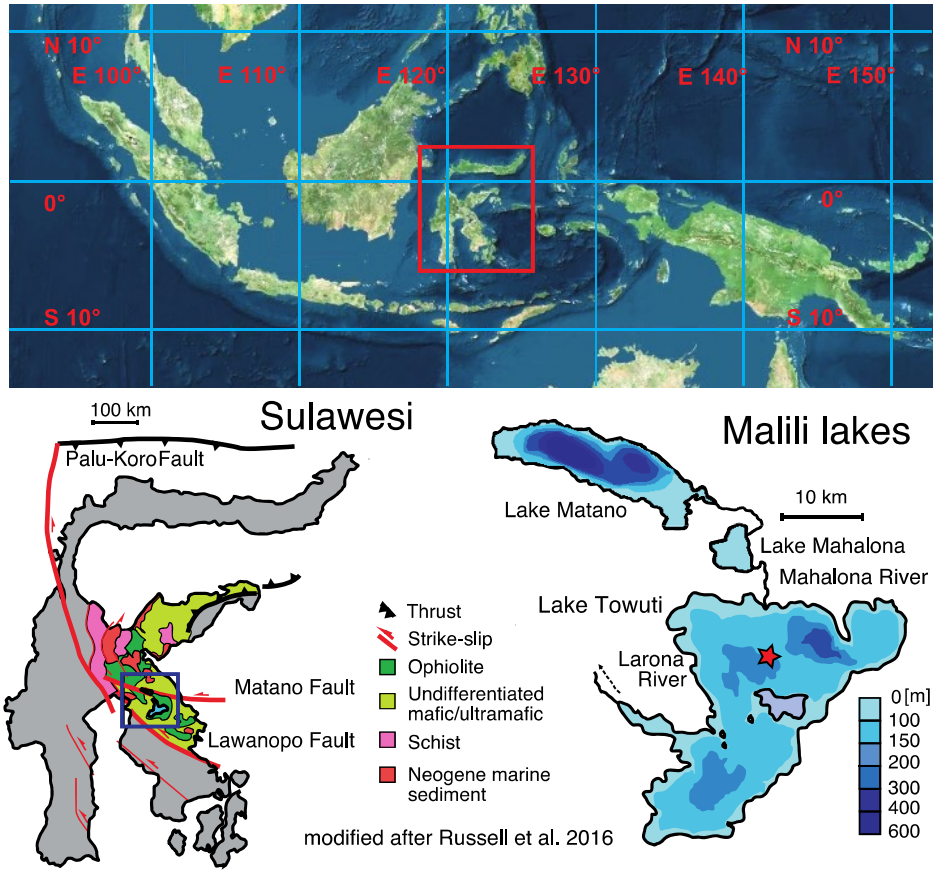

Figure 9.10: *Modified after Russell et al. (2014). Location of Lake Towuti within the Malili Lakes system, Sulawesi, Indonesia. The drilling site, TDP Site 1, is indicated by the red star.*

Our samples (n=166) are derived from a drill core composite stratigraphic section of the upper 113 meters of site TDP-TOW15-1 (Figure 9.10), including holes 1A, 1B, 1D, and 1F. The upper ~100 m of sediments in this section were continuously deposited in a lacustrine environment and likely represent hundreds of thousands of

years of lake history (Russell et al., 2016). Sediments below 100 m indicate deposition in shallow lacustrine, riverine, and swamp environments (Russell et al., 2016).

Lake Towuti's sediments principally consist of an alternation of two types of unconsolidated clays: green clays and red clays, the latter of which contain variable concentrations of siderite (Russell et al., 2014, 2016; Vogel et al. 2015). Mineralogical analyses of surficial sediments and shallow cores show that fine-grained sediments are primarily composed of phyllosilicates, namely serpentine, smectite and kaolinite with variable but generally low amounts of silt-sized siliciclastics, and diverse occurrence of Fe-phases such as siderite, magnetite and Fe^{3+}-oxides (Tamuntuan et al., 2015; Vogel et al., 2015; Goudge et al., 2017; Hasberg et al., 2018; Morlock et al., 2018). Fine-grained pelagic sediments in the core are occasionally interspersed with coarser grained turbidites and concretionary levels rich in siderite (Russell et al., 2016). Despite the low primary productivity today, OM can be abundant in larger quantities, such as the few diatomaceous lithologies, which have been observed at depth in the cores (Russell et al., 2016).

Methods

The Rock-Eval method

All samples were freeze-dried and homogenized using a mortar and pestle. Rock-Eval analyses were performed with a Rock-Eval 6 pyrolyser (Vinci Technologies) at the Institute of Earth Sciences of the University of Lausanne (Switzerland). Between 55 and 70 mg of freeze-dried and powdered sample material were placed in Incoloy crucibles for analyses. The Rock-Eval analytical process consists of two sequential heating steps under different ambient conditions (Espitalié et al., 1985; Lafargue et al., 1998; Behar et al., 2001) while recording the different volatile fractions of the OM as a function of the increasing temperature. The first step is a pyrolysis under an inert atmosphere (N_2). Free hydrocarbons (HC) are first released isothermally at 200°C for 3 minutes and measured as signal S1 (expressed in mg HC g^{-1} sediment) by a flame ionization detector (FID). Samples are then progressively heated up to 650 °C at a rate of 25°C $minute^{-1}$. Long-chained C-compounds and kerogen crack and release HC, which is recorded as the S2 fraction (mg HC g^{-1} sediment, Figure 9.11A). Hydrocarbons released during these steps are measured by a flame ionization detector (FID), and the abundance of hydrocarbons measured as a function of time is called a thermogram. Simultaneously, the cracking of

kerogen and OM also releases carbon dioxide (CO_2) and carbon monoxide (CO) that are measured by an infrared-cell (IR). Carbon oxide thermograms are expressed in mg CO_2 and mg CO per g of sediment, respectively (Figure 9.11), and are referred to as S3 and S3CO. Using the S1, S2, S3 and S3CO thermograms, the pyrolysed carbon (PC, wt%), or the fraction of TOC which is proportional to the amount of hydrogen and oxygen in the OM, is measured. The second step in the Rock-Eval method is a combustion under oxidative conditions (N_2/O_2 : 80/20). Following a short cooling step, samples are progressively reheated from 300 up to 850 °C. The combusted CO is recorded as the S4CO thermogram and CO_2 as $S4CO_2$ and S5. Both oxides are measured (by IR) to quantify the residual fraction of the TOC, referred to as residual carbon (RC – wt%), which requires external oxygen to be combusted and volatilized. Low PC/RC ratios are typical of OM rich in long-chained carbon polymers such as organic compounds of vascular plants (Meyers, 1997; Carrie et al., 2012) or residual/degraded OM (Henrichs, 1993). While the measured HC is exclusively of organic origin, carbonates also contribute to the production of CO_2 and CO within the S3 fraction, with different cracking temperatures depending on their composition (Pillot et al., 2014).

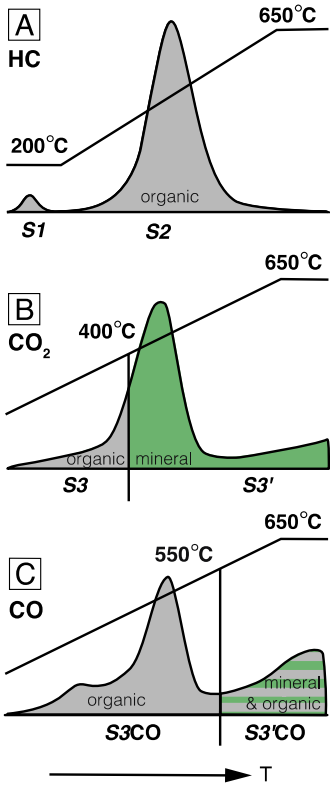

Figure 9.11: *Standard Rock-Eval temperature ranges for HC (A), CO_2 (B) and CO (C) thermograms in Lake Towuti sediments, modified after Behar et al. (2001). The illustration explains how intensities are conventionally split into organic and mineral carbon integrals.*

Table 9.2: *Rock-Eval parameters and their respective equations after Lafargue et al. (1998). Signals S1 and S2 correspond to HC recorded during pyrolysis. CO_2 and CO from the C_{org} fraction are given by signals S3 and S3CO. CO_2 and CO from the C_{inorg} fraction are given by signals S3' and S3'CO. At the oxidation step, signals $S4CO_2$ and S4CO correspond to the C_{org} fraction and S5 to the C_{inorg}. In grey, the revisited formulas where total intensity of CO and CO_2 thermograms was proportionally redistributed into organic and inorganic fractions obtained by End-Member Analysis. They replace classic signals such as S3, S3', S3CO and S3'CO.*

Rock-Eval Parameter	Formula
TOC (wt%), Total Organic Carbon	PC + RC
PC (wt%), Pyrolysed Carbon	(S1+S2) x 0.083 + (S3 x 12/440) + (S3CO + 1/2S3'CO) x 12/280
RC (wt%), Residual Carbon	(S4CO2 x 12/440) + (S4CO x 12/280)
MinC (wt%), Mineral Carbon	PyroMinC + OxiMinC
PyroMinC (wt%)	S3' x 12/440 + 1/2S3'CO x 12/280
OxiMinC (wt%)	S5 x 12/440
HI (mg HC g^{-1} TOC), Hydrogen Index	S2 x 100/TOC
OI_{RE6} (mg O_2 g^{-1} TOC), Oxygen Index	$OICO_2$ x 32/44 + OICO x 16/28
OI or $OICO_2$ (mg CO_2 g^{-1} TOC)	S3 x 100/TOC
OICO (mg CO g^{-1} TOC)	S3CO x 100/TOC
EMA-TOC (wt%)	EMA-PC + RC
EMA-PC (wt%)	((S1+S2) x 0.083) + ($C_{org}CO_2$ x 12/440) + (C_{org}CO x 12/280)
EMA-MinC (wt%)	EMA-PyroMinC + OxiMinC
EMA-PyroMinC (wt%)	($C_{inorg}CO_2$ x 12/440) + (C_{org}CO x 12/280)
EMA-OI	$C_{org}CO_2$ x 100/ EMA-TOC
EMA-OICO	C_{org}CO x 100/ EMA-TOC
EMA-OI_{RE6} (mg O_2 g^{-1} TOC)	(EMA-OI x 32/44) + (EMA-OICO x 16/28)

Standard Rock-Eval parameters (TOC; MinC; HI; OI) and the OI_{RE6} (a variety of OI, calculated in mg O_2 g^{-1} TOC) were calculated from thermograms using the areas between boundary temperatures based on the empirically determined equations of Lafargue et al. (1998; Tab. 9.2). The thermal boundary between organic and mineral carbon in CO_2 thermograms from the first step is set at 400°C (Lafargue et al., 1998), below which CO_2 is considered to be of organic origin (S3, Fig. 9.11B). Above 400°C, CO_2 is considered to have a mineral origin (S3', Figure 9.11B). Conversely, the thermal boundary in CO thermograms is variable and defined where a minimum of CO-intensity is observed (400-600°C). If no minimum could be measured, 550°C is taken as a default value (Fig 9.11C). At lower temperatures CO intensities are considered exclusively organic (signal S3CO, Figure 9.11C). As temperature increases, CO additionally evolves from the reaction of CO_2 with residual organic carbon, following the

Boudouard equilibrium reaction (CO_2 + C ↔ 2CO; Lafargue et al., 1998). At high temperatures, it is assumed that the CO_2 involved in the reaction is predominantly originating from carbonates. Therefore, above the defined minimum, CO is considered to evolve from a mixture of organic and inorganic sources (signal S3'CO, Figure 9.11C).

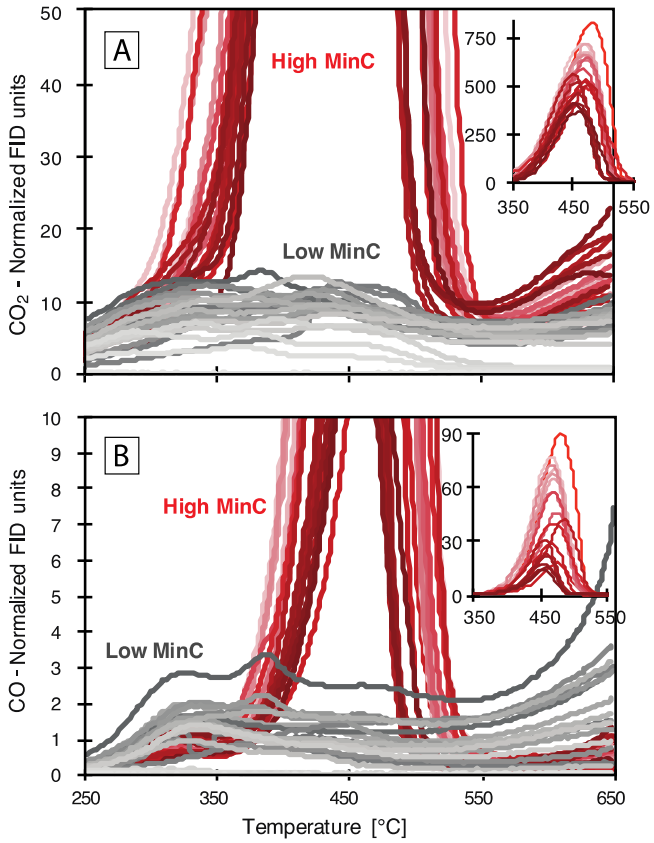

Figure 9.12: *Representative CO_2 (A) and CO (B) thermograms for siderite rich (High MinC, red colors) and siderite-poor (Low MinC, grey colors) samples. The High MinC group displays high intensities between 350 and 550 °C, which corresponds to the cracking-temperature range of siderite (Espitalié et al., 1985). Intensities are normalized to sample mass.*

The presence of siderite exerts a significant complication as it overlaps with the commonly used Rock-Eval thermal boundaries. This is because siderite starts to thermally decompose below 400 °C, well within the range of the cracking of OM. This challenges the use of standard Rock-Eval parameters because siderite -MinC can contribute to intensities used for the calculation of TOC and OI_{RE6}, as well as parameters that are normalized against TOC such as the HI. However, detecting and correcting siderite effects is possible. It can be differentiated from other carbonates because it simultaneously produces both CO and CO_2 at relatively low temperatures due to the additional reaction of CO_2 with Fe^{2+}-oxides ($FeCO_3$ → FeO + CO_2 ; 3FeO + CO_2

→ Fe_3O_4 + CO). Consequently, thermograms from siderite-rich samples will show twin features on CO_2 and CO thermograms (Figure 9.12, simultaneous CO_2 and CO peaks), whereas other carbonates will not (Espitalié et al., 1980).

Besides TOC and MinC, the Rock-Eval method allows the determination of OM quality-related indices such as HI, OI and OI_{RE6}. Plotted within a Pseudo Van-Krevelen diagram, they display endmembers of OM sources contributing to the sediment pool of OM preserved after deposition (Tissot and Welte, 1984; Tyson, 1995; Meyers and Lallier-Vergès, 1999). Owing to the application of Rock-Eval analysis in the context of hydrocarbon exploration, source endmembers are characterized as kerogen types (Tissot and Welte, 1984; Peters, 1986). The Type I kerogen is rich in hydrocarbons and lipids (high HI) and is typically attributed to microbial biomass and/or the waxy coatings of leaves from land plants (Meyers, 1997; Carrie et al., 2012). Type II kerogen originates from protein-rich algal biomass. Despite a potential contribution from fresh terrestrial inputs, I and II are often considered as aquatic OM. The Type III kerogen is defined by OM poor in hydrocarbons and rich in carbohydrates and lignins (main component in plant cell wall materials). It typifies woody plants, terrestrial OM, or highly degraded aquatic or terrestrial OM (Katz, 1983; Meyers and Lallier-Vergès, 1999). This typology, and in particular interpreting the source of Type III kerogen, can be ambiguous, but it has successfully been applied in many paleoenvironmental studies utilizing HI and OI variations in lacustrine sediments to deduce changes in aquatic productivity and/or OM degradation in lacustrine systems (Ariztegui et al., 2001; Steinmann et al., 2003).

In addition to the previously mentioned indices typifying OM sources, two S2-derived indices, the I- and R-indices (Disnar et al., 2003; Sebag et al., 2006, 2016; Marchand et al., 2008; Albrecht et al., 2014), have been used to qualitatively characterize OM degradation. The S2 thermograms, which measure the amount of pyrolysed HC, are normalized to 100% and divided into 5 temperature ranges, from the most thermally labile to the most thermally refractory organic fraction (A1: 280-340 °C, A2: 341-400 °C, A3: 401-460 °C, A4: 461-550 °C, A5: 551-650 °C). The I-index (I = log [(A1+A2)/A3]) is commonly used to assess the contribution of the most thermally labile fraction to the sedimentary OM and may be used to estimate the degree of OM preservation. Albrecht et al. (2014), showed that the I-index is sensitive to degradation of biological tissues into soil and sedimentary OM. Conversely, the R-index (R = (A3+A4+A5)/100) provides a qualitative measure of the thermal stability of bulk OM

and can therefore be used to estimate the degree of OM degradation. Together, these indices can be used as indicators for OM degradation and mineralization. Indeed, by default, both indices are strongly inversely correlated when thermal stability is driven by preferential mineralization of the labile fraction; i.e. when the refractory fraction increases at the expense of the labile fraction during the degradation of OM.

X-ray diffraction and elemental CHNS analysis

To confirm the presence or absence of siderite in samples with high and low MinC values, we performed X-ray diffraction (XRD) analyses on freeze-dried and powdered bulk sediment samples, with detection limits fluctuating between 0.2 and 0.5 wt% of MinC. Whole sediment compositions were determined using a Thermo Scientific ARL X-TRA diffractometer at the Institute of Earth Sciences (University of Lausanne, Switzerland), following the methods described by Adatte et al. (1996). Reported intensities of siderite were observed at $2\theta=32°$.

Additionally, total carbon (TC) and TOC, were measured on 6 samples, covering the range of TOC and MinC values inferred by Rock-Eval analyses, with a Carlo Erba EA 1108 Elemental Analyser at the Institute of Geological Sciences, University of Bern, to evaluate the Rock-Eval dataset before and after EMA. Inorganic carbon was removed using 1M HCl at 70°C prior to TOC content determination. Total inorganic carbon (TIC) was calculated as the difference between TC and TOC.

End-member analysis

Thermal boundaries used in the equations for the determination of Rock-Eval parameters (Lafargue et al., 1998) were empirically defined considering the cracking temperature ranges of organic and inorganic carbon phases. The accuracy of the empirically determined thermal boundaries was tested in this study using End-Member Analysis (EMA). In particular, EMA was applied to better constrain the contribution of siderite C to quantify the MinC.

We used AnalySize, a Matlab-based Graphic User Interface typically used for processing and unmixing of grain-size distribution data (Paterson and Heslop, 2015). We followed a Single-Specimen Unmixing (SSU) method, which unmixes individual

grain-size distributions (GSD) into unimodal parametric distributions using a least squares approach. Applications of EMA on GSD are commonly used to characterize sediment transport processes. Thermograms are in many ways similar to grain-size distribution spectra. This is because they consist of overlapping peaks resulting from OM and mineral carbon phases cracking at variable temperature ranges. Likewise to its application on GSD, EMA on Rock-Eval thermograms may facilitate unmixing of the thermograms into carbon endmembers and help to qualitatively characterize carbon composition in sediments.

There are two main constraints with SSU. The statistical approach presumes that intensities can be described as a linear mixture of the end-member components in which the abundances of each end-member must be nonnegative and sum to one (100%) (Paterson and Heslop, 2015). CO and CO_2 intensities in thermograms are already nonnegative values. To allow our dataset to sum to one, thermograms were normalized to 100%, i.e. intensities at each temperature increment (°C) of each thermogram were divided by the integral of the entire signal (200°C-650°C). The parametric EMA was applied to CO and CO_2 thermograms using a lognormal distribution fit. Thermograms measured at the oxidation step (S4CO, S4CO_2, S5; Tab. 9.2) were not considered for EMA since all siderite should have been degraded during the pyrolysis stage (Espitalié et al., 1985). This is clearly visible in thermograms (Figure 9.12) with siderite intensities negligible after 550°C. Each end-member's intensity was integrated and included in the equations of Rock-Eval parameters (Behar et al., 2001). Results of EMA and in particular the resulting relative amounts of siderite in our samples were compared to the parameters obtained via the Rock-Eval classic thermal boundaries.

Results

Uncorrected standard Rock-Eval parameters

TOC ranges between 0.18 and 6.05 wt%, which is within the range of modern surface sediments (0.17 and 6.43 wt%; Hasberg et al., 2018). RC (residual carbon) values are generally higher than PC (pyrolysed carbon), barely reaching PC/RC ratios >1. Only 18 out of the 166 samples have a PC/RC >1. MinC ranges between 0.11 and 4.65 wt%.

HI (15-300 mg HC g^{-1} TOC) is positively related to the TOC content. OI and OI_{RE6} are very high, reaching values above 1000 mg CO_2 and mg O_2 g^{-1} TOC,

respectively, especially where TOC contents are below 2 wt%. Such high values are comparable to those reported (up to 1500 mg O_2 g^{-1} TOC) from Gabonese lake sediments with a relatively high contribution of sand and charcoal (Sebag et al., 2013). The I index, an estimate of the preservation of the labile OM, ranges between -0.61 and 0.56. Conversely, the R index, representing the relative abundance of the thermally stable (refractory) OM, ranges between 0.50 and 0.89.

Siderite content and matrix effect

XRD measurements confirmed macro- and microscopic observations of the presence and absence of siderite. Siderite was systematically detected by XRD in samples with variable MinC (0.5-3 wt%, Fig. 9.13). However, siderite was only occasionally detected at MinC values <0.5 wt% (i.e. 0.3 wt%, Fig. 9.13). Although XRD cannot provide precise estimates of siderite content, the comparison of XRD peak intensities with the Rock-Eval MinC shows very good agreement (R^2=0.91) and both values are positively correlated. Moreover, other carbonate minerals were not detected by XRD. It can therefore be assumed that MinC originates from siderite while other carbonate phases are either absent or below the detection limit of XRD. This is in good agreement with previous combustion tests (Pillot et al., 2014), which show that the amount of siderite is proportional to the signal of CO_2 and CO thermograms, used in the calculation of MinC.

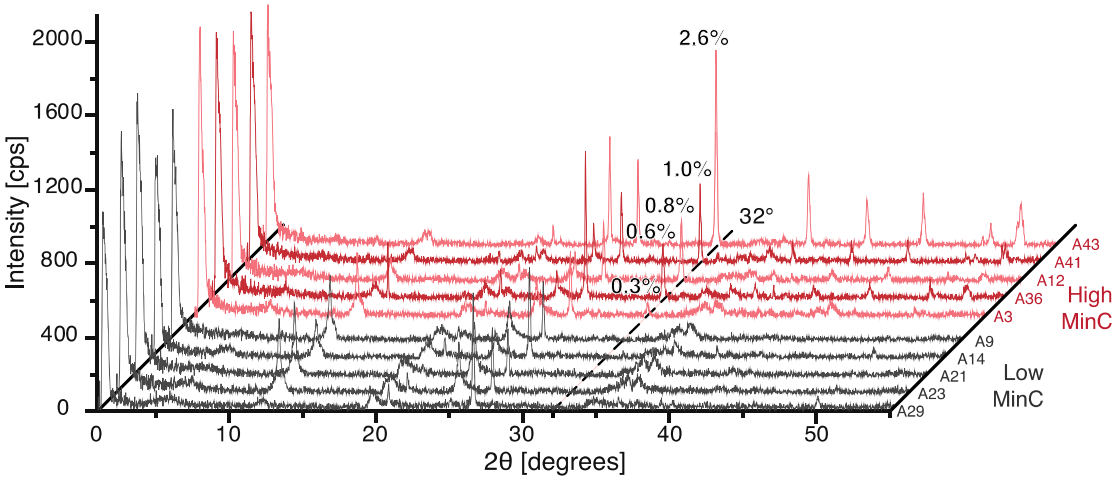

Figure 9.13: *X-ray diffractograms of samples from the High MinC (MinC>0.3%) and Low MinC (MinC<0.3%) groups showing the presence or absence of the characteristic siderite diffraction at 2θ=32°.*

As revealed by previous studies (Espitalié et al., 1985; Sebag et al., 2018), siderite can contribute to the S3 and S3CO integrals (used to calculate the PC and TOC; Table 9.2). This affects Rock-Eval TOC and MinC assessment and can strongly bias the

calculation of OI and OI_{RE6} values which are particularly sensitive to these matrix effects on S3 and S3CO thermograms. Lake Towuti sediments with low TOC and high siderite content are particularly prone to these siderite-induced matrix effects and therefore require an evaluation and eventually a correction prior to calculating Rock-Eval parameters. To objectively determine whether siderite is accountable for the assumed matrix effects, we followed an approach totally independent of the lithological facies and focused only on our Rock-Eval thermograms. Thus, we divided the entire dataset into two groups using the median (0.31 wt%) of MinC: *high MinC* (siderite-rich samples) and *low MinC* (siderite-poor samples). This was done under the assumption that in Lake Towuti sediments MinC calculated from uncorrected Rock-Eval thermograms indicates the presence of siderite as suggested by the correlation of MinC with the XRD intensity peaks at 32.1°. The CO_2 and CO thermograms of the *high MinC* group show high intensities between 350 and 550°C, whereas intensities in this

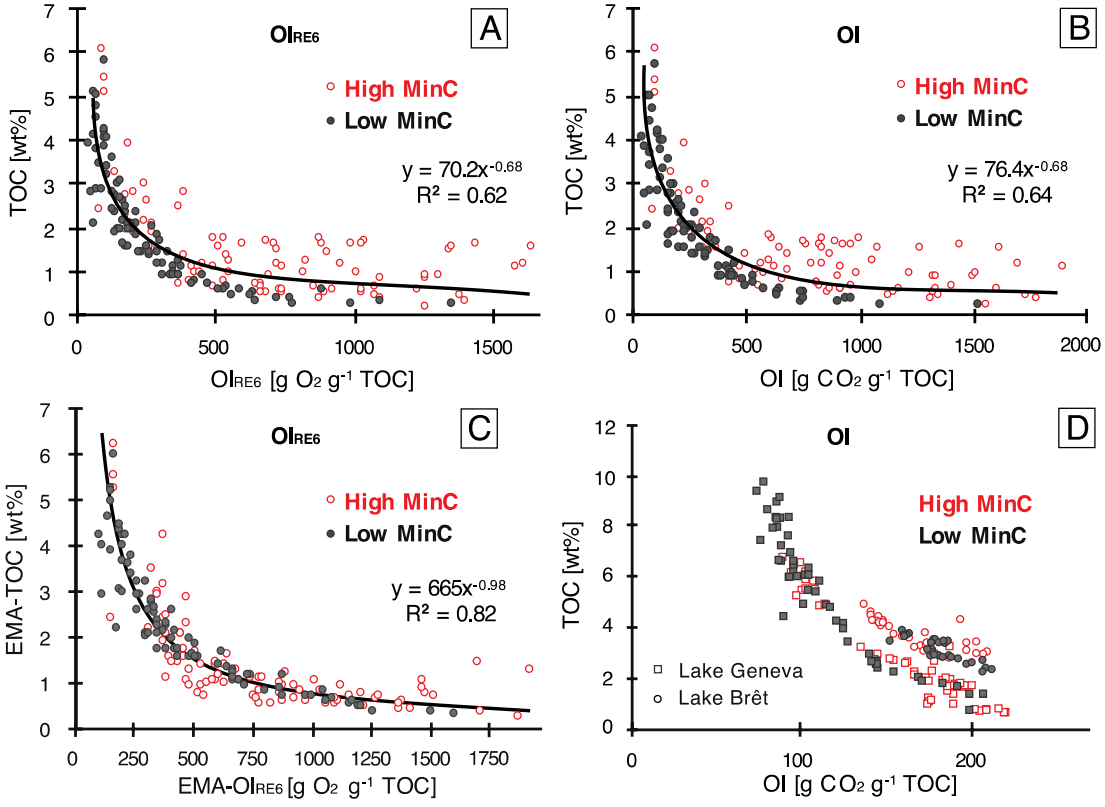

Figure 9.14: *High MinC (siderite-rich) and Low MinC (siderite-poor) samples reveal different TOC vs. OI_{RE6} (A) and TOC vs. OI (B) properties. (C) With End-Member Analysis (EMA), the trend defined by TOC vs OI_{RE6} is tight-clustered whether samples contain high or low/no siderite. (D) Scatterplot of TOC vs. OI presents tight clustering in lakes with low/no siderite (Lake Geneva, Gascón Díez et al., 2017; Lake Brêt, Thevenon et al., 2013). MinC in these systems is principally composed of calcite. Note the different scales in the different panels.*

temperature range are low in the *low MinC* sample set (Fig. 9.12). These observations are also consistent with Pillot et al. (2014) and Sebag et al. (2018) who demonstrated strong correlation between siderite content and intensity at these temperature ranges in Rock-Eval thermograms.

Based on the grouping assigned to the Lake Towuti sample set, oxygen indexes (OI and OI_{RE6}) and TOC, two parameters sensitive to siderite effects on S3 and S3CO integrals, also reveal two distinct populations related to siderite abundance (Figs. 9.14A and 9.14B). While both parameters present an outstanding correlation in the *low MinC* group, those of the *high MinC* spread out, particularly in samples with TOC <2 wt%. This suggests possible matrix effects on OI, OI_{RE6} and TOC.

Carbon distribution by End-Member analysis

We tested different parametric distributions and optimized the linear independence of the end members (EM) by choosing the lowest maximum squared linear correlation factors (R^2) between the different fitted EM. Indeed, a low linear correlation between end members is convenient since high EM correlation is an indication of overfitting where one end member is a near duplicate of another (Paterson and Heslop, 2015). A lognormal parametric distribution in CO_2 thermograms with 6 EM accounted for a specimen median R^2 value of 98.6% and a maximum EM linear correlation of R^2=0.07. The same parametric distribution in CO thermograms with 5 EM accounted for a specimen median R^2 value of 95.8% with a maximum EM linear correlation of R^2=0.20. Using alternative parametric distributions and/or forcing the analysis to fewer or more EM, did not improve the EM linear correlation factors.

Considering a temperature of 380-560°C for siderite and the temperature peaks given by the algorithm, two EM in the CO and three EM in the CO_2 thermograms were assigned to inorganic carbon (Fig. 9.15A). Deconvolution of the siderite signal of CO and CO_2 thermograms into 2 (at 444°C and 473°C) and 3 (at 419°C, 450°C and 479°C) peaks respectively could be the result of a thermal shift-matrix effect caused by carbonate mass variations, different degrees of crystallinity, or other mineral matrix effects (Espitalié et al., 1980; Marchand et al., 2008; Pillot et al., 2014; Kang et al., 2015).

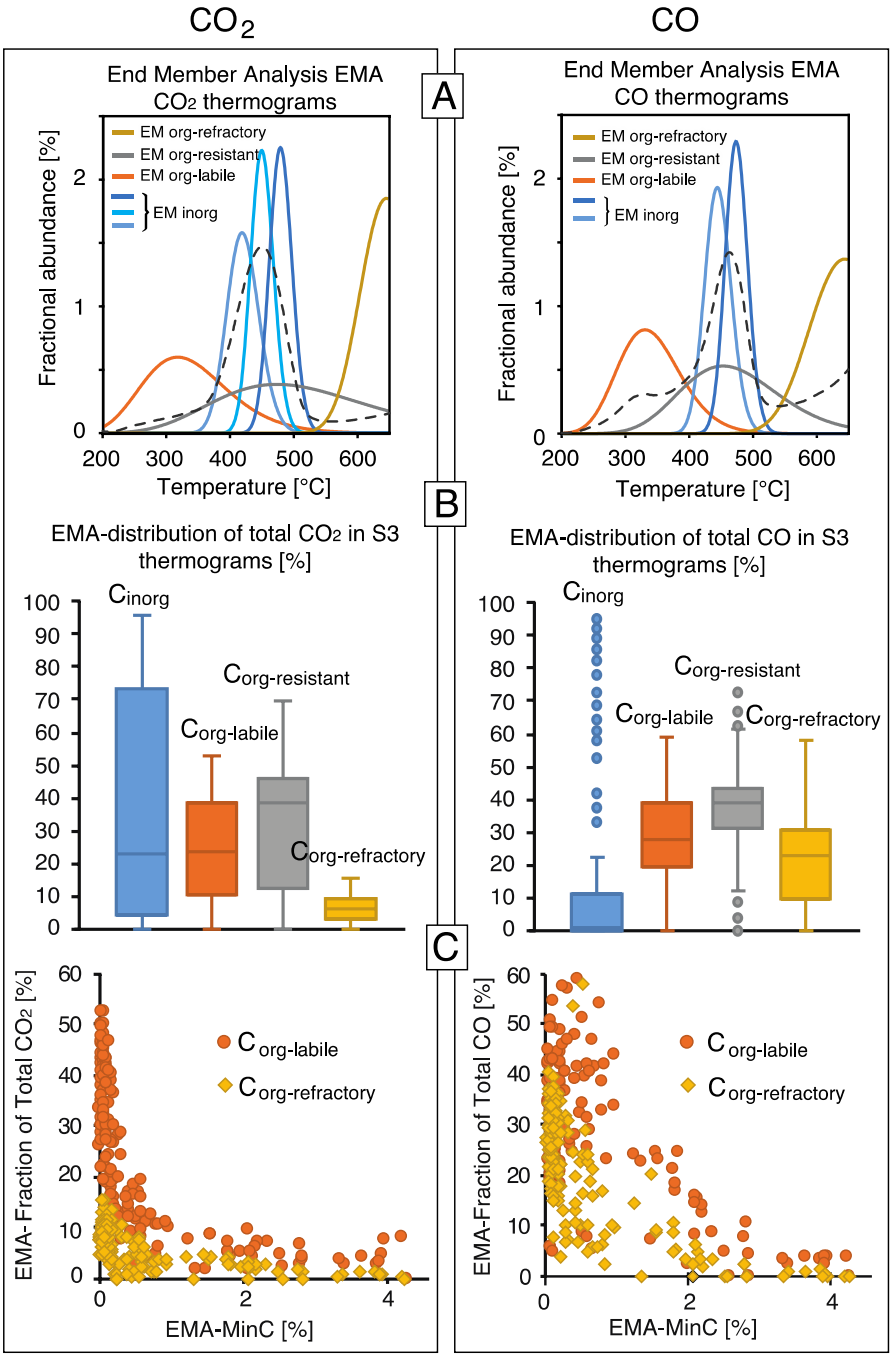

Figure 9.15: *Results of the End Member Analysis (EMA) performed on thermograms to identify and quantify carbon phases. (A) End-Members (EM) density obtained by EMA in CO_2 and CO thermograms. Three and two EM, respectively, were assigned to siderite. Three End-members were attributed to organic phases. Dashed lines indicate the relative average intensity of thermograms. (B) EM were identified as siderite (C_{inorg}), labile C_{org} ($C_{org\text{-}labile}$), refractory C_{org} ($C_{org\text{-}refractory}$), and an intermediate C_{org} phase moderately refractory ($C_{org\text{-}intermediate}$). Integrated intensities were included in the equations of Rock-Eval parameters (Behar et al., 2001) such as MinC and TOC. (C) $C_{org\text{-}labile}$ and $C_{org\text{-}refractory}$ are both negatively correlated to the MinC calculated by EMA (EMA-MinC) suggesting consumption of both C_{org} phases. However, $C_{org\text{-}labile}$ is generally more abundant than $C_{org\text{-}refractory}$ even at high MinC, indicating resilience of $C_{org\text{-}labile}$ to mineralization processes.*

Pillot et al. (2014) combusted rocks containing different degrees (5-40 mg) of pure siderite under oxidative conditions and suggested mass variations as having a small effect in the temperature at which they release their maximum of CO_2 (515-519°C). However, the content of siderite in Lake Towuti sediments seems to influence considerably its peak of cracking temperature. Indeed, samples with MinC values >1 wt% show that CO_2 intensity peaks with a mineral origin evolve in temperature with varying MinC at a rate of ca. 12°C per 1 wt% of MinC ($R^2 = 0.7$). Considering the mass range of the samples (55-70 mg) and the molar mass of siderite (115.8 g mol^{-1}) this corresponds to rates between 1.8 and 2.3 °C mg^{-1} of siderite, respectively.

The temperature peaks at which siderite decomposes in our samples are considerably lower than those found by Pillot et al. (2014) who combusted the carbonates (i.e. under oxidative conditions). Marchand et al. (2008) tested the decomposition of pure siderite and rhodochrosite under pyrolysis conditions and obtained results similar to those of Pillot et al. (2014) suggesting, hence, that oxidative conditions will not particularly shift the peak at which carbonates decompose. It is likely that crystal size neither has a substantial impact on the temperature at which carbonates decompose. Indeed, it has been demonstrated (Pillot et al., 2014) that different crystal sizes of pure calcite (chalk and marble) changed the temperature of maximal release of CO_2 by only 2-4 °C.

Conversely, other mineral matrix-effects might considerably impact the cracking of carbonates. Experimental thermal decomposition of pure siderite (Marchand et al., 2008) or siderite within a rock matrix (Pillot et al., 2014) occurs above 510°C. Carbonates within a clayey matrix decompose at a lower range, between 400 and 475°C (Marchand et al., 2008; Sebag et al., 2018; this study). Moreover, the presence of Fe-oxides might reduce the thermal stability of siderite by more than 100 °C (Kang et al., 2015). Sediments in Lake Towuti and many other tropical environments (Sebag et al., 2018) contain abundant Fe-oxides thus making a shift towards lower siderite decomposition temperatures more likely. Additionally, SEM-EDX analyses of siderite in Lake Towuti sediments show substitution of Fe by Mn with an average Mn atomic/Fe atomic of 0.13 (Vuillemin et al., 2018a). Since rhodochrosite decomposes at higher temperatures (Marchand et al., 2008; Pillot et al., 2014), its presence could also explain some of the variability of the cracking temperature of siderite.

The three remaining EM in CO (peaks at 331°C, 453°C and 644°C) and CO_2 (peaks at 317°C, 473°C and 646°C) thermograms were assigned to organic carbon. Considering the different temperature peaks of the EMs and the thermal properties of OM, we indexed them as labile organic carbon ($C_{org\text{-}labile}$), resistant organic carbon ($C_{org\text{-}resistant}$), and refractory organic carbon ($C_{org\text{-}refractory}$) (Figure 9.15A). Intensities of EM attributed to siderite were combined and indexed as inorganic carbon (C_{inorg}). In light of the EMA results, The $C_{org\text{-}resistant}$ appears to be a substantial source of CO and CO_2 in pyrolysis (Figure 9.15B). However, CO and CO_2 in some sediments are almost exclusively derived from carbonates. The $C_{org\text{-}refractory}$ has as well an important contribution, possibly enhanced by the interaction with Fe-oxides (Grand et al., 2018).

EMA-derived organic and inorganic carbon in CO and CO_2 thermograms were used to calculate TOC (EMA-TOC), MinC (EMA-MinC), and Rock-Eval indices (EMA-HI and EMA-OI_{RE6}). Briefly, the total intensity of CO and CO_2 thermograms was proportionally redistributed into organic and inorganic moieties based on the discriminatory EM's ($C_{org}CO_2$ and $C_{inorg}CO_2$; $C_{org}CO$ and $C_{inorg}CO$), replacing classic CO_2 and CO signals (S3 and S3' ; S3CO and S3'CO). EM based values were then included in the standard formulas (Table 9.2) to calculate Rock-Eval parameters. The Boudouard effect, assuming CO above 550°C as half organic and half mineral (Fig. 9.11), was not considered in calculations because a) siderite is thought to be entirely consumed above 550 °C; b) the effect is negligible below 550°C (Espitalié et al., 1985); and c) other carbonates are absent. Therefore, all CO from $C_{org\text{-}refractory}$ peaks is assumed as exclusively organic.

Rock-Eval thermal boundaries by End-Member analysis

Parameters obtained using EMA are in agreement with those obtained with classic Rock-Eval thermal boundaries although there are slight differences in the TOC and MinC distribution between both approaches. EMA-TOC concentrations (0.70-6.22 wt%) increased by up to 0.39 wt% at the expense of the EMA-MinC (0.01-4.26 wt%), suggesting an overestimation of the initial MinC. This overestimation is almost exclusive to samples with MinC < 1 wt%. Samples with MinC > 1 wt% are usually underestimated. Additionally, using EMA allowed to constrain MinC values of zero. This is consistent with lithological observations in most of the green clays, where siderite is absent. EMA-OI values range from 109 to 2392 mg CO_2 g^{-1} TOC and EMA-

OI_{RE6} values are comprised between 110 and 1872 mg O_2 g^{-1} TOC, much higher than values obtained using conventional Rock-Eval thermal boundaries.

In any case, both approaches produce OI and OI_{RE6} values that are exceptionally high and exceed by far those of previously reported values (up to ~ 500 mg CO_2 g^{-1} TOC) in studies carried out in diverse environments (Meyers and Lallier-Vergès, 1999; Li et al., 2000; Steinmann et al., 2003; Vannière et al., 2008; Debret et al., 2014; Omodeo-Salé et al., 2016). These studies have similar and coherent OI values suggesting a specific type of OM even though their settings are different. Conversely, very high OI_{RE6} values (up to 1500 mg O_2 g^{-1} TOC) have been reported (Sebag et al., 2013; Mabicka Obame et al., 2014) in tropical environments and thus possibly indicate highly degraded OM. OI_{RE6} values higher than 1000 mg O_2 g^{-1} TOC have as well been reported in C horizons from cambisols in mountain areas where OM is scarce and strongly degraded (Giguet-Covex et al., 2011; Bajard et al., 2017). Despite the high values, EMA-OI_{RE6} correlate very well with EMA-TOC (Fig. 9.14C) and the *High* and *Low MinC* constitute this time a more tightly clustered single group as it is the case in samples with low or no siderite from one Alpine (Lake Geneva; Gascón Díez et al., 2017) and one artificial lake in Switzerland (Lake Brêt; Thevenon et al., 2013; Figure 9.14D). This suggests that EMA-derived Rock-Eval parameters are widely unbiased by siderite matrix effects.

Discussion

End-Member Analysis for siderite matrix effect-free Rock-Eval parameters

TOC, MinC, and Rock-Eval indices for OM characterization calculated from uncorrected Rock-Eval thermograms are clearly affected by siderite matrix effects in Lake Towuti sediments. Our approach corrects these Rock-Eval matrix induced biases, improves estimates of OM content in sediments, and optimizes indices used for OM characterization. Here we used the TOC vs. OI_{RE6} scatterplot as a matrix effect proxy. Samples with low or no siderite have an exponential relationship with tight clustering (*Low MinC*, Figure 9.14A) as previously shown in other lacustrine environments containing low or no siderite (Figure 9.14D; Thevenon et al., 2013; Gascón Díez et al., 2017). Samples with an excess or deficiency in CO_2 with a siderite origin spread out in a much looser clustering (*High MinC*; Fig. 9.14A) as for Lake Towuti sediments

containing siderite. The improvements from our EMA correction on TOC and OI_{RE6} values are clearly demonstrated in Figure 9.14C, where the relation of TOC with OI_{RE6} for High and Low MinC samples is similar after correction.

In Lake Towuti, siderite matrix effects only affect TOC moderately since most of the TOC (76% for *Low MinC* and 72% *High MinC*) is composed of RC, which is not affected by matrix effects because it is measured during the oxidation step. This emphasizes that the co-pyrolysis of siderite and most of the OM is limited and that the overlap of signals is low. Conversely, some PC values, the fraction of TOC (24% for *Low MinC* and 28% *High MinC*) measured during the pyrolysis step, were corrected for matrix effects and increased at the expense of MinC, after EMA. The underestimation of PC values can be explained by the limit set at 400°C by the conventional approach to split the organic and inorganic carbon pools (Figure 9.11), despite the refractory OM pyrolysing above that limit (Figure 9.15) and even beyond 550 °C, as shown in our thermograms (Figure 9.12). This is why MinC is overestimated when its values are lower than 1 wt%. Conversely, if siderite is abundant (MinC >1 wt%), intensities below 400 °C are high enough to trigger a bias, and as a result MinC is underestimated. Moreover, EMA showed an abundant $C_{org\text{-}resistant}$ component (32% of total CO_2 and 35% of total CO) in Lake Towuti sediments, potentially combusting along with siderite (Figure 9.15). However, siderite-rich sediments in this study contain low TOC, and hence also low total $C_{org\text{-}resistant}$. Therefore, the bias is generally modest and specific to a few samples with high PC and abundant siderite. For instance, after EMA, samples with EMA-PC and EMA-MinC values >1 wt% showed a carbon redistribution between 0.26 and 0.39 wt%, much larger than the average correction (0.14 wt%).

The EMA routine allowed us to evaluate and better constrain TOC and MinC in samples with variable amounts of organic carbon and siderite compared to other Rock-Eval siderite-matrix effect corrections (Milesi et al., 2016; Sebag et al., 2018). Samples with low PC and abundant siderite, as it is the case for the majority, present low to moderate matrix effects. However, EMA appears particularly valuable in settings where PC and MinC values are high. Moreover, our novel approach allowed us to satisfactorily estimate siderite content in Lake Towuti sediments. Based on EMA-MinC, modal concentrations of siderite in the bulk sediment range from 0 to 45 wt%, with an average of 7 wt%, which is consistent with macro- and microscopic observations. Conversely, the already high OI_{RE6} values considerably increased after correction.

Similar increases in OI_{RE6} after correcting carbonate matrix effects have been reported in other studies; indeed, this is expected as the correction removes carbon from estimates of TOC. For instance, Baudin et al. (2015) performed Rock-Eval analyses in Timor Sea sediments and showed simultaneous CO_2 production from residual carbon (RC) and poorly crystallized calcite. In that study, after correction of TOC values (0.81 wt% ± 0.04), OI increased to values as high as 750 mg CO_2 g^{-1} TOC. Likewise, in this study, EMA showed that a small fraction of $C_{org\text{-}resistant}$ was erroneously accounted as C_{inorg} and TOC correction resulted in an increase of OI_{RE6} values. Therefore, low TOC content and particularly low PC values are sufficient to generate extremely high OI values, especially in Towuti sediments which are already enriched in refractory oxygenated OM. This phenomenon was previously described as a decrease in the signal-to-noise ratio with decreasing TOC (Katz, 1983; Peters, 1986; Espitalié et al., 1985) generating a low TOC-matrix effect.

Finally, to validate Rock-Eval parameters, we measured TOC and TIC in selected samples with an Elemental Analyser (EA) and siderite intensities by XRD. Although MinC and TOC, before EMA, correlate very well with TIC and TOC measured by EA respectively, the slope of the linear regression deviates from the 1:1 line (e.g. MinC = 1.23 TIC + 0.09, R^2 = 0.97), suggesting systematic offsets between the two methods. Differences in Rock-Eval carbon distribution (organic versus inorganic) before and after EMA are relatively small but still relevant considering the low OM content of some Lake Towuti lithologies. However, corrections are not large enough to have an impact on the correlation factors and the slope of Rock-Eval parameters versus those obtained by the Elemental Analyser and XRD. This points to methodological inconsistencies. For instance, the EA, requires prior acidification and separate measurements to constrain the inorganic carbon content. Acidification techniques are known to partially remove labile and soluble organic matter (Marchand et al., 2008; Levesque et al., 2009; Larson et al., 2010; Brodie et al., 2011) possibly leading to an underestimation of TOC values. Conversely, using weak acids can prevent the complete dissolution of carbonates, especially siderite, which is more resistant to acid dissolution than other carbonates (Larson et al., 2010; Brodie et al., 2011; Schlacher and Connolly, 2014). This could explain why C_{org} measurements of acidified samples are systematically lower than their equivalent TOC, obtained by pyrolysis.

Although EMA could improve our Rock-Eval dataset, methodological inconsistencies are still obvious and require further investigation.

Sources of sedimentary organic matter in Lake Towuti

Carbonate matrix effect-free Rock-Eval parameters constitute a more reliable basis to characterize OM in lacustrine sediments. This is particularly true for HI and OI (and OI_{RE6}) indices which, plotted in the Pseudo Van-Krevelen diagram (Figure 9.16A), typify OM sources. Typically, OI and OI_{RE6} increase with OM rich in highly oxidized carbon chains whether they are transported from the catchment or formed by dehydrogenation and oxidation processes during early diagenesis (Jacob et al., 2004; Sebag et al., 2018). EMA-OI_{RE6} in this study (110-1872 mg O_2 g^{-1} TOC) reach anomalously high values, most of them far beyond the usual range to characterize OM sources (Peters, 1986) in aquatic sediments (Meyers, 1997; Meyers and Lallier-Vergès, 1999; Ariztegui et al., 2001; Steinmann et al., 2003; Baudin et al., 2015) and soils (Disnar et al., 2003). Some studies have reported high OI_{RE6} values from lignins (800 mg O_2 g^{-1} TOC; Carrie et al., 2012), C horizons in cambisols (>1000 mg O_2 g^{-1} TOC; Giguet-Covex et al., 2011; Bajard et al., 2017) and predominantly clastic lake sediments with abundant terrestrial OM in lateritic environments (>850 mg O_2 g^{-1} TOC; Mabicka Obame et al., 2014; Sebag et al., 2018). However, high EMA-OI_{RE6} values could likely be the result of other matrix-effects, which in our case subsist the carbonates matrix-effect correction and affect the EMA-OI_{RE6} index. For instance, Fe-oxides may interact with OM (Grand et al., 2018) and clays may exert a thermal shielding effect (Espitalié et al., 1980) with, as consequence, an increase in the temperature at which OM cracks. Espitalié et al. (1985) empirically defined OI as reliable if TOC was >2 wt% and unreliable if <0.5 wt% because low TOC, causing high OI, complicates the conventional use of OI as an indicator of OM provenance. Half of our dataset presents EMA-TOC values >1.5 wt% and can up to a certain point be associated to highly oxidized carbon chains. However, OI_{RE6} values should be interpreted with caution and OM characterization in similar settings requires complementary analyses such as $\partial^{13}C$ and/or biomarkers.

Unlike OI_{RE6}, EMA-HI values are within the usual range of OM characterization and were unaffected by carbonate matrix-effects. The entire dataset presents a relatively narrow range of EMA-HI (14-289 mg HC/g EMA-TOC), with low values consistent

with allochthonous or highly oxidized OM and high values generally attributed to OM sourced from aquatic organisms (Tissot and Welte, 1984; Meyers and Lallier-Vergès, 1999). However, our EMA-HI values are still significantly lower than those of lipids characterizing algae (>500 mg HC g^{-1} TOC; Meyers and Lallier-Vergès, 1999; Carrie et al., 2012). Therefore, samples with moderate EMA-HI values support intermittent inputs of algal lacustrine OM to a terrestrial-like bulk OM that characterizes OM preserved in Lake Towuti sediments.

HI/OI ratios <0.5, as it is largely the case for Towuti samples, have been assigned to terrestrial/soil OM (Carrie et al., 2012; Sebag et al., 2018), and this is consistent with highly-degraded allochthonous OM originating from lateritic soils in the Lake Towuti catchment. Additionally, 87% of Lake Towuti sediments have EMA-PC/EMA-RC ratios <1 and are equivalent to those of carbohydrates (cellulose, pectin) and fresh materials such as conifer needles or tree bark (Carrie et al., 2012). Although such indicators suggest OM in Lake Towuti as being primarily of terrestrial origin, long-chained carbon polymers can also originate from the accumulation of recalcitrant phases following oxidation and diagenetic degradation of the labile fraction (Henrichs, 1993; Jacob et al., 2004).

Depositional environments and early diagenesis in Lake Towuti

I and R indices can indicate the preservation and degradation state of organic matter and, unlike OI_{RE6} values, they are derived from S2 thermograms and thus unbiased by siderite and low TOC-matrix effects. In the I-R diagram (Figure 9.16B), the whole dataset indicates a strong correlation between these two indices. Following Sebag et al. (2016), this correlation indicates that the thermal stability of sedimentary OM is controlled by degradation processes. Indeed, an OM mixture from different sources would generate poorly related I-R indices (Sebag et al., 2016). Towuti water temperatures ranging between 28 and 30°C (Costa et al. 2015) likely enhance degradation, which is further facilitated by methanogenesis, the most important OM mineralization pathway (444 ± 172 mmol m^{-2} yr^{-1} of organic carbon) after burial in Towuti sediments (Friese et al., 2018; Vuillemin et al., 2018).

According to the I-R indices (Figure 9.16B), degradation is more substantial in samples with high EMA-TOC. Additionally, the few samples with a clear dominant algal component (EMA-HI > 130 g HC g^{-1} EMA-TOC) present the lowest I-index for a

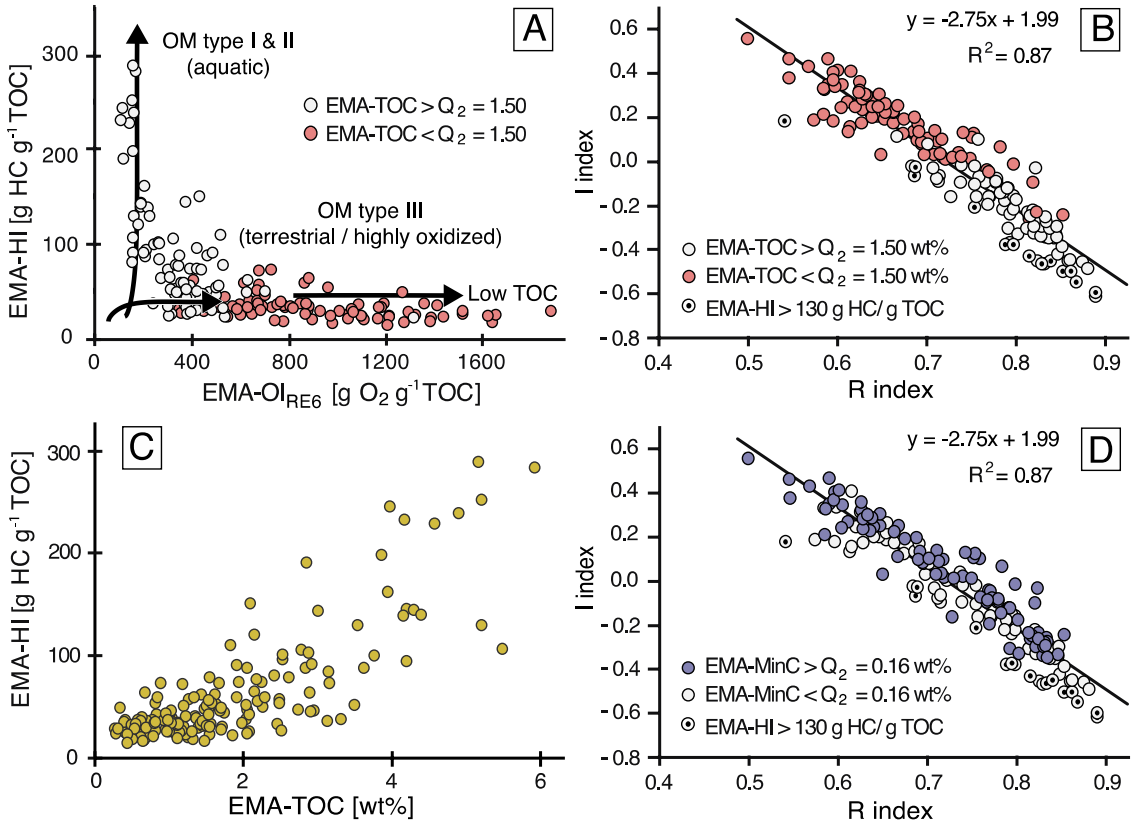

Figure 9.16: *(A) Pseudo Van Krevelen diagram and its main endmembers typifying OM: type I and II, aquatic OM; type III, terrestrial or highly oxidized OM. Very high OI_{RE6} values are explained by low TOC content in Lake Towuti sediments. (B) I-R diagram suggesting larger degradation in samples with higher EMA-HI and EMA-TOC values. (C) EMA-TOC vs. EMA-HI showing linear dependence at TOC contents between 1 wt% and 6 wt%. (D) I-R diagram suggesting degradation independent of the EMA-MinC.*

given R-index, suggesting substantial loss of the most labile OM, and appear more degraded than samples with low EMA-TOC. This supports different rates of OM degradation, which are particularly high in sediments with abundant algal OM (Figure 9.16B). Greater productivity can explain the highest values of EMA-TOC and, if the OM is of planktonic origin, it is preferentially degraded compared to the more resistant terrestrial OM (Tyson et al., 1995). Moreover, EMA-HI correlates positively with EMA-TOC (Figure 9.16C). A decrease of EMA-HI along with EMA-TOC suggests a loss of the labile fraction following degradation. According to previous studies (Huc et al., 1990; Tyson, 1995), HI values level out when sediments attaint optimal preservation conditions, usually at TOC values between 3 and 6 wt% for siliciclastic marine and lacustrine sediments. At that stage, HI can be used to determine eventually the nature of the original sources of lipidic material (Tyson et al., 1995). Since our HI values do not level out, optimal OM preservation conditions were not achieved in Lake Towuti

sediments and our EMA-TOC versus EMA-HI indicates intense degradation of labile autochthonous OM.

Hence, buried OM in our high EMA-TOC samples is depleted in the labile and likely residually enriched in the more recalcitrant OM and thus shows a predominance of terrestrially sourced OM. This is in agreement with the moderately high EMA-OI_{RE6} values with a terrestrial-like signature. If extremely high EMA-OI_{RE6} are due to a low EMA-TOC-matrix effect, as seen in 5.1, moderately high EMA-OI_{RE6} from kerogens could be the result of accumulation of refractory phases. However, differentiating kerogens with a terrestrial origin from those formed by in-situ degradation in samples with low EMA-HI and moderately high EMA-OI_{RE6} requires further investigation and possibly a detailed organic geochemical approach.

Finally, unlike EMA-TOC, EMA-MinC do not define a clear relation with the I-R indices (Figure 9.16D) and degradation processes seem not to be related to the abundance of siderite. This points to a substantial contribution of siderite forming post-burial and thus after the majority of the OM has already been degraded. Indeed, according to EMA, $C_{org\text{-}labile}$ and $C_{org\text{-}refractory}$ both decrease with increasing C_{inorg}, suggesting that "labile" and "refractory" fractions are indistinctly mineralized (Figure 9.15C) into intermediate phases such as CH_4 and CO_2 (Friese et al., in prep.) prior to siderite formation. This brings to light different degradation processes of OM followed by a subsequent (diagenetic) transition of organic carbon to siderite (Vuillemin et al., 2018).

Conclusions

Despite its many advantages, a potential problem with Rock-Eval analysis arises from the bias introduced by matrix effects that hamper the robust determination of OI_{RE6}, MinC and TOC values. Samples with abundant siderite thus require a suitable matrix-correction approach to generate unbiased Rock-Eval parameters.

Using End-Member Analysis (EMA) we were able to correct Rock-Eval thermograms for siderite matrix effects allowing for a more accurate determination of widely used parameters for quantitative and qualitative organic matter characterization. Carbonate matrix effects slightly affected TOC and MinC values since the major component of the organic carbon was obtained during the oxidation step and thus was not synchronous with the pyrolysis of siderite. However, very low TOC contents, and

probably the presence of clays and Fe-oxides, induced anomalously high OI_{RE6} values, which could not be exploited using classic Rock-Eval interpretation schemes and should be interpreted with caution.

Standard Rock-Eval indices obtained by EMA combined with alternative indices derived from S2 thermograms (I-R) can be used as valuable indicators for OM sourcing and degradation in geochemically exceptional Lake Towuti sediments. The I- and R-indices suggested different degradation processes: in combination with high EMA-HI-values, they indicated an intermittent algal input to the sediments, followed by intense loss of the labile organic fraction; associated to high EMA-TOC and moderately high EMA-OI_{RE6} they indicated strong degradation and substantial accumulation of terrestrial-like OM in the sediments. Moreover, a correlation of I-R indices with the MinC could not be determined, suggesting that the majority of OM degradation processes precede siderite formation.

In summary, our EMA-Rock-Eval approach improves identification of the sources and the intensity of degradation of OM in ferruginous and siderite bearing sediments. Due to the relatively low amount of sample preparation required and rapid analysis EMA Rock Eval approaches are particularly useful for generating high-resolution datasets for OM sourcing and quality and for targeting specific sediment intervals out of long sediment succession for more time-consuming analyses.

Acknowledgements

The Towuti Drilling Project was partially supported by grants from the International Continental Drilling Program, the US National Science Foundation, the German Research Foundation, the Swiss National Science Foundation (20FI21_153054/1 and 200021_153053/1), Brown University, Genome British Columbia, and the Ministry of Research, Technology, and Higher Education (RISTEK). PT Vale Indonesia, the US Continental Drilling Coordination Office, the GeoForschungs-Zentrum Potsdam and DOSECC Exploration Services are acknowledged for logistical assistance to the project. This research was carried out with permission from the Ministry of Research and Technology (RISTEK), the Ministry of Trade of the Republic of Indonesia, and the Natural Resources Conservation Center (BKSDA) and Government of Luwu Timur of Sulawesi. We thank the valuable comments and suggestions of F. Baudin and Ch. Giguet-Covex to an early version of this manuscript as well as editor S. Rowland.

Dataset

Ordoñez, Luis; Vogel, Hendrik; Adatte, Thierry; Sebag, David; Ariztegui, Daniel; Russell, James; Kallmeyer, Jens; Vuillemin, Aurèle; Bijaksana, Satria; Crowe, Sean; Friese, André (2019), "Empowering conventional Rock-Eval pyrolysis for organic matter characterization of the siderite-rich sediments of Lake Towuti (Indonesia) using End-Member Analysis.", Mendeley Data, v1

http://dx.doi.org/10.17632/nrzksn8jzc.1

References

Adatte, T., Stinnesbeck, W., Keller, G., 1996. Lithostratigraphic and mineralogic correlations of near K/T boundary clastic sediments in northeastern Mexico: implications for origin and nature of deposition. Geolical Society of America Special Papers 307, 211–226.

Albrecht, R., Sebag, D., Verrecchia, E., 2014. Organic matter decomposition: bridging the gap between Rock–Eval pyrolysis and chemical characterization (CPMAS13C NMR). Biogeochemistry 122, 101–111.

Ariztegui, D., Chondrogianni, C., Lami, A., Guilizzoni, P., Lafargue, E., 2001. Lacustrine organic matter and the Holocene paleoenvironmental record of Lake Albano (central Italy). Journal of Paleolimnology 26, 283–292.

Bajard, M., Develle, A.-L., Arnaud, F., David, F., Giguet-Covex, C., Pignol, C., Jacob, J., Crouzet, C., Poulenard, J., Sabatier, P., 2017. Progressive and regressive soil evolution phases in the Anthropocene. Catena 150, 39–52.

Baudin, F., Disnar, J.-R., Aboussou, A., Savignac, F., 2015. Guidelines for Rock–Eval analysis of recent marine sediments. Organic Geochemistry 86, 71–80.

Behar, F., Beaumont, V., De B. Penteado, H.L., 2001. Rock-Eval 6 Technology: Performances and Developments. Oil & Gas Science and Technology 56, 111–134.

Brodie, C.R., Casford, J.S.L., Lloyd, J.M., Leng, M.J., Heaton, T.H.E., Kendrick, C.P., Yongqiang, Z., 2011. Evidence for bias in C/N, δ13C and δ15N values of bulk organic matter, and on environmental interpretation, from a lake sedimentary sequence by pre-analysis acid treatment methods. Quaternary Science Reviews 30, 3076–3087.

Carrie, J., Sanei, H., Stern, G., 2012. Standardisation of Rock-Eval pyrolysis for the

analysis of recent sediments and soils. Organic Geochemistry 46, 38–53.

Costa, K.M., Russell, J.M., Vogel, H., Bijaksana, S., 2015. Hydrological connectivity and mixing of Lake Towuti , Indonesia in response to paleoclimatic changes over the last 60 , 000 years. Palaeogeography, Palaeoclimatology, Palaeoecology 417, 467–475.

Dean, W.E., Gardner, J. V., Piper, D.Z., 1997. Inorganic geochemical indicators of glacial-interglacial changes in productivity and anoxia on the California continental margin. Geochimica et Cosmochimica Acta 61, 4507–4518.

Debret, M., Bentaleb, I., Sebag, D., Favier, C., Nguetsop, V., Fontugne, M., Oslisly, R., Ngomanda, A., 2014. Influence of inherited paleotopography and water level rise on the sedimentary infill of Lake Ossa (S Cameroon) inferred by continuous color and bulk organic matter analyses. Palaeogeography, Palaeoclimatology, Palaeoecology 411, 110–121.

Disnar, J.R., Guillet, B., Keravis, D., Di-Giovanni, C., Sebag, D., 2003. Soil organic matter (SOM) characterization by Rock-Eval pyrolysis: Scope and limitations. Organic Geochemistry 34, 327–343.

Espitalié, J., Deroo, G., Marquis, F., 1985. La pyrolyse Rock-Eval et ses applications. Deuxième partie. Revue de l'Institut français du Pétrole 40, 755–784.

Espitalié, J., Madec, M., Tissot, B., 1980. Role of mineral matrix in kerogen pyrolysis: influence on petroleum generation and migration. American Association of Petroleum Geologists Bulletin 64, 59–66.

Friese, A., Kallmeyer, J., Glombitza, C., Vuillemin, A., Simister, R., Bijaksana, S., Vogel, H., Melles, M., Russell, J.M., Nomosatryo, S., Bauer, K., Heuer, V.B., Henny, C., Crowe, S.A., Ariztegui, D., Wegner, D., 2018. Methanogenesis predominates organic matter mineralization in a ferruginous , non-sulfidic sedimentary environment. EGU General Assembly Conference Abstracts 20, 7446.

Gascón Díez, E., Corella, J.P., Adatte, T., Thevenon, F., Loizeau, J.L., 2017. High-resolution reconstruction of the 20th century history of trace metals, major elements, and organic matter in sediments in a contaminated area of Lake Geneva, Switzerland. Applied Geochemistry 78, 1–11.

Giguet-Covex, C., Arnaud, F., Poulenard, J., Disnar, J.-R., Delhon, C., Francus, P., David, F., Enters, D., Rey, P.-J., Delannoy, J.-J., 2011. Changes in erosion patterns during the Holocene in a currently treeless subalpine catchment inferred

from lake sediment geochemistry (Lake Anterne, 2063 m a.s.l., NW French Alps): The role of climate and human activities. The Holocene 21, 651–665.

Goudge, T.A., Russell, J.M., Mustard, J.F., Head, J.W., Bijaksana, S., 2017. A 40,000 yr record of clay mineralogy at Lake Towuti, Indonesia: Paleoclimate reconstruction from reflectance spectroscopy and perspectives on paleolakes on Mars. Bulletin of the Geological Society of America 129, 806–819.

Grand, S., Viret, F., Sebag, D., Verrecchia, E., 2018. Rock-Eval pyrolysis of density fractions from tropical soils of Western Uganda. RST Société géologique de France 638.

Haffner, G.D., Hehanussa, P.E., Hartoto, D., 2001. The biology and physical processes of large lakes of Indonesia: Lakes Matano and Towuti. The Great Lakes of the World. Food-web, Health and Integrity. Backhuys Publishers, Leiden 183192.

Hasberg, A.K.M., Bijaksana, S., Held, P., Just, J., Melles, M., Morlock, M.A., Opitz, S., Russell, J.M., Vogel, H., Wennrich, V., 2018. Modern sedimentation processes in Lake Towuti, Indonesia, revealed by the composition of surface sediments. Sedimentology.

Henrichs, S.M., 1993. Early Diagenesis of Organic Matter: The Dynamics (Rates) of Cycling of Organic Compounds BT - Organic Geochemistry: Principles and Applications, in: Engel, M.H., Macko, S.A. (Eds.), . Springer US, Boston, MA, pp. 101–117.

Huc, A.Y., Le Fournier, J., Vandenbroucke, M., Bessereau, G., 1990. Northern Lake Tanganyika - an example of organic sedimentation in an anoxic rift lake, in Lacustrine Basin Exploration: Case Studies and Modern Analogs. AAPG Memoir 50, 169–185.

Jacob, J., Disnar, J.R., Boussafir, M., Sifeddine, A., Turcq, B., Albuquerque, A.L.S., 2004. Major environmental changes recorded by lacustrine sedimentary organic matter since the last glacial maximum near the equator (Lagoa do Caçó, NE Brazil). Palaeogeography, Palaeoclimatology, Palaeoecology 205, 183–197.

Kadarusman, A., Miyashita, S., Maruyama, S., Parkinson, C.D., Ishikawa, A., 2004. Petrology, geochemistry and paleogeographic reconstruction of the East Sulawesi Ophiolite, Indonesia. Tectonophysics 392, 55–83.

Kang, N., Schmidt, M.W., Poli, S., Franzolin, E., Connolly, J.A.D., 2015. Melting of siderite to 20GPa and thermodynamic properties of FeCO3-melt. Chemical Geology 400, 34–43.

Katz, B.J., 1983. Limitations of "Rock-Eval" pyrolysis for typing organic matter. Organic Geochemistry 4, 195–199.

Konecky, B., Russell, J., Bijaksana, S., 2016. Glacial aridity in central Indonesia coeval with intensified monsoon circulation. Earth and Planetary Science Letters 437, 15–24.

Lafargue, E., Marquis, F., Pillot, D., 1998. Rock-Eval 6 Applications in Hydrocarbon Exploration, Production, and Soil Contamination Studies. Oil & Gas Science and Technology 53, 421–437.

Larson, T.E., Heikoop, J.M., Perkins, G., Chipera, S.J., Hess, M.A., 2010. N-Nitrosopiperazines form at high pH in post-combustion capture solutions containing piperazine: a low-energy collisional behaviour study. Rapid communications in mass spectrometry : RCM 24, 3567–3577.

Lehmusluoto, P., Machbub, B., Terangna, N., Rusmiputro, S., Achmad, F., Boer, L., Brahmana, S.S., Priadi, B., Setiadji, B., Sayuman, O., 1997. National inventory of the major lakes and reservoirs in Indonesia. Expedition Indodanau Technical Report, Edita Oy.

Levesque, C., Juniper, K., Planas, D., 2009. Organic matter loss during hydrochloric acid treatment of aquatic samples: implications for elemental and stable isotopic analyses, in: AGU Fall Meeting Abstracts.

Li, L., Keller, G., Adatte, T., Stinnesbeck, W., 2000. Late Cretaceous sea-level changes in Tunisia: a multi-disciplinary approach. Journal of the Geological Society 157, 447–458.

Mabicka Obame, R., Copard, Y., Sebag, D., Abdourhamane Touré, A., Boussafir, M., Bichet, V., Garba, Z., Guillon, R., Petit, C., Rajot, J.L., Durand, A., 2014. Carbon sinks in small Sahelian lakes as an unexpected effect of land use changes since the 1960s (Saga Gorou and Dallol Bosso, SW Niger). Catena 114, 1–10.

Marchand, C., Lallier-Vergès, E., Disnar, J.R., Kéravis, D., 2008. Organic carbon sources and transformations in mangrove sediments: A Rock-Eval pyrolysis approach. Organic Geochemistry 39, 408–421.

Meyers, P.A., 1997. Organic geochemical proxies of paleoceanographic, paleolimnologic, and paleoclimatic processes. Organic Geochemistry 27, 213–250.

Meyers, P.A., Lallier-Vergès, E., 1999. Lacustrine sedimentary organic matter of Late Quaternary paleoclimates. Journal of Paleolimnology 21, 345–372.

Milesi, V., Prinzhofer, A., Guyot, F., Benedetti, M., Rodrigues, R., 2016. Contribution of siderite-water interaction for the unconventional generation of hydrocarbon gases in the Solimões basin, north-west Brazil. Marine and Petroleum Geology 71, 168–182.

Monnier, C., Girardeau, J., Maury, R.C., Cotten, J., 1995. Back-arc basin origin for the East Sulawesi ophiolite (eastern Indonesia). Geology 23, 851–854.

Morlock, M.A., Vogel, H., Nigg, V., Ordoñez, L., Hasberg, A.K.M., Melles, M., Russell, J.M., Bijaksana, S., 2018. Climatic and tectonic controls on source-to-sink processes in the tropical, ultramafic catchment of Lake Towuti, Indonesia. Journal of Paleolimnology.

Omodeo-Salé, S., Suárez-Ruiz, I., Arribas, J., Mas, R., Martínez, L., Josefa Herrero, M., 2016. Characterization of the source rocks of a paleo-petroleum system (Cameros Basin) based on organic matter petrology and geochemical analyses. Marine and Petroleum Geology 71, 271–287.

Paterson, G.A., Heslop, D., 2015. Geochemistry, Geophysics, Geosystems. Geochemistry Geophysics Geosystems 18, 1541–1576.

Peters, K.E., 1986. Guidelines for Evaluating Petroleum Source Rock Using Programmed Pyrolysis. American Association of Petroleum Geologists Bulletin 70, 318–329.

Pillot, D., Deville, E., Prinzhofer, a., 2014. Identification and Quantification of Carbonate Species Using Rock-Eval Pyrolysis. Oil & Gas Science and Technology – Revue d'IFP Energies nouvelles 69, 341–349.

Russell, J.M., Bijaksana, S., Vogel, H., Melles, M., Kallmeyer, J., Ariztegui, D., Crowe, S., Fajar, S., Hafidz, A., Haffner, D., Hasberg, A., Ivory, S., Kelly, C., King, J., Kirana, K., Morlock, M., Noren, A., 2016. The Towuti Drilling Project : paleoenvironments , biological evolution , and geomicrobiology of a tropical Pacific lake 29–40.

Russell, J.M., Vogel, H., Konecky, B.L., Bijaksana, S., Huang, Y., Melles, M., Wattrus, N., Costa, K., King, J.W., 2014. Glacial forcing of central Indonesian hydroclimate since 60,000 y B.P. Proceedings of the National Academy of Sciences of the United States of America 111, 5100–5.

Schlacher, T.A., Connolly, R.M., 2014. Effects of acid treatment on carbon and nitrogen stable isotope ratios in ecological samples: A review and synthesis. Methods in Ecology and Evolution 5, 541–550.

Sebag, D., Debret, M., M'voubou, M., Obame, R.M., Ngomanda, A., Oslisly, R., Bentaleb, I., Disnar, J.-R., Giresse, P., 2013. Coupled Rock-Eval pyrolysis and spectrophotometry for lacustrine sedimentary dynamics: Application for West Central African rainforests (Kamalete and Nguene lakes, Gabon). The Holocene 23, 1173–1183.

Sebag, D., Disnar, J.R., Guillet, B., Di Giovanni, C., Verrecchia, E.P., Durand, A., 2006. Monitoring organic matter dynamics in soil profiles by "Rock-Eval pyrolysis": Bulk characterization and quantification of degradation. European Journal of Soil Science 57, 344–355.

Sebag, D., Garcin, Y., Adatte, T., Deschamps, P., Ménot, G., Verrecchia, E.P., 2018. Correction for the siderite effect on Rock-Eval parameters: Application to the sediments of Lake Barombi (southwest Cameroon). Organic Geochemistry 123, 126–135.

Sebag, D., Verrecchia, E.P., Cécillon, L., Adatte, T., Albrecht, R., Aubert, M., Bureau, F., Cailleau, G., Copard, Y., Decaens, T., Disnar, J., Hetényi, M., Nyilas, T., Trombino, L., 2016. Geoderma Dynamics of soil organic matter based on new Rock-Eval indices. Geoderma 284, 185–203.

Steinmann, P., Adatte, T., Lambert, P., 2003. Recent changes in sedimentary organic matter from Lake Neuchâtel (Switzerland) as traced by Rock-Eval pyrolysis. Eclogae Geologicae Helvetiae 96, 109–116.

Tamuntuan, G., Bijaksana, S., King, J., Russell, J., Fauzi, U., Maryunani, K., Aufa, N., Ode, L., 2015. Variation of magnetic properties in sediments from Lake Towuti , Indonesia, and its paleoclimatic significance 420, 163–172.

Thevenon, F., Alencastro, L.F. de, Loizeau, J.L., Adatte, T., Grandjean, D., Wildi, W., Poté, J., 2013. A high-resolution historical sediment record of nutrients, trace elements and organochlorines (DDT and PCB) deposition in a drinking water reservoir (Lake Brêt, Switzerland) points at local and regional pollutant sources. Chemosphere 90, 2444–2452.

Tissot, B.P., Welte, D.H., 1984. From Kerogen to Petroleum, in: Petroleum Formation and Occurrence. Springer Berlin Heidelberg, Berlin, Heidelberg, pp. 160–198.

Tyson, R. V, 1995. Abundance of Organic Matter in Sediments: TOC, Hydrodynamic Equivalence, Dilution and Flux Effects, in: Sedimentary Organic Matter: Organic Facies and Palynofacies. Springer Netherlands, Dordrecht, pp. 81–118.

Vannière, B., Colombaroli, D., Chapron, E., Leroux, A., Tinner, W., Magny, M., 2008.

Climate versus human-driven fire regimes in Mediterranean landscapes: the Holocene record of Lago dell'Accesa (Tuscany, Italy). Quaternary Science Reviews 27, 1181–1196.

Vogel, H., Russell, J.M., Cahyarini, S.Y., Bijaksana, S., Wattrus, N., Rethemeyer, J., Melles, M., 2015. Depositional modes and lake-level variability at Lake Towuti, Indonesia, during the past ~29 kyr BP. Journal of Paleolimnology.

Vuillemin, A., Benning, L.G., Luecke, A., Mayr, C., Friese, A., Kallmeyer, J., Wirth, R., Kemnitz, H., Schuessler, J.A., Bijaksana, S., Vogel, H., Melles, M., Russell, J.M., Bauer, K., Henny, C., Crowe, S.A., 2018a. Diagenetic siderites and vivianites in ferruginous sediment from Lake. EGU General Assembly Conference Abstracts 20, 4855–1.

Vuillemin, A., Friese, A., Alawi, M., Henny, C., Nomosatryo, S., Wagner, D., Crowe, S.A., Kallmeyer, J., 2016. Geomicrobiological features of ferruginous sediments from lake Towuti, Indonesia. Frontiers in Microbiology 7, 1–16.

Vuillemin, A., Horn, F., Alawi, M., Henny, C., Wagner, D., Crowe, S.A., Kallmeyer, J., 2017. Preservation and significance of extracellular DNA in ferruginous sediments from Lake Towuti, Indonesia. Frontiers in Microbiology 8, 1–15.

Vuillemin, A., Horn, F., Friese, A., Winkel, M., Alawi, M., Wagner, D., Henny, C., Orsi, W.D., Crowe, S.A., Kallmeyer, J., 2018b. Metabolic potential of microbial communities from ferruginous sediments. Environmental Microbiology 00, 1–17